



## **Deliverable 2.4: Treatment of chemical evolutions in national programmes**

Work Package 2

The project leading to this application has received funding from the European Union's Horizon 2020 research and innovation programme under grant agreement No 847593.



<http://www.ejp-urad.eu/>

## Document information

Project Acronym	<b>EURAD</b>
Project Title	<b>European Joint Programme on Radioactive Waste Management</b>
Project Type	<b>European Joint Programme (EJP)</b>
EC grant agreement No.	<b>847593</b>
Project starting / end date	<b>1<sup>st</sup> June 2019 – 30 May 2024</b>
Work Package No.	<b>2</b>
Work Package Title	<b>Assessment of Chemical Evolution of ILW and HLW Disposal Cells</b>
Work Package Acronym	<b>ACED</b>
Deliverable No.	<b>2.4</b>
Deliverable Title	<b>Treatment of chemical evolution in National Programmes</b>
Lead Beneficiary	<b>COVRA</b>
Contractual Delivery Date	<b>1 November 2019</b>
Actual Delivery Date	<b>26 November 2020</b>
Type	<b>Report</b>
Dissemination level	<b>PU</b>
Authors	<b>Erika Neeft (COVRA), Eef Weetjens (SCK•CEN), Antonín Vokal (SURAO), Markku Leivo (VTT), Benoît Cochepin, Christelle Martin, Isabelle Munier (ANDRA), Guido Deissmann (FZJ), Vanessa Montoya (UFZ), Povilas Poskas, Dalia Grigaliuniene, Asta Narkuniene (LEI), Enrique García (ENRESA), Javier Samper, Luis Montenegro and Alba Mon (UDC)</b>

### To be cited as:

Neeft, E., Weetjens E., Vokal A., Leivo M., Cochepin B., Martin C., Munier I., Deissmann G., Montoya V., Poskas P., Grigaliuniene D., Narkuniene A., García E., Samper J., Montenegro L., Mon A. (2019): Treatment of chemical evolution in National Programmes, D 2.4 of the HORIZON 2020 project EURAD. EC Grant agreement no: 847593.

### Disclaimer

All information in this document is provided "as is" and no guarantee or warranty is given that the information is fit for any particular purpose. The user, therefore, uses the information at its sole risk and liability. For the avoidance of all doubts, the European Commission has no liability in respect of this document, which is merely representing the authors' view.

### Acknowledgement

This document is a deliverable of the European Joint Programme on Radioactive Waste Management (EURAD). EURAD has received funding from the European Union's Horizon 2020 research and innovation programme under grant agreement No 847593.

Status of deliverable		
	By	Date
Delivered (Lead Beneficiary)	COVRA	11-Dec-2019
Verified (WP Leader)	SCK CEN	20-Dec-2019
Reviewed (Reviewers)	RATEN & ANDRA	23-07-2020
Approved (PMO)	ANDRA	25-11-2020
Submitted to EC (Coordinator)	ANDRA	08-12-2020

## Executive Summary

The broader scope of the workpackage ACED is the assessment of the chemical evolution at the disposal cell scale involving interacting materials and thermal, hydraulic and/or chemical gradients by considering ILW and HLW disposal concepts representative for different concepts throughout Europe. There are a number of elements, especially at the interface scale, which are common for both HLW and ILW disposal cells. On the other hand, the disposal cells for ILW and HLW also have specific elements only relevant for either one of the two such as involved processes, features et cetera. Therefore having both ILW and HLW as separate study objects in the evaluation of the methodologies for process integration and model abstraction will allow for a much broader application of the outcomes of this work package for the different national programmes. Processed waste is considered in ACED and includes a vitrified waste form for High Level Waste (HLW) and a cementitious waste form for Intermediated Level Waste (ILW). Disposal of these waste forms in a geological disposal facility hosted in either crystalline or sedimentary rock types are investigated. Both rock types are porous materials and the chemical composition of their pore waters may induce mineral changes in the engineered barrier system. The virgin pore water chemistry in these host rocks is influenced by carbonates and clay minerals but thermodynamic modelling is required to determine the pore water chemistry in clay host rocks while this modelling may not always be appropriate to determine the pore water chemistry in fractures in crystalline rocks due mixing of groundwaters and biological processes that also have an impact on the porewater chemistry at the depth of the disposal facility. The evolved pore waters from the engineered system chemically affect the host rock locally. A systematic understanding of the chemical evolution from the waste form up till the host rock can be used for a robust assessment of the impact of these processes.

Disposal cells in ACED treat the chemical evolution from the waste form until the host rock. An integration of the available knowledge of the chemical evolution can be performed in a safety assessment. There may be current European practices why the chemical evolutions for disposal are included in safety assessments and safety cases and how the chemical evolutions at disposal cell scale have been treated. A collection of the conceptualisations of the chemical evolutions and which parts have been modelled in Europe could prevent duplication of work already done. Organisations from eight EU countries participate in the ACED task for the current handling of the chemical evolution: Belgium, Czech, Finland, France, Germany, Lithuania, Netherlands and Spain They have described the characteristics of the disposal cells considered in their national programmes and the considered chemical evolutions. Organisations from other European countries with nuclear power plants that participate in EURAD and Switzerland have been asked to contribute to this deliverable. Waste management Organisations (WMOs) usually write the safety cases and the safety assessments is the backbone in the safety case. Therefore preferably WMOs from the missing European countries have been asked to complete a template in which details were asked, specifically references for the materials in the disposal cell, a narrative of the post-closure phase, conceptual and mathematical model for the disposal cell. These country contributions in this Deliverable 2.4 as well as Deliverable 2.5: Analysis of experiments and numerical studies on interfaces, are contributions to the initial State of the Art (Deliverable 2.1). The country contributions can also be used to define experimental conditions that are representative for the chemical evolution of the disposal concepts considered in Europe such as temperature at interfaces and these contributions have been used to define the disposal cells that are used for the modelling work in ACED.

### Vitrified HLW

HLW requires shielding and cooling during handling and storage. The quantities of heat need to be included in the design of the disposal facility. The reprocessing of spent fuel removes unused uranium and plutonium, which can be used again in fresh fuel. After reprocessing, less than 5% of the initial

volume of high-level radioactive waste remains for disposal. One of the waste products is vitrified HLW. Vitrified HLW is envisaged to be disposed in a facility at a depth at which the pore water chemistry of the host rock is not expected to vary due to climate change at Earth's surface when the hazard potential of this waste is large. The collection in this report shows that all disposal cells can be characterised as containing HLW with an encapsulation of the waste canister in a steel overpack to prevent contact between pore water and the waste form when the waste generates heat. This overpack is usually surrounded by a bentonite buffer or concrete buffer in order to be able to assume a corrosion mechanism and a well-chosen corrosion rate to determine the durability of the overpack. These disposal concepts and designs ensure that radionuclide release does not occur when thermal gradients in the host rock are present; this feature reduces the uncertainty of potential radionuclide migration within the host rocks.

The eight contributions for heat generating waste show that a temperature limit of 100°C has been set for the bentonite buffer as well as concrete buffer in order to preserve its properties on the long-term. The chemical evolution is not included in the safety assessment but especially the Spanish and Czech contributions show that the chemical interaction between solid materials can be bounded from calculating the chemical evolution as a function of time and space. For example, iron corrosion has been calculated to reduce the porosity of the bentonite buffer till a maximum of 15 cm after 100.000 years or even 1 million years by precipitation of corrosion species and iron-carbonate species; the carbonate originates from the granitic pore water i.e. a fraction of the bentonite buffer is chemically affected in the local vicinity of the steel-bentonite interface. These calculations are however made at 25°C since most thermodynamic data are related to this temperature.

Such calculations have not been made for the steel overpack interfacing the concrete buffer in the national current treatments of the chemical evolution by the eight organisations participating in ACED. There is however information available from the Swedish ILW disposal cells for the chemical evolution of the steel-concrete interface. From these participating organisations, the chemical evolution for HLW disposal cells has been focussed on the pH of the concrete buffer, the pH as a function of time at the interface between the concrete buffer and carbon steel overpack has been calculated in order to determine the period for the beneficial alkaline conditions in which steel is passivated and very small corrosion rates can be chosen. These alkaline conditions have been calculated to last for 80.000 years in the Belgian programme. Constant diffusion values have been used and this may optimize the envisaged durability of the concrete buffer especially when the clay pore water is saline even brackish since the crystallisation of calcium-sulphate minerals may result in the formation of cracks within the concrete buffer. The presence of these cracks changes the transport properties, an increase in diffusion values as identified for the chemical evolution of concrete barriers in the Swedish programme.

It has been deduced from the references that the Swiss approach is similar to the Spanish and Czech approaches i.e. calculating the potential extent of the chemical interaction and determine whether or not these effects are safety relevant in order to judge whether or not these chemical processes need to be included in the safety assessment. The Spanish, Czech and Swiss programmes calculate the chemical evolution of the interface between the steel overpack and bentonite buffer. Mainly anaerobic conditions are available in the post-closure phase and the anaerobic corrosion of iron results into the release of dissolved iron species, hydrogen gas and hydroxyl ions. An increase of the pH, until a pH of 10, has been calculated at the steel-bentonite interface. A potential impact of an increasing pH is the transformation of clay minerals in zeolites. The solubility of corrosion species and iron-carbonate species is limited by which the concentration of positively charged dissolved iron species is small. The sorption capacity of the bentonite buffer can be reduced by sorption of dissolved iron species.

Eventually, there will be contact between pore water and the vitrified HLW. Glass has been known to be very insoluble, A passivation layer on the exposed surfaces of glass has been known to be formed in neutral as well as alkaline media. This layer also constitutes a barrier against transport of water towards glass and of solvated glass into solution. The long term dissolution rate of the vitrified waste form is therefore expected to be very small after fracture of the overpack. Congruent dissolution of glass is used to determine the radionuclide release in safety assessments but the incorporation of radionuclides in the passivating layer may be element-specific. There will be always steel present when there is contact

between pore water and the non-cracked parts of vitrified HLW and the glass dissolution rate is larger in the vicinity of steel. The impact of steel on the glass dissolution rate is mainly excluded in the current treatment of the chemical evolution.

Chemical interactions between the engineered barrier system and the host rock are also included in ACED. The pH of the pore waters in bentonite buffers and crystalline pore waters are similar i.e. there can be no alkaline plume. The granitic host rock has only the safety function to isolate the waste. The focus in the current handling of the chemical evolution is therefore on the potential changes within the bentonite buffer by the advective crystalline water flow. The crystalline chemical pore waters compositions in the Czech and Spanish cases are both of sodium bicarbonate types by which there is an inflow of bicarbonate into the bentonite buffer and sulphate and chlorine outflow. The sulphate can originate from the oxidation of trace amounts of pyrite within the bentonite buffer; the pore water chemistry of their granitic rocks is fresh.

All clay host rocks have disposal concepts in which the clay host rocks interfaces with concrete. The alkaline plumes in the clay host rock have been calculated to be limited to 2 to 2.5 meter for poorly indurated clay in the Belgian programme after a period of 100.000 years. The porosity of poorly indurated clay is between 30-35% and the extent of an alkaline plume was calculated to be 0.7 meter after a period of 1 million years in the Spanish programme for such a porous clay. Indurated clay is less porous and the alkaline plume extends to less than 0.1 metre in the Swiss programme. Consequently, the current handling of disposal cells shows that the extent of the chemical interaction is limited to the vicinity of interfaces in a period of 100.000 years or sometimes even 1 million years.

### Cemented ILW

ILW requires shielding during handling and storage. ILW is already disposed in Europe, operational facilities are present in Hungary, Slovenia, Sweden, Finland, France and Spain. Following IAEA convention, a distinction can be made between short lived and long-lived ILW. Disposal of short-lived ILW is usually governed in facilities located at less than 100 metre depth in which the pore water chemistry of the host rock can be changed due to climate change at Earth's surface but the hazard potential of this waste has then reduced significantly. The amount of long-lived radionuclides i.e. radionuclides with a half-life of about 30 years, is limitedly present. This limited amount mainly determines the potential radiological exposure in the long-term period till 100.000 years. For long-lived ILW, disposal depths similar to a disposal depth of HLW are studied in Europe as well as smaller than the HLW disposal depth but always larger than this depth for short-lived ILW.

The chemical processes associated with the interactions at the 6 studied interfaces, except glass-steel, are assumed to be similar for HLW and ILW. The evolution of the pH of the concrete barriers has been studied in-depth e.g. in the Swedish programme since the pH has an impact on the corrosion processes affecting the durability of these barriers and concentration of complexing agents for radionuclides.

Fracture of the concrete barriers may take place when the strain associated with an increasing thickness of corrosion products surrounding the rebars cannot be accommodated by creep of concrete. Passivation layers on steel surfaces can only be present at high pH and anaerobic conditions. Anaerobic conditions within the disposal facility can be assumed some time after closure due to consumption of the encapsulated oxygen by aerobic corrosion of metals, especially structural steel, and insufficient access of oxygen from the environment surrounding the disposal facility. These passivation layers limit also the corrosion rate by which the generated corrosion products can sufficiently be dissipated by diffusion reducing the potential mechanical stresses within concrete. Also, the hydrogen generation rate may be sufficiently small when these passivating layers are present by which damage to these concrete barriers by generation of gas is unlikely.

Metallic ILW can be steel but also Zircaloy, aluminium and zinc. Zircaloy also has a passivation layer at high pH which limits the corrosion rate and the generated hydrogen is picked-up for the formation of zirconium-hydride. These passivation layers are not present at high pH for aluminium and zinc. A waste product with a sufficient quality may not be achieved during waste processing of these metals with cement, especially when the reactive surface area is high. Additives are used to make a passivation layer during waste processing such as  $\text{LiNO}_3$  for processing aluminium to gain cemented waste with a sufficient quality. Other chemical interactions between this processed waste and cementitious material such as grout than between pure metals and grout need to be included in order to determine the chemical evolution of these processed waste types.

The degradation of organic waste results in the formation of complexing organic agents but the degradation rates highly depend on the type of organic waste. A reliable degradation rate has not yet been defined for spent ion exchange resins because the chemical resistance is so high, also in cementitious materials. The formation of organic complexing agents by degradation of these resins does not need to be included in a safety assessment. But cellulose degrades faster at high pH and its degradation is associated with the formation of iso-saccharinic acid, a complexing agent for radionuclides. A high pH and high calcium content reduce the concentration of many of these organic complexing agents limiting the radionuclide exposure when ultrafiltration of these complexes does not take place by the host rock.

Ultrafiltration of these organic agents can be excluded as a retardation mechanism in granitic rocks due to the presence of fractures but this mechanism can be used for clay host rocks provided that the generated gas has not perturbed the clay host rock. Perturbation of the granitic host rock by gas generation as a result of degradation of waste can be excluded due to the presence of these fractures that allows sufficient fast dissipation of gas.

## Table of content

Executive Summary.....	4
Table of content.....	8
List of figures .....	13
List of Tables .....	18
Glossary.....	20
1. Introduction .....	21
1.1 Background.....	21
1.2 Objectives .....	21
1.3 Realization .....	21
1.4 Explanation contents .....	22
2. Features of facilities in crystalline rock and clay .....	23
2.1 Virgin pore water chemistry, mineralogy and porosity.....	23
2.1.1 Clay host rocks .....	23
2.1.2 Crystalline rocks .....	25
2.2 Construction.....	26
2.2.1 Clay host rocks .....	26
2.2.2 Crystalline rocks .....	28
2.3 Operation .....	28
2.4 Rock characteristics at start of the post-closure phase.....	29
3. Bentonite and concrete.....	30
3.1 Bentonite.....	30
3.1.1 Pore water chemistry .....	30
3.1.2 Mineralogy and porosity .....	30
3.2 Concrete .....	31
3.2.1 Pore water chemistry.....	31
3.2.2 Mineralogy and porosity .....	34
4. Disposal cells with vitrified HLW .....	39
4.1 Characterization of disposal cells in granite and clay.....	39
4.1.1 Interface between carbon steel overpack and buffer .....	42
4.1.2 Interface between engineered materials and host rock.....	44
4.2 Calculated chemical interactions and their impact .....	44
4.2.1 Interface between steel overpack and buffer .....	44
4.2.2 Interface between engineered materials and host rock.....	46
5. Disposal cells with cemented ILW .....	49

5.1	Metallic waste .....	50
5.2	Organic waste.....	53
6.	Belgium.....	54
6.1	Characterization of the HLW disposal cell in clay .....	54
6.1.1	Description of materials in disposal cell.....	54
6.1.2	Thermal gradients / Thermal and hydraulic gradients .....	57
6.1.3	Pore water compositions .....	61
6.2	Chemical evolution of the HLW disposal cell .....	62
6.2.1	Narrative .....	62
6.2.2	Conceptual model.....	65
6.2.3	Mathematical model.....	67
6.3	Characterization of an ILW disposal cell in clay .....	68
6.3.1	Description of materials in disposal cell.....	68
6.3.2	Hydraulic gradients .....	69
6.3.3	Pore water compositions .....	70
<b>6.4</b>	<b>Chemical evolution of the ILW disposal cell .....</b>	<b>70</b>
6.4.1	Narrative .....	70
6.4.2	Conceptual model.....	70
7.	Bulgaria.....	71
8.	Czech Republic.....	72
8.1	Characterization of the HLW disposal cell in granite .....	72
8.1.1	Description of materials in disposal cell.....	72
8.1.2	Thermal gradients.....	74
8.1.3	Hydraulic gradients .....	77
8.1.4	Pore water compositions .....	78
8.2	Chemical evolution of the HLW disposal cell .....	80
8.2.1	Narrative .....	80
8.2.2	Conceptual model.....	81
8.2.3	Mathematical model.....	83
8.2.4	Calculated results .....	84
9.	Finland .....	91
9.1	Characterization of an ILW disposal cell in granite .....	91
9.1.1	Description of materials in disposal cell.....	91
9.2	Hydraulic gradients .....	91
9.3	Pore water compositions .....	92
9.4	. Chemical evolution of the ILW disposal cell .....	92

9.4.1	Narrative .....	92
9.4.2	Conceptual model.....	92
9.4.3	Mathematical model.....	93
9.4.4	Calculated results .....	93
10.	France.....	95
10.1	Characterization of the HLW disposal cell in clay .....	95
10.1.1	Description of materials in disposal cell.....	95
10.1.2	Thermal gradients.....	98
10.1.3	Pore water compositions .....	99
10.2	Chemical evolution of the HLW disposal cell .....	101
10.2.1	Narrative .....	101
10.2.2	Conceptual and mathematical model .....	104
10.3	Characterization of an ILW disposal cell in clay .....	105
10.3.1	Description of materials in disposal cell.....	105
10.3.2	Pore water compositions .....	109
10.4	Chemical evolution of the ILW disposal cell .....	111
10.4.1	Narrative .....	111
10.4.2	Conceptual model.....	114
10.4.3	Mathematical model.....	115
11.	Germany.....	116
11.1	Characterization of the HLW disposal cell in crystalline-and clay- rock.....	118
11.1.1	Description of materials in disposal cell.....	118
11.1.2	Thermal and hydraulic gradients .....	120
11.1.3	Pore water compositions .....	120
11.2	Chemical evolution of the HLW disposal cell .....	121
11.2.1	Narrative .....	121
11.2.2	Conceptual model.....	121
11.3	Characterization of an ILW disposal cell .....	121
11.3.1	Description of materials in disposal cell.....	121
11.3.2	Hydraulic gradients .....	122
11.3.3	Pore water compositions .....	122
11.4	Chemical evolution of the ILW disposal cell .....	123
11.4.1	Narrative .....	123
11.4.2	Conceptual model.....	123
12.	Hungary .....	124
13.	Lithuania .....	125

13.1	Characterization of an ILW disposal cell in granite .....	125
13.1.1	Description of materials in disposal cell.....	125
13.1.2	Hydraulic gradients .....	126
13.1.3	Pore water compositions .....	126
13.2	Chemical evolution of the ILW disposal cell .....	126
13.2.1	Narrative .....	126
13.2.2	Conceptual model.....	127
13.2.3	Mathematical model.....	127
14.	Netherlands .....	130
14.1	Characterization of the HLW disposal cell in clay .....	130
14.1.1	Description of materials in disposal cell.....	130
14.1.2	Thermal gradients.....	133
14.1.3	Pore water compositions and porosity.....	137
14.2	Chemical evolution of the HLW disposal cell .....	138
14.2.1	Narrative .....	138
14.2.2	Conceptual model.....	142
14.2.3	Mathematical model.....	143
14.3	Characterization of an ILW disposal cell in clay .....	143
14.3.1	Description of materials in disposal cell.....	143
14.3.2	Pore water compositions .....	144
14.4	Chemical evolution of the ILW disposal cell .....	144
14.4.1	Narrative .....	144
14.4.2	Conceptual model.....	145
14.4.3	Mathematical model.....	145
15.	Romania .....	146
16.	Slovenia .....	147
17.	Spain.....	148
17.1	Characterization of the HLW disposal cell in granite.....	148
17.1.1	Description of materials in disposal cell.....	148
17.1.2	Thermal and hydraulic gradients .....	151
17.1.3	Pore water compositions .....	159
17.2	Chemical evolution of the HLW disposal cell .....	159
17.2.1	Narrative .....	159
17.2.2	Conceptual model.....	160
17.2.3	Mathematical model.....	163
17.2.4	Calculated results .....	163

17.2.5	Recent updates of the predictions of the chemical evolution of the HLW cell in granite	165
17.3	Characterization of the HLW disposal cell in clay .....	167
17.3.1	Description of materials in disposal cell.....	167
17.3.2	Thermal and hydraulic gradients .....	169
17.3.3	Pore water compositions .....	176
17.4	Chemical evolution of the HLW disposal cell .....	177
17.4.1	Narrative .....	177
17.4.2	Conceptual model.....	177
17.4.3	Mathematical model.....	179
17.4.4	Calculated results .....	179
17.4.5	Improvements in the chemical evolution of the HLW cell in clay.....	182
17.5	Characterization of an ILW disposal cell in clay or granite.....	183
18.	Sweden.....	184
18.1	Characterization of the LILW disposal cell in granite .....	184
18.2	Chemical evolution of the ILW disposal cell .....	185
19.	Switzerland .....	186
19.1	Characterization of the HLW disposal cell in clay .....	186
19.2	Chemical evolution of the HLW disposal cell .....	187
19.2.1	Clay-cement interaction .....	187
19.2.2	Steel-bentonite interaction .....	187
20.	United Kingdom .....	188
21.	References .....	189
Appendix A.	Presentation kick-off meeting from Hungary .....	200
Appendix B.	Completed template from Romania.....	204
Appendix C.	Presentation kick-off meeting from Slovenia .....	208
Appendix D.	Mathematical formulation of chemical reactions .....	212
Appendix E.	Completed template from Sweden .....	217
Appendix F.	Completed template from United Kingdom .....	221
Appendix G.	Complete template from Czech Republic.....	228

## List of figures

<i>Figure 1-1: EU countries with power plants in orange; image from website of the European Nuclear Safety Regulators Group (ENSREG).</i> .....	22
<i>Figure 2-1: Evolution of the thermal power of a typical residue UOX: 44000 MWd/tU initial enrichment 3.8% <sup>235</sup>U and mixed with MOX: 45.000 MWd/tU initial enrichment [AREVA, 2007]. Decay of many short-lived radionuclides takes place in the period smaller than 30 years. Their contribution to the thermal power is assumed not be included.</i> .....	39
<i>Figure 2-2: Abstracted disposal cells containing vitrified HLW considered in Europe for the host rocks: granite, poorly indurated clay and indurated clay. Blue = vitrified HLW, black = steel overpack, bentonite (purple) or concrete buffer (grey) surrounds the overpack and grout = light grey.</i> .....	41
<i>Figure 2-3: A conceptual framework for EDZ fracture closure in Opalinus Clay, covering the key phenomena and features from the early post excavation phase until static formation pressure recovery [Alcolea, 2014].</i> .....	<b>Erreur ! Signet non défini.</b>
<i>Figure 2-4: Pourbaix diagrams for the system Fe-H<sub>2</sub>O at 75°C and 22°C with an activity of iron dissolved species of 10<sup>-7</sup>; 0.002 M Cl is a reasonable concentration for tap water. Magnetite (green) is Fe<sub>3</sub>O<sub>4</sub>(s) and Hematite (orange) is Fe<sub>2</sub>O<sub>3</sub>(s).</i> .....	43
<i>Figure 2-5: Evolution of the pH as a function of the distance from the steel overpack at start 100, 1000, 10.000 and 100.000 years.</i> .....	45
<i>Figure 2-6: Cement-bentonite interaction as a coupled linear system [Savage, 2014]</i> .....	48
<i>Figure 3-1: Abstracted disposal cells containing cemented metallic ILW considered in Europe for the host rocks: granite (left) and poorly indurated clay (right). Blue = metallic ILW in tetramoulds left, in CSD-C's right, concrete shielding and support (grey), grout = light grey, washed granitic rock = green.</i> .....	51
<i>Figure 3-2: Pourbaix diagrams at 22°C for the systems Fe-Cr-H<sub>2</sub>O and Al-H<sub>2</sub>O with an activity of iron, chromium and aluminium dissolved species of 10<sup>-7</sup> M; 0.002 M NaCl is a reasonable concentration for tap water. Chromite (green) is FeCrO<sub>4</sub>(s).</i> .....	52
<i>Figure 4-1: Supercontainer type SC-1 for vitrified HLW (left) and indicative figure of a disposal gallery cross-section in Boom clay host rock (right, dimensions not to scale).</i> .....	54
<i>Figure 4-2: Materials and interfaces in a disposal cell for HLW according to the Belgian disposal design. Note that the reference inner diameter for a disposal gallery recently increased from 3.0 m to 3.5 m, which would increase the outer radius to 2.05 instead of 1.8 m [ONDRAF/NIRAS, 2019].</i> .....	55
<i>Figure 4-3: Thermal power evolution of a HLW canister (the figure corresponds to a loading of 1.33 tHM/canister from the reprocessing of spent fuel with a burn-up of 33 GWd/tHM. More details in paragraph 2.1 of [Sillen and Marivoet, 2007].</i> .....	56
<i>Figure 4-4: Model geometry: only half of a supercontainer needs to be modelled for symmetry reasons.</i> .....	57
<i>Figure 4-5: Near field temperature profiles for disposal of vitrified HLW in a supercontainer-based repository (cooling time: 60 years)</i> .....	58
<i>Figure 4-6: Temperature evolution at different interfaces in the near field of a disposal gallery filled with vitrified HLW (cooling time: 60 years).</i> .....	61
<i>Figure 4-7: Main chemical characteristics of concrete (engineered barriers) and clay (host formation) pore waters in a HLW disposal cell</i> .....	62
<i>Figure 4-8: Evolution of pH at the overpack and the stainless steel (SS) envelope as a function of time (X-axis, years); top figures are a zoom of the bottom figures.</i> .....	66

<i>Figure 4-9: pH evolution as function of distance from the concrete – clay interface in the short term (left) and long term (right).</i> .....	67
<i>Figure 4-10: The monolith CB-2 for disposal of compacted waste (left), and cross-section view of a typical CSD-C canister</i> .....	68
<i>Figure 4-11: Materials and interfaces in a disposal cell for ILW according to the Belgian disposal design. Note that the reference inner diameter for a disposal gallery recently increased from 3.0 m to 3.5 m [ONDAF/NIRAS, 2019].</i> .....	68
<i>Figure 6-1: Scheme for disposal of spent fuel in a horizontal layout.</i> .....	73
<i>Figure 6-2: A simplified scheme of disposal cell</i> .....	73
<i>Figure 6-3: Thermal power of canisters with spent fuel assemblies as a function of time</i> .....	74
<i>Figure 6-4: Scheme for calculations of maximal thermal gradients</i> .....	75
<i>Figure 6-5: Temperature at the interface between bentonite and host rock for various sites in the repository in a horizontal layout (SIVB2 – centre of block B2, SIIIB1 – centre of the block 1, O1 edge of block 1, O2 edge of block 2, O3 edge of block 3,.....</i> .....	77
<i>Figure 6-6: Hydraulic head in the depth of a repository with highlighted polygons representing DGR (Milicky, Uhlík et al., 2019).</i> .....	78
<i>Figure 6-7: Geochemical models tested in Czech programme [Červinka et al., 2018].</i> .....	81
<i>Figure 6-8: Domains of 1D and 2D models in the plane of a fracture</i> .....	82
<i>Figure 6-9: 1D model for reactive modelling</i> .....	82
<i>Figure 6-10: 2D model domain</i> .....	83
<i>Figure 6-11: The results of modelling of the change of pH and Eh after the opening of the undisturbed rock</i> .....	84
<i>Figure 6-12: Reference model: Evolution of pH, Eh, iron concentration and precipitated magnetite as a function of the distance from the corrosion cell at 100, 1,000, 10,000 and 100,000 years from the beginning of the simulations</i> .....	87
<i>Figure 6-13: Hydraulic head pressures in the model domain with direction of flow and positions of observation points A and B.</i> .....	88
<i>Figure 6-14: Evolution of pH and pe at observation points A and B for model variant under anoxic conditions.</i> .....	89
<i>Figure 7-1: Conceptual representation of components within the disposal system. (Nummi 2018)</i> .....	91
<i>Figure 7-2: The modelling chain in the performance assessment.(Nurmi 2018)</i> .....	93
<i>Figure 7-3: Leaching depth of concrete barrier due to groundwater.</i> .....	94
<i>Figure 8-1: Image of a HLW vitrified waste primary package</i> .....	95
<i>Figure 8-2: R7-T7 disposal package with at top right, a detailed view of its gripping groove.</i> .....	96
<i>Figure 8-3: Cross section through a HLW1/HLW2 disposal cell: shown here at the end of loading (illustration from end of basic engineering design stage).</i> .....	97
<i>Figure 8-4: Section of a HLW disposal cell with identification of the different materials.</i> .....	97
<i>Figure 8-5: Cigéo underground facility.</i> .....	98
<i>Figure 8-6: Temperature change over time at various points in and around the warmest HLW2 cell (temperature change in the clay rock at the cell wall is given by the yellow curve).</i> .....	99

Figure 8-7: Stages of nuclear glass corrosion and related potential rate-limiting mechanisms (Gin et al., 2013)..... 104

Figure 8-8: Alteration of a glass surface and associated release of radionuclides - (1) sealed container (2) alteration under unsaturated conditions in the vicinity of the glass  $\Rightarrow$  no release (3) as resaturation occurs near the hydrated glass, release of the radionuclides present in the hydrated glass and alteration in  $V_0$  (4) alteration in  $V_R$  - At each moment, until the total resaturation, one part of the glass will alter under unsaturated conditions and another part under saturated conditions thus leading to gradual release of radionuclides..... 105

Figure 8-9: Design Principle ILW-LL cell..... 106

Figure 8-10: Standard section of ILW-LL disposal cell with support and liner. Example of CS1 disposal cells (end of basic engineering design stage). ..... 107

Figure 8-11: Filling of disposal cells with packages type CS5 (at end of basic engineering design).. 107

Figure 8-12: CS4 ILW-LL disposal container with lid secured by screws ..... 108

Figure 8-13: Chronogram of main processes occurring in ILW cells during the operating and the post-closure periods. .... 113

Figure 9-1: Schematic 3D-geological sections (right) of the repository site models for Northern (a) and Southern (b) Germany and simplified geological profiles (left) illustrating the position of the clay layers (Jobmann et al. 2017b)..... 119

Figure 9-2: Schematic of the concepts for borehole disposal and drift emplacement (Jobmann et al. 2017b)..... 120

Figure 11-1: Repository concept ..... 125

Figure 12-1: Materials used in the disposal cell [Verhoef, 2017] ..... 130

Figure 12-2: Evolution of the thermal power of a typical residue UOX: 44000 MWd/tU initial enrichment 3.8%  $^{235}\text{U}$  and mixed with MOX: 45.000 MWd/tU initial enrichment [AREVA, 2007]. Decay of many short-lived radionuclides takes place in the period smaller than 30 years. Their contribution to the thermal power is assumed not be included. .... 132

Figure 12-3: Schematics of CSD-v; dimensions in millimetres [AREVA, 2007]..... 133

Figure 12-4: Geometry for the calculation of the thermal phase with 100 metre thickness of clay and a magnification with the waste (right). Midpoints are calculated with the line in each positive section in order to obtain maxima in calculated temperatures. The images should be turned 90 degrees in order to visualize these geometries in the disposal concept i.e. horizontal emplacement of disposal packages is envisaged..... 134

Figure 12-5: Calculated temperatures at different interfaces after a storage period of 130 years for CSD-v; at midpoints; 2D axi-symmetry with thermal power as supplied by AREVA and cooling period of 130 years. .... 135

Figure 12-6: Pore water compositions and CaO/SiO<sub>2</sub> ratios for concrete used in the disposal cell... 137

Figure 12-7: Salt deposits at joints between concrete segments in HADES URL. Image from EURIDICE website: presentation 01 EURIDICE general. .... 138

Figure 12-8: Diffusional ingress and egress of dissolved species at start of the post-closure phase. 139

Figure 12-9: Diffusion of dissolved species and gas generation (left) and thermodynamic calculation made with Phreeplot and thermochimie database(right)..... 140

Figure 12-10: Diffusion of dissolved species and gas generation at an evolved stage. .... 141

Figure 12-11: Schematics of CSD-c with 6 pucks (compacted drums); dimensions in millimetres [AREVA, 2001] ..... 144

Figure 15-1: Underground installations in the Spanish repository concept in granite (ENRESA, 2001). ..... 148

Figure 15-2: Longitudinal section of a disposal drift in the Spanish repository concept in granite (ENRESA, 2001). ..... 149

Figure 15-3: Dimensions of an individual disposal cell in the Spanish repository concept in granite (ENRESA, 2001). ..... 149

Figure 15-4: Finite element mesh used in the THM numerical model (ENRESA, 2001). ..... 153

Figure 15-5: Calculated saturation degree time evolution in the Spanish repository concept in granite (ENRESA, 2001). ..... 156

Figure 15-6: Calculated temperature time evolution in the Spanish repository concept in granite (ENRESA, 2001). ..... 157

Figure 15-7: Geometry and 1-D axisymmetric mesh used in the first stage of the geochemical model (ENRESA, 2001). ..... 160

Figure 15-8: Temperature boundary conditions at the first stage of the geochemical model (ENRESA, 2001). ..... 161

Figure 15-9: Geometry and 1-D axisymmetric mesh used in the second stage of the geochemical model (ENRESA, 2001). ..... 162

Figure 15-10: Temperature boundary conditions at the second stage of the geochemical model (ENRESA, 2001). ..... 162

Figure 15-11: Time evolution of the calculated calcium, magnesium, sodium and potassium at the middle point in the bentonite (ENRESA, 2001). ..... 164

Figure 15-12: Time evolution of the calculated bicarbonate, chloride and sulphate at the middle point in the bentonite (ENRESA, 2001). ..... 164

Figure 15-13: Time evolution of the calculated pH and pE at the middle point in the bentonite (ENRESA, 2001). ..... 165

Figure 15-14: Underground installations in the Spanish repository concept in clay (ENRESA, 2004). ..... 167

Figure 15-15: Schematic diagram of a disposal drift in the Spanish repository concept in clay (ENRESA, 2004). ..... 168

Figure 15-16: Boundary conditions of the numerical model of the near field (ENRESA, 2004). ..... 171

Figure 15-17: . Calculated saturation degree time evolution in the Spanish repository concept in clay (ENRESA, 2004). ..... 173

Figure 15-18: Calculated temperature time evolution in the Spanish repository concept in clay (ENRESA, 2004). ..... 174

Figure 15-19: Dimensions and 1-D axisymmetric mesh used in the first stage of the geochemical model (ENRESA, 2004). ..... 177

Figure 15-20: Temperature boundary conditions at the first stage of the geochemical model (ENRESA, 2004). ..... 178

Figure 15-21: Dimensions and 1-D axisymmetric mesh used in the second stage of the geochemical model (ENRESA, 2004). ..... 178

Figure 15-22: Temperature boundary conditions at the second stage of the geochemical model (ENRESA, 2004). ..... 179

Figure 15-23: Spatial distribution of the calculated calcium, magnesium, sodium, potassium, chloride, bicarbonate, sulphate and silica once bentonite is fully saturated (ENRESA, 2004). ..... 180

Figure 15-24: Spatial distribution of the calculated pH once bentonite is fully saturated (ENRESA, 2004). ..... 180

Figure 15-25: Spatial distribution of the calculated pH at different times (ENRESA, 2004). ..... 181

Figure 15-26: Time evolution of the calculated calcium, magnesium, sodium, potassium, chloride, bicarbonate, sulphate and silica at a point located at the middle of bentonite (ENRESA, 2004). ..... 182

Figure 16-16-1: Disposal cell containing ILW operating (left, 1BMA) and considered in Sweden (right, 2BMA) in the host rock granite, adapted from SKB's report [SKB, 2014a]. Blue = cemented ILW and steel ILW, black = steel sacrificial stirrer, rebar or walls tetramoulds, crushed rock (green), air (white), shotcrete = light grey. A constraining wall of concrete is casted to prevent crushed rock entering the access tunnels. A concrete plug and bentonite seals are fabricated against the constraining wall. ... 185

Figure 17-1: Disposal cell containing vitrified HLW considered in Switzerland for the host rock indurated clay. Grey = vitrified HLW, black = steel overpack, bentonite (purple) surrounds the overpack and cementitious liner = light grey. .... 186

## List of Tables

<i>Table 4-1: Characteristics and role of the components in a disposal cell for HLW according to the Belgian disposal design and safety concept. Information taken from [ONDRAF/NIRAS 2017a,b, von Lensa et al. 2008].</i>	55
<i>Table 4-2: Description of parameters for thermal gradients</i>	59
<i>Table 4-3: Characteristics and role of the components in a disposal cell for ILW according to the Belgian disposal design and safety concept. Information taken from [ONDRAF/NIRAS 2017bc, von Lensa et al 2008].</i>	69
<i>Table 6-1: The change of maximal temperature at the surface of canisters on the change of thermal conductivity of compacted bentonite</i>	74
<i>Table 6-2: Description of parameters for thermal gradients</i>	76
<i>Table 6-3: Initial physico-chemical parameters and chemical composition of different types of waters which were used for geochemical modelling</i>	80
<i>Table 6-4: Parameters of the geochemical porewater model for the bentonite</i>	86
<i>Table 8-1: Number of packages per disposal cell and distance between cells for disposal of highly exothermic HLW approximately 100m long</i>	99
<i>Table 8-2: Example of mineralogical composition of the Callovo-Oxfordian claystone and molar volumes of the different minerals and secondary minerals (Marty et al. 2014a)</i>	100
<i>Table 8-3: Example of exchangers composition of the Callovo-Oxfordian claystone (Idiart &amp; Laviña; 2019)</i>	100
<i>Table 8-4: Example of water composition of the Callovo-Oxfordian claystone (Marty et al. 2014a)</i>	100
<i>Table 8-5: Simplified mineralogical composition of concrete CEM I considering amorphous "CSH 1,6" (the high proportion of calcite is related to the nature of the aggregate incorporated in the concrete).</i>	110
<i>Table 8-6: Simplified mineralogical composition of concrete CEM V considering amorphous "CSH 1,6" (the high proportion of calcite is related to the nature of the aggregate incorporated in the concrete).</i>	110
<i>Table 8-7: Examples of water composition of CEM I and CEM V cement modelled with ThermoChimie</i>	111
<i>Table 9-1: Prediction of the amounts of waste expected from reprocessing that will have to be disposed of in the Federal Republic of Germany (BMUB, 2015a)</i>	117
<i>Table 9-2: Waste containers permitted for the Konrad repository (BfS, 2014).</i>	122
<i>Table 9-3: Mine water composition (Brewitz, 1982 and Tittel et al., 1986)</i>	122
<i>Table 9-4: Element specific time for radionuclide mobilisation form the waste.</i>	123
<i>Table 9-5: Solubility limits used for the near field within the permitting process for Konrad.</i>	123
<i>Table 11-1: Groundwater composition [Vaitkeviciene, 2017]</i>	127
<i>Table 11-2: MX-80 data [Ochs, 2004]</i>	128
<i>Table 11-3: Data for chemical reactions</i>	128
<i>Table 12-1: Dimensions for the supercontainer for CSD-v</i>	131
<i>Table 12-2: Description of parameters for thermal gradients</i>	136

<i>Table 12-3: Pore water compositions at start of the post-closure phase</i> .....	137
<i>Table 15-1: Bentonite parameters used in the THM numerical model (ENRESA, 2001)</i> .....	154
<i>Table 15-2: Description of parameters for thermal gradients</i> .....	158
<i>Table 15-3: Initial chemical composition of the bentonite porewater and the granite hydration water (ENRESA, 2001).</i> .....	159
<i>Table 15-4: Initial mineral volume fraction in the bentonite (ENRESA, 2001)</i> .....	159
<i>Table 15-5: Calculated chemical composition of the bentonite porewater after saturation (ENRESA, 2001)</i> .....	163
<i>Table 15-6: Main parameter considered in the THM model of the Spanish reference concept in clay (ENRESA, 2004).</i> .....	172
<i>Table 15-7: Mechanical parameters of the cansiter, bentonite and clay of the Spanish reference concept in clay (ENRESA, 2004).</i> .....	172
<i>Table 15-8: Description of parameters for thermal gradients</i> .....	175
<i>Table 15-9: Initial chemical composition (mol/L) of the bentonite porewater, the concrete water and the clay porewater at 25 °C (ENRESA, 2004).</i> .....	176
<i>Table 15-10: Initial mineral volumen fraction in the bentonite, the concrete and the clay (ENRESA, 2004)</i> .....	176

## Glossary

BWR	Boiling Water Reactor
CP	Corrosion Product
CSD-V	Conteneur Standard de Déchets Vitrifiés'
CSD-C	Conteneur Standard de Déchets Compactés
CSH	calcium silicate hydrate
DGR	Deep Geological Repository
DSSC	Disposal System Safety Case
EBS	Engineered Barrier System
EDZ	Excavation Damaged Zone
ENSREG	European Nuclear Safety Regulators Group
GDF	Geological Disposal Facility
HLW	High level waste
HM	Heavy Metal
ILW	Intermediate Level Waste
ISA	Iso-saccharinic acid
KBS-3	kärnbränslesäkerhet (Swedish nuclear fuel safety) version 3
LILW-LL	Low and Intermediate level waste – Long Lived
LWR	Light Water Reactor
MOX	uranium/plutonium mixed oxide
MSA	Monosulphoaluminate
MTR	Materials Testing Reactor
NPP	Nuclear Power Plant
NRVB	Nirex Reference Vault Backfill
OPC	Ordinary Portland Cement
PEHD	PolyEthylene High Density
SC	Supercontainer
SCC	Supercontainer concrete
SGW	Synthetic granite groundwater
SFR	Slutförvaret för kortlivat radioaktivt avfall; disposal facility for short lived LILW in Sweden
SNF	Spent Nuclear Fuel
TDS	Total Dissolved Solutes
URF	Underground Research Facility
URL	Underground Research Laboratory
WMO	Waste Management Organisation

## 1. Introduction

### 1.1 Background

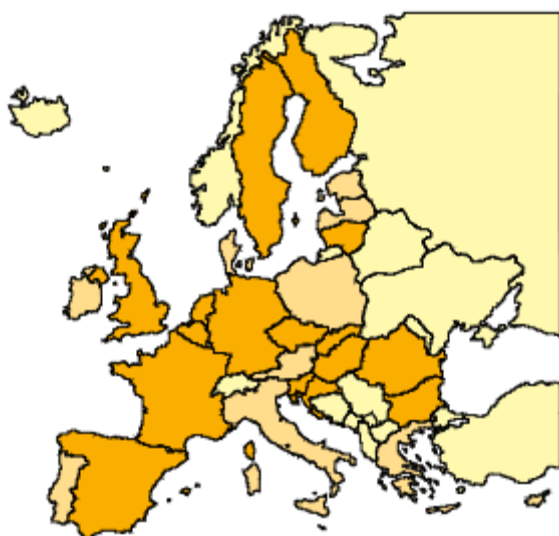
Waste management organisations prepare safety reports or safety cases to show how and why disposal of waste is to be safely performed. The backbone of a safety case is a safety assessment. This assessment quantifies the containment behaviour of natural and engineered barriers to calculate potential releases of radionuclides from the waste into the accessible human environment and the resulting radiation exposures which are then compared with a yardstick e.g., a dose constraint. The information needed to quantify the behaviour of the barriers is varied and is subject to different types and levels of uncertainty. A balanced view between realism (somewhere close to the expected behaviour) and showing robustly and simply that the system is safe, even with in-built conservatism is necessary to make informed decisions on design optimisation and, eventually, on acceptable site characteristics. ACED is seeking which geochemical processes need to be included for representative assessments of the chemical evolution. The investigated geological disposal facilities are hosted in either crystalline or sedimentary rock types. Disposal cells containing vitrified HLW and cemented ILW are considered in this EURAD Work Package.

### 1.2 Objectives

There may be current European practices why the chemical evolutions for disposal are included and how the chemical evolutions at disposal cell scale have been treated. A collection of the conceptualisations of the chemical evolutions and which parts have been modelled in Europe shows the already conducted work and could prevent duplication of work. The aim of this report is to describe the current handling of the chemical evolutions of disposal cells in national programmes. Every geological disposal facility is unique but there are many similarities between disposal cells and an attempt has been made to integrate the collected country contributions into three disposal cells for GDFs hosted in crystalline rock, indurated clay and poorly indurated clay. Also a disposal cell with a different approach to other national programmes, from France, has been included. These descriptions of chemical evolutions involving interacting materials and how these are derived from scientific bases serves as input for the desk-top studies in the initial State-of the Art (SOTA), Deliverable 2.1. Deliverable 2.5: Experiments and numerical model studies on interfaces is also a contribution to this initial SOTA.

### 1.3 Realization

Characteristics of disposal cells from eleven national programmes have been presented at the ACED kick-off meeting held in July 2019, 10 EU countries and Switzerland. The expected contributions from ACED was also collected in order to get a grasp of potential end-user aspects. Organisations from eight of these countries have been given one month to describe the characteristics of the disposal cells considered in their national programmes and chemical evolutions of these disposal cells. Four of these countries do not need to dispose vitrified HLW but spent nuclear power fuel. An agreement was made on the table of contents for each country contribution at the kick-off meeting; aspects of disposal of spent fuel that are of interest to ACED is the heat generation by spent fuel and the temperature evolution at one of the following six interfaces: glass-steel, cementitious material-granite, cementitious material-clay, steel or iron-bentonite, steel or iron-cementitious material and steel or iron-granite and the associated chemical interactions. A one page description is made of presentations that have given permission to be used in this deliverable; the presentation can be found in the Appendix. But there are more than 11 EU countries that need to deal with disposal of radioactive waste. *Figure 1-1* shows that there are 16 EU countries with nuclear power plants.



FusionCharts XT Trial

Figure 1-1: EU countries with power plants in orange; image from website of the European Nuclear Safety Regulators Group (ENSREG).

Contacts for the missing 6 EU countries have been found from the list of the EURAD General Assembly, except for Croatia because there is no Croatian organisation taking part in EURAD. Waste Management Organisations usually coordinate research programmes and write the safety cases and therefore preferably WMOs from these other countries have been asked to complete a template in which details were asked, specifically references for the materials in the disposal cell, a narrative of the post-closure phase, conceptual and mathematical model for the disposal cell. A one or two-page document has been made from the completed template and reading the references; the completed templates can also be found in the Appendix.

## 1.4 Explanation contents

The integration of the collected country contributions into disposal cells for GDFs hosted in crystalline rock, indurated clay and poorly indurated clay is shown in the chapter 2, 3, 4 and 5. These chapters are followed by the current handling of the chemical evolution in each country that provided contributions.

## 2. Features of facilities in crystalline rock and clay

Disposal cells in ACED treat the chemical evolution from the waste form until the host rock. The chemical alteration of the host rock due to climate change is not considered in ACED. Vitrified HLW and long-lived ILW are disposed at such large depth that climate changes foreseen in the next 100.000 years have a negligible impact on the chemistry of the host rocks. The geochemical evolution of engineered materials can be highly influenced by the properties of the host rock. The properties of the host rock in the vicinity of the engineered materials changes during excavation of the host rock and may change during the operation of the facility. This Chapter describes the characteristics of crystalline rocks and clay rocks that have been and can be used as input of the host rock to model the chemical evolution of facilities containing waste in these host rocks as well as the extent of changes in these properties by constructing and operating the facility for the chemical evolution in the post-closure phase.

### 2.1 Virgin pore water chemistry, mineralogy and porosity

The chemical gradients in pore water compositions between engineered porous material and host rocks are usually the driving forces for the chemical evolution. The following two paragraphs show the chemical characteristics of clay and crystalline host rocks. As much as possible, primary references of the published pore water chemistries, porosity and mineralogy have been used.

#### 2.1.1 Clay host rocks

Measured pore water compositions for clay host rocks are influenced by experimental artefacts e.g. [De Craen, 2004], [Gaucher, 2009]:

- the partial pressure of CO<sub>2</sub> is larger at depth of the disposal facility and degassing of CO<sub>2</sub> takes place when the samples are taken. This degassing has an impact on the measured bicarbonate (HCO<sub>3</sub><sup>-</sup>) content and pH in the pore water composition;
- redox potentials cannot be measured with a sufficient accuracy and therefore these potentials are usually calculated from a thermodynamic equilibrium;
- the clay host rock in the deep underground has usually been depleted in oxygen for millions of years. Pieces of host rock can be sensitive to the oxidized conditions above ground e.g. pyrite (FeS<sub>2</sub>) can be oxidized and this oxidizing reaction acidifies the sample with which a too high concentration of sulphate (SO<sub>4</sub><sup>2-</sup>) and cation concentrations are measured as a result of dissolution of carbonates. The carbonates buffer the pH.

Data of clay core samples e.g. obtained by mechanical squeezing or aqueous leaching can be used as input for the thermodynamic modelling. These chemistries for poorly indurated clay i.e. Boom Clay in Belgium [De Craen, 2004] and Netherlands [Griffioen, 2017], indurated clay i.e. Callovo-Oxfordian clay [Gaucher, 2006/2009], the reference host rock in France and Opalinus Clay [Mäder, 2009], the reference host rock in Switzerland, are shown in the next table.

Table 2-1: Modelled pore water chemistries in clay host rocks

Parameter	Unit	Belgian	Dutch	French	Swiss (reference)	Swiss (sea case)
Temperature	°C	16	26	25	25 <sup>1</sup>	25
pH	-log(H <sup>+</sup> )	8.5	6.9	7.28	7.203	7.009
pe	-log(e <sup>-</sup> )	-4.7	-2.8	-2.64	-2.781	-2.563
pCO <sub>2</sub>	log(bar)	-2.62	-1.5	-1.96	-2.2	-2.5
Na <sup>+</sup>	mmol/kg	15.6	460.9	32.1	164.4	527.5
K <sup>+</sup>	mmol/kg	0.2	9.8	7.10	2.604	1.77
Ca <sup>2+</sup>	mmol/kg	0.05	13.2	15.0	12.51	49.71
Mg <sup>2+</sup>	mmol/kg	0.06	56.1	14.2	9.625	37.55
Sr <sup>2+</sup>	mmol/kg			1.12	0.2106	0.422
Fe <sup>2+</sup>	mmol/kg	0.003	0.0000031	0.332	0.0524	0.246
Al <sup>3+</sup>	mmol/kg	0.000024	0.000033	0.00000695		
SiO <sub>2</sub> (aq)	mmol/kg	0.1	0.3	0.0940	0.1779	0.172
Cl <sup>-</sup>	mmol/kg	0.7	541.0	30.1	160.0	662.0
SO <sub>4</sub> <sup>2-</sup>	mmol/kg	0.02	28.4	33.9	24.72	21.06
HCO <sub>3</sub> <sup>-</sup>	mmol/kg	14.4	7.2	2.78	2.043	0.631

The concentration of all cations can depend on the measured occupancy and selectivity of the clay minerals but the limiting concentration for the cations Ca<sup>2+</sup>, Mg<sup>2+</sup>, Fe<sup>2+</sup> and Sr<sup>2+</sup> can also be the formation of carbonates i.e. calcite (CaCO<sub>3</sub>), dolomite (CaMg(CO<sub>3</sub>)<sub>2</sub>), siderite (FeCO<sub>3</sub>) and strontianite (SrCO<sub>3</sub>). The aluminium concentration is limited by the dissolution products of clay minerals e.g. kaolinite or chlorite [Mäder, 2009] and the dissolved SiO<sub>2</sub> content by the quartz or chalcedony [De Craen, 2004] solubility. The partial pressure of CO<sub>2</sub> determines the bicarbonate concentration and can be controlled by a mineral assemblage [Mäder, 2009], [Wang, 2010]. The chlorine, Cl<sup>-</sup>, and sulphate, SO<sub>4</sub><sup>2-</sup>, concentrations can be fixed in the modelling but celestite (SrSO<sub>4</sub>) may control the sulphate concentration [Gaucher, 2009], [Mäder, 2009]. Traces of sulphide are also present in clay pore water due to presence of pyrite in the clay mineralogy. The presence of pyrite is the clear indication that clay formations have reducing conditions and pyrite can be used in the modelling to determine the redox potential.

The mineralogy of the clay host rocks for poorly indurated clay i.e. Boom Clay in Belgium (Mol) [Honty, 2012] and Netherlands [Griffioen, 2017]. indurated clay i.e. Callovo-Oxfordian clay (Bure) [Wenk, 2008], the reference host rock in France and Opalinus Clay [Traber, 2013], the reference host rock in Switzerland are shown in the next table. The porosities of the virgin host rock are 36-40 vol% for Boom Clay in Belgium at HADES at 223 metres depth (Mol) [De Craen 2004], 31-35 vol% for Boom Clay in the Netherlands at around 500 metres depth [Verweij, 2016] 17 vol% for Callovo-Oxfordian clay [Gaucher, 2009] and 15 vol% for Opalinus Clay [Alcolea, 2014].

<sup>1</sup> The pore water chemistries have been calculated at 25°C since the temperature dependency of a lot of phases are unknown. The deviation is also expected to be sufficiently small if the temperature is within a range of 10 K from 25°C [Mäder, 2009].

Table 2-2: Average or reference mineralogical compositions of clay host rocks in wt%

Mineral	Chemical formula	Belgian	Dutch	French	Swiss
Muscovite	$KAl_2(AlSi_3O_{10})(F,OH)_2$				
Illite/Muscovite		18.8			
Illite	$K^aAl^b_3Si^c_3O_{10}(OH)_2$		10.9	33.9	24
Ill/Sm mixed layer		21.8		1.9	9
Smectite <sup>montmorillonite</sup>	$(Na,Ca)_{0.33}(Al,Mg)_2(Si_4O_{10})(OH)_2 \cdot nH_2O$		25.4		
Kaolinite	$Al_2Si_5O_5(OH)_4$	7.4	4.1	3.3	18
Chlorite	$(Mg,Fe)_3(Si,Al)_4O_{10}(OH)_2 \cdot (Mg,Fe)_3(OH)_6$	2.2	1.1	3.8	9
Chl/Sm mixed layer					0
Clinoptilolite/ Heulandite	$((Na,K,Ca)_{4-6}Al_6Si_{30}O_{72} \cdot 24H_2O / ((Na,Ca)_{4-6}Al_6Si_{30}O_{72} \cdot 24H_2O$		0.6		
Quartz	$SiO_2$	38.9	42.0	24.0	20
Calcite	$CaCO_3$	0.6	5.3	24.3	13
K-feldspar	$KAlSi_3O_8$	4.8	6.7		2
Albite	$NaAlSi_3O_8$	2.0	2.4		
Plagioclase	from $NaAlSi_3O_8$ till $CaAl_2Si_2O_8$			3.9	0.9
Anorthite	$CaAl_2Si_2O_8$				
Dolomite/ankerite	$CaMg(CO_3)_2$	0.3		3.5	0.4
Siderite	$FeCO_3$	0.1			4
Pyrite	$FeS_2$	2.1	1.4	1.4	1
Apatite	$Ca_5(PO_4)_3(F,Cl,OH)$	0.2			

<sup>a</sup> can also be H<sub>3</sub>O, <sup>b</sup> can also be Mg or Fe, can also be Al

## 2.1.2 Crystalline rocks

The water flowing in a borehole through fractures can be measured in granitic rocks. Pumping rates are adjusted in order to obtain the representative groundwater samples. There were not always modelled pore water chemistries available for granitic rocks, the redox conditions may be controlled by microbial activity and the groundwater composition may be also determined by mixing of ground waters in these host rocks i.e. thermodynamic modelling may not always result in representative pore water chemistries. The measured and modelled pore water chemistries in granitic host rocks pore water chemistries for granitic rocks in Czech [Červinka, 2018] in Spain [ENRESA, 2001], in Sweden [SKB, 2005] [Aukué, 2006] and in Finland [Pitkänen, 1996] with a temperature between 10-11°C around a depth of 400 metre [Sedighi, 2014] are shown in the next table.

Table 2-3: Modelled and measured pore water chemistries in granitic host rocks

Parameter	Unit	Czech (600 m)	Czech (1000 m)	Spanish	Swedish (512 m)	Finnish (446.0-558.5 m)
Temperature	°C	25	25	30	11.35	11
pH	-log(H <sup>+</sup> )	8.2	9.4	7.9	7.2	7.9
pe	-log(e <sup>-</sup> )	+4.00	+4.00	-2.907	-2.54	-4.33
Na <sup>+</sup>	mmol/kg	0.865	3.81	4.350	89	122
K <sup>+</sup>	mmol/kg	0.0537	0.0179	0.05371	0.9	0.35
Ca <sup>2+</sup>	mmol/kg	0.864	0.0324	0.1522	23	41.2
Mg <sup>2+</sup>	mmol/kg	0.342	0.00412	0.1604	9.3	2.35
Sr <sup>2+</sup>	mmol/kg					0.171
Fe <sup>2+</sup>	mmol/kg	0.00179	0.00179	0.8953	0.033	0.00013
Al <sup>3+</sup>	mmol/kg	0.00371	0.00371			0.002
SiO <sub>2</sub> (aq)	mmol/kg	0.520	0.481	0.3761		0.072
Cl <sup>-</sup>	mmol/kg	0.0931	0.528	0.3949	153	214
SO <sub>4</sub> <sup>2-</sup>	mmol/kg	0.219	0.109	0.01561	5.2	0.114
HCO <sub>3</sub> <sup>-</sup>	mmol/kg	2.77	2.68	5.048	2.2	

The following table shows the mineralogy's of granitic host rocks for granite in Czech Republic with the main mineral components quartz, feldspars, mica and amphibole [Vondrovic, 2015], El Berrocal granite in Spain [Siitari-Kauppi, 2007], granite (to granodiorite) at Forsmark with an average porosity of 0.43 vol% [Drake, 2006] and migmatitic gneiss, the dominant rock type at Olkiluoto in Finland [Kärki, 2006]. But, the mineralogy in granitic rocks may not be as relevant as the mineralogy of the fracture fillings for the pore water chemistry in granitic rocks. The granitic rock is practically impervious due to its porosities of less than 1 vol%; transport of dissolved species mainly takes place through fractures. Precipitation of calcite, chlorite and clay minerals can be fracture fillings [Drake, 2006].

Table 2-4 Average mineralogical compositions of granitic host rocks in vol%.

Mineral	Chemical formula	Czech	Spanish	Swedish	Finnish
Quartz	SiO <sub>2</sub>	+	40	35.6	30.3
Plagioclase	from NaAlSi <sub>3</sub> O <sub>8</sub> till CaAl <sub>2</sub> Si <sub>2</sub> O <sub>8</sub>	+	30	35.6	17.0
K-feldspar	KAlSi <sub>3</sub> O <sub>8</sub>	+	20	22.5	8.6
Biotite	K(Mg,Fe) <sub>3</sub> AlSi <sub>3</sub> O <sub>10</sub> (OH) <sub>2</sub>	+	+	5.1	22.7
Muscovite	KAl <sub>2</sub> (Si <sub>3</sub> Al)O <sub>10</sub> (OH,F) <sub>2</sub>	+	+		0.9
Hornblende	Ca <sub>2</sub> (Mg,Fe,Al) <sub>5</sub> (Al,Si) <sub>8</sub> O <sub>22</sub> •(OH) <sub>2</sub>				0.1
Chlorite	(Mg,Fe) <sub>3</sub> (Si,Al) <sub>4</sub> O <sub>10</sub> (OH) <sub>2</sub> •(Mg,Fe) <sub>3</sub> (OH) <sub>6</sub>	+	+	0.2	2.6
Corderite	Mg <sub>2</sub> Al <sub>4</sub> Si <sub>5</sub> O <sub>18</sub>				4.0
Pinite	Muscovite and clay minerals				5.9
Sillimanite	Al <sub>2</sub> SiO <sub>5</sub>				1.8
Epidote	Ca <sub>2</sub> Al <sub>2</sub> Fe(SiO <sub>4</sub> )(Si <sub>2</sub> O <sub>7</sub> )(O,OH) <sub>2</sub>			0.6	0.0
Apatite	Ca <sub>5</sub> (PO <sub>4</sub> ) <sub>3</sub> (F,Cl,OH)				0.1
Saussurite	Mixture with epidote and feldspars				3.7
Sericite	Usually muscovite, illite or paragonite with small crystals				0.8
Opagues	Mainly magnetite Fe <sub>3</sub> O <sub>4</sub> and small content of FeS <sub>2</sub>			0.3	1.0
Titianite / sphene	CaTiSiO <sub>5</sub>			0.2	0.1
Allanite	(Ca,Mn,Ce,La,Y,Th) <sub>2</sub> (Fe,Ti)(Al,Fe) <sub>2</sub> O•OH [Si <sub>2</sub> O <sub>7</sub> ][SiO <sub>4</sub> ]			0.3	

## 2.2 Construction

The construction of the disposal facility requires excavation of the rock. The excavation technique and excavation diameter determines the extent of fractures that have been generated in host rocks. The disposal galleries to emplace HLW packages are usually smaller in diameter than the disposal galleries to emplace packages containing ILW and the excavation procedure can be different. The outcome of both features is that the Excavation Damaged Zone (EDZ) is smaller for galleries to dispose HLW than for galleries to dipose ILW. Bolts for mechanical support need to be used for ILW disposal cells in indurated clay as well as crystalline rocks. The change in properties of the host rock by construction in the vicinity of the engineered barrier sytem can be relevant for the chemical evolution at disposal cell scale.

### 2.2.1 Clay host rocks

Fractures in the surrounding of a gallery are made during excavation of clay host rocks but the water flow through these fractures diminishes as a function of time. The characterisation of the EDZ in clay host rocks has been investigated in the 5<sup>th</sup> framework programme SELFRAC [Bernier, 2007]. Poorly indurated clays have a high self-healing capacity due to their high content of swelling clay minerals such as smectite of which montmorillonite is the most famous species. The occurrence of swelling clay minerals is limited in indurated clays [Mazurek, 2011] (see also

Table 2-2) and those clays exhibit only self-sealing of fractures i.e. self-sealed fractures are preferential pathways for new fracturing. Three fracture zones can be distinguished: a zone with interconnected fractures, a zone with discrete fractures that are not interconnected and a zone without macroscopic fractures but a slightly higher permeability than the virgin permeability of the host rock. The zone with interconnected fractures is the EDZ [Bock, 2010].

The driving forces for the closure of the generated fractures are compressive load or confining pressure and access to water. The closure of fractures can be measured as the increase in pore water pressure. The conceptual understanding has been provided in the Swiss programme [Alcolea, 2014] in which water suction towards the generated fractures occurs; these fractures have an atmospheric pressure ( $P_{atm}$ ) immediately after excavation. Equilibrium has been achieved when the formation pressure ( $P_{fmt}$ ) is achieved.

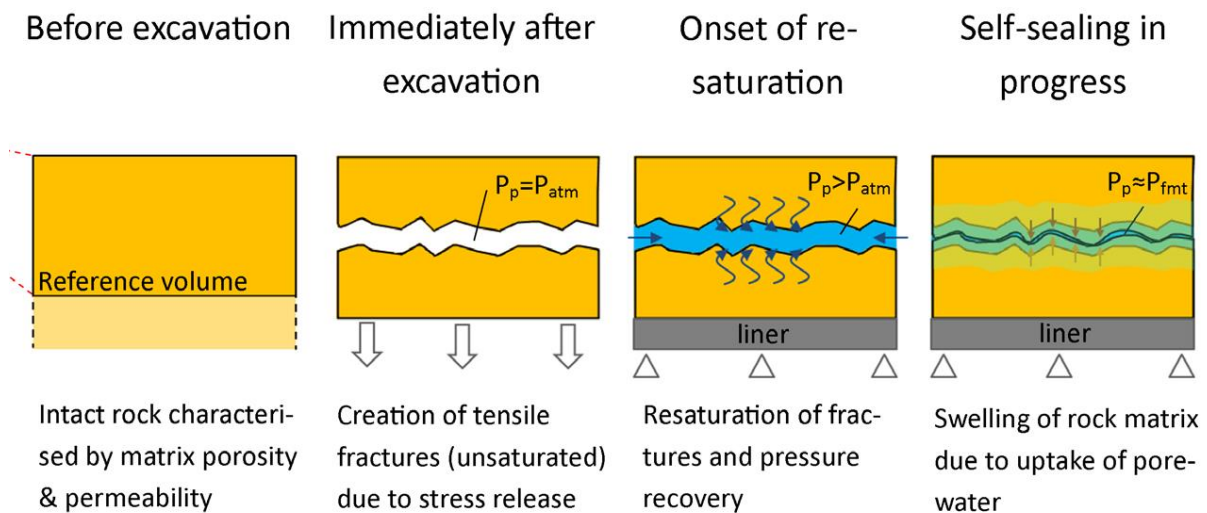


Figure 2-1: A conceptual framework for EDZ fracture closure in Opalinus Clay, covering the key phenomena and features from the early post excavation phase until static formation pressure recovery [Alcolea, 2014].

For modelling the chemical evolution of the disposal cell, the EDZ can be characterised as a zone with a larger porosity and permeability than the virgin host rock and can be abstracted from the fracture pattern; the heterogeneous distribution of hydraulic properties is then averaged by integration of the axial flux around the tunnel. The values for hydraulic conductivity or permeability are largest near the interface between concrete and clay. These values asymptotically reduce as a function of the radial distance till the values measured for the virgin host rock after about 6 metres from this interface. For indurated clay such as Opalinus Clay, the measured local transmissivities as a representation for the hydraulic properties were from a maximum distance of the gallery wall of 1.25 metre and characterized as the EDZ:  $10^{-10}$  to  $5 \times 10^{-7}$  m<sup>2</sup>/s while the measured range was  $5 \times 10^{-13}$  to  $10^{-12}$  m<sup>2</sup>/s at a distance of the gallery wall between 2.00 and 4.00 metre [Bock, 2010]. In-situ permeability measurements show that the permeability is increased by several (up to 6 or 7) orders of magnitude within 20 to 40 cm from the tunnel wall. The hydraulic conductivity for virgin indurated clay such as Opalinus clay is  $4.4 \times 10^{-14}$  m/s [Alcolea, 2014].

Larger hydraulic conductivities are measured for virgin poorly indurated clay e.g. the geometric mean of the vertical hydraulic conductivity over the thickness of the Boom Clay in Mol is  $1.7 \times 10^{-12}$  m/s [NIROND, 2013] and specifically near the HADES facility about  $6 \times 10^{-12}$  m/s and the self-healing process for poorly indurated clay can be fast e.g. the connecting gallery in HADES (Mol) with an external diameter of 4.6 metre showed an EDZ of 1 metre after excavation that diminished to less than 60 cm after 2 years [Bernier, 2007]. The research in HADES also provided experimental evidence that the fracture extent

depends on the excavation technique and excavated diameter. In poorly indurated clay, the connecting gallery was constructed with a larger overcut than the PRACLAY gallery [NIRONDA, 2013] i.e. diminishing the necessary stress release. The PRACLAY gallery has an external diameter of 2.5 metre. The measured hydraulic properties near the interface between concrete and clay has been measured to be similar to these properties measured further away from this interface [Dizier, 2017]. A larger hydraulic conductivity has been measured for clay near the concrete liner for the larger gallery of 4.6 metre i.e. less than a factor of 3 at less than 1.5 metres from the interface between concrete and clay i.e. outside the interconnected fracture zone, after a few months and less than a factor of 2 after 8 years [Bernier, 2007; NIRONDA 2013].

All clay host rocks considered for geological disposal have reached reducing chemical conditions by which sulphide-minerals are present e.g. pyrite. The excavation may result in sufficient access of oxygen to these minerals and the oxidation reaction releases acid. Grouts are sprayed on indurated clay surfaces after excavation of the indurated clay rocks. The grout is injected to neutralise the potential acidity in the French disposal design. The Swiss disposal design and procedures are different and the Swiss research results indicate that only 1% of the pyrite originally present in the EDZ will be altered for a HLW disposal gallery i.e. the long term impact will be insignificant in their disposal design. This bounding is based on field studies of tunnels open for a few years in an Underground Research Lab in Switzerland (Mont Terri) and a traffic tunnel open for more than 100 years [Leupin, 2016a]. The cementitious liner in the Swiss disposal design has a mechanical support function during construction and operation. Abstractions of both disposal designs are presented in Chapter 4.

Direct emplacement of hardened concrete segments is necessary against the convergence of poorly indurated clay and this procedure also limits the further oxidation of clay. The oxidation induced by construction is believed to be limited to a zone of about 1 meter around the disposal galleries in the Belgian programme.

The ILW disposal cells are lined with concrete in-situ for indurated clay sometime after excavation; bolts made of injected resins may be needed for indurated clay host rock before the liner is casted as shown in the French disposal design. Bolts, also called anchors, are also used in Slovenia for constructing a silo. Also for ILW disposal cells, hardened concrete segments are directly emplaced after excavating poorly indurated clay. .

### 2.2.2 Crystalline rocks

Crystalline rock specific excavation procedures have been defined in Finland and Sweden to make galleries to dispose HLW with an acceptable limited water inflow through fractures to emplace the engineered material bentonite [e.g. Baxter, 2018]. The water flow from the host rock into the disposal cells needs also to be limited for the post-closure phase to limit ingress of species from shallow and deep ground water [Vieno, 2003]. Excavation of rock to construct disposal galleries for short-lived ILW can be drilling and blasting. Rock support are bolts and shotcrete; the density of applied bolts as well as non-reinforced or or reinforced shotcrete is determined by the fracture extent of the rock [e.g. Carlsson, 2007].

## 2.3 Operation

The constructed disposal galleries within clay host rocks are kept dry by ventilation. The porosity and permeability of the concrete liner used for indurated clay host rocks is larger than the (virgin) porosity and permeability of the clay host rock. Some drying of the indurated clay host rock takes place in the operational phase leading potentially to shrinkage cracks.

The porosity and permeability of the concrete segments in the liner used for poorly indurated clay host rocks is smaller than the (virgin) porosity and permeability of poorly indurated clay. Salt deposits become visible at the joints between concrete segments. These deposits arise due to clay pore water flowing into the disposal gallery and interacting with air, concrete segments and evaporation. The small inflow of poorly indurated clay pore water at the joints between the concrete segments is evaporated by ventilation i.e. pumping of water out of facility within the clay host rock is not necessary.

Pumps need to be used to keep the disposal facility in crystalline rock dry. The main inflow of water into this facility are the access tunnels, not the disposal galleries [Carlsson, 2007] [SKB, 2015].

All the chemical changes by the clay host rock induced by the oxygen in the ventilation air is similar to the earlier processes described for construction and paragraph 2.1.1.

## 2.4 Rock characteristics at start of the post-closure phase

The processes previously described for the construction and operation of the disposal facility can have an impact on the characteristics of the host rock for the chemical evolution of the disposal cell in the post-closure phase.

The indurated clay in the vicinity of the disposal section of the facility has been dried in the operational phase. The start of the post-closure phase is characterised with resaturation, the period in time to achieve the formation water pressure has been estimated to be 10.000 years in the French contribution for ILW disposal cells. The limited access of water for indurated clays in the construction and operational phase makes that the self-sealing process of these clays in the vicinity of the engineered materials may start somewhere in the post-closure phase. The thickness of the EDZ for the long-term for a disposal gallery for HLW was estimated to be 1.25 metre with an increase in porosity of 3% i.e. 15% instead of 12% for the virgin host rock. The calculated averaged hydraulic conductivity was  $2 \times 10^{-13}$  m/s,  $4.4 \times 10^{-14}$  m/s is the hydraulic conductivity for the virgin host rock [Leupin, 2016a]. Apart from some unrecovered cracks, the potential diffusional path of water from this clay host rock into the engineered materials is rather homogeneous since there are no large discrete features.

The poorly indurated clay is not dried during the operational phase by ventilation since the immediate placement of the thick concrete segments that are necessary against the fast convergence of these clays also prevents drying of these clays due to their small water permeability. The clays have a water higher permeability than the concrete segments and there is evidence of water inflow of clay pore water at the joints between concrete segments. There seems to be no limited access of water in the operational phase for self-healing of these clays. A permeability of the clay host rock equal to the virgin permeability may already be assumed at the start of the post-closure phase, especially for galleries made for disposal of HLW since their diameter can be as small as the PRACLAY gallery. The potential diffusional path of water from this clay host rock into the disposal cell is heterogeneous since the joints between the concrete segments can be considered as the preferential pathways. This in-diffusion is restricted by the pore structure of the clay host rock.

The crystalline host rocks are also considered to be as wet as the virgin host rock except with some additional fractures caused by excavation of the host rock. Existing and made fractures are the preferential pathways for unrestricted diffusional flow of water into the disposal cell. In the long-term, fractures can be filled with carbonates and clay minerals i.e. a self-sealing process that diminishes the water flow from the crystalline rock into the engineered materials of the disposal cell.

Apart from a change in physical properties, there can also be a change in chemistry. The difference between the clay host rock in the vicinity of engineered materials due to operation and construction and the virgin clay host rock are a higher concentration of sulphates in the pore water chemistry due to pyrite oxidation and higher cation concentrations as a result of dissolution of carbonates to buffer the associated decrease in pH by this oxidation. Gypsum is precipitated especially on fractured clay surfaces.

### 3. Bentonite and concrete

Bentonite and concrete are frequently used as engineered materials in disposal cells. A grasp of the potential chemical gradients between the host rocks and these engineered materials can be deduced from a description of the pore water chemistry of these engineered materials.

#### 3.1 Bentonite

##### 3.1.1 Pore water chemistry

Bentonite buffers are usually 'dry' emplaced. Dry can mean for bentonite buffers a water content of 17 wt% e.g. [Johansson, 2020] or 10% e.g. [Atabek, 1991]. The pore water chemistry of this engineered barrier is therefore determined by the inflow of host rock water and establishment of equilibria between dissolved species present in this host rock water and minerals present in bentonite i.e. there is no initial pore water chemistry as in concrete. There is a pore water composition of bentonite calculated in the Spanish programme with and without saturation with granitic host rock pore water (ENRESA 2001). The comparison of these pore water compositions and the knowledge of the available soluble salts in bentonite clearly indicates that the bentonite pore water becomes more diluted during the chemical interaction between bentonite and the Spanish granitic host rock water as shown in the following table. A smaller dilution would be expected for the Swedish and Finnish granitic ground waters since these waters are more saline.

Table 3-1: Modelled bentonite pore water compositions [ENRESA, 2001]

Parameter	Unit	As emplaced	After saturation
Temperature	°C	RT	83.07
pH	-log(H <sup>+</sup> )	7.75	6.6
pe	-log(e <sup>-</sup> )	12.85	-0.197
Na <sup>+</sup>	mmol/kg	145.5	93.42
K <sup>+</sup>	mmol/kg	1.253	0.811
Ca <sup>2+</sup>	mmol/kg	20.78	11.19
Mg <sup>2+</sup>	mmol/kg	22.30	16.07
Sr <sup>2+</sup>	mmol/kg		
Fe <sup>2+</sup>	mmol/kg	1.612×10 <sup>-3</sup>	6.583×10 <sup>-2</sup>
Al <sup>3+</sup>	mmol/kg		
SiO <sub>2</sub> (aq)	mmol/kg	0.2646	0.9913
Cl <sup>-</sup>	mmol/kg	159.9	106.2
SO <sub>4</sub> <sup>2-</sup>	mmol/kg	36.59	20.94
HCO <sub>3</sub> <sup>-</sup>	mmol/kg	0.4361	1.714

##### 3.1.2 Mineralogy and porosity

Bentonite has a high smectite content of which montmorillonite is the most famous species. The smectite content can be 88 wt% as used in the Czech and 75 wt% in the Swiss programme in which smectite is further specified as Na-montmorillonite in Wyoming MX-80 [Müller-Vonmoos, 1983]. Wyoming MX-80 bentonite is also used in the Swedish programme [Wanner, 1994]. The structural formula for Na-montmorillonite is (Si<sub>3.96</sub>Al<sub>0.04</sub>)(Al<sub>1.55</sub>Fe<sup>3+</sup><sub>0.20</sub>Fe<sup>2+</sup><sub>0.01</sub>Mg<sub>0.24</sub>)O<sub>10</sub>(OH)<sub>2</sub>Na<sub>0.30</sub> [Müller-Vonmoos, 1983] that seems to be later refined into (Si<sub>3.98</sub>Al<sub>0.02</sub>)(Al<sub>1.55</sub>Fe<sup>3+</sup><sub>0.09</sub>Fe<sup>2+</sup><sub>0.08</sub>Mg<sub>0.28</sub>)O<sub>10</sub>(OH)<sub>2</sub>Na<sub>0.38</sub> [Bradbury, 2014]. The second contributor to the mineralogical composition is quartz. The Wyoming MX-80 bentonite also contains feldspar. Carbonates are the third contributor to the mineralogical composition. Pyrite and soluble salts (NaCl, KCl, CaSO<sub>4</sub>) are present in trace amounts in Wyoming MX-80 bentonite and bentonite used in the Spanish and Czech programmes. The Czech programme also has the soluble

salts  $\text{Mg}(\text{NO}_3)_2$  and  $\text{NaHCO}_3$ . The porosity,  $\varepsilon$ , of bentonite is determined by the dry density,  $\rho_{\text{dry}}$ , and specific density  $\rho_{\text{sp}}$  [Ochs, 2004]:

$$\varepsilon = 1 - \frac{\rho_{\text{dry}}}{\rho_{\text{sp}}}$$

For example, a specific density of  $2760 \text{ kg m}^{-3}$  is made with a dry density of  $1590 \text{ kg m}^{-3}$  and the porosity becomes 0.43 (43 vol%). There is also a perfect correlation between the dry density and hydraulic conductivity, also for MX-80 bentonite but the stress state is important for determination of the hydraulic conductivity [Atabek, 1991]

## 3.2 Concrete

### 3.2.1 Pore water chemistry

The concrete pore water compositions may be solely determined by the cement minerals generated during hydration assuming that the aggregates have not reacted with cement.

Table 3-3 and

Table 3-4 show different types of cement according to the cement classification EN-197-1. The pH of the concrete pore water depends on the presence of portlandite( $\text{Ca}(\text{OH})_2$ ) i.e. a pH > 12.5 is possible if this cement mineral is present. This presence is measured using X-ray diffraction in CEM I as well as CEM III/B [Kempl, 2015] although the calcium/silicium ratio in CEM III/B is smaller than 3. In thermodynamic modelling of completely reacted phases, portlandite is not present in CEM III/B and this absence of portlandite also gives calculated pH values below 12.5 e.g. 12.4 in CEM III/B [Cloet, 2019]. The following table shows the measured pore water chemistries from cement pastes by which the pore solutions were gained by a high-pressure apparatus and the main element concentrations were measured using ICP-OES [Kempl, 2015] and the modelled pore water chemistries for CEM-I [Wang, 2009], the French contribution and for CEM-III/B [Cloet, 2019]<sup>2</sup>. The pore solutions obtained with a high-pressure apparatus seem to approximate best the pore water chemistries [Atkins, 1991] and therefore other techniques to obtain pore solutions such as crushing hardened cement paste and let the crushed paste come into contact with water are not considered.

Table 3-2: Modelled and measured pore water chemistries in cements

Parameter	Unit	CEM-I			CEM-III/B	
		Measured	Modelled (Belgian)	Modelled (French)	Measured	Modelled
Temperature	°C	RT	25		RT	20
pH	$-\log(\text{H}^+)$	13.1	13.5	13.26	13.0	12.4
pe	$-\log(\text{e}^-)$	-	-	7.74	-	-10.3
Na <sup>+</sup>	mmol/kg	99.0	141	90	70.9	800
K <sup>+</sup>	mmol/kg	68.1	367	220	39.8	800
Ca <sup>2+</sup>	mmol/kg	2.1	0.7	1.5	2.8	7
Mg <sup>2+</sup>	mmol/kg	0.02	$\approx 10^{-7}$	$3.2 \times 10^{-7}$	0.02	$6 \times 10^{-5}$
Sr <sup>2+</sup>	mmol/kg	*		-	*	-
Fe <sup>2+</sup>	mmol/kg	*		$6.2 \times 10^{-4}$	*	-
Al <sup>3+</sup>	mmol/kg	*	0.06	0.77	*	0.8
SiO <sub>2</sub> (aq)	mmol/kg	*	0.05/0.3	$7.7 \times 10^{-2}$	*	0.1
Cl <sup>-</sup>	mmol/kg			40		100
SO <sub>4</sub> <sup>2-</sup>	mmol/kg	0.5	2	0.32	1.7	500
CO <sub>3</sub> <sup>2-</sup>	mmol/kg		0.3			0.07

A measured pH of concrete pore water larger than 13 is also available for similar cement pastes and measured from pore solutions that were gained by a high-pressure apparatus cement pastes containing fly ash e.g. [Andersson, 1989] but it is difficult to understand these pore water chemistries without X-ray diffraction. Therefore, reference has been made to a paper that contained both pore water chemistry as well as X-ray diffraction [Kempl, 2015]. Reducing i.e. negative, redox potentials for cements were measured for cements containing blast furnace slag, otherwise oxidising i.e. positive, redox potentials had been measured [Andersson, 1989] [Atkins, 1991].

The initial redox potential in concrete strongly depends on the type of cement used for its manufacturing. For Ordinary Portland Cement (OPC) i.e. CEM I, CaO is made by baking carbonate in limestone without a specific control of the heating environment. OPC concrete lacks electroactive species and is therefore largely unbuffered, being slightly oxidizing after fabrication. Blast furnace slag (BFS) is made in reducing environments as a by-product of steel. Concrete made with cement in which OPC is blended with BFS, contains traces of pyrite, FeS<sub>2</sub> and has therefore a reducing environment after fabrication. An oxygen penetration front into the concrete is observed as a loss of the blueish colour in above ground civil infrastructure.

<sup>2</sup> Concentrations for the Table in this report have been read from Fig 4.13 in this report assuming mol/m<sup>3</sup> ≈ mmol/kg

The calcium concentrations in this *Table 3-2* are an order in magnitude smaller than the maximum modelled concentration of calcium in equilibrium with CSH-gels of 20 mmol/kg [Berner, 1992] and [Vehmas, 2019a] without alkalis since the pH is controlled by the alkali content at a pH > 12.5 [van Eijk, 2000]. As the alkali content and pH is reduced upon leaching, the calcium concentration will increase.

### 3.2.2 Mineralogy and porosity

The mineralogy of concrete is determined by the calculated presence of cement minerals and aggregates. The calculated presence of cement minerals is determined by the compositions of oxides, amount of reacted phases with water and thermodynamic database. The following table shows the compositions of oxides as reported by the cement industry [CCM, 2016], [HCM, 2020] the total amount may not approach 100% due to rounding off. The groundwater compositions in clay host rocks and also the oxidation of pyrite can generate high sulphate contents. The content of tricalciumaluminate in these cements should therefore be small enough to prevent delayed ettringite formation, especially for CEM I cements an additional identification is assigned for this chemical resistance: Sulphate Resistance (SR), SR3 i.e. a tricalciumcontent smaller than 3 wt%. CEM II and III are blended cements containing a fraction of portlandite cement with either fly ash slag (V) or blast furnace slag to have a sufficient high pH to activate reaction of these slags. The amount of clinker in these cements are for CEM I 95-100 wt%, CEM II/B-V 65-79 wt%, CEM III/ A 35-64 wt% and CEM III/B 20-34 wt% according to this cement classification following the European standard EN-197-1. The maximum amount of other additions than slag is 5 wt%. The largest proportion is preserved for gypsum ( $\text{CaSO}_4 \cdot 2\text{H}_2\text{O}$ ) or anhydrite ( $\text{Ca}_2\text{SO}_4$ ) that is added to cements and determines the  $\text{SO}_3$  content. The alkalis are also present as readily soluble sulphates. Gypsum acts as a retarder but there is a limit of 4 wt% to limit ettringite formation. The alkali equivalents (LA) are small enough to prevent alkali-silica reactions if  $\text{SiO}_2$  aggregates were to be used. The types of cement used for the waste packaging or building the disposal facility have the same ingredients but with a smaller range in proportions than specified in this European standard.

Table 3-3: Average oxide compositions of different types of cement in wt%

Cement type	CaO	SiO <sub>2</sub>	Al <sub>2</sub> O <sub>3</sub>	MgO	Fe <sub>2</sub> O <sub>3</sub>	SO <sub>3</sub>	Na <sub>2</sub> O	K <sub>2</sub> O
CEM I 52.5 N SR3 LA	63.5	21.3	3.5	2.0	4.3	2.6	0.10	0.63
CEM II/B-V 42.5 N	53	27	6.8	1.2	5.8	2.9	0.30	0.30
CEM III/A 42.5 N	48	28	9.6	4.9	2.0	2.3	0.16	0.91
CEM III/B 42.5 N LH/SR LA	48	29	9.9	6.0	1.3	2.4	0.29	0.61

The numbers 52.5 and 42.5 refer to the compressive strength that is to be achieved after 28 days. One of those specified concretes is the Cebama reference mix that was designed for plugs for a disposal facility hosted in granitic rock. The CaO and SiO<sub>2</sub> in Cebama reference mix are 36.0 wt% and 50.7 wt% based on the specified contents of CEM I, silica fume and blast furnace slag [Vehmas, 2019b]. The Ca/Si ratio is significantly smaller than the cements listed in

Table 3-3.

Hydration models are used to model the composition of hydrated cement but the calculated mineralogy may not be validated and may be less representative for geological disposal than measured mineralogy's. There are many articles of X-ray diffraction results of hydrated cement and the following Rietveld analysis but Calcium Silicate Hydrates identification remains difficult due to their poor crystallinity, complex solid solution formation with alkali elements, occurrence of polymorphs and varying water concentrations [Kempl, 2015]. Portlandite, Ettringite and carbonate minerals can be well measured. Portlandite and Ettringite are shown in the following table since calcium carbonate is only measured in carbonated cement samples i.e. a cement mineral composition with calcite ( $\text{CaCO}_3$ ) does not represent initial state, although it can be calculated from an hydration model e.g. [Höglund, 2014] and [Cloet, 2019]. In historical concrete, the presence of portlandite, ettringite and calcite are identified with their characteristic temperature peaks in the differential thermal analysis [Mallison, 1987].

Portlandite is measured in CEM I as well as CEM III/B, the amount is in CEM III/B three times less than CEM I [Kempl, 2015]. Ettringite is controlled by the added amount of gypsum, hydrotalcite is controlled by the available magnesium [Neall, 1994] and the left-over for iron and aluminium control the amount of hydrogarnets. These phases have been calculated e.g. [Höglund, 2014] and [Neall, 1994]. A CSH-gel and a low Ca-CSH gel have been used earlier [Neall, 1994] and in the following table the CSH gels that are C1.8SH and C1.1SH [Höglund, 2014] are used. C1.8SH could also be afwillite [Wang, 2009]. Although afwillite and other well crystallised minerals are considered in the analyses, these well crystallised CSH-phases are not measured [Kempl, 2015] [Atkins, 1991]. The weights in

*Table 3-3* and molar weights of cement minerals have been used to determine the mineralogical compositions in the following table.

Table 3-4: Mineralogical composition from average oxide compositions

Mineral	Chemical formula	Molar weight [gram/mol]	Mineralogical composition in wt%			
			CEM I	CEM II/B-V	CEM III/A	CEM III/B
Portlandite	Ca(OH) <sub>2</sub>	74.1	18	6	4	5
CSH-gel	C1.8SH1.8	193	55	1	1	0
Low Ca-CSH gel	C1.1SH1.8	154	0	53	55	56
Hydrotalcite	Mg <sub>4</sub> Al <sub>2</sub> O <sub>7</sub> •10H <sub>2</sub> O	443	4	3	10	13
Hydrogarnet	(CaO) <sub>3</sub> Al <sub>2</sub> O <sub>3</sub> •3H <sub>2</sub> O	378	5	16	18	16
Fe-hydrogarnet	(CaO) <sub>3</sub> Fe <sub>2</sub> O <sub>3</sub> •3H <sub>2</sub> O	436	9	12	4	3
Ettringite	Ca <sub>6</sub> Al <sub>2</sub> (SO <sub>3</sub> ) <sub>4</sub> (OH) <sub>12</sub> •26H <sub>2</sub> O	1254	8	9	7	7
Pyrite	FeS <sub>2</sub>	120	0	0	0.14	0.20

The ratio of portlandite and CSH-gel is similar as calculated with the hydration model [Höglund, 2014]. Monosulphate is the location for sulphate in hydration models e.g.[Höglund, 2014], [Berner, 1992] but only ettringite has been measured and therefore used as the location for sulphate in the mineralogical composition. This is also assumed in the Belgian programme[Wang, 2009]. Monosulphate is however metastable with respect to ettringite but in some studies monosulphate instead of ettringite is measured with XRD [Atkins, 1991]. All suggested mineralogical compositions are stoichiometric with the average oxide compositions but the blended cements could only contain low Ca-CSH gel in order to have some portlandite as measured in cement pastes made with CEM III/B [Kempl, 2015].

The porosity in the cementitious materials is controlled according to their application. Concrete buffers, concrete segments and plugs are made with aggregates that usually have no porosity. The concentration of quartz aggregates ranges between 1700 and 2000 kgm<sup>-3</sup>. The porosity is mainly located within the hydrated cementitious phase provided there is a good bonding between hydrated cement and aggregates, otherwise there also some additional porosity at the interface between hydrated cement and aggregates. Kerosine porosimetry seems to give the best reliable result and a porosity of 12.5% was measured for the concrete designed for plugs in the disposal facility for results to be obtained on a short time [Vehmas, 2019b]. Reliable porosity measurements can also be gravimetrically determined but require a long period in laboratory time. Higher porosities are present for cementitious materials that are used as a backfill and shotcrete e.g. between 25-35 vol% [NAGRA, 2008]. The porosity of concrete made with blended cements is similar to concrete made with OPC based cement with the same factors such as cement content, water/cement ratio, curing conditions et cetera but CEM I (i.e. OPC) based concrete has a relative open pore structure compared to blended cements containing slag. Concrete made with these blended cements are called low-permeability concretes due to the refined pore structure [Atkins, 1991] [Atabek, 1991] [Jackson, 2017].

## 4. Disposal cells with vitrified HLW

The spent fuel from nuclear power plants (NPP) can be reprocessed. Reprocessing involves extracting fissile materials (uranium and plutonium) for recycling to reduce the volume of high-level waste. The main process for reprocessing is Plutonium Uranium Refining Extraction (PUREX), in which spent fuel is dissolved in nitric acid and tri-butyl-phosphate is used to extract the actinides [Gruppelaar, 1998]. The High-Level Liquid Waste (HLLW) contains fission products. Actinides and traces of plutonium and uranium are present in the liquid as well. For vitrified HLW present in Western European countries, HLLW has been poured with a melted glass frit into a stainless steel container. The result is vitrified waste in which radionuclides are homogeneously distributed in a borosilicate glass matrix. In a few Eastern European countries, there are existing treaties with the Russian Federation and the negotiations of the waste form in which the radionuclides are to be incorporated after reprocessing, are currently running. In this ACED deliverable, we study the vitrified waste products as made in Sellafield and la Hague. The largest amount comes from France and therefore frequently, the French abbreviation for this waste product is used: Conteneur Standard de Déchets Vitrifiés, CSD-V.

### 4.1 Characterization of disposal cells in granite and clay

The heat generating power of vitrified HLW diminishes as a function of time by decay of radionuclides. The following figure shows the heat generating power per waste canister as a function of time.

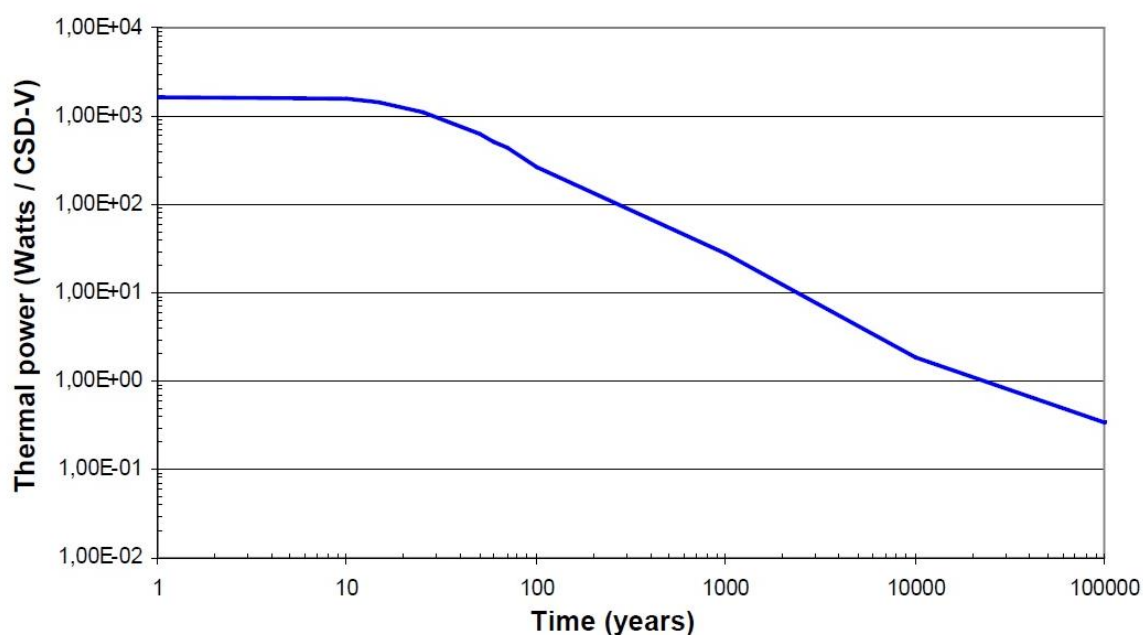


Figure 4-1: Evolution of the thermal power of a typical residue UOX: 44000 MWd/tU initial enrichment 3.8%  $^{235}\text{U}$  and mixed with MOX: 45.000 MWd/tU initial enrichment [AREVA, 2007]. Decay of many short-lived radionuclides takes place in the period smaller than 30 years. Their contribution to the thermal power is assumed not be included.

The heat generating power induces thermal and hydraulic gradients within the disposal cell and the participating organisations have been asked to provide information on these gradients in order to obtain a general view of these gradients of the chemical processes. The following table shows the provided information. ACED evaluates the chemical evolution for vitrified HLW but heat generated by spent fuel

can be of also be of interest to ACED provided that information concerning the temperature is available for at least one of the six interfaces investigated in ACED:

- glass-steel
- cementitious material-granite
- cementitious material-clay
- steel or iron-bentonite
- steel or iron-cementitious material
- steel or iron-granite

Table 4-1: Provided information about thermal and hydraulic gradients for HLW disposal cell

Country	Organisation	HLW	Calculated information concerning gradients
Belgium	SCKCEN	Vitrified	Temperature
Czech	SURAO	Spent fuel	Temperature
Finland	VTT	No contribution for HLW disposal cell <small>None of the six interfaces investigated in ACED may be present in the Finnish programme for spent fuel.</small>	
France	ANDRA	Vitrified	Temperature
Germany	FZJ & UFZ	Vitrified	No calculated information
Lithuania	LEI	No contribution for HLW disposal cell	
Netherlands	COVRA	Vitrified HLW	Temperature
Spain	ENRESA & UDC	Spent fuel	Temperature and saturation degree

From the table it becomes clear that from the participating organisations only the Spanish contribution can be used to provide information on hydraulic gradients within the disposal cell, the saturation degree at several positions in the bentonite buffer as a function of time has been calculated including the steel-bentonite interface. The Spanish contribution calculated that the required time for saturation of the bentonite buffer is 16.4 years for disposal cells hosted in granitic host rocks and 18.2 years for disposal cells hosted in plastic (i.e poorly indurated) clays. Consequently, hydraulic gradients within the disposal cell may be negligible for post-closure phase in these host rocks. The diffusional inflow of water from indurated clays is smaller than granitic and poorly indurated clays and larger periods in time for saturation are therefore expected as explained in paragraph 2.4.

Almost any disposal cell has a steel overpack that encapsulates the waste canisters for this heat generating period in order to prevent contact between any pore water and the vitrified waste form. Potential migration of radionuclides in the host rock can then only take place without thermal gradients which reduces the parameter uncertainty and model uncertainty in safety assessments. The period in time it requires to have no thermal gradients in the host rock also maximises the temperature of glass when it would in contact with pore water. The temperature of glass would at least be less than 35 degrees Celsius when the thermal gradient in the clay host rock is negligible as calculated in the Dutch and Belgian case. The French case has a waste temperature criterion i.e. 50 degrees Celsius for vitrified waste disposed before 2075 and 70 degrees Celsius for waste disposed after 2075. The higher temperature criterion after 2075 is explained by the advances in knowledge about the behaviour of vitrified waste and of radionuclides in solution. The following figure shows an abstraction of the disposal cells considered in Europe for the following host rocks: granite, poorly indurated clay and indurated clay.

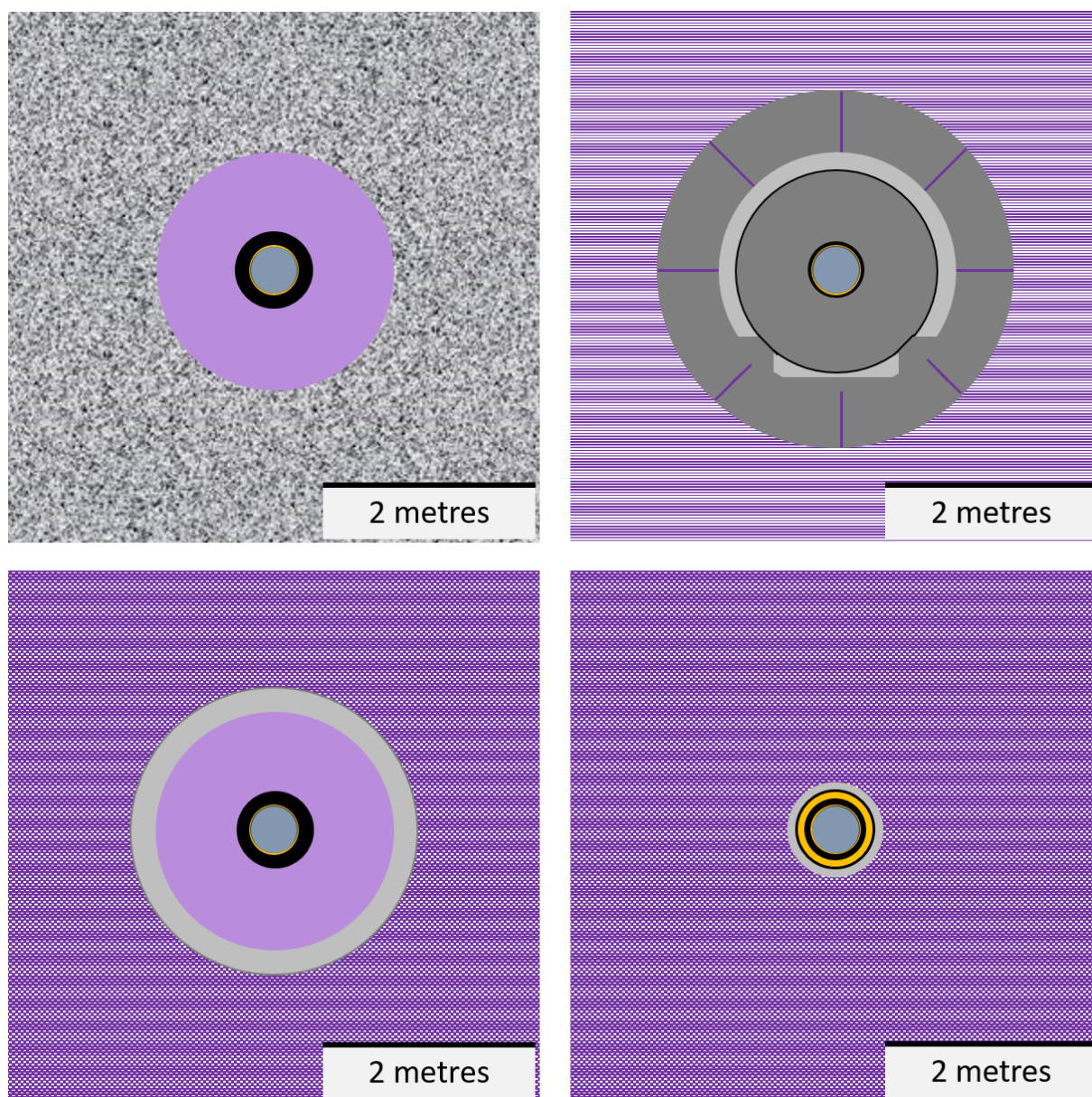


Figure 4-2: Abstracted disposal cells containing vitrified HLW considered in Europe for the host rocks: granite, poorly indurated clay and indurated clay. Blue = vitrified HLW, orange = void, black = steel, bentonite (purple) or concrete buffer (grey) surrounds the overpack and grout = light grey.

The carbon steel overpack is usually surrounded by a buffer that provides beneficial conditions for the durability of the overpack. Bentonite buffers are used in the Czech, English, German, Spanish and Swiss program and concrete buffers are considered in Belgian and Dutch disposal programmes. An exception is the French programme, in which the carbon steel overpack is not surrounded by a buffer; there is a void between the steel overpack and steel tube in order to facilitate retrieval of the waste package.

Grouts are envisaged to be injected in most disposal facilities hosted in clay host rocks, the only found exception is the Spanish disposal cell that envisages a disposal concept in which bentonite interfaces concrete hardened segments. The reason for grouting in facilities built in poorly indurated clay is to eliminate empty volume in order to have sufficient heat dissipation to the host rock. The French programme considers a mixture of bentonite and cement interfacing the clay host rock in order to

neutralise the potential acidity resulting from the pyrite oxidation due to excavation work and thus limit the corrosion rate of the steel tube.

It has been chosen to provide more detailed characteristics at interfaces of the disposal cells since the interactions between materials have a specific focus within ACED.

#### 4.1.1 Interface between carbon steel overpack and buffer

The bentonite buffer has a typical pore structure by which two physical beneficial conditions for this durability are present:

- 1) no advection at the interface between steel and bentonite;
- 2) no growth of microbes.

Advection could accelerate corrosion by increasing the removal speed of the corrosion species from the vicinity of the steel surface. Microbial corrosion rate is usually larger than chemical corrosion rate but the initiation of microbial corrosion does not take place when the microbial activity is absent. This absence is possible by space restriction. The beneficial physical conditions for bentonite are also present in concrete buffer on the long-term, but the slow leaching of cementitious phases slightly increases the porosity of the concrete buffer. These typical pore structures of small connecting pore throats have also safety relevant features since potential radionuclide migration can be assumed to be limited to diffusion and retardation of colloids and radionuclide complexes takes place by ultrafiltration. Other retardation mechanisms are sorption and co-precipitation. Positively charged dissolved radionuclide species can be sorbed by negatively charged clay minerals and negatively charged radionuclides can be sorbed by cementitious minerals that are positively charged at a pH larger than 11.8 [Poiteau, 2008].

Both buffers have a temperature limit of 100 degrees Celsius in many disposal programmes. The reason for this temperature limit in the Czech and Spanish programmes is to limit degradation or mineral alteration of the bentonite buffer in order to limit the uncertainty in the long-term predictability of this buffer. For the concrete buffer, this temperature limit has been set to limit the formation of a gaseous phase. The basis for the design of a geological disposal facility is this temperature limit and therefore all calculated temperature evolutions interfacing the steel overpack are below 100 degrees Celsius.

At room temperature, the pH of the bentonite buffer is around 8 and the concrete buffer starts the post-closure phase with a pH around 13 (see Chapter 3). The difference in pH between both buffers has some interesting features steel. The following figure shows the thermodynamic diagrams of iron with the same chemical thermodynamic input but at two different temperatures. Only the part of the Pourbaix diagram with a negative redox potential is relevant since the anaerobic conditions for steel corrosion are obtained either within the operational phase or soon in the post-closure phase since the disposal depth for HLW is usually deep enough for the existence of reducing conditions.

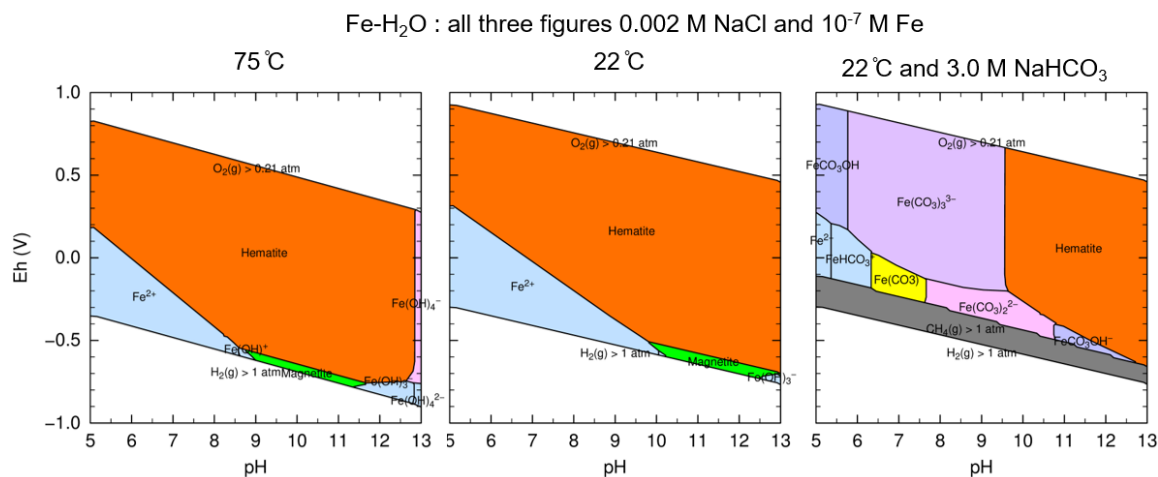


Figure 4-3: Pourbaix diagrams for the system Fe-H<sub>2</sub>O at 75 °C and 22 °C with an activity of iron dissolved species of 10<sup>-7</sup>; 0.002 M Cl is a reasonable concentration for tap water. Magnetite (green) is Fe<sub>3</sub>O<sub>4</sub>(s), Hematite (orange) is Fe<sub>2</sub>O<sub>3</sub>(s) and Siderite (FeCO<sub>3</sub>) is yellow.<sup>3</sup>

The heat generation of vitrified HLW will increase the temperature of the concrete pore water and this increase results in a decrease of the pH. Passivation of the carbon steel overpack is expected when the pH and redox potential in the magnetite stability field. Magnetite on the carbon steel no longer dissolves if the solution is saturated with dissolved iron species. Please note that the supersaturated iron solutions have been used in the calculated Pourbaix diagrams; the actual range in pH of the thermodynamically stable magnetite is smaller. The minimum in solubility has been calculated to be 10<sup>-9</sup> M at 100°C and 10<sup>-10</sup> M at 25°C [Hermansson, 2004]. This layer also constitutes a barrier against transport of water towards steel and of dissolved iron species into solution. This passivation is expected to extend beyond the thermal phase for concrete buffers. The pH of bentonite is around 8 and especially at higher temperatures, passivation of the carbon steel overpack may thermodynamically be expected but not at room temperature. A surface oxide film has not been measured to be formed on the surfaces of carbon steel exposed at 15°C to synthetic ground water at a pH of 8 and made with a bentonite buffer but the measured corrosion rates remained slow i.e. 0.09 µm per year [Fujisawa, 1997]. Precipitation of magnetite as a corrosion product in bentonite has been modelled at 25°C in the Czech and Spanish disposal programmes due to an increase of pH till 10 by iron corrosion at the vicinity of the bentonite-iron interface. A rise in pH near the steel surface, which makes precipitation of magnetite thermodynamically possible, can be caused by insufficient dissipation of the generated hydroxyl ions in bentonite while there may be sufficient dissipation of these ions in synthetic groundwater. The presence of carbonate in bentonite pore water may also result in the formation of siderite; modest concentrations of carbonate have been attributed a risk of hydrogen induced cracking (HIC) [Padovani, 2017]. Sufficient high carbonate concentrations in concrete pore water for HIC is not expected as the cement minerals will react with carbonate to form calcium carbonate.

The thickness of the steel overpack is at least three times smaller for countries considering a concrete buffer compared to countries that have chosen a bentonite buffer. The minimum corrosion rate of 0.5 µm per year at steel-bentonite interfaces used in the Spanish programme is also significantly larger than the long-term corrosion rate of carbon steel of 0.01 µm per year as found in alkaline media at

<sup>3</sup> These figures have been made with Phreeplot [Kinniburgh & Cooper, 2018], a free available software programme that makes geochemical plots using Phreeqc [Parkhurst & Appelo, 2013]. The SIT database has been used as input for these calculations. This database corresponds to the PHREEQCi version of the ThermoChimie v.7.b, developed by Amphos 21, BRGM and HydrAsa for ANDRA, the French National Radioactive Waste Management Agency. Thermodynamic calculations made with Phreeplot and thermochemie database.

temperatures 25°C and 80°C<sup>4</sup>. It may take some several tens of hours of exposure to obtain this small corrosion rate; this long term corrosion rate 0.01 µm per year was the rate measured after 10,000 hours [Smart, 2017]. Carbon steel specimens exposed to mortar solutions for a shorter period than 10,000 hours measured a temperature-dependency to the corrosion rate at a pH of 12.6 i.e. 0.004 µm per year at 15°C, 0.002 µm per year at 30°C and 0.02 µm per year at 45°C [Fujisawa, 1997].

#### 4.1.2 Interface between engineered materials and host rock

Figure 4-2 shows that the outer diameter of bentonite interfaces granite. The difference in pH between the bentonite buffer and granitic pore water is negligible. Dry bentonite buffers are emplaced and therefore the initial hydraulic gradient is large. The porosities used in the Czech and Spanish programmes for bentonite buffers are around 40%. The potential granitic pore water flow is entirely determined by flow through fractures since the porosity of a granitic rock piece is negligible. This advective flow of granitic pore water ensures quickly saturation but it can be non-homogeneously distributed by which the geochemical evolution is also non-homogeneous. The temperature at this interface has been calculated to remain below 80 degrees Celsius.

Hydraulic gradients are negligible in disposal systems with poorly indurated clay due to the high saturation degree of emplaced concrete segments and their small porosity. The porosities of the cementitious materials used in these disposal cells are smaller than the clay host rock. The concrete liner also prevents dehydration in the operational phase. The temperature at this interface has been calculated to remain below 60 degrees Celsius.

Drying of clay host rock in the operational phase is considered in indurated clay host rocks; the porosity of these clay host rocks is smaller than the hardened grout. Hydraulic gradients are therefore assumed to be present at the start of the post-closure phase as explained in paragraph 2.4.

## 4.2 Calculated chemical interactions and their impact

The chemical evolution of the disposal cell containing vitrified HLW is not included in any safety assessment but parts of the chemical evolution of the disposal cell have been calculated. The country contributions show that calculating the chemical interaction between materials requires the porosity, the pore water, mineralogical composition at start of the post-closure phase and the diffusional speed of dissolved species. An assumption is made of reactive minerals in the chemical evolution and their thermodynamic data are used calculations. The current handling of disposal cells containing a bentonite buffer show that the extent of the chemical interaction is limited to the vicinity of interfaces for a period of 100.000 years or sometimes even 1 million years.

#### 4.2.1 Interface between steel overpack and buffer

##### 4.2.1.1 Disposal cells with an interface between steel and bentonite

The chemical interaction between steel and bentonite has been experimentally investigated in the 6<sup>th</sup> framework programme NF-PRO [Sneyers, 2008]. The country contributions from the Spanish, Czech and Swiss programmes show the modelled the chemical interaction between steel and bentonite. The conceptual geochemical model included the following reactions 1) aqueous complexation, 2) acid/base reactions 3) redox reactions, 4) mineral dissolution and precipitation and 5) cation exchange processes. Anoxic corrosion of steel generates dissolved iron species, hydroxyl ions and hydrogen. The hydroxyl

<sup>4</sup> These experiments also have been performed with a radiation rate of 0.25 Gy per hour and 25 Gy per hour. A difference in corrosion rate as a function of temperature, radiation and chlorine concentrations has not been measured [Smart, 2017].

ions increase the pH of the bentonite buffer till a pH of 10. The following figure shows the evolution of the pH in the bentonite buffer and the precipitation of magnetite from the Czech programme.

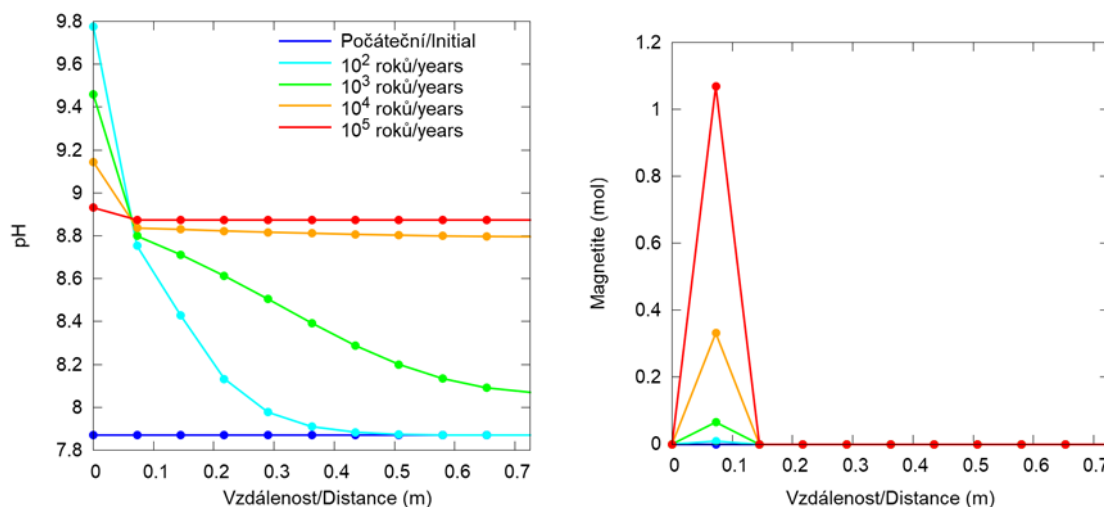


Figure 4-4: Evolution of the pH as a function of the distance from the steel overpack at start 100, 1000, 10.000 and 100.000 years.

The potential impact of an increasing pH is the transformation of (swelling) clay minerals into zeolites like analcime. The dissolved iron species precipitate in the bentonite as magnetite and siderite. The carbonate for the precipitation of siderite comes from the granitic pore water. The zones with reduced porosity in the bentonite buffer have been calculated to depend on the corrosion rate of iron and advective flow of granitic water. The potential impact of a reduction in porosity is pore clogging but the bentonite buffers in the Spanish and Czech programme have an initial porosity of 40% by which sufficient escape paths for the hydrogen gas remain i.e. built-up gas pressure by pore clogging may be unlikely. The zones with reduced porosity have been calculated to be smaller than 5 cm for a corrosion rate of 5  $\mu\text{m}$  per year and 12 cm for a corrosion rate of 0.5  $\mu\text{m}$  per year in the Spanish programme. Magnetite precipitation has been calculated to be limited to 15 cm in the Czech programme. The dissolved iron species may also sorb on the negatively charged clay mineral surfaces by which sorption capacity of the bentonite buffer is reduced. But the concentration of dissolved iron species in equilibrium with magnetite and siderite is very small. These geochemical calculations have been made at 25°C since most thermodynamic data are related to this temperature. The influence of temperature on dissolution and precipitation of mineral phases could reduce the uncertainty in the calculated results. The Swiss programme refers to Savage's work that noted the potential impact of the released hydrogen: hydrogen could further reduce the sorbed iron species [Savage, 2014]. This reduction could increase the surface charge of the clay minerals and thereby decreasing the swelling pressure by which the hydraulic conductivity of bentonite is increased. This process has, however, also in the Swiss programme, been quantified as a process that is not likely to happen and reference is made to the work by Didier et al [Didier, 2012].

Eventually there will be contact between the pore water and vitrified HLW. Glass has been known to be very insoluble in natural environments that have a neutral pH. Glass will be passivated by the formation of an amorphous layer at the exposed surface. This passivation layer hardly dissolves if the solution is saturated with Si, Zr, Al, Ca etcetera. This layer also constitutes a barrier against transport of water towards glass and of solvated glass into solution. The dissolution rate of the vitrified waste form is therefore expected to be very slow after fracture of the overpack. Glass dissolution rates are usually used in assessments to calculate the potential radionuclide release. The country contribution from the French programme shows that the glass alteration rate increases in the vicinity of iron and corrosion

products. The solvation of glass into solution is promoted by sorption of dissolved silicon by corrosion products and precipitation of iron silicates.

#### 4.2.1.2 Disposal cells with an interface between steel and concrete

The fate of iron complexes within the concrete buffer has not been modelled for HLW but has been calculated for ILW disposal cells [Höglund, 2014]. The potential impact could be cracking of concrete surrounding steel due to the volume increase of corrosion products. This cracking has been known to be prevented for reinforced concrete by a sufficient concrete cover for the rebars. But this practical experience is too limited for the long-term and may not yet be sufficiently understood for modelling. The pH at the interface between the steel overpack and the concrete buffer has been modelled in the Belgian programme by assuming the concrete buffer being exposed to Boom Clay pore water i.e. neglecting the limited migration of leached species in clay and pore clogging in the clay host rock. Diffusional leaching of cementitious minerals has been calculated. The concrete buffer was made by Ordinary Portland cement. The pH at the interface between the steel overpack and concrete buffer has been calculated to be reduced till 12.5 within 1200 years. It is calculated to remain a pH of 12.5 for 80.000 years.

Eventually there will be contact between the pore water and vitrified HLW. The dissolution rate of the vitrified waste form has been known to be larger at higher pH but also at high pH, a passivation layer on the exposed surfaces is formed. In the country contribution from the Belgian programme it is assumed that the release of silicic acid by the glass will react with calcium released by portlandite to form calciumsilicatehydrate phases (CSH) that may also incorporate aluminium from the glass (CASH). These reactions trigger the dissolution of the silica matrix and slow down the decrease of the dissolution rate. Si from glass can also react with CSH phases in the concrete to form CSH phases with low Ca/Si ratios which may also have a triggering effect.

### 4.2.2 Interface between engineered materials and host rock

#### 4.2.2.1 Disposal cells with an interface between bentonite and granitic rock

*Figure 4-2* shows that the engineered material interfacing the granitic host rock is bentonite. The pH of the pore waters in bentonite buffers and granitic pore waters are similar i.e. there is no alkaline plume. The granitic host rock usually has only the safety function to isolate the waste and local chemical interactions with the engineered materials have no impact on this safety function. The focus in the current handling of the chemical evolution is limited to the potential changes on the bentonite buffer on the advective granitic water flow. The granitic chemical pore waters compositions in the Czech and Spanish cases are both of sodium bicarbonate types by which there is an inflow of bicarbonate into the bentonite buffer and sulphate and chlorine outflow. The sulphate may originate from the oxidation of trace amounts of pyrite within the bentonite buffer or the bentonite buffer the dissolution of gypsum within the bentonite buffer.

#### 4.2.2.2 Disposal cells with an interface between cementitious material and clay

*Figure 4-2* shows that all disposal concepts in clay host rocks have disposal concepts in which the clay host rocks interfaces with concrete. The big difference between poorly indurated clay and indurated clay is that the concrete hardened segments are used for poorly indurated clay and grout is hardened when interfacing the indurated clay host rock. In both cases, the pH of the pore waters in concrete materials is higher than the clay host rocks. The measured chemical profiles of concrete encapsulated in poorly indurated clay for more than 40 years show sharp pH gradients at the edges of the concrete samples [Atkinson, 1985]. The reduction in pH is caused by leaching of alkali hydroxides and calcium by

dissolution and decalcification of cement minerals. The dissolution of cement minerals may increase the porosity of concrete and thereby reduce its mechanical strength. The impact on the mechanical strength of concrete and resulting variation in transport parameters in concrete has been evaluated in the Swedish programme i.e. a concrete-granite interface. The same trend in the evolution in pH occurs as identified by Atkinson [1985] and predicted by thermodynamic calculations [Berner, 1990] for CEM I cement based concrete that starts with a calcium, silicium ratio larger than 1.7 i.e.:

- Initial pH of 13.5 that is reduced till 12.5 by leaching of alkali hydroxides;
- Dissolution of the cement mineral Portlandite at pH=12.5;
- Decalcification and dissolution of CSH-gels ( $1.7 > \text{Ca/Si} > 0.85$ ) until a similar pH of granitic or clay pore water is achieved.

Calcium aggregates that are used as the concrete buffer in the Belgian disposal concepts and in the NIREX Buffer Vault Backfill for granitic host rocks also have a pH buffering function between a pH of 8.5 and 10.5.

The evolution of the pH within concrete and clay has been calculated by mass balance in the Belgian programme. The conceptual geochemical model included the following reactions 1) aqueous speciation, 2) acid/base reactions 3) clay mineral dissolution and dissolution and precipitation of secondary phases in Boom Clay 4) pH independent cation exchange processes with a fixed charge on clay minerals 5) pH dependent cation exchange processes to represent the buffer capacity of organic matter in clay and 6) a non-electrostatic surface complexation model to simulate the protonation and deprotonation on illite and montmorillonite but changes in porosity and transport parameters have been excluded. The pore water in Belgium (Boom Clay) is fresh and this approach may therefore have no impact on the chemical evolution. The sharp pH gradients that have been calculated in the Belgian programme to evolve within the concrete at the edges have also been observed in Atkinson's study.

The Swedish investigations on reactive transport modelling with concrete show that precipitation of minerals that degrade the mechanical strength of concrete may not be identified by assuming constant transport parameters when exposed to brackish pore water [Höglund, 2014]. As saline or brackish water or more saline are expected in granitic and clay pore waters in Finland, Sweden, Belgium for the Ypresian clay host rock, France, Netherlands and Switzerland. The use of Fick's law for diffusion instead of the more correct Poisson-Nernst-Planck equations also affects the prediction of precipitation minerals within concrete [SKB, 2014b; p.68].

The alkaline plumes in the clay host rock have been calculated to be limited to 2 to 2.5 meter for poorly indurated clay in the Belgian programme after a period of 100.000 years. Boom Clay is poorly indurated clay and other examples are London Clay and Ypresian Clay. The porosity ranges between 30-45% [Mazurek, 2011]. Precipitation of calcite, brucite and sepiolite has been calculated to buffer hyperalkaline plume in the Spanish programme. The extent of an alkaline plume was calculated to be 0.7 meter after a period of 1 million years in a clay host rock with a porosity of 32.8%. A potential impact of the alkaline plume is the loss in the self-healing capacity of these poorly indurated clays in the vicinity of what is left of the disposal facility. This loss in self-healing has been evaluated for bentonite in which it has been elucidated that the interaction between cement and this engineered swelling clay material is highly non-linear, with a complex interplay between fluid transport, clay ion exchange and dissolution, secondary mineral growth and consequent changes in physical properties: porosity, permeability, swelling pressure [Savage, 2014].

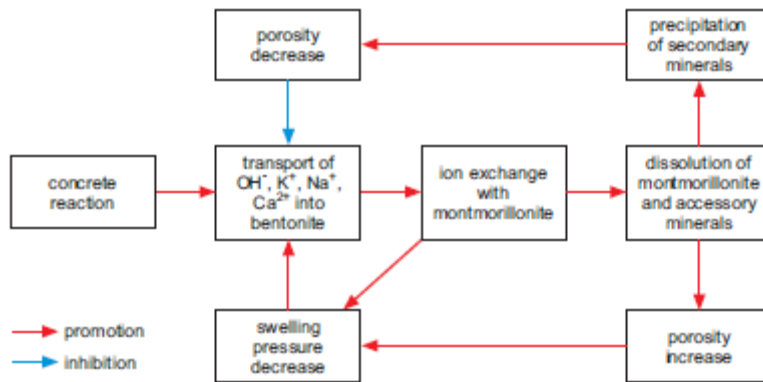


Figure 4-5: Cement-bentonite interaction as a coupled linear system [Savage, 2014]

Indurated clay is less porous than poorly indurated clay, indurated clay porosities are at least smaller than 20% [Mazurek, 2011]. The alkaline plume has been calculated to extend to less than 0.1 metre in the Swiss programme. Consequently, the current handling of disposal cells shows that the extent of the chemical interaction is limited to the vicinity of interfaces in a period of 100.000 years or sometimes even 1 million years i.e. the clay host rock remains its containment properties on the long-term.

## 5. Disposal cells with cemented ILW

For ACED, it has been chosen to concentrate on the two types of cemented ILW: a metallic waste form and organic waste form. The nature of organic waste and metallic waste is diverse and therefore preferences of specified types of cemented ILW have been asked in order to prioritize potential cases to be studied in ACED. The following tables show the characteristics of ILW and highest interest for types of ILW.

Table 5-1: Reported waste characteristics and interest

Country	Metallic or organic	Further specification	Comment
Belgium*	Metallic	CSD-c i.e. mainly Zr	Given the similarity of engineered materials in a ILW disposal cell and HLW disposal cell, the chemical evolution may be assumed to occur alike but no specific assessment has been done.
Czech*	ILW disposal cell without choice in organic or metallic waste presented at kick-off meeting July 2019		
Finland*	Mainly activated materials and solidified liquid waste ILW is packed in concrete waste packages		
France*	Metallic and organic	Metallic waste is mainly composed by technological waste (black steel) and structural waste (stainless steel, Ni alloys and Zr alloy etc.)  Organic waste, especially interest in the behaviour of PVC and cellulose. Degradation of both polymers lead to release of phthalate and iso-saccharine acid	
Germany*	Element specific time for radionuclide mobilisation from the waste. Cementitious materials e.g. 0 years for Cs, Rb and Cl and 600 years for actinides. After 600 years, the complete radionuclide inventory is released from the waste packages. Host rock is an iron ore formation i.e. outside scope of ACED.		
Lithuania*	Graphite blocks and sleeves from the reactor core, activated metallic core components and parts of spent fuel assemblies		
Netherlands*	Metallic	CSD-c, hulls of Zicaloy, other metallic parts are usually Inconel.	Chemical evolution of ILW disposal container would be similar to HLW disposal container. Instant release of radionuclides at assumed periods, chemical evolution is excluded.
Spain*	No specific studies and therefore no contribution.		
Hungary	organic	resins	Stabilisation of organic waste has not been solved and there is a large amount of this type of waste.
Romania	organic	resin	Spent ion exchange resins have a high content of carbon-14 and do therefore not satisfy waste acceptance criteria for near surface disposal and needs to be geologically disposed off.
Sweden	metallic	Carbon steel/ stainless steel	Need to know if corrosion products can cause fractures in the concrete on long time scales. Also need to know how to quantify these eventual cracks and how to change the hydraulic properties of the concrete.

\*The conceptualisations of the chemical evolutions and which parts have been modelled in the national programmes have been described by organisations working in these countries.

From Table 5-1, it can be deduced that for a few countries further specification metallic or organic waste is not performed and that the chemical evolution of ILW disposal cells is frequently not included in the assessment. There seems to be limited current handling of the chemical evolution of ILW disposal cells in Europe. No specific studies have been made for the chemical evolution of disposal cells containing cemented ILW in the Netherlands, Czech and Spain. In the Dutch case, the exclusion of the chemical evolution in the safety assessment means that radionuclides within the waste form and packages are

assumed to be released into the host rock as a function of the element-specific solubility i.e. radionuclides below an element-specific solubility are instantaneously released into the host rock. No post-closure safety function of the engineered barrier system has been used in the safety assessment. The durability of the waste form has been included in the German case in which specific periods in time have been used for the release of radionuclides. These approaches may sound conservative but the negligence of accompanying degradation products as a result of the chemical evolution may have an impact on the calculated radiological exposure. The most important two ones are:

- 1) the generation of gas during anaerobic corrosion of many metallic waste types which may damage or perturb the containment behaviour of the engineered barrier system and the clay host rock;
- 2) the formation of complexing agents with radionuclides during degradation of organic waste such as iso-saccharinic acid.

These two features are the main issues for ILW disposal cells. The consumption of oxygen by steel in the disposal facility generates anaerobic conditions after closure of the GDF. Gas is generated since water instead of oxygen, is used as an oxidant in the corrosion process. The gas generation rates can be very small for metallic surfaces that are exposed to high pH concrete pore water conditions due to presence of a passivation layer such as magnetite on steel in *Figure 4-3*. High pH and high calcium concentrations in concrete pore water reduce the concentration of the complexing organic agents by precipitation of calcium-solids [SKB, 2015; p.154]. The evolution of the pH of concrete barriers has therefore been intensively studied for operational disposal facilities such as in Sweden.

The waste packaging and caissons in the disposal facility can be made with reinforced concrete. The interest of Finland and Sweden is the long-term evolution of reinforced concrete in their disposal facilities hosted in granite since the corrosion process may have an impact on the durability of concrete because an increasing thickness of corrosion products around rebars may no longer be accommodated by the creep of concrete. The pH of concrete pore water reduces by leaching of alkali hydroxides and calcium by dissolution of portlandite followed by dissolution of CSH gels as explained in paragraph 4.2.2.2. The chemical processes within concrete interfacing clay host rocks and crystalline host rocks are similar since there are many similarities in pore water composition but the speed of concrete alteration can be different due to a different diffusional ingress and outgress of species. The brackish granitic pore water conditions to which the disposal facility is exposed in the first thousands of years results in ingress of sulphate and chlorine in the concrete barriers. The Swedish investigations shows that the ingress of chlorine results in the precipitation of Friedel's salt which may counteract the reduction in porosity by leaching of calcium. The ingress of sulphate and bicarbonate is considered as a deleterious process due to the formation of calcium-sulphate minerals that crystallize as fine needles which makes concrete losing its strength and integrity by peeling off parts of the concrete along moving reaction fronts within the concrete. The values for diffusion are significantly increased when the calculated porosity becomes smaller than the initial porosity of concrete in order to include the potential impact of the crystallisation of these calcium-sulphate minerals in which the surrounding concrete cracks. The pore waters in Slovenia and Belgium (Boom Clay) are fresh and the risk of formation of these calcium-sulphate minerals within the concrete may be negligible.

## 5.1 Metallic waste

Metallic waste can be Zircaloy that arises from reprocessing of spent fuel, scrap metal during maintenance outages when equipment is discarded, modified or renovated, decommissioning and dismantling of nuclear plants e.g. corrosion resistant inner parts of nuclear power plant are made of stainless steel. Scrap metal can also come from non-nuclear power activities e.g. spent radiation sources, equipment containing radiation sources, waste from radiotherapy units, radioactively contaminated material and may contain apart from steel also aluminium. Another scrap metal is zinc. The following figure shows the metallic ILW:

- scrap metal contained in tetramoulds;
- compacted Zircaloy hulls, Inconel ends and other stainless parts contained in standardized containers.

These standardised containers are made in France as another waste product from the reprocessing of spent nuclear power fuel. The French abbreviation for these waste products is frequently used: Conteneur Standard de Déchets Compactés, CSD-C.

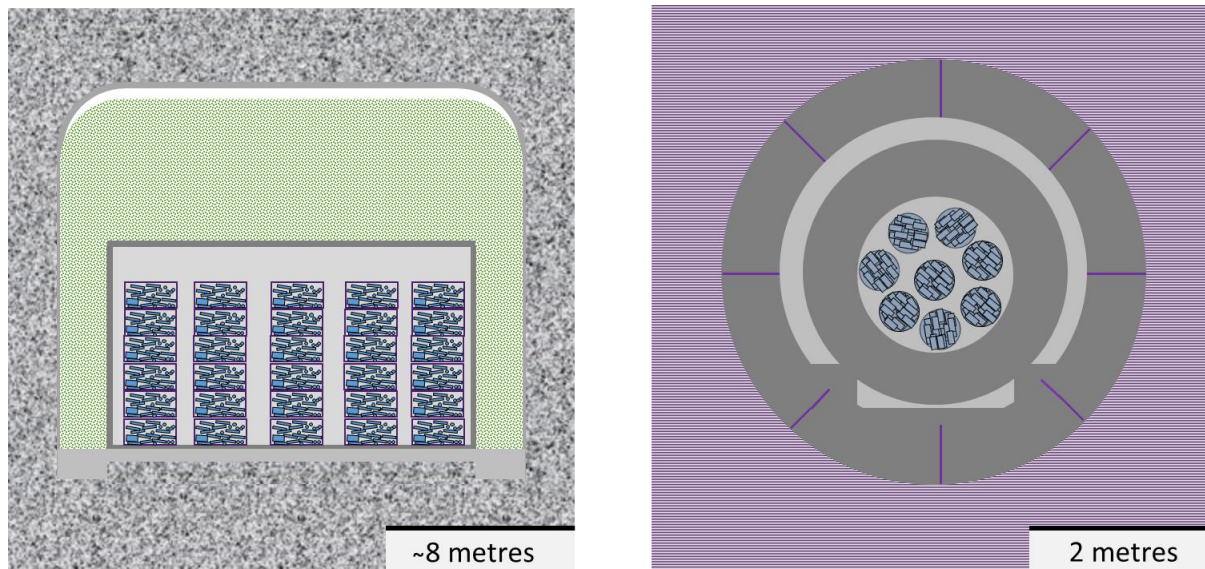


Figure 5-1: Abstracted disposal cells containing cemented metallic ILW considered in Europe for the host rocks: granite (left) and poorly indurated clay (right). Blue = metallic ILW in tetramoulds left, in CSD-C's right, concrete shielding and support (grey), grout = light grey, washed granitic rock = green.

Zircaloy and steel at relevant disposal conditions have been studied in the 7<sup>th</sup> framework programme Carbon-14 Source Term (CaST). The passivating oxide layers found after irradiation in a nuclear power plant and preserved in cementitious materials have a large impact on the corrosion rate since the corrosion process is bounded by an equilibrium between diffusion of water through the oxide layer and dissolution at the solid-liquid interface. Many corrosion experiments are performed with rinsed metallic specimens [e.g. Fusjisama, 1997; Smart, 2017] in which the presence of any oxide layer at start of the experiment has been removed. Consequently, the initial corrosion rates are larger than the long-term corrosion rates at which a passivating metallic oxide layer has become present during the corrosion experiment. The long-term corrosion rates may be more representative for steel ILW since the metallic surface of scrap metal is not expected to be rinsed before processing this waste with cementitious material. CSD-C's are expected to contain metals of which the oxide layer that is formed in the nuclear plant, is damaged due to cutting, shearing and high compaction.

Hydrogen is not released to the surrounding at every anaerobic corroding metallic surface. The hydrogen generated by anaerobic corrosion of Zircaloy is picked up for the formation of a zirconium-hydride. The Japanese studies measured a hydrogen pick-up of at least 90% at 30 degrees Celsius when Zircaloy is exposed to alkaline water as well as pure water. The hydrogen pick-up decreases with increasing temperature [Sakuragi, 2017]. Hydride formation for zirconium, vanadium and titanium has been known for decades and is thermodynamically understood [Lacher, 1937]. An underestimation of the corrosion rate would be measured by measuring the released zirconium due to the small solubility product of zirconia. The Zircaloy corrosion rates from measured adsorbed and released hydrogen are as low as the corrosion rates determined from released non-radioactive nickel and chromium: below 1 nm per year. [Necib, 2018]. With such small corrosion rates, long-lived radionuclides such as carbon-14 may therefore decay within this waste form and not released to the encapsulation, the cementitious material, provided that the Zircaloy surface remains exposed to alkaline conditions. The corrosion rate

can suddenly be increased when the Zircaloy claddings are exposed to  $\text{CaCl}_2$  solutions with a concentration higher than 0.05 M due to the formation of a ternary complex  $\text{Ca}_3[\text{Zr}(\text{OH})_6]^{4+}$  [Gras, 2014]. These concentrations of calcium and chlorine are possible by ingress of chlorine in concrete. This sudden increase in corrosion rate can be excluded by choosing the waste packaging material on the chemical understanding of the disposal environment.

The hydrogen pick-up for steel, aluminium and zinc is negligible; hydrogen is endothermically dissolved in these metals. An upper limit for corrosion of stainless steel during anaerobic corrosion at alkaline conditions is 0.01  $\mu\text{m}$  per year due to the presence of the passivated oxide layer [Mibus, 2018]. The higher corrosion resistance for stainless steel compared to carbon steel in a nuclear plant is the formation of chromite. The following figure shows the Pourbaix diagrams for stainless steel showing the passivated oxide layer is chromite and not magnetite as shown in Figure 4-3.

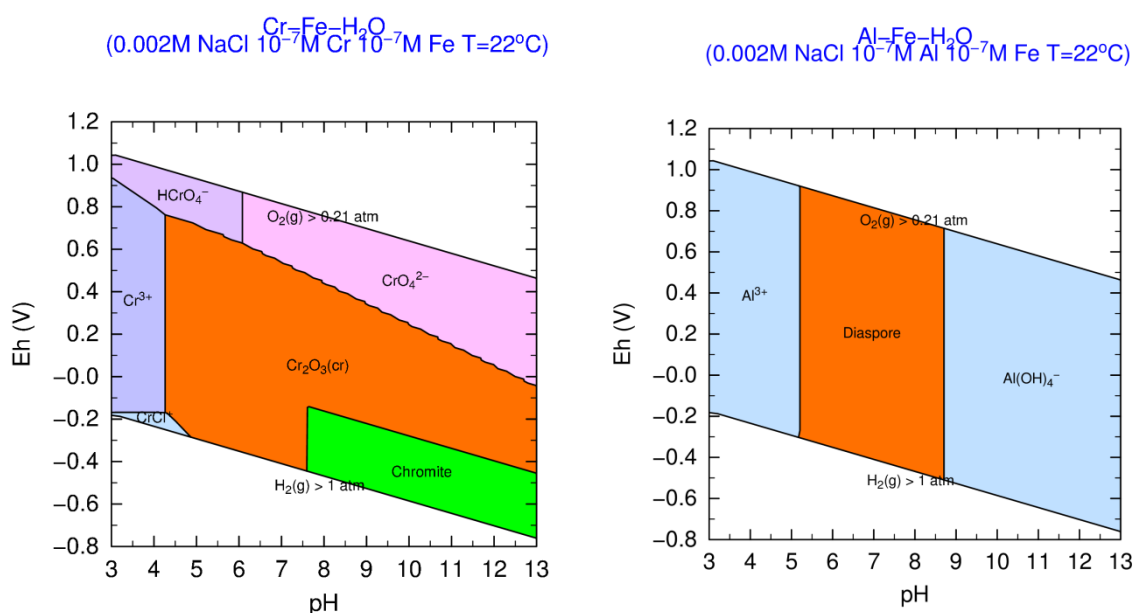


Figure 5-2: Pourbaix diagrams at 22 °C for the systems Fe-Cr-H<sub>2</sub>O and Al-H<sub>2</sub>O with an activity of iron, chromium and aluminium dissolved species of 10<sup>-7</sup> M; 0.002 M NaCl is a reasonable concentration for tap water. Chromite (green) is  $\text{FeCrO}_4(\text{s})$ .<sup>5</sup>

A passivated oxide layer is thermodynamically not present at high pH for zinc and aluminium (see above figure) with the chosen components. The corrosion rates can be large at high pH but it depends on the chemical composition whether or not a film is formed. For example, a sufficient supply of calcium and sufficient slow removal of calcium from a corroding aluminium surface allows the formation of an Al-Ca complex that suppresses corrosion. The initial corrosion rate of 20 mm per year may then reduce till 0.01 and 0.001 mm per year [Fujisama, 1997]. These long-term rates are however still 100 till 1000 times larger than the long-term corrosion rates found for stainless steel. Aluminium waste processing with cementitious materials usually results in too high gas generation rates when the reactive surface area is large. A waste product with a sufficient quality for e.g. safe stacking of waste packages and other mechanical loads cannot be generated when this gas formation occurs.  $\text{LiNO}_3$  is then added to the cementitious solution in order to form an insoluble Li-Al film during the cement solidification [Matsuo, 1996].

<sup>5</sup> These figures have also been made with Phreeplot and SIT database.

## 5.2 Organic waste

Organic waste can be spent ion exchange resins, plastics, rubbers and cellulose e.g. paper and clothing. The degradation studies are focussed on whether organic complexing agents for radionuclides can be formed.

Disposal of spent ion exchange resins have been studied in the 7<sup>th</sup> framework programmes CaST and also in this programme, a chemical degradation rate of resins representative for disposal conditions did not become available. Chemical degradation of organic materials can be initiated by a nucleophilic attack of OH<sup>-</sup> ions on a carbon atom with a partial positive charge. Such carbon atoms are generally not present in polystyrene, the basic material for ion exchange resins [Van Loon, 1995]. The resins may swell by uptake of water and fracture the surrounding cementitious material. A maximum amount of 20 vol% is therefore recommended to prevent crack formation due to the swelling pressure of resins [Matsuda, 1992]. No organic degradation products are considered in the Swedish programme due to the high chemical resistance of these resins, also at cementitious conditions.

The information of the other types of organic waste has been taken from the Swedish programme [SKB, 2015; SKB, 2014b]. Plastics are usually resistant towards degradation, but degradation highly depends on their size. Rubbers are less degradable than plastics. Most of the known degradation products of plastics and rubber e.g. hydrogen, hydrogen chloride, have no significant complexing ability and can therefore be ignored.

At high pH and a Ca<sup>2+</sup> rich environment, cellulose will degrade to shorter chained organic compounds. The organic acids released are two types of iso-saccharinic acids (ISAs) that experimentally been measured in leachates from the degradation of cellulose in the presence of different cement types [SKB, 2015]. ISAs are organic complexing agents.

All organic complexing agents are present as the anionic compound of acids. There are several mechanisms in cementitious materials to limit the transport of these organic complexing agents to the surroundings. The high pH and high calcium concentrations in cementitious materials reduce the concentration of some organic complexing agents such as oxalate and ISA due to precipitation of salts [SKB, 2015, p.154]. This precipitation provides a sink for dissolved calcium by which cementitious minerals are dissolved at the expense of precipitation of these salts. At a pH larger than 11.8, these anionic compounds can be sorbed on positively charged minerals [Poiteau, 2008] [Wieland, 2016]. The connecting pore throat for many intact concrete types can be so small that diffusion is allowed to be assumed and ultrafiltration of complexing agents as large as ISAs takes place. Other organic degradation products are not charged but can have an impact on the changing rate of the chemical and physical properties of concrete such as CO<sub>2</sub>. The generated CO<sub>2</sub> will react with cementitious minerals to form calcite and the cementitious minerals need to buffer the associated hydroxonium ions upon dissolution of CO<sub>2</sub> in concrete pore water. The ingress and egress of diffusional species from the host rocks also has an impact on the changing rate of these properties of concrete; this rate is expected to be smaller in disposal facilities hosted in clay than in crystalline rocks due to the diffusional transport regime in clay compared to the advective transport in crystalline host rocks.

## 6. Belgium

SCK•CEN - Eef Weetjens

### 6.1 Characterization of the HLW disposal cell in clay

#### 6.1.1 Description of materials in disposal cell

In Belgium, the concept of geological disposal in clay formations is studied for more than 40 years as a reference option for the long-term management of both category B (LILW-LL) and category C (HLW) waste. In absence of a policy decision, the waste management organisation NIRAS/ONDRAF proposes disposal in a concrete-based repository located at a depth between 200 m and 600 m in a poorly indurated clay formation. The national geological disposal programme can thus be considered to be in the conceptualisation stage.

For disposal of vitrified HLW, the so-called ‘supercontainer concept’ is considered [ONDRAF/NIRAS, 2017a]. A supercontainer is a prefabricated cylindrical concrete container in which a carbon steel overpack containing the HLW can be inserted, forming as such a shielded disposal waste package (*Figure 6-1*). In the case of vitrified HLW, such a supercontainer can accommodate two CSD-V<sup>6</sup> canisters, one after the other.

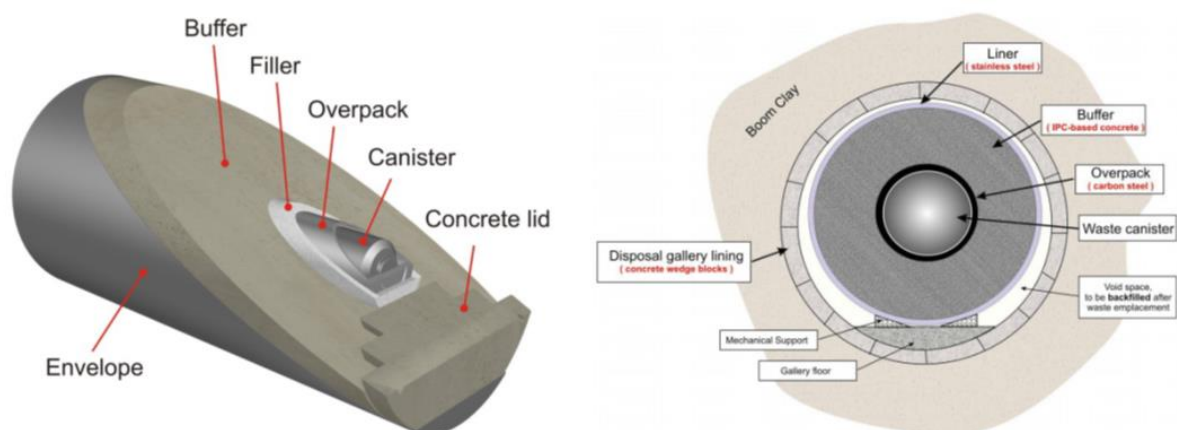


*Figure 6-1: Supercontainer type SC-1 for vitrified HLW (left) and indicative figure of a disposal gallery cross-section in Boom clay host rock (right, dimensions not to scale).*

This disposal concept was developed in order to meet a number of high-level requirements, that are derived from both operational and long-term safety considerations. A key feature of the supercontainer concept is that the concrete made from Ordinary Portland Cement (OPC) should buffer the pH at high values for as long as possible (at least during the thermal phase) in order to keep the carbon steel overpack passivated and thereby limit corrosion. Passivation occurs at  $\text{pH} > 9.5 - 10.5$ .

The materials and interfaces in such a disposal cell are depicted schematically in *Figure 6-2*. For each of the considered components, the materials and dimensions, the role in the safety concept and possible additional requirements are briefly described in *Table 6-1* (for as far as information is available at this stage).

<sup>6</sup> CSD-V: ‘Conteneur Standard de Déchets Vitrifiés’, the standard canister for vitrified waste that is the product of reprocessing at the ORANO facilities at La Hague, France.

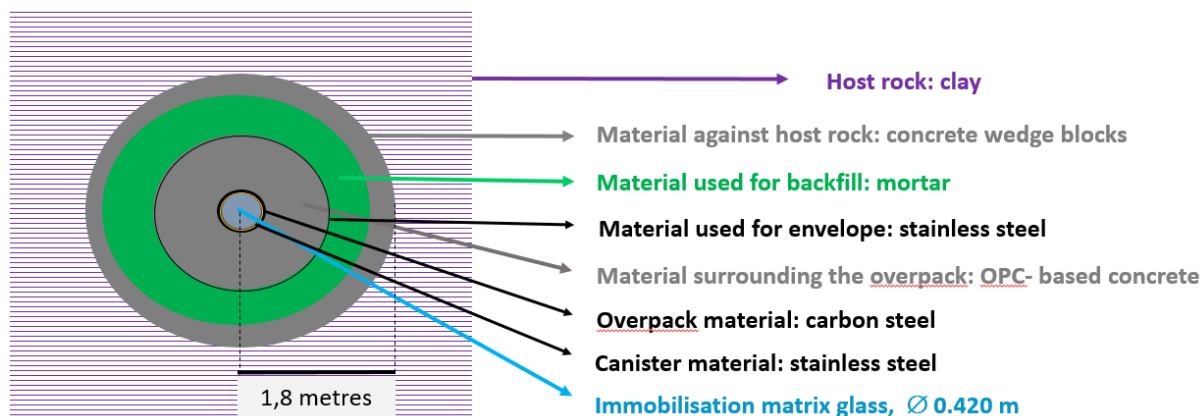


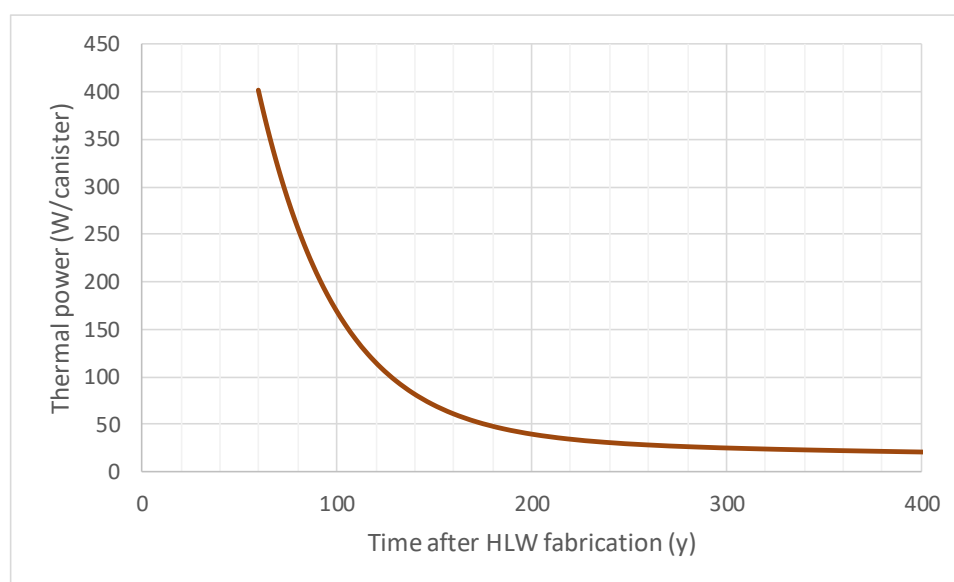
Figure 6-2: Materials and interfaces in a disposal cell for HLW according to the Belgian disposal design. Note that the reference inner diameter for a disposal gallery recently increased from 3.0 m to 3.5 m, which would increase the outer radius to 2.05 instead of 1.8 m [ONDRAF/NIRAS, 2019].

Table 6-1: Characteristics and role of the components in a disposal cell for HLW according to the Belgian disposal design and safety concept. Information taken from [ONDRAF/NIRAS 2017a,b, von Lensa et al. 2008].

Component	material	dimensions	Role in the safety concept and design criteria (if relevant/available)
Clay host formation	Host formation and site dependent	Host formation and site dependent	<ul style="list-style-type: none"> <li>Both physical (thickness and depth, low permeable) and chemical (retention) barrier</li> <li>Fast self-sealing properties to limit excavation disturbed zone</li> </ul>
Disposal gallery lining	Concrete wedge blocks	30 cm thick	<ul style="list-style-type: none"> <li>Provide mechanical stability and limit clay convergence</li> <li>Material compatibility with EBS and host rock</li> </ul>
Backfill	Mortar	48 – 74 cm thick	<ul style="list-style-type: none"> <li>Minimise void spaces</li> <li>Material compatibility with EBS and host rock</li> </ul>
Envelope	Stainless steel (AISI 316 LhMo)	0.6 cm thick	<ul style="list-style-type: none"> <li>Provide mechanical strength and confinement during transport and handling</li> <li>Prevent ingress of aggressive species (salts) that potentially build up at the clay/concrete interface during the operational phase</li> <li>Facilitate retrievability</li> </ul>
Supercontainer buffer	OPC concrete: CEM I/42.5N HSR LA, W/C = 0.5, limestone aggregate	Ø 2.132 m, radial thickness 75 cm, top thickness 60 cm; bottom thickness 69 cm	<ul style="list-style-type: none"> <li>Provide shielding during underground operations</li> <li>Limit corrosion of the overpack by establishing a highly alkaline environment</li> <li>To some extent provide additional, and sometimes complementary, sorption to the clay host formation</li> </ul>

			<ul style="list-style-type: none"> <li>•</li> </ul>
Overpack	P355 QL2 grade carbon steel <sup>7</sup> according to EN 10028-6	Outer Ø 0.532 m, radial thickness 3 cm; top and bottom thickness 6 cm; length 2.725 m	<ul style="list-style-type: none"> <li>• Provide the main barrier to radionuclide release during the thermal phase: exhibit good resistance to localized corrosion and an acceptable general corrosion rate</li> </ul>
Gap		2.1 cm	
Canister	AISI 309 grade stainless steel (C: 0.15%; Cr: 24%; Ni: 13%)	Outer Ø 0.43 m, thickness 0.5 cm	
HLW Waste form	R7T7 borosilicate glass	Ø 0.42 m; length 1.338 m	<ul style="list-style-type: none"> <li>• Leaching resistance</li> </ul>

The decay of some radionuclides in the HLW will generate significant amounts of heat during hundreds of years. Even after a cooling period of 60 years before disposal, the thermal power of a HLW canister would still be in the order of 400 W (see *Figure 6-3* for the thermal power of a vitrified waste canister as function of time). Note that this is dependent on factors with respect to the reprocessed fuel (e.g. type, burn-up) and vitrification technology (e.g. waste loading)



*Figure 6-3:* Thermal power evolution of a HLW canister (the figure corresponds to a loading of 1.33 tHM/canister from the reprocessing of spent fuel with a burn-up of 33 GWd/tHM. More details in paragraph 2.1 of [Sillen and Marivoet, 2007].

<sup>7</sup> Commercial name: CarElso 70 SOHIC

The temperature of the virgin host formation is function of type and depth. Assuming disposal at the midplane of the Boom Clay layer in Mol at ~230 m depth<sup>8</sup>, the temperature of the virgin clay material would be about 16°C.

### 6.1.2 Thermal gradients / Thermal and hydraulic gradients

A number of temperature calculations in the near and far field of a supercontainer-type HLW disposal cell in Boom Clay have been performed and reported (e.g., as reported in [Weetjens and Sillen 2005, Weetjens 2009, Sillen and Marivoet 2007]). In the near field of a backfilled repository, heat transport is generally limited to conduction. For a two-dimensional radial (axisymmetric) geometry, and assuming constant parameters, the governing equation can be written as:

$$\frac{\partial T}{\partial t} = \frac{\partial}{\partial r} \left( \frac{\lambda}{\rho c_p} \frac{\partial T}{\partial r} \right) + \frac{1}{r} \frac{\partial T}{\partial r}$$

where  $\lambda$  (W/(m·K)) is the thermal conductivity of the medium,  $\rho$  (kg/m<sup>3</sup>) is the bulk density of the medium and  $c_p$  (J/(kg·K)) is the specific heat capacity of the medium. Indicative values for the thermal parameters of the components in a HLW disposal cell are given in *Table 6-2*, together with their source. The model geometry is schematically depicted in *Figure 6-4*. All boundaries are no heat flux boundaries (symmetry) except the outer radial boundary, which is chosen far enough (continuity) not to influence the outcome of calculated near field temperatures for the first hundreds of years. The additional temperature increase due to a neighbouring gallery (at 50 m distance) was calculated separately and is in the order of 3°C after 50 years and almost 4°C after 100 years [Weetjens and Sillen, 2005].

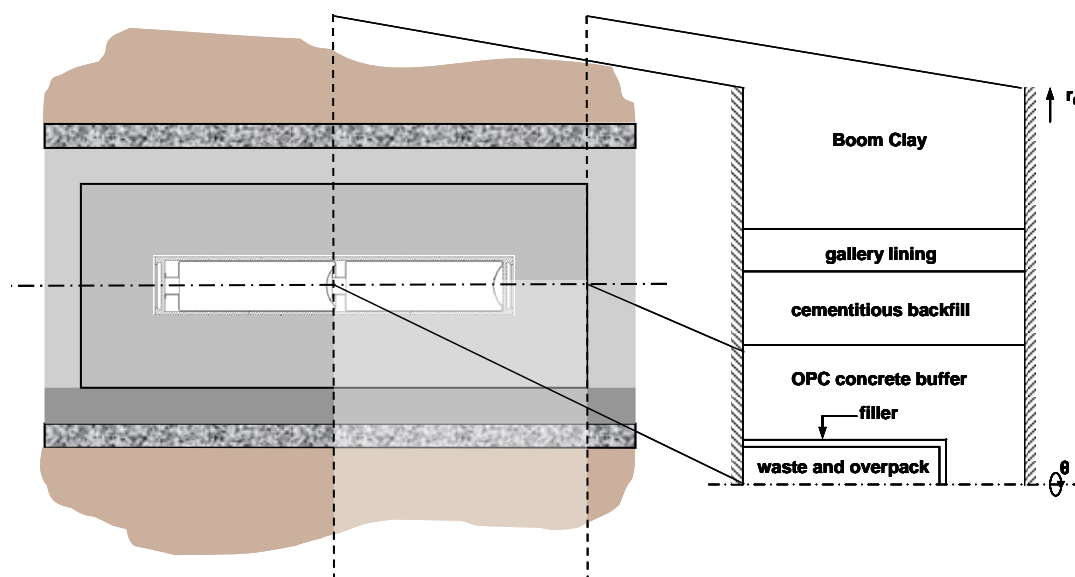


Figure 6-4: Model geometry: only half of a supercontainer needs to be modelled for symmetry reasons.

<sup>8</sup> This was the reference site for methodological studies in past decades.

The results in terms of radial temperature profiles and temperature evolution at the interfaces are given in Figure 6-5 and Figure 6-6.

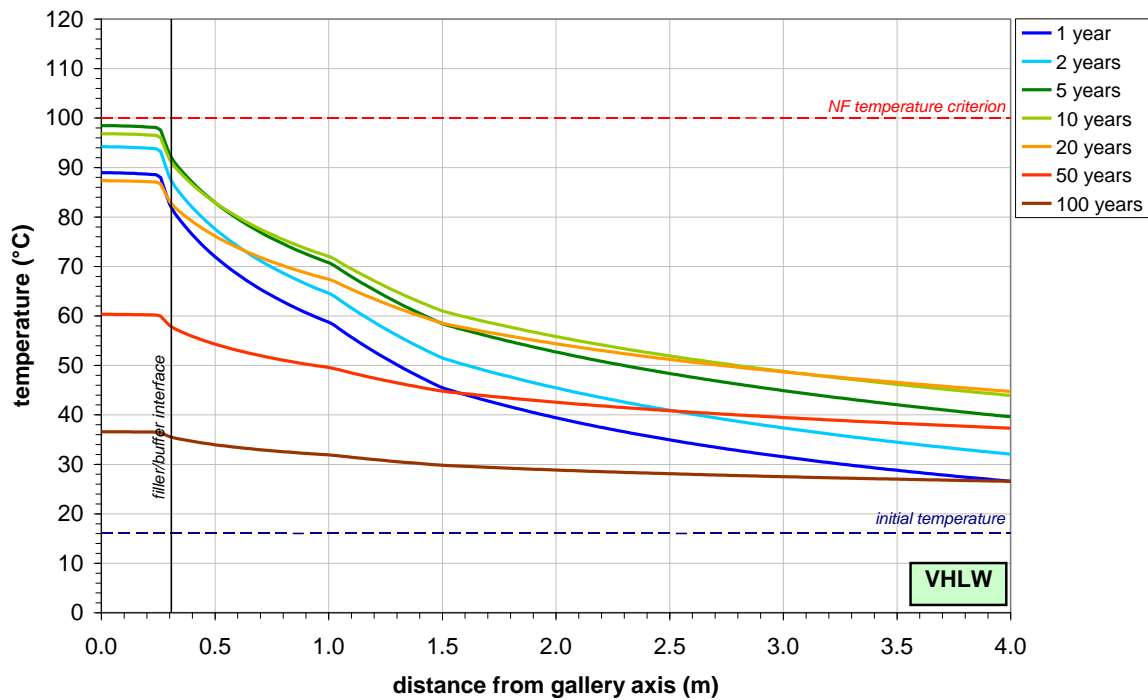


Figure 6-5: Near field temperature profiles for disposal of vitrified HLW in a supercontainer-based repository (cooling time: 60 years)

Table 6-2: Description of parameters for thermal gradients

Feature	Examples of parameter	Value and unit	Source	Justification / comments
Heat source	Thermal power as a function of time	See Figure 6-3	[Sillen and Marivoet 2007]	
Heat volume	Volume of heat source	150 l	[von Lensa et al. 2008]	Volume of vitrified waste inside a canister
Waste form glass	Heat conductivity	NA		Thermal properties of waste form are not taken into account as it is assumed that at the time of disposal the heat is uniformly distributed inside the overpack.
	Specific density	NA		
	Specific heat capacity	NA		
Air gap	Thermal conductivity	NA		See above. Possibly the gap will be filled with glass frit in order to saturate the interface in Si and slow down glass dissolution.
	Specific density	NA		
	Specific heat capacity	NA		
Overpack	Thermal conductivity	40 W/(m·K)	[Weetjens 2009]	
	Specific density	7850 kg/m <sup>3</sup>	[Craeye et al 2009]	
	Specific heat capacity	500 J/(kg·K)		
Supercontainer buffer (self-compacting concrete)	Thermal conductivity	1.89 W/(m·K)		
	Specific density	NA		Lumped in volumetric heat capacity
	Specific heat capacity	2.42x10 <sup>6</sup> J/(m <sup>3</sup> ·K)		Volumetric value
Backfill / filler	Thermal conductivity	1 W/(m·K)		
	Specific density	2400 kg/m <sup>3</sup>		

EURAD Deliverable 2.4 – Treatment of chemical evolutions in national programmes

	Specific heat capacity	880 J/(kg·K)	
Host rock	Thermal conductivity	1.45 W/(m·K)	In a 2D axisymmetric geometry, the average value is used of horizontal (1.7 W/(m·K)) and vertical (1.25 W/(m·K)) thermal conductivity of Boom Clay
	Specific density	NA	Lumped in volumetric heat capacity
	Specific heat capacity	2.9x10 <sup>6</sup> J/(m <sup>3</sup> ·K)	Volumetric value
	Temperature	16°C	At Boom Clay midplane

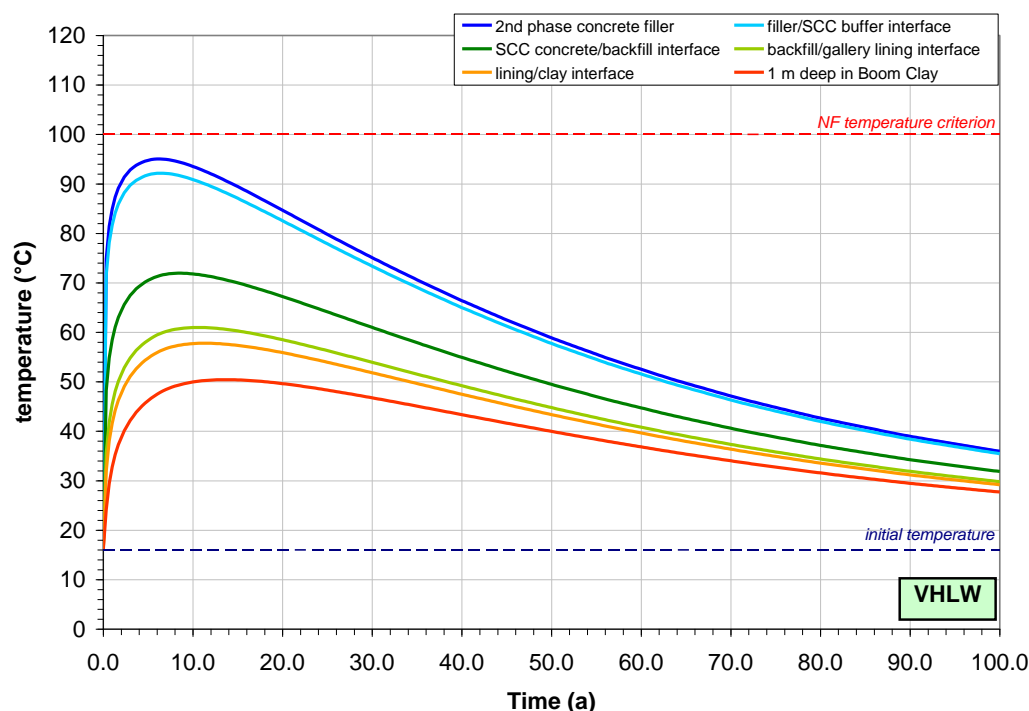


Figure 6-6: Temperature evolution at different interfaces in the near field of a disposal gallery filled with vitrified HLW (cooling time: 60 years)

During the excavation of the disposal gallery and shaft, a fracture zone is inevitably formed in the first meter of Boom Clay around the gallery as a result of the mechanical failure caused by stress redistribution. Beyond this fracture zone, an eye-shaped damaged zone with enhanced hydraulic conductivity due to effective stress variation is observed around the gallery into the Boom Clay up to 1.25-1.7 times the gallery diameter. The increase in hydraulic conductivity in the damaged zone is limited to one order of magnitude [Yu et al 2011], thus roughly from  $\sim 10^{-12}$  m/s to  $\sim 10^{-11}$  m/s.

During the operational phase, ventilation of the repository induces limited desiccation in the clay formation close to the tunnel wall. However, the repository tunnels will be backfilled and closed soon after waste emplacement and the disposal galleries will become saturated with pore water fairly rapidly (within a few decades). Pressure equilibration of the repository's porous materials to in situ hydrostatic pressure (about 23 bar at 230 m depth) proceeds more slowly, but equilibrium is assumed to be reached after a century [Weetjens et al 2006].

### 6.1.3 Pore water compositions

As the Belgian disposal concept is essentially a concrete-clay concept, the initial pore water compositions in equilibrium with concrete and clay and their interaction will largely determine the evolution of chemical gradients in the near field. Main equilibrium characteristics are given in Figure 6-7. More details about pore water compositions can be found in e.g. [De Craen 2004] (Boom Clay), [Wang 2009] and [Wang et al. 2010] (Supercontainer concrete).

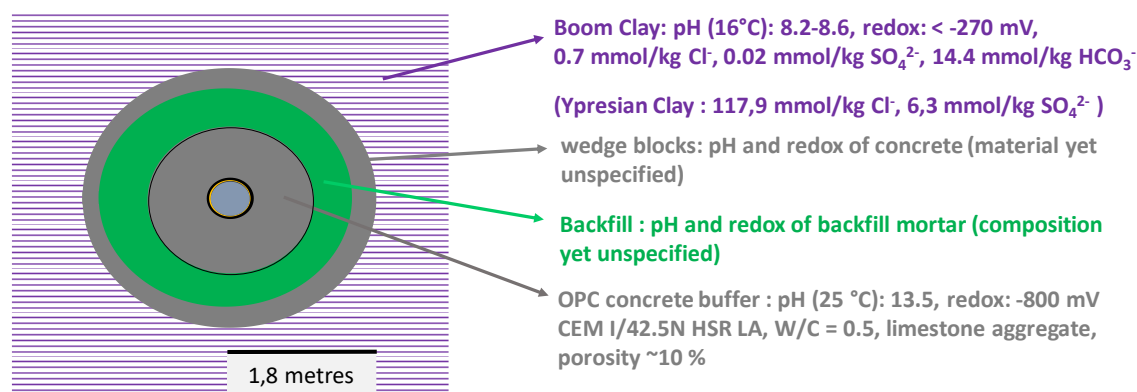


Figure 6-7: Main chemical characteristics of concrete (engineered barriers) and clay (host formation) pore waters in a HLW disposal cell

## 6.2 Chemical evolution of the HLW disposal cell

### 6.2.1 Narrative

A realistic analysis and the demonstration of an adequate level of understanding of the evolution of the disposal system in general are essential parts of the safety assessment. The chemical evolution in particular is of key importance as it will determine the solubility and speciation, and hence release and mobility of radionuclides in the repository near field.

Prior to repository construction, the ground water at the repository location is assumed to be in equilibrium with the clay mineralogy. In case of Boom Clay, a silty clay or argillaceous silt with pyrite and variable carbonate and organic matter contents, the more reactive mineralogical components are calcite, siderite and pyrite, which will control the concentrations of dissolved calcium and iron, and the redox potential of the pore water. The equilibrium pore water can be considered as a dilute NaHCO<sub>3</sub> solution with relatively high concentration of organic matter, a pH of ~8.2-8.6 and a redox potential (Eh) of about -270 mV/SHE (see 6.1.3).

#### 6.2.1.1 Chemical evolution from repository closure to overpack failure

The excavation of the galleries and the introduction of cementitious materials introduce large chemical gradients in the repository near field. Furthermore, the equilibrium state of geochemical reactions varies with temperature, as do reaction rates. Elevated temperatures increase the solubility of most solids (with carbonates and sulphates and cement minerals as portlandite as exception), decrease the solubility of most gases and increase reaction rates. For the expected temperature gradients, see 6.1.2.

With respect to the **clay pore water**, two relatively short-term processes might have an influence in the near field: oxidation of clay minerals due to the excavation and ventilation of galleries, and production of CO<sub>2</sub> from Boom Clay kerogen under thermal stress. These processes are reported in detail in [De Craen et al. 2011] and [Bruggeman and De Craen 2012] respectively, and only main conclusions are briefly captured in the paragraphs below.

During excavation of the clay and operation of the repository oxidation effects are unavoidable. Boom Clay is very sensitive to oxidation because of the presence of pyrite and organic matter. Pyrite oxidation leads to release of H<sup>+</sup>, affecting the pH of the clay. Moreover, the production of sulphates and intermediate thiosulphates may be directly or indirectly detrimental to steel components: in the presence of sulphate reducing bacteria (SRB), these sulphates may be converted back to sulphides, which in turn could intensify corrosion of steel. It has been demonstrated that oxidation of pyrite is limited to the fracture surfaces in the excavation disturbed zone (EDZ). Ventilation of the galleries, and in-diffusion of

dissolved oxygen, will not lead to additional pyrite oxidation. Therefore, oxidation is believed to be limited to a zone of about 1 m around the disposal galleries [De Craen et al 2011].

Compared to other argillaceous formations studied in the European context of geological disposal of radioactive waste, the Boom Clay contains substantial amounts of low-maturity organic matter (TOC content of 1 to 5% [De Craen 2009]), distributed between the liquid and the solid phase. A very small fraction (~0.05%) of the total organic matter content is in solution and is considered to be mobile. In a porous medium such as Boom Clay, the mobility of organic species in solution also depends on their molecular size, the largest molecules being immobilised in the pores by ultrafiltration [Durce et al 2018]. The cut-off equivalent to ultrafiltration is estimated to be  $3 \times 10^5$  Da or about 20 nm. In the current phenomenological models it is assumed that all dissolved organic matter molecules smaller than this cut-off are potentially mobile and will not be filtered out by the Boom Clay. Furthermore, all mobile dissolved organic matter (DOM) is considered to show sufficiently similar characteristics and can thus be regarded as one homogeneous pool.

The composition and fractionation of the Boom Clay organic matter may be affected by thermal stress. The thermal gradient associated with the disposal of vitrified HLW is considered to result mainly in the dissociation of carboxylic functional groups, leading to a release of  $\text{CO}_2(\text{g})$ . In turn, this  $\text{CO}_2$  leads to a decrease of pH (acidification) and dissolution of carbonate minerals (by  $\text{H}_2\text{CO}_3$ ) [Weetjens et al 2012].

The foreseen thermal gradient is not assumed to result in a substantial cracking of the *solid* organic matter pool. On the other hand, the alkaline plume and oxidation processes occurring in the near field considered would mainly have an impact on the solid organic matter composition and would likely result in a local increase of the dissolved organic matter concentration [Bruggeman and De Craen 2012].

Inside the disposal galleries, and prior to overpack failure, the **concrete pore water** is largely determined by the slow degradation of concrete phases by the Boom clay pore water. The following evolution is expected:

- Stage 1: a pH around 13.5, controlled by the dissolved alkalis (Na and K)
- Stage 2: characterised by a pH of 12.5, controlled by the solubility of portlandite ( $\text{Ca}(\text{OH})_2$ )
- Stage 3: a pH between 12.5 and 10.5, regulated by the equilibrium of C-S-H phases with the in-diffusion of clay pore water solutes
- Stage 4: the final stage is characterised by a pH lower than 10.5 but higher than 8.5, buffered by calcite ( $\text{CaCO}_3$ )

All pH values mentioned are for 25°C.

Concrete degradation is diffusion controlled, and is expected to occur extremely slowly. For the supercontainer concrete, the first two stages will be dominant in the considered assessment time frame of one million years, although stage 3 cannot be ruled out. The concrete buffer is not expected to reach stage 4 in the considered assessment timeframe, based on conservative geochemical calculations (see 6.2.2.1).

#### 6.2.1.2 Chemical evolution post overpack failure

Three broad causes for overpack failure are possible: (i) a pH lower than 10 when the concrete has evolved to stage 3, (ii) loss of integrity due to mechanical stresses (early canister failure), and (iii) when aggressive species (chloride, thiosulphate) reaches critical concentrations. They do not have all the same probability and may have different consequences for the chemical evolution.

After the overpack failure, concrete pore water will fill up the gap between the overpack and the stainless steel canister containing the waste glass. The canister wall will prevent contact of the concrete pore water with the waste glass for another period of time, depending on the composition of the concrete pore water (for the concrete pore water evolution, see Section 6.2.1.1). Ultimately, the canister wall will also be perforated, first locally and then more generally, and the glass will come in contact with the concrete pore water. The composition of the pore water at that time depends on the cause of the failure.

#### Early canister failure due to mechanical stresses

In case of some early canister failure (due to mechanical stresses), the composition of this water is assumed to be the same as the composition of the pore water in the concrete buffer (high pH, stage I or II water), although it may be affected by the contact with the overpack/canister steel and corrosion products.

The overpack will be covered by a layer of steel corrosion products, but the thickness of this layer at the time of perforation is not known. In this condition, the layer of steel corrosion products and corroding steel is considered as a purely physical barrier separating the glass and the concrete buffer, with negligible chemical effects on its environment. Hydrogen gas will be generated by anaerobic corrosion inside the glass canister, and may slow down the intrusion of water if the generation rate exceeds the rate of transport towards the near field. Alpha-radiolysis of the water inside the canister will also generate hydrogen and oxygen gas, which may have a similar effect.

Upon contact of the glass surface with the high pH concrete pore water, the glass matrix will start to dissolve and release the confined radionuclides. The exact dissolution rate will depend on the composition of the pore water. The dissolution of the glass will locally modify the composition of this pore water. Calcium, potassium and sodium from the pore water will be incorporated in the glass alteration layer and secondary phases formed on the glass surface. The hydrolysis of the silica network with the release of weak acids (silicic acid, boric acid) will cause a pH decrease. Precipitation of secondary phases can accelerate or slow down the pH decrease, depending on the type of phases that is formed. The dissolved glass layers will be replaced by a growing alteration layer. This layer, and the secondary phases it includes (phyllosilicates or zeolites), will adsorb part of the radionuclides released from the initial silica matrix.

Some surfaces of the glass may temporarily be in contact with water vapour only. This can locally condensate and form a water film on the glass. The pH of this water film will increase by ion exchange (mainly release of  $\text{Na}^+$  from the glass, accompanied by an increase of the  $\text{OH}^-$  concentration), and thus also favour silica network dissolution and secondary phase formation.

Because local saturation is reached much faster in narrow fissures in the glass due to the higher local glass surface/contacting solution volume (S/V) ratio, these fissures are expected to become less accessible for pore water soon by the precipitation of secondary phases. This will slow down the dissolution of these glass surfaces.

More in general, in confined areas inside the canister with little water (or solute) renewal, the dissolution rate will soon decrease by several orders of magnitude, compared to the dissolution rate at first contact with stage 1 concrete pore water. The longer-term evolution of the glass will depend on the rate of transport of concrete components towards the glass, and of glass components towards the concrete.

Silicic acid released by the glass will react with Ca released by the portlandite to form calcium silicate hydrate phases (C-S-H) that may also incorporate aluminium from the glass (C-A-S-H). These reactions trigger the dissolution of the silica matrix and slow down the decrease of the dissolution rate. Si from the glass can also react with C-S-H phases in the concrete to form C-S-H phases with low Ca/Si ratios, which may also have a triggering effect.

By these reactions, the portlandite in the concrete close to the glass will dissolve and reprecipitate as C-(A)-S-H phases. Because the overpack/canister/glass system contains some cavities that will initially be filled with pore water, it is expected that these cavities will gradually be filled with the precipitating phases, while the porosity of the first layer of concrete may increase because of the dissolution of the portlandite.

The resulting altered near-field system will constitute a transport barrier isolating the glass from the unreacted concrete. Transport through this barrier will be mainly diffusion controlled. The composition of the water in contact with the glass will at this stage be different from the composition of the pore water in the concrete buffer, depending on the effectiveness of the transport barrier. As a result of the buffering capacity of the glass, the composition of the water in contact with the glass, will be less aggressive towards the glass (lower pH, higher Si concentrations, lower Ca concentrations).

On the long-term, the surface area of the glass exposed to water will change. Remaining stresses in the glass block may cause stress corrosion cracking, increasing the surface area. The dissolution of the glass fragments will decrease the surface area. The micro-surface area of the glass will increase by local preferential dissolution, or decrease because it is covered by a precipitation layer. The net effect of all these processes on the evolution of the surface area cannot be quantified sufficiently well. The change of glass surface area will change the local S/V ratio, which will further change the glass dissolution rate; it has been reported that glass dissolution rate decreases with increasing S/V ratio. The application of an experimental parameter like S/V to the real disposal situation is not evident, though. Because the tests at high S/V are representative of the more advanced reaction progress, they are more representative of the later stages of dissolution also in a real disposal situation.

### **Early canister failure due to aggressive species**

There is a large uncertainty on the composition of the pore water composition and the composition of the buffer, mainly because the time of failure due to aggressive species is very uncertain. As a consequence, the pore water of the concrete in contact with the canister can be in any stage between stage 1 and 3. If the composition is close to stage 1 and 2, the chemical processes will be similar to those described in “early canister failure due to mechanical stresses”. When it is close to stage 3, the chemical processes are described in “canister failure due to pH decrease”

### **Canister failure due to pH decrease**

The pore water composition will be in equilibrium with concrete in stage 3 thus without portlandite and may include also elements from the canister, overpack and corrosion products. The dissolution of the glass will locally modify the composition of this pore water, but because the conditions are less aggressive towards the glass, the glass will dissolve at a lower rate.

## 6.2.2 Conceptual model.

### 6.2.2.1 Chemical evolution from repository closure to overpack failure

For this timeframe, geochemical modelling efforts in past decades primarily focused on the pH evolution as function of concrete-clay interactions. Especially the pH evolution at the interface with the carbon steel overpack is of interest, as this forms the fundamental argumentation for the safety function “engineered containment” in the safety concept.

The conceptual model is usually simplified into geochemical equilibrium calculations taking into account diffusive transport in a 1D radial geometry. Two variant approaches are reported in detail in [Wang 2009] and [Wang et al 2010]. In [Wang 2009], a conservative assessment is done of the timescale of pH decrease as a result of contact with Boom Clay pore water. Boom Clay is modelled as a fixed boundary condition in this model, thereby neglecting transport limitations in the clay. Results in terms of pH evolution at the carbon steel-concrete interface (overpack) and the concrete-stainless-steel interface (envelope) are provided in *Figure 6-8*. This shows that it is expected that it takes a minima 80 000 years before the pH starts to drop at the overpack interface.

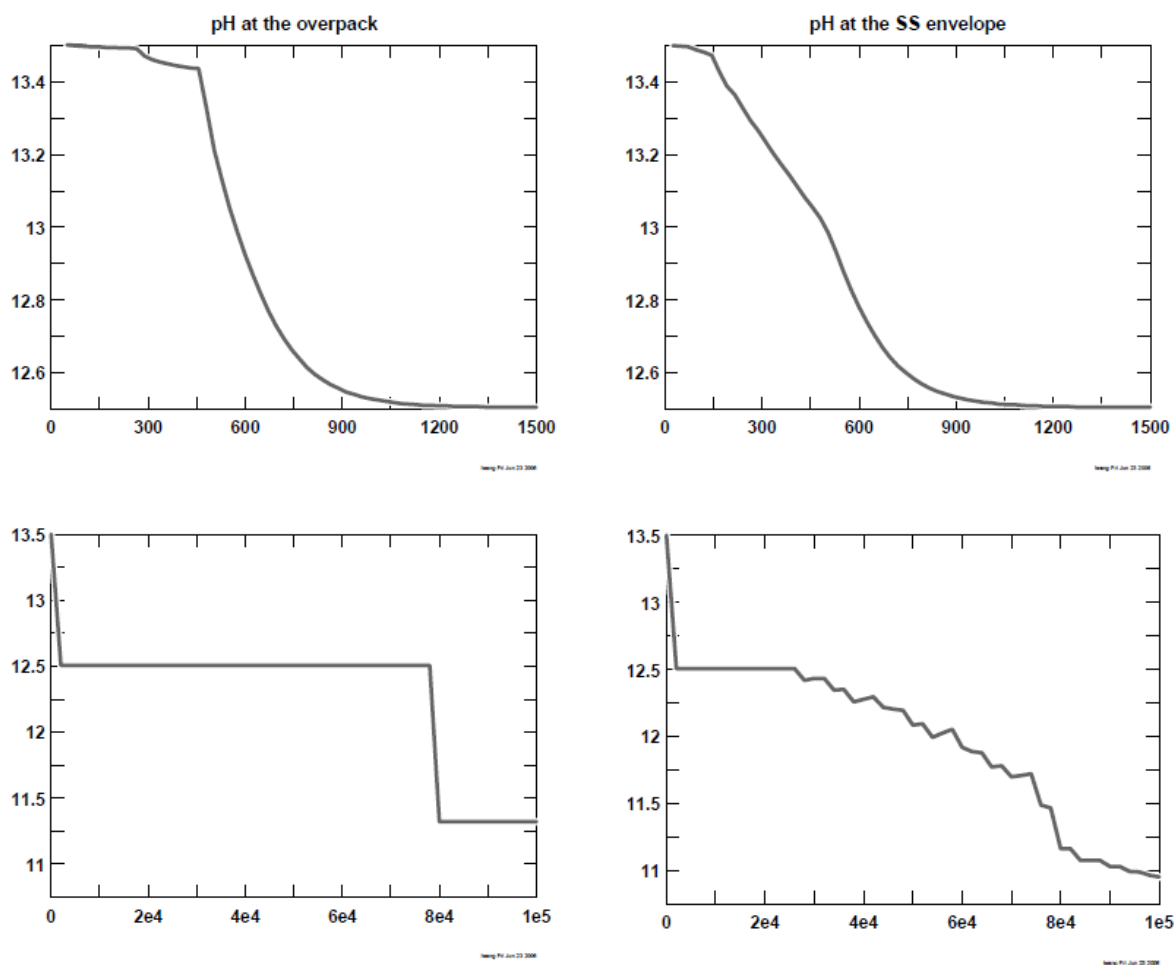


Figure 6-8: Evolution of pH at the overpack and the stainless steel (SS) envelope as a function of time (X-axis, years); top figures are a zoom of the bottom figures.

A variant calculation was performed in [Wang et al. 2010] in which a certain volume of Boom Clay was included in the model, in order to take into account transport limitations and to better represent concrete-clay interactions. In this calculation, the end of stage 2 was calculated to occur after more than 100 000 years (see Figure 6-9 right).

The latter geochemical modelling exercise also allows for assessing the perturbation of the Boom Clay by the alkaline plume. A sensitivity analysis based on a supercontainer containing HLW shows that the spatial extent of the alkaline plume is limited to 2 – 2.5 m after 100 000 years (Figure 6-9). This is further supported by mass balance calculations. Note that these calculations did not take into account any thermal gradients, or any changes in porosity or other transport parameters.

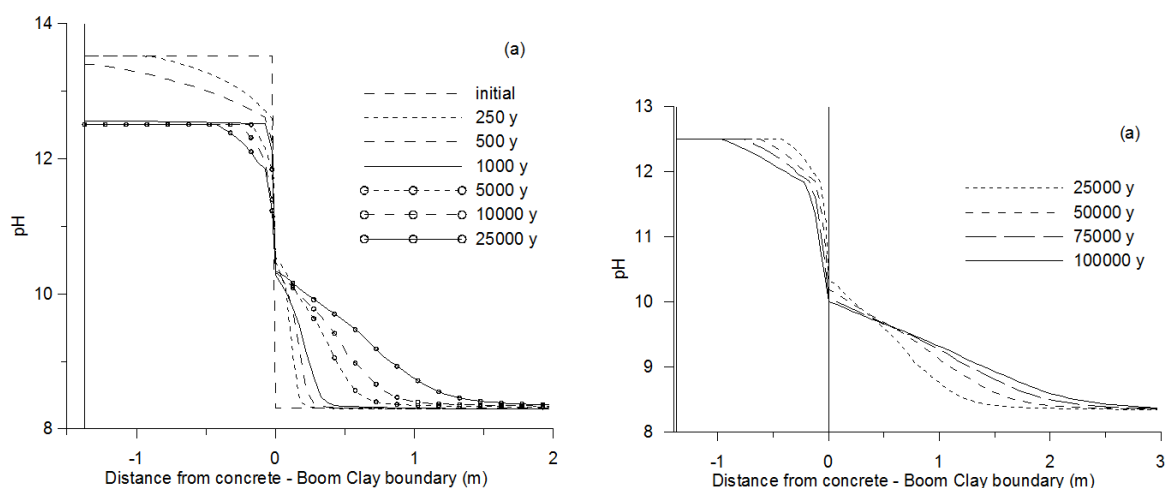


Figure 6-9: pH evolution as function of distance from the concrete – clay interface in the short term (left) and long term (right).

### 6.2.3 Mathematical model

#### 6.2.3.1 Description of mathematical model of Boom Clay – Concrete interactions.

In this paragraph, a concise description of the model assumptions and mathematical model that lead to the simulation results presented in *Figure 6-9* is given. A more detailed description and all governing equations was reported in [Wang et al 2010].

The model aim was to assess the diffusion of an alkaline plume within the Boom Clay. However, to account for the variation in composition of the alkaline plume with time (different states of concrete), the concrete material in the near field is explicitly included in the model (between 0.22 and 0.162 m from a 1D radial transport field). The model included following geochemical processes in the Boom Clay:

- Aqueous speciation
- Dissolution of the clay minerals – 2 alternatives were used with the clay minerals; either they are in thermodynamic equilibrium or they are dissolving kinetically. Given the large computational time for the kinetic approach and the small differences between the two approaches, only the equilibrium approach was taken forward
- Equilibrium precipitation/dissolution of secondary phases in the Boom Clay
- A pH independent cation exchange process to represent exchange of cations with the fixed charge on the clay minerals
- A pH dependent multisite cation exchange process to represent buffer capacity by the organic matter in the Boom Clay
- A non-electrostatic surface complexation model to simulate the protonation and deprotonation on illite and montmorillonite

Thermodynamic principles including activity correction coefficients were used to calculate the equilibrium state during transport using mass action laws (see the PHREEQC manual for details [Parkhurst and Appelo, 1999]). Transport was described by an 1D radial diffusion equation.

### 6.3 Characterization of an ILW disposal cell in clay

#### 6.3.1 Description of materials in disposal cell

In the current lay-out of the geological disposal facility under study by ONDRAF/NIRAS, disposal of ILW will occur in a dedicated section of the repository, called the B-zone [ONDRAF/NIRAS 2019] and [ONDRAF/NIRAS 2017b]. In the frame of the ACED project, we limit the scope to disposal of compacted waste, containing mainly hulls, end-pieces (cladding residues), spacing grids and springs from reprocessing activities at La Hague. ONDRAF/NIRAS foresees a concrete monolith (type CB-2) disposal package, which contains 8 CSD-C<sup>9</sup> canisters, and is filled with mortar for immobilisation purposes [ONDRAF/NIRAS 2017c] (see *Figure 6-10*).

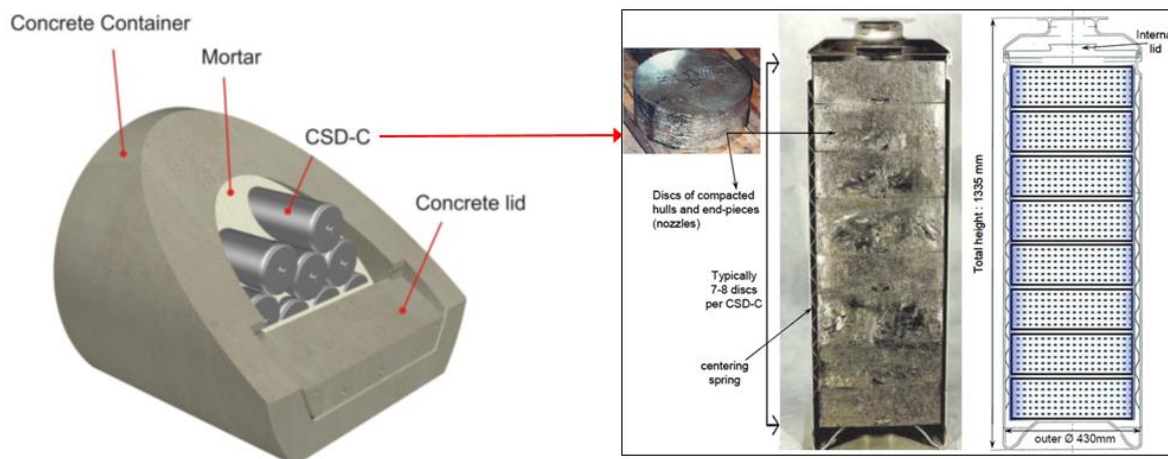


*Figure 6-10:* The monolith CB-2 for disposal of compacted waste (left), and cross-section view of a typical CSD-C canister

The materials and interfaces in a ILW disposal cell are depicted schematically in *Figure 6-11*. For each of the considered components, the materials and dimensions, the role in the safety concept and possible additional requirements are briefly described in *Table 6-3* (for as far as information is available at this stage).

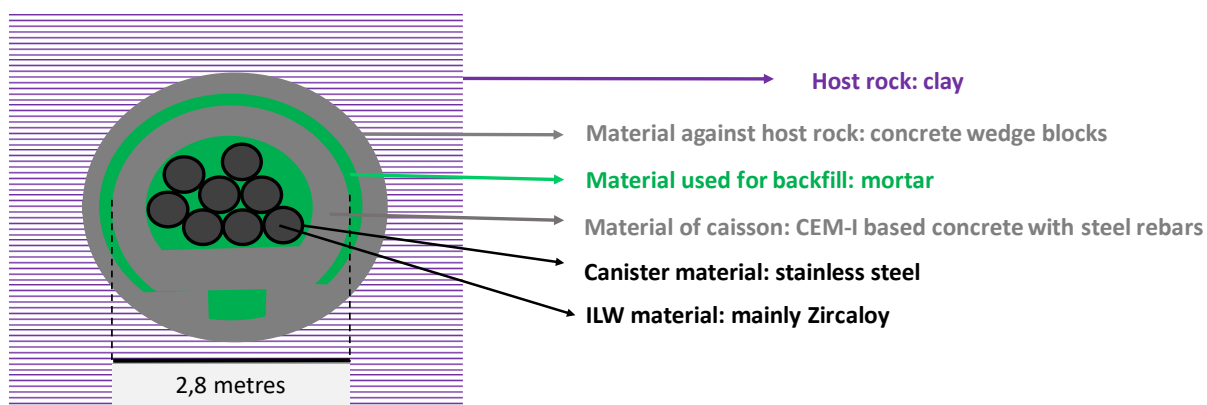


*Figure 6-11:* Materials and interfaces in a disposal cell for ILW according to the Belgian disposal design. Note that the reference inner diameter for a disposal gallery recently increased from 3.0 m to 3.5 m [ONDRAF/NIRAS, 2019].

<sup>9</sup> CSD-C: 'Conteneur Standard de Déchets Compactés', the standard canister for compacted waste that is the product of reprocessing at the ORANO facilities at La Hague, France.

Table 6-3: Characteristics and role of the components in a disposal cell for ILW according to the Belgian disposal design and safety concept. Information taken from [ONDRAF/NIRAS 2017bc, von Lensa et al 2008].

Component	material	dimensions	Role in the safety concept and design criteria (if relevant/available)
Clay host formation	Host formation and site dependent	Host formation and site dependent	<ul style="list-style-type: none"> <li>Both physical (thickness and depth, low permeable) and chemical (retention) barrier</li> <li>Fast self-sealing properties to limit excavation disturbed zone</li> </ul>
Disposal gallery lining	Concrete wedge blocks	30 cm thick	<ul style="list-style-type: none"> <li>Provide mechanical stability and limit clay convergence</li> <li>Material compatibility with EBS and host rock</li> </ul>
Backfill	Mortar	10 – 35 cm thick	<ul style="list-style-type: none"> <li>Minimise void spaces</li> <li>Material compatibility with EBS and host rock</li> </ul>
Caisson	concrete: CEM I 42.5 N LA HSR LH, W/C = 0.47, limestone aggregate	∅ 2.8 m, radial thickness 52 cm, axial thickness 56 cm	<ul style="list-style-type: none"> <li>Provide shielding during underground operations</li> <li>Maintaining alkaline conditions to limit corrosion</li> <li>To some extent provide additional, and sometimes complementary, sorption to the clay host formation</li> </ul>
Immobilisation mortar	CEM III/C 32,5N, W/C = 0.36, limestone aggregate	NA	<ul style="list-style-type: none"> <li>Immobilise CSD-C canisters</li> <li>To some extent provide additional, and sometimes complementary, sorption to the clay host formation</li> </ul>
Canister	Stainless steel	∅ 0.43 m, thickness 0.5 cm	
ILW Waste form	Mainly Zircaloy-4, also Inconel and stainless steel	∅ 0.42 m; length 1.3355 m	<ul style="list-style-type: none"> <li>Leaching resistance</li> </ul>

### 6.3.2 Hydraulic gradients

As co-disposal of HLW and ILW is considered at the same depth, with same-sized disposal galleries, the hydraulic gradients would a priori be similar.

However, considerable uncertainty exists with respect to the potential development of a gas phase. For compacted waste (CSD-C), hydrogen is produced through the corrosion of caisson reinforcement bars, primary canisters and metals contained in the waste forms. The relative importance of each source term depends on the reactive surface area and corrosion rate in disposal conditions (anaerobic, alkaline). It is assumed that development of a free gas phase can be avoided if corrosion rates are low enough: *i.e.* in the order of a few nm/y [Yu and Weetjens 2012].

### 6.3.3 Pore water compositions

Similar to HLW. See 6.1.3.

## 6.4 Chemical evolution of the ILW disposal cell

### 6.4.1 Narrative

Given the similarity of engineered materials in a ILW disposal cell (Monolith-B concept for CSD-C) and HLW disposal cell (Supercontainer concept for CSD-V), the chemical evolution may be assumed to occur alike, at least in broad terms. It can be anticipated that the relatively larger amount of metallic components in a ILW disposal cell might affect redox conditions. No specific assessments have been done so far, to the authors' knowledge.

### 6.4.2 Conceptual model

See 6.2.2.1

## 7. Bulgaria

Ivan Ivanov from the Technical University of Sofia has contacted the Bulgarian WMO SERAW. The following text could be included in this report for the current handling in the Bulgarian programme:

Bulgaria does not have processed spent nuclear fuel yet in their country.

According to the existing treaties with the Russian Federation, the HLW from the SNF processing will be returned to Bulgaria within 10 years after the specific volume has been determined according to the methodology agreed by the parties in accordance with international practices in this field.

The methodology, cited above, has not yet been agreed between the two parties.

The project for dismantling of the Controlled Areas of units 1 to 4 of the Kozloduy NPP has not started. Therefore, the volume of Intermediate Level Waste (ILW) cannot be determined at this stage. Their estimated value is up to 10 cubic meters according to the Bulgarian National Program.

## 8. Czech Republic

SURAO - Antonín Vokál

The Czech Republic has no suitable salt domes or large clay soil areas so that only crystalline rocks can be considered for the construction of a deep geological repository. The Czech DGR concept assumes that waste packages containing spent fuel assemblies will be enclosed in steel-based canisters placed in vertical or horizontal boreholes at a depth of ~ 500m below the surface. The space between the canisters and the host crystalline rock will be backfilled with compacted bentonite. The reference canister design contained in the Czech DGR concept is composed of two layers, an outer layer of carbon steel which will corrode very slowly under anaerobic conditions and a second inner layer of stainless steel which will corrode at an almost negligible general corrosion rate and exhibit a low tendency to local corrosion under anaerobic conditions. The reference buffer and backfill materials consist of compacted bentonite from Czech Ca, Mg bentonite deposits. Research activities focusing on confirming of these reference options are ongoing.

### 8.1 Characterization of the HLW disposal cell in granite

#### 8.1.1 Description of materials in disposal cell

The criteria/requirements for materials in disposal cells “waste package, buffer, backfill, and host rock surrounding boreholes” are derived from the Czech basic legislative requirement, which is the maximal effective dose for a representative person from population, which should not be higher than 0,25 mSv in a year [Atomic Act, 2016]. The most important barriers in the Czech concept are canisters. Practically no canister should fail in the range of several hundred thousand years under the DGR normal evolution scenario. The main safety functions of materials surrounding the canisters are to protect canisters from all possible processes and events that could contribute to the canister failure. The material surrounding the canisters in boreholes (buffer) should not allow:

- 1) migration of corrosion accelerating species to the surface of canister by advection,
- 2) grow of microbes that could initiate microbial corrosion and
- 3) movement of canisters in boreholes.

The buffer composition should not itself contribute to corrosion of canisters by high concentration of corrosive agents. The similar, but not so strict requirements are on the backfill, that should keep buffer in bore holes and limit the flow of water through DGR disposal tunnels.

The temperature at the interface between canister and buffer should not exceed 100 °C (with margin 95 °C) to decrease the possibility of fast rate of degradation of materials above 100 °C and also to prevent difficulties of the evaluation of processes occurring above this temperature.

The retardation properties (sorption, diffusion coefficients) of buffer and backfill should contribute to the slow migration of long-term radionuclides after canister failure to the host rock, but there are not any requirements on these properties.

The requirements concerning the dimensions of selected engineered barriers are derived from the dimensions of spent fuel assemblies and thermal dimensioning of the repository. The dimension of a disposal cell proposed in the reference design of the Czech repository for a horizontal layout is given in *Figure 8-1* [Špinko, 2017]. The horizontal layout was used in preliminary geochemical studies [Červinka, 2018].

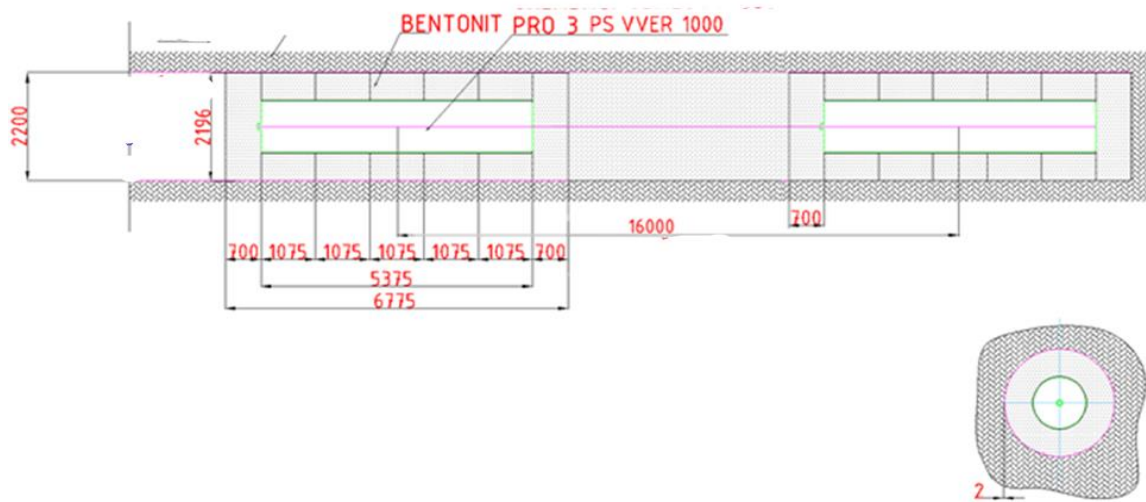


Figure 8-1: Scheme for disposal of spent fuel in a horizontal layout

A simplified scheme of a disposal cell *Figure 8-2* was used for modelling chemical changes in compacted bentonite [Červinka et al., 2018].

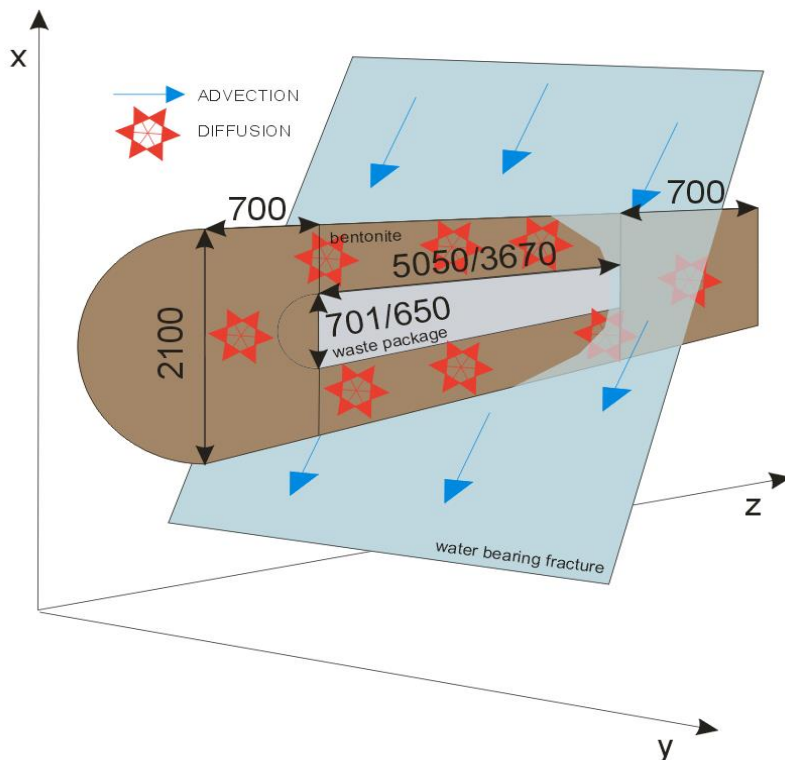


Figure 8-2: A simplified scheme of disposal cell

### 8.1.2 Thermal gradients

Thermal power of canisters with spent fuel assemblies as a function of time is given in *Figure 8-3*. The initial time for calculations is related to the expected 65 years of cooling of spent fuel assemblies in dry storage facilities located near nuclear power plants.

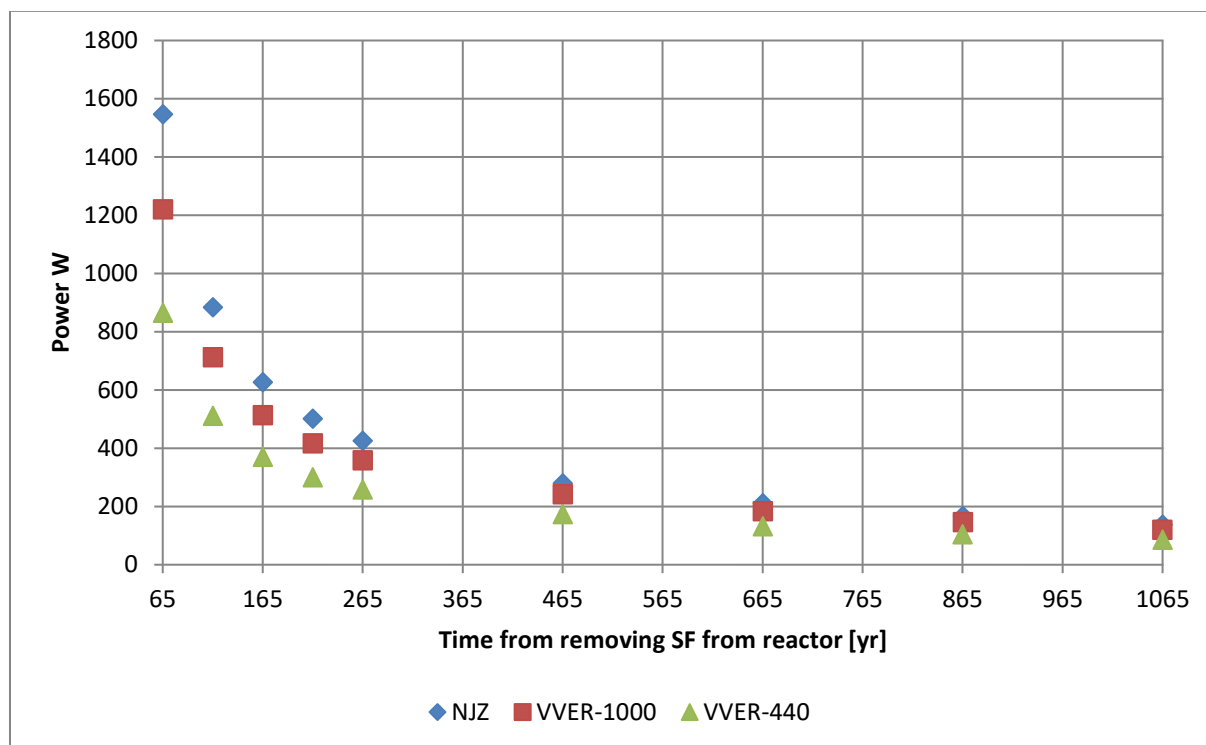


Figure 8-3: Thermal power of canisters with spent fuel assemblies as a function of time

Thermal gradients in disposal cells depend on the thermal power of canisters with spent fuel assemblies, design of a repository and thermal properties of the host rock and engineered barriers surrounding canisters with spent fuel assemblies. The first studies in the Czech programme [Blaheta, Malík, 2012] were aiming to get basic understanding of the heat transfer from canisters to the host rock. It was found that the most important parameters, besides the thermal power of canister with spent fuel assemblies, are thermal conductivities of bentonite and host rock, thickness of bentonite and degree of bentonite saturation. Various analytical and numerical approaches have been used for thermal calculations.

A dependence of the temperature at the interface between the canister and bentonite blocks for selected thickness of 100 cm of bentonite on the bentonite thermal conductivity is given in the Table 1 for the canister with an initial power 1900 W.

Table 8-1: The change of maximal temperature at the surface of canisters on the change of thermal conductivity of compacted bentonite

$\lambda(\text{Wm}^{-1}\text{K}^{-1})$	0.7	0.8	0.9	1.0	1.1	1.2	1.3
Temperature °C	121.33	112.87	106.30	101.07	96.78	93.23	90.23

The calculations confirmed the importance of bentonite thermal conductivity for the values of thermal gradients. The problem of determination of thermal conductivity at the transient period is that the saturation of bentonite can significantly change particularly in the transient period after repository closure. From the host rock site, the bentonite is saturated by water and from the canister the bentonite is desaturated due to the heating by decay heat from canister. Conservatively the value of the thermal conductivity of bentonite for most of calculations was taken  $0.7 \text{ Wm}^{-1}\text{K}^{-1}$ .

For thermal dimensioning of the repository (determination of distances between disposal boreholes with canisters and between disposal tunnels), calculations were carried out by Kobyłka, 2017. The dimensioning of the repository was based on the limit of  $95 \text{ }^\circ\text{C}$  ( $100 \text{ }^\circ\text{C}$  minus  $5 \text{ }^\circ\text{C}$  margin) at the interface between the canister and bentonite in the repository (see *Figure 8-4*).

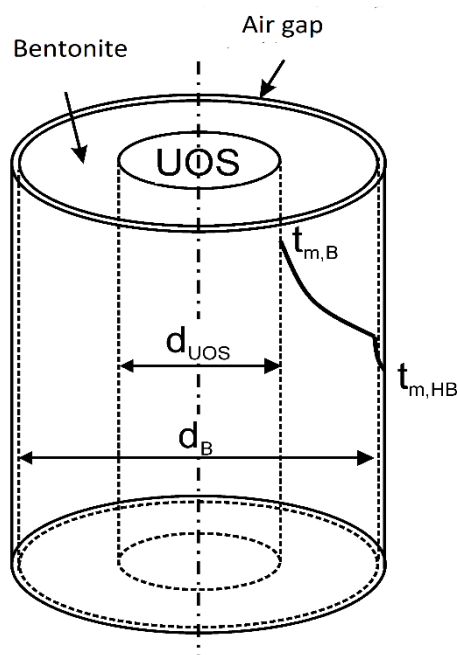


Figure 8-4: Scheme for calculations of maximal thermal gradients

The calculations of thermal gradients have been conducted for all Czech candidate sites, which differs in the values of thermal conductivities in the range from  $2.1 \text{ Wm}^{-1}\text{K}^{-1}$  to  $3.2 \text{ Wm}^{-1}\text{K}^{-1}$  (Kobyłka, 2017). For all candidate sites it was assumed that temperature at the depth of 500m below surface is  $25 \text{ }^\circ\text{C}$ . The data used in calculations are given in *Table 8-2*.

Table 8-2: Description of parameters for thermal gradients

Feature	Examples of parameter	Value and unit	Comments
Heat source in	Thermal power as a function of time	1125 W	3 SF WWER 1000 after 65 yrs
Heat volume	Volume of heat source	4.6 m <sup>3</sup>	Total volume of canister, but only medium part with SF (4.7 m was considered)
Spent fuel/overpack	Heat conductivity	200 W m <sup>-1</sup> K <sup>-1</sup>	The same values were taken for all materials in the canister
	Specific density	7000 kg m <sup>-3</sup>	
	Specific heat capacity	400 J kg <sup>-1</sup> K <sup>-1</sup>	
Air gap	Thermal conductivity	0.0258 W m <sup>-1</sup> K <sup>-1</sup>	2 mm
	Specific density	1.2 kg m <sup>-3</sup>	
	Specific heat capacity	1010 J kg <sup>-1</sup> K <sup>-1</sup>	
Material surrounding the overpack	thermal conductivity	0.7 W m <sup>-1</sup> K <sup>-1</sup>	Compacted bentonite
	specific density	1600 kg m <sup>-3</sup>	
	specific heat capacity	2500 J kg <sup>-1</sup> K <sup>-1</sup>	
Host rock	thermal conductivity	2,59 W m <sup>-1</sup> K <sup>-1</sup>	
	specific density	2679 kg m <sup>-3</sup>	
	specific heat capacity	761 J kg <sup>-1</sup> K <sup>-1</sup>	
	temperature	25 °C	

The analytical solution of Fourier differential equation of heat transfer with linear source, according to Ikonen, Raiko, 2015, have been used. The variable parameters in calculations were distances between tunnels and between canisters with spent fuel assemblies. The results of calculations of temperature at the interface between bentonite and host rock (tmHB) for a horizontal layout for one of the candidate sites are given in *Figure 8-5*.

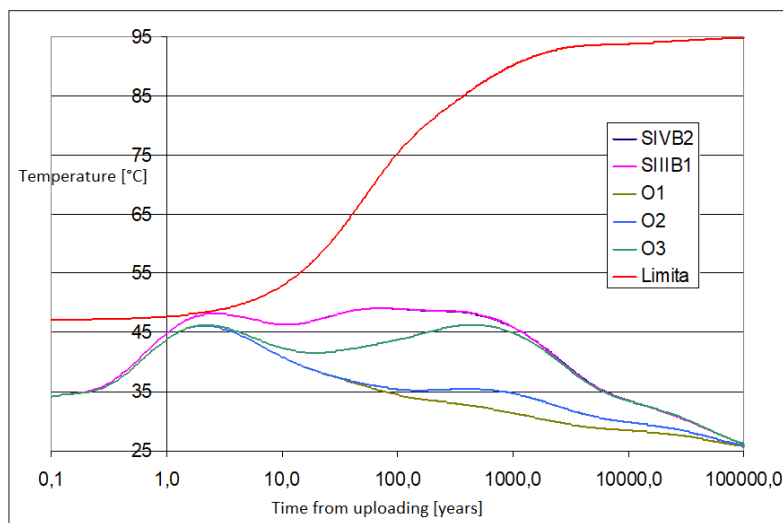


Figure 8-5: Temperature at the interface between bentonite and host rock for various sites in the repository in a horizontal layout (SIVB2 – centre of block B2, SIIIB1 – centre of the block 1, O1 edge of block 1, O2 edge of block 2, O3 edge of block 3,

The thermal gradient, difference of temperatures between the interface steel/bentonite and the interface bentonite/host rock, can be easily calculated from the difference between limit of 95 °C (red line) and the temperature at the interface between bentonite blocks and the host rock. The maximal thermal gradient across bentonite in the central part of a repository is 48 °C, approximately ten years after uploading of canisters with spent fuel assemblies.

### 8.1.3 Hydraulic gradients

Groundwater flow in ground and upper bedrock is caused mainly by differences in topography and the structure and hydraulic properties of the bedrock. The hydraulic heads at the candidate site Kravi hora are shown in Figure 8-6. The hydraulic gradient is a vector gradient between two or more hydraulic heads over the length of the flow path. The average hydraulic gradient was here estimated to be about the value of 3 %.

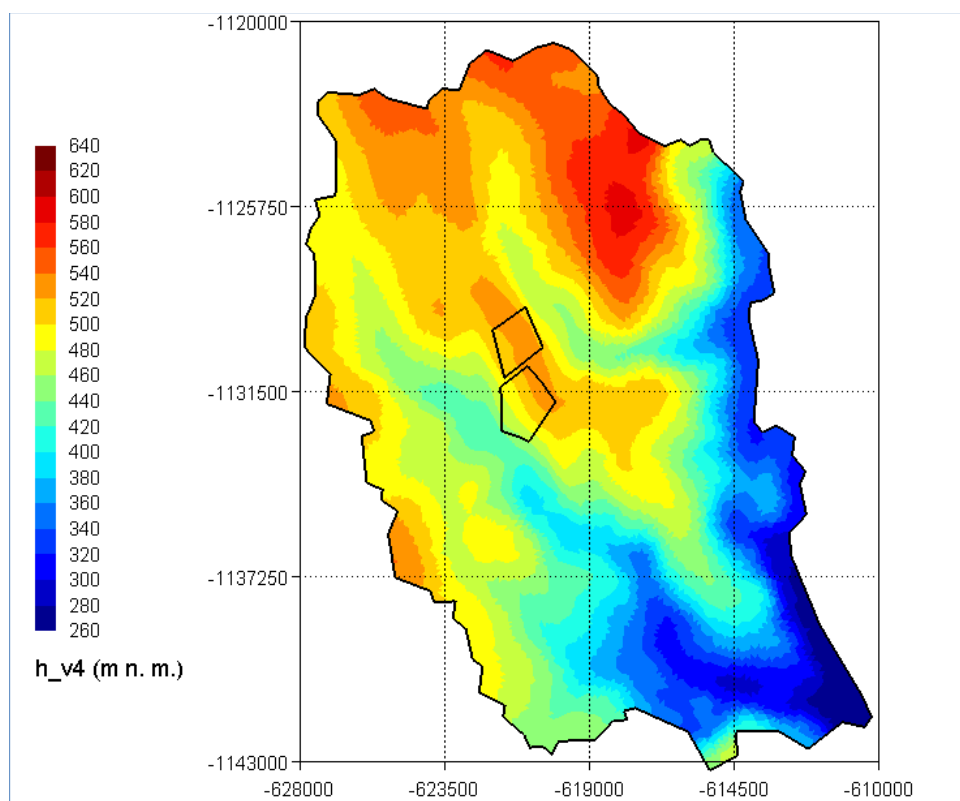


Figure 8-6: Hydraulic head in the depth of a repository with highlighted polygons representing DGR (Milicky, Uhlík et al., 2019)

Hydraulic gradients at the scale of disposal cells in depth of 500m below surface in crystalline rocks might be, however, highly heterogeneous (Nordqvist et al., 2008) and depend on the local conditions around the disposal cells. Usually the hydraulic gradients are less than 1 %.

Due to very low hydraulic conductivities of the host rock at the depth of 500m, for most of the disposal cells the main process governing chemical changes in the crystalline rock surrounding disposal cells will be therefore diffusion and not advection. Conservatively, however, it was in geochemical calculations assumed that the flow in the fracture intersecting disposal cell *Figure 8-2* is advective.

#### 8.1.4 Pore water compositions

Overview of the chemical composition of groundwaters and porewaters considered in geochemical modelling studies (Červinka et al., 2018) is given in *Table 8-3*. The following types of water have been used for geochemical modelling

- SGW2 is a synthetic granite groundwater whose physico-chemical parameters and chemical composition were derived from the average physico-chemical parameters and average chemical composition of real groundwater at the Bukov Underground Research Facility (URF Bukov) about 600 m below the surface. Its composition corresponds to the groundwater in deeper circulation in the fracture environment of the crystalline rocks of the Bohemian Massif, type Ca-HCO<sub>3</sub>. Composition was calculated as the average of 11 analyses. The selection was subsequently verified on a larger sample data set of 18 analyses.
- SGW3 is a synthetic granite groundwater whose physico-chemical parameters and chemical composition were derived from the physico-chemical parameters and chemical analysis of groundwater at the Rožná mine from the 22-24 level about 1000 m below the surface. The groundwater composition represents a very slow circulation of deep

groundwater in the fracture environment of the crystalline rocks of the Bohemian Massif, type Na-HCO<sub>3</sub>. The composition was calculated as the average of 5 analyses. The selection was subsequently verified on a larger sample data set of 18 analyses.

- B-SGW2-OX is bentonite porewater (bentonite BaM) calculated for SGW2 groundwater in interaction with bentonite under oxic conditions (equilibrium with atmospheric oxygen having a partial pressure of 0.21 atm).
- B-SGW2-ANOX is bentonite porewater (bentonite BaM) calculated for SGW2 groundwater in interaction with bentonite under anoxic conditions (oxygen-free environment).
- B-SGW3-OX is bentonite porewater (bentonite BaM) calculated for SGW3 groundwater in interaction with bentonite under oxic conditions (equilibrium with atmospheric oxygen having partial pressure of 0.21 atm).
- B-SGW3-ANOX is bentonite porewater (bentonite BaM) calculated for SGW3 groundwater in interaction with bentonite under anoxic conditions (oxygen-free environment).

Table 8-3: Initial physico-chemical parameters and chemical composition of different types of waters which were used for geochemical modelling

Parameter	Unit	SGW2	B-SGW2-OX	B-SGW2-ANOX	SGW3	B-SGW3-OX	B-SGW3-ANOX
pH		8.2	8.24	7.87	9.4	8.24	8.13
Eh	mV	236.6	731.6	-212.4	236.6	731.7	-257.3
Temperature	°C	25	25	25	25	25	25
Al <sup>3+</sup> *	mol kgw <sup>-1</sup>	3.71E-06	6.34E-08	2.76E-08	3.71E-06	6.32E-08	4.96E-08
Ca <sup>2+</sup>	mol kgw <sup>-1</sup>	8.64E-04	5.12E-05	1.76E-04	3.24E-05	5.11E-05	1.64E-04
Cl <sup>-</sup>	mol kgw <sup>-1</sup>	9.31E-05	2.07E-03	2.06E-03	5.28E-04	2.50E-03	2.49E-03
Fe <sup>2+</sup> *	mol kgw <sup>-1</sup>	1.79E-06	3.60E-12	9.50E-07	1.79E-06	3.60E-12	8.15E-07
HCO <sub>3</sub> <sup>-</sup>	mol kgw <sup>-1</sup>	2.77E-03	9.68E-04	1.32E-03	2.68E-03	9.65E-04	7.55E-04
K <sup>+</sup>	mol kgw <sup>-1</sup>	5.37E-05	8.80E-04	9.04E-04	1.79E-05	8.87E-04	8.80E-04
Mg <sup>2+</sup>	mol kgw <sup>-1</sup>	3.42E-04	1.18E-03	1.03E-03	4.12E-06	1.19E-03	9.78E-04
NO <sub>3</sub> <sup>-</sup>	mol kgw <sup>-1</sup>	0.00E+00	3.18E-03	3.16E-03	0.00E+00	3.18E-03	3.16E-03
Na <sup>+</sup>	mol kgw <sup>-1</sup>	8.65E-04	1.01E-02	1.03E-02	3.81E-03	1.02E-02	1.02E-02
SO <sub>4</sub> <sup>2-</sup>	mol kgw <sup>-1</sup>	2.19E-04	3.59E-03	3.57E-03	1.09E-04	3.48E-03	3.46E-03
SiO <sub>2</sub> (aq)	mol kgw <sup>-1</sup>	5.20E-04	9.67E-05	9.50E-05	4.18E-04	9.67E-05	9.60E-05
Calculated							
H <sup>+</sup>	mmol kgw <sup>-1</sup>	-4.84E-02	-9.92E-03	2.16E-02	-5.02E-01	-9.98E-03	-2.91E-03
Dissolved solids	mg L <sup>-1</sup>	298.9	1005	1021	319.5	1012	986
Charge imbalance error		-0.06%	0.14%	-0.16%	-0.16%	-0.18%	0.15%
Water type		Ca-CO3	Na-SO4	Na-SO4	Na-CO3	Na-SO4	Na-SO4
CO <sub>2</sub> (g)	log fugacity	-2.99	-3.52	-3.01	-4.25	-3.52	-3.51
O <sub>2</sub> (g)	log fugacity	-34.30	-0.68	-65.98	-29.50	-0.67	-67.98
Goethite	log Q/K	5.69	0.00	0.00	5.49	0.00	0.00
Kaolinite	log Q/K	5.03	-0.10	-0.10	2.22	-0.10	-0.09
Calcite	log Q/K	0.53	-1.27	-0.97	0.12	-1.27	-0.98
Quartz	log Q/K	0.71	-0.03	-0.03	0.49	-0.03	-0.03

Note 1: The composition of SGW2 and SGW3 groundwaters entering the models was reduced with respect to minor elements, for example F<sup>-</sup>, NH<sub>4</sub><sup>+</sup>, NO<sub>3</sub><sup>-</sup>, Li<sup>+</sup> etc. In contrast, dissolved elements important for evaluating saturation with respect to minerals of the host rock or fracture infill (SiO<sub>2</sub>(aq), Al<sup>3+</sup> and Fe<sup>2+</sup>) were preserved. Concentrations of aluminium and iron have considerable variance in the analyses (in the case of iron values, ranging from several hundred to several units of mg l<sup>-1</sup>). Choosing the Fe<sup>2+</sup> and Al<sup>3+</sup> concentrations based on the arithmetic mean, due to its variance, did not appear to be the appropriate procedure. Consequently, the concentrations of Al<sup>3+</sup> and Fe<sup>2+</sup> in both groundwaters were selected on the expert estimation of their probable values, namely 0.1 mg l<sup>-1</sup>.

Note 2: Partial pressures of carbon dioxide (log PCO<sub>2</sub>) were calculated as an average of all analyses and for SGW2 verification against the gas analysis was done (S1 outflow). For SGW2 log PCO<sub>2</sub> is equal to -3.00, which corresponds to the CO<sub>2</sub> analysis from the S1 outflow with PCO<sub>2</sub> equal to -3.12. The partial pressure of CO<sub>2</sub> was then for groundwater SGW2 cca 2.8x higher than in the air. In the case of SGW3, the determination of average value was problematic with respect to the incomplete analysis of carbonates speciation for pH > 9.5. Nevertheless, the value of PCO<sub>2</sub> was selected to be -3.50, which corresponds to the CO<sub>2</sub> partial pressure atmosphere.

## 8.2 Chemical evolution of the HLW disposal cell

### 8.2.1 Narrative

Evolution of geochemical changes in the DGR in crystalline rocks can be divided into the following periods:

- 1) The change of chemical composition of groundwater at the time of opening the undisturbed rock, which brings out the ingress of oxygen into the host rock environment.

- 2) Consumption of the oxygen and the creation of oxygen-free environment and gradual resaturation of the GDR.
- 3) Chemical evolution at the scale of disposal cells
  - a. Transient changes due to the leveling of hydraulic and chemical gradients after repository closure and oxygen consumption
  - b. Migration of corrosion products (iron species and hydrogen for carbon steel) from the canisters to the surrounding materials under changing temperatures
- 4) Changes after glaciation periods, particularly possible dilution of the ground water with infiltrating water after ice melting water.

The processes studied in the Czech programme are described in *Figure 8-7* (Červinka et al., 2018. Gondolli et al., 2018)

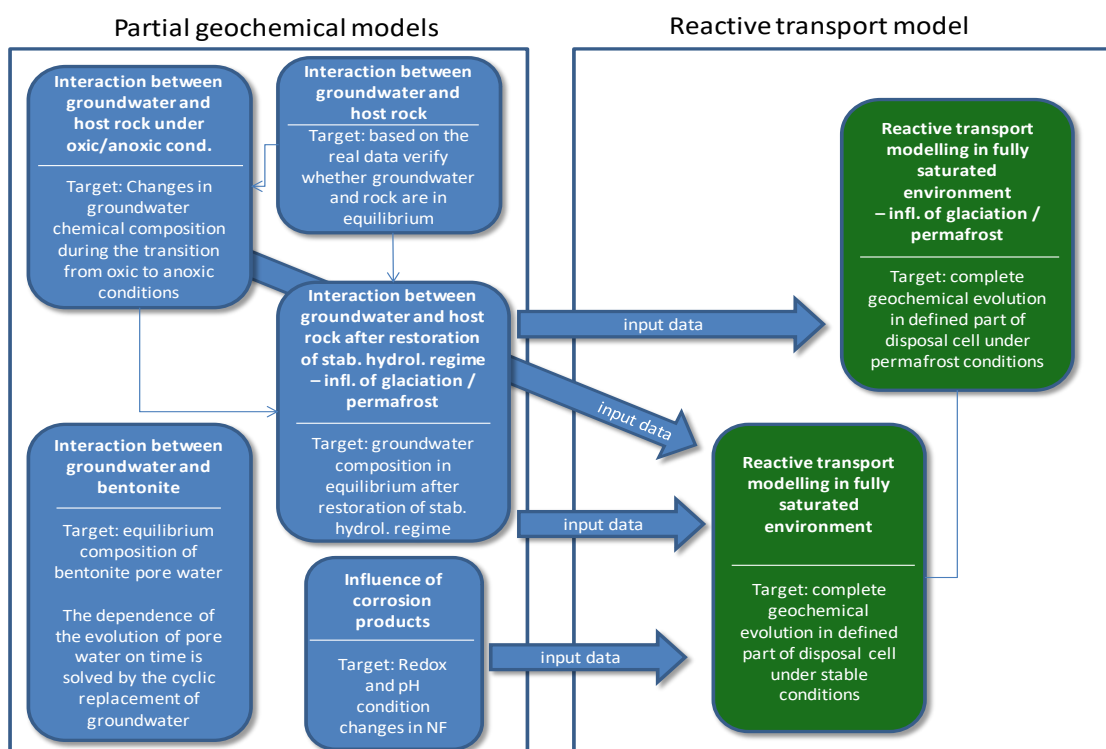


Figure 8-7: Geochemical models tested in Czech programme [Červinka et al., 2018].

### 8.2.2 Conceptual model

Both the one-dimensional and two-dimensional models were located in the plane of a conductive fracture, intersecting the block of the host rock with the canister *Figure 8-8*.

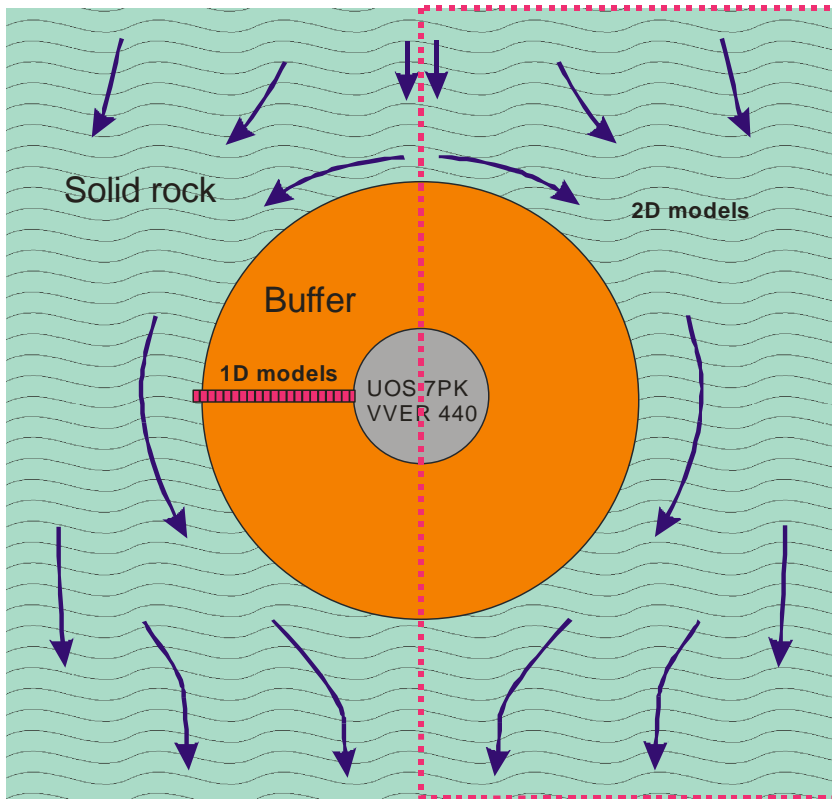


Figure 8-8: Domains of 1D and 2D models in the plane of a fracture

A one-dimensional model of reactive transport through a bentonite buffer with the fracture with flowing water was set up in the initial step of modelling. The length of the domain was 730 mm, which consisted of 5 mm in the fracture and 725 mm in the bentonite *Figure 8-9*. Spatial discretisation was 5 mm (length 730 mm was divided into 146 model cells).

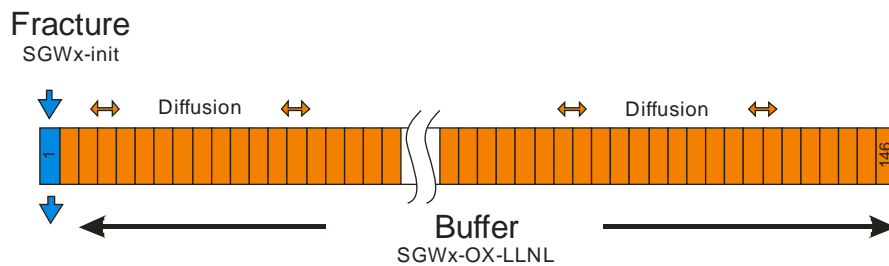


Figure 8-9: 1D model for reactive modelling

A set of two-dimensional models was compiled in the second step of modelling. These models were set up as a one half of the circular ring in the plane of fracture, intersecting the block of host rock with supercontainer (utilising the planar symmetry of supercontainer). The length of the modelling domain was 3.52 m, width was set to 1.76 m and thickness to 0.1 m *Figure 8-10*.

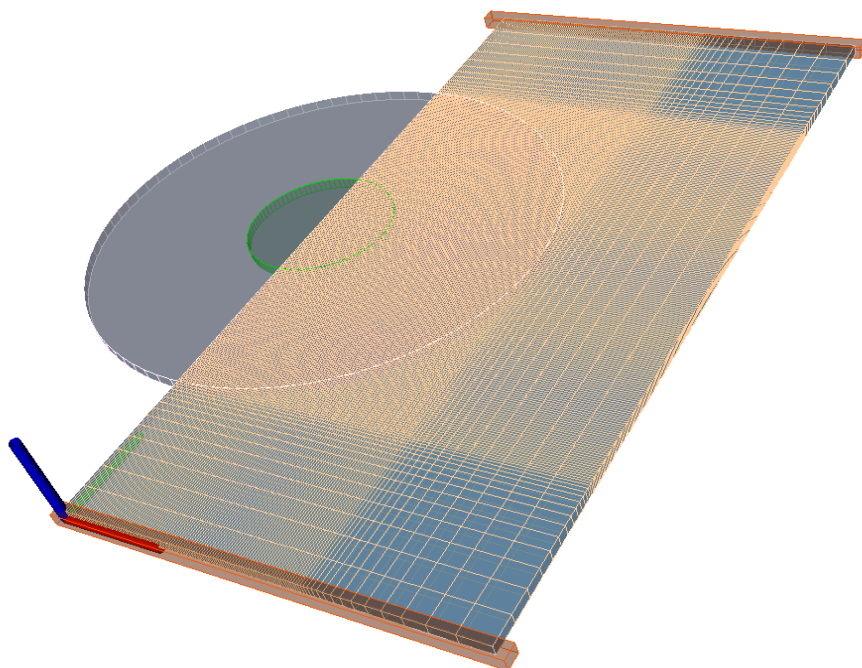


Figure 8-10: 2D model domain

The modelled domain corresponded to a situation when groundwater flowing through the fracture washed the perimeter of the bentonite buffer of the canister. Exchange of the dissolved species occurred in the model domain between the water in the fracture and the porewater of the bentonite buffer along the perimeter (at the outer boundary) of the buffer. The fracture was approximated as a zone of porous media. The hydraulic conductivity was set to 0.158 m per year ( $5.0 \cdot 10^{-9}$  m.s<sup>-1</sup>), effective porosity to 0.05 and tortuosity to 1.0. The used hydraulic gradient (2.8%) corresponded with the results of the regional flow model (Uhlík et al. 2016). It was assumed that the area of the fracture contained the background model groundwater while the buffer was saturated with the relevant bentonite porewater.

The modelled 2D domain was discretised in space in the modelling grid, which consisted of 120 computation nodes (119 cells) in x direction, 239 computation nodes (238 cells) in y direction and 2 nodes (1 cell) in z direction. Homogeneous spacing of nodes with distance 1 cm ( $\Delta x$ ,  $\Delta y$ ) was used in the area of the bentonite buffer to a distance of 105 cm from the axis of the supercontainer. Out of this area, the distance between nodes increased by a factor of 1.2 to the boundary of the model domain.

### 8.2.3 Mathematical model

Two geochemical reaction modelling codes were used in the work of Červinka et al, 2018

The Geochemist's Workbench® Professional software (GWB), Release 11 (Bethke and Yeakel 2018), which includes a number of program modules for, e.g., evaluating geochemical and hydrochemical data, modelling geochemical equilibrium, calculating complex phase diagrams and water speciation, etc.

PHREEQC version 3 geochemical code (Parkhurst and Appelo 2013). PHREEQC is a freeware modelling tool developed by USGS which is suitable for modelling aqueous solutions, both equilibrium and kinetic batch reaction modelling, and one-dimensional (1D) reactive transport modelling. PHREEQC can also be used for so-called inverse geochemical modelling.

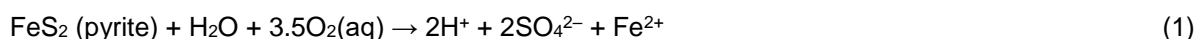
In both modelling tools, the Lawrence Livermore National Laboratory database (denoted 'thermo.com.V8.R6+.t.dat' in GWB and 'LLNL.DAT' in PHREEQC) was utilized (Johnson et al. 2000).

The model of reactive transport in 1D and 2D was built in PHAST software version 3.3 (Parkhurst et al. 2004, 2010), which used as a reaction module the actual version of the PHREEQC geochemical code (Parkhurst and Appelo 2013). Consistency of the thermodynamic data was maintained by using the same thermodynamic database LLNL.DAT. The Model Viewer version 1.6 software (Hsieh and Winston 2002) was used to visualise the 2D models' results.

## 8.2.4 Calculated results

### Chemical evolution after repository opening

The main chemical reaction involved in the change of the physico-chemical parameters and the chemical composition of the groundwater after exposure to the atmosphere and atmospheric oxygen and carbon dioxide are the oxidation of pyrite and other sulfides:

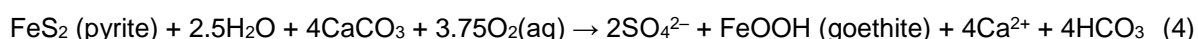
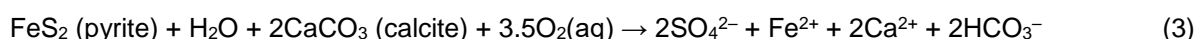


and further oxidation of iron with precipitation of goethite



According to these equations there is considerable acidity production.

The evolution of pH and ORP depends on the calcite concentration in the rocks. In the presence of calcite, the above equations can be overwritten (3 and 4)



The dissolution of calcite and generally carbonates effectively buffer pH changes and ensure that groundwater pH values do not shift into the acidic area. If a strongly acidic environment develops, there is also significant destruction of primary minerals and more significant dissolution of the secondary products of their transformation.

Example of the evolution of the selected physico-chemical parameters of groundwater during the oxidative action of atmospheric oxygen in the presence of atmospheric carbon dioxide for non-affected deep circulating groundwaters at the site of interest is shown in *Figure 8-11*.

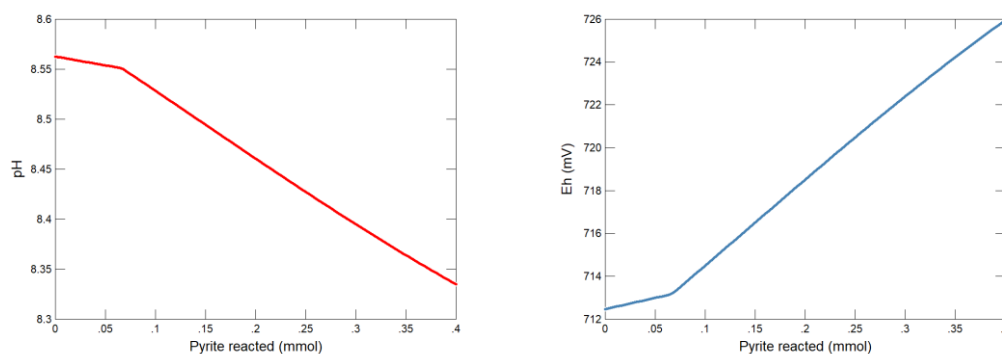
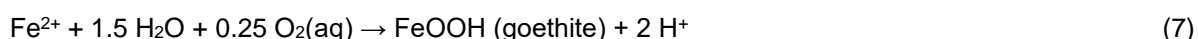


*Figure 8-11: The results of modelling of the change of pH and Eh after the opening of the undisturbed rock*

### Chemical evolution of the repository after closure

The reduction environment will be ensured after the closure and flooding of the repository by two factors. The first factor is that the rocks of the underground repository will be isolated from the atmosphere by groundwater, thereby preventing further access of oxygen from the atmosphere. The oxygen present in rocks and originally dissolved in groundwater will be consumed by the oxidation processes of sulfides and principally of divalent iron and manganese, which are contained in rock-forming minerals or dissolved in groundwater.

An example is oxidation of siderite or dissolved iron (5,6 and 7):



These processes create an oxygen-free (anoxic) environment and consequently contribute to the creation of a reducing environment.

The second factor that significantly contributes to the creation of a reducing environment and has sufficient reduction capacity is the infiltration of decomposing organic matter originating from organic debris on the surface.

### Migration of corrosion products

Probably the most important chemical processes in the Czech concept with the steel based canisters surrounded by bentonite processes are generation and migration of iron corrosion products.

In anoxic conditions, the iron corrosion reaction can be written as (8):



As the result of reaction (8),  $\text{Fe}^{2+}$  ions, hydroxyl ions and hydrogen are released to an aqueous solution, which results in changes in the physico-chemical parameters such as an increase in pH due to the higher  $\text{OH}^-$  concentration and increase in Fe concentration. These changes are, however, compensated by the hydrolysis of  $\text{Fe}^{2+}$  ions, the formation of  $\text{Fe}(\text{OH})_2$  and other reactions in the system, such as precipitation of magnetite ( $\text{Fe}_3\text{O}_4$ ) or other stable corrosion products. Some of the corrosion products can also be considered as bentonite alteration products, for example, greenalite and chamosite (i.e. fytosilicate minerals containing Fe) at anoxic conditions (e.g., Gondolli et al., 2018).

The basic assumptions, parameters and characteristics of the reference model are as follows:

- Temperature 25 °C and anoxic conditions.
- The geometry of the 1D reaction transport model was based on the parameters of the bentonite barrier considered for the "WP VVER 440" container. A bentonite barrier with a thickness of 725 mm was divided into 10 model cells, each of them with a thickness of 72.5 mm. A corrosion cell was also attached (72.5 mm) in the system. In each cell, 1 l of bentonite porewater B-SGW2-ANOX (see *Table 8-3*) was considered as the initial liquid phase.
- The transport of dissolved species was represented by simple diffusion with the effective diffusion coefficient of  $\text{Deff} = 1,3 \cdot 10^{-10} \text{ m}^2 \text{ s}^{-1}$  for each species.
- The iron corrosion given by equation (8) was considered to be kinetically controlled (e.g. Savage et al., 2010)
- For the reference model in this project, an average corrosion rate of  $1 \mu\text{m year}^{-1}$  was considered, which corresponds to  $k = 4.47 \cdot 10^{-9} \text{ mol m}^{-2} \text{ s}^{-1}$ . The corrosion rate of  $1 \mu\text{m year}^{-1}$  or similar was considered, for example, in modelling studies conducted by Wersin et al. (2008) and de Combarieu et al. (2007).
- The reactive surface area of iron (S) in the corrosion rate equation was calculated to be  $1.4 \cdot 10^{-2} \text{ m}^2$  based on the assumption of the cylindrical shape of the corrosion cell. This value represents the area of iron available for the corrosion reaction and was used in the model.

- The amount of solid iron was set to 100 mol, which guarantees a sufficient extent of iron in the system.
- Cation exchange reactions were described using the reactions in *Table 8-4*. In addition, the cation exchange reaction for  $\text{Fe}^{2+}$  was added to the model:  $\text{Fe}^{2+} + 2 \text{X}^- = \text{FeX}_2$  ( $\log K = 0.44$  according to Parkhurst and Appelo (2013)). As a result,  $\text{Fe}^{2+}$  can also be involved in the cation exchange reactions in the model.
- In each of the bentonite cells, 3.86 kg of the bentonite BaM was considered, which corresponds to a porewater volume of 1 l, a bentonite porosity of 41.5%, and a density of compacted bentonite of  $1600 \text{ kg m}^{-3}$ . The number of cation exchange sites and surface complexation sites was calculated based on 3.86 kg of bentonite.
- In the model, both dissolution and precipitation of the bentonite primary minerals was not allowed. The only corrosion product was magnetite. Precipitation of magnetite was only allowed in the bentonite cells, as suggested by Hunter et al. (2007).
- In the model, carbonate, sulphate, and nitrate reduction were suppressed, as suggested by Hunter et al. (2007).

Table 8-4: Parameters of the geochemical porewater model for the bentonite

Density of compacted bentonite	1600 $\text{kg m}^{-3}$		
Porosity	0.415		
Solid/liquid ratio	3.86 $\text{kg l}^{-1}$		
Temperature	25 °C		
<b>Minerals</b>	<b>Weight %</b>	<b>Cation exchange reactions</b>	<b>log K</b>
Smectite	87.770	$\text{Na}^+ + \text{X}^- = \text{NaX}$	0.000
Quartz	5.251	$\text{K}^+ + \text{X}^- = \text{KX}$	0.700
CaMg-siderite	3.108	$\text{Ca}^{2+} + 2 \text{X}^- = \text{CaX}_2$	0.800
Calcite	-	$\text{Mg}^{2+} + 2 \text{X}^- = \text{MgX}_2$	0.602
Dolomite	-		
Goethite	-		
Kaolinite	-		
<b>Well-soluble salts</b>	<b>mmol <math>\text{kg}^{-1}</math></b>	<b>Equivalent fractions (<math>\beta</math>)</b>	<b>meq <math>\text{kg}^{-1}</math></b>
$\text{Mg}(\text{NO}_3)_2$	0.41	NaX 0.072	39
$\text{NaHCO}_3$	40.0	KX 0.063	34
Gypsum	0.87	$\text{CaX}_2$ 0.213	117
Halit	0.51	$\text{MgX}_2$ 0.652	357
		CEC	547

The results of the reference (base case) model are shown in *Figure 8-12*. They are illustrated in the form of the values of the studied parameters as functions of the distance from the corrosion cell at four different times from the beginning of the simulations: 100, 1,000, 10,000 and 100,000 years.

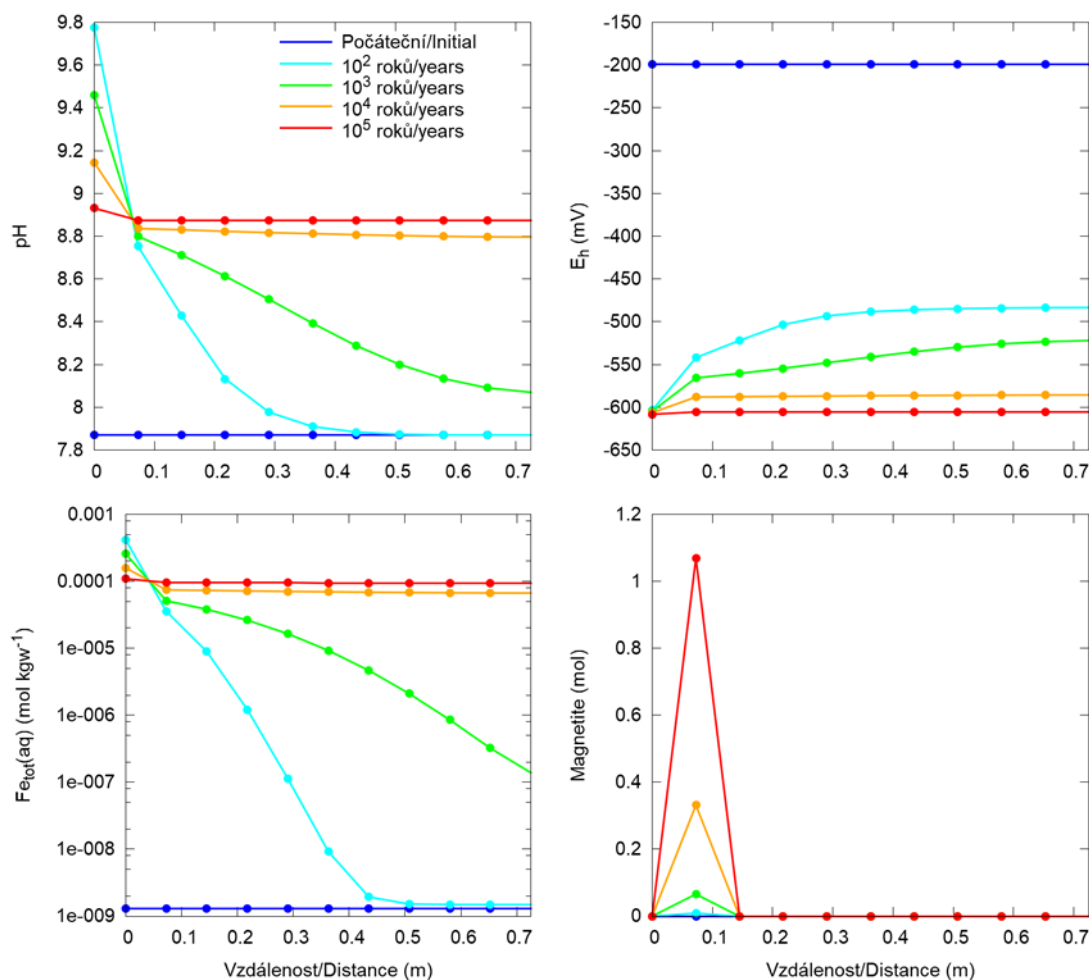


Figure 8-12: Reference model: Evolution of pH, Eh, iron concentration and precipitated magnetite as a function of the distance from the corrosion cell at 100, 1,000, 10,000 and 100,000 years from the beginning of the simulations

### Results of reactive transport modelling

The aim of the modelling was to assess the hydrogeochemical interactions that can occur in the repository in granite and identify important processes and issues on which SURAO should focus in future.

The physical and chemical interactions allowed for 2D reactive transport models were:

- speciation of the solutions
- mixing of the solutions
- equilibrium dissolution and precipitation of selected phases
- cation exchange on the surface of smectite

The results of the primary variants of 2D models using colour scales were visualised in the plane of the model domain (i.e. fracture) for time 0 (first equilibration of input solutions) and six selected output times 100, 500, 1,000, 10,000, 100,000 and 1,000,000 years. To illustrate the results, two observation points A and B were selected in the model domain *Figure 8-13*.

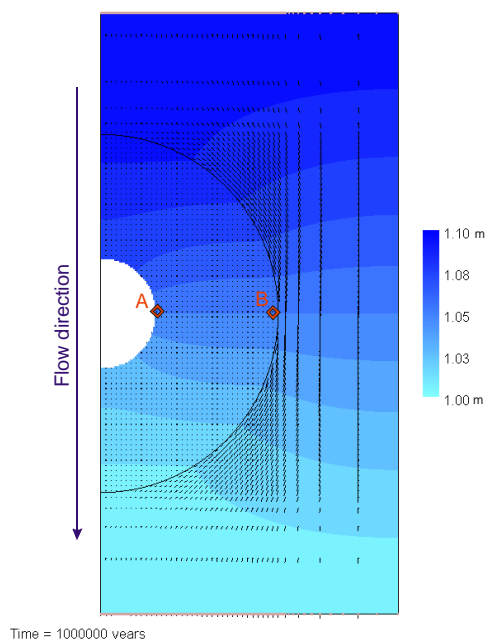


Figure 8-13: Hydraulic head pressures in the model domain with direction of flow and positions of observation points A and B

Hydrochemical interactions were driven by deviation from the local equilibrium between the bentonite porewater and primary or secondary minerals allowed in the system. Diffusive transport of all compounds was driven by the concentration gradient between the bentonite porewater and groundwater flowing through the fracture. The final distribution of each compound in the model domain and in time was the result of combination of transport processes and hydrochemical interactions. The initial content of gypsum in bentonite was dissolved immediately in the porewater of the buffer in all model variants. Sulfates and chlorides did not take part in any hydrochemical reaction in the simulated system. They were only transported by diffusion out of the bentonite buffer to the fracture and subsequently by advective transport out of the model domain. Distribution of all other compounds was more or less affected by hydrogeochemical interactions.

Dissolution of kaolinite occurred in all model variants based on model groundwater SGW2 (*Table 8-3*), especially in the fringe along the contact of the buffer with the fracture. The total dissolved mass of kaolinite after 1,000,000 years was negligible compared to the initial content of kaolinite (less than 1%). On the other hand, dissolution of kaolinite led to an increase of the pH of the bentonite porewater. Examples of the results for change of pH and pe are given in *Figure 8-14*.

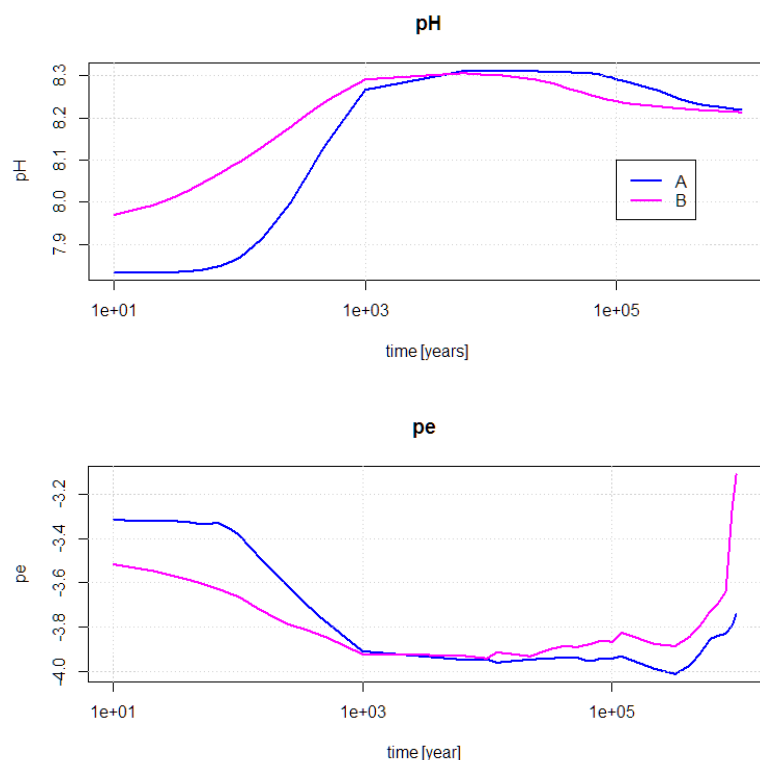


Figure 8-14: Evolution of pH and pe at observation points A and B for model variant under anoxic conditions.

## Conclusion

Geochemical modelling allowed SURAO to highlight, identify and qualitatively describe the processes that would take place at the interface of the bentonite buffer material and fracture with the flowing groundwater. Models included the transport processes (diffusion and advection) and hydrogeochemical interactions (dissolution and precipitation of selected mineral phases and ion exchange reaction within the clay minerals of the smectite group).

Some processes and phenomena were not included in the individual geochemical models or in the reactive transport model for several reasons. The primary reason was to preserve the consistency and simplicity of the whole system so that the different processes could be distinguished and the system properly interpreted. Another reason was a significant uncertainty in the full understanding of these processes and their proper implementation into the models. These not included processes are:

- Thermally induced transport – the bentonite engineered barrier and surrounding host rock will be heated as a result of heat generation from the waste package. Subsequently the groundwater will be heated up, resulting in a substantial temperature gradient between heated groundwater near the DGR and the surrounding groundwater. It is possible that this temperature gradient will generate a flow in the direction from the DGR to its surroundings, i.e. in the direction of the temperature drop. Fully saturated bentonite can be expected in the hundreds up to the first thousand years. The return of the temperature to the original state (i.e. ambient temperature) is estimated to be in the first tens of thousands of years. In a fully saturated environment with a temperature gradient, a significant proportion of the thermally induced transport and changes in the original steady flow can be expected.
- Non-homogenous saturation of bentonite – the non-homogenous saturation of bentonite will occur in rock environment dominated by fractures, and it is highly probable that some disposal areas will be fully saturated significantly later than others. Until complete saturation of the bentonite and system stabilisation occurs, geochemical evolution (e.g. the

composition of porewaters) may be inhomogeneous. Influence can also be expected on the groundwater flow and the formation of preferential pathways.

- Influence of temperature on dissolution and precipitation of mineral phases – the temperature has a considerable effect on the dissolution and precipitation of minerals. Solubility generally increases with temperature, but this does not apply, for example, to carbonates, where, on the contrary, increasing temperature decreases solubility. It has a significant influence on geochemical reactions and can significantly affect the results of the geochemical model. Some individual geochemical models can include the influence of temperature. However, the reactive transport model took place in the "cold" phase where the temperature of the system will not be affected by the heat generated by the SNF. A temperature of 25 ° C was considered, since most thermodynamic data are related to this temperature.
- Uncertainties in groundwater saturation with respect to minerals – although the basic silicates and aluminosilicates, such as plagioclases, feldspars, pyroxenes, etc., are usually thermodynamically stable for the given composition of groundwater in the presence of dissolved SiO<sub>2</sub> and aluminium, other phases containing the same main components originate under the surface and near-surface conditions of the Earth's crust, for example, the formation of clay minerals, various modifications of SiO<sub>2</sub>, precipitation of trivalent iron oxyhydroxides (e.g. goethite, ferrihydrite) instead of more stable hematite, etc. One reason is the different kinetics of reactions where the rate of formation of the latter minerals is several orders higher than of the original rock-forming aluminosilicates of crystalline rocks. Another reason is that the composition of groundwater corresponds to a stationary state rather than to thermodynamic equilibrium with certain minerals. This stationary state is the result of differences in the rate of dissolution of the primary minerals and the rate of consumption of the individual components in the newly formed mineral phases. Because of this stationary concentration, the primary minerals are undersaturated and the secondary minerals are oversaturated, while from the long-term perspective the groundwater composition is stable and does not change significantly over time.
- Potential effects of other processes – for example, the protonation/deprotonation of the surface sites of clay minerals of the smectite group within the bentonite in the reactive transport model.

The significance of these processes with respect to the current results of individual geochemical models will be tested in further phases of SURAO DGR development programme.

## 9. Finland

VTT - Markku Leivo

### 9.1 Characterization of an ILW disposal cell in granite

#### 9.1.1 Description of materials in disposal cell

In Finland both operational LILW repositories are excavated in crystalline rock about 100 m depth. The disposal system is conceptually divided into components as shown in *Figure 9-1*. The waste cavern on the left represents low level waste disposal without engineered barriers of backfilling in the cavern. On the right is intermediate level waste and packages surrounded by concrete barriers inside backfilled waste cavern.

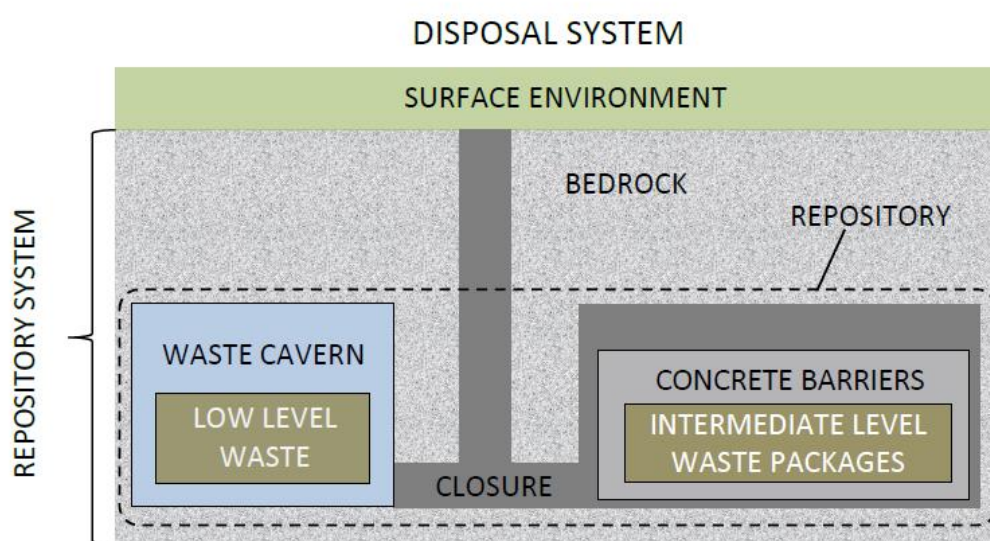


Figure 9-1: Conceptual representation of components within the disposal system. (Nummi 2018)

The components can be expressed as:

- *Low level waste* disposed in the repository without additional engineered barriers. Low level waste mainly consist of contaminated materials and the waste containers are usually steel drums. Some low level wastes are also disposed without a container.
- *Intermediate level waste* includes mainly activated materials and solidified liquid waste. They are packed in concrete waste packages.
- *Concrete barriers* around the intermediate level waste packages.
- *Waste caverns* excavated in the crystalline bedrock.
- *Closure* is to separate the repository from the surface environment and provide mechanical support for the concrete barriers. Closure includes concrete plugs and backfilling in the waste caverns and tunnels.

### 9.2 Hydraulic gradients

For example the groundwater system of the Hästholmen island (Loviisa) can be divided into several distinctive layers. Above 50-100 meters is the so-called fresh  $\text{HCO}_3^-$  -rich water lens and close to the coastline this layer contains also water from the present Baltic Sea. At approximately 100 to 400 meters is a  $\text{SO}_4$ -rich brackish Na-Cl water layer, which mainly originates from the Litorina sea. Below the depth of 400 m pre-Litorina water containing glacial meltwater is found, and below 600 m saline preglacial and Pre- Cambrian and Eemian Sea water. However, groundwater flow is dominated by the upper groundwater layers, and the lower levels are essentially stagnant. (Snellman et al. 1998)

Repository is expected to be saturated after the closure. The water will be brackish groundwater. Due to the land uplift fresh water will replace the brackish water later on.

### 9.3 Pore water compositions

Brackish groundwater with TDS ranging from 2 000-9 800 mg/l has been observed at both Finnish sites. At Olkiluoto brackish Na-Cl or Na-Ca-Cl-type groundwater occurs from a depth of 60m to a depth of 400-500m. At Loviisa, brackish Na-(Ca)-Cl-type groundwater has been met from a depth of about 50m down to about 600m.

In the upper part of the bedrock to a depth of 50-100m, quite young, fresh-brackish  $\text{HCO}_3^-$ -rich groundwater occurs, which is a mixture of the present Baltic Sea water and water infiltrating from the surface. Deeper, at 100-400m the  $\text{SO}_4$ -rich groundwater has strong influence of the preceding Litorina Sea water, and below this is a groundwater containing a greater portion of glacial meltwater. Below, at about 500-600m there is saline groundwater containing increasing amounts of water older than the Weichselian glaciation, however remnants of cold-climate water have been mixed in this ground water. (Snellman et.al. 1998).

## 9.4 . Chemical evolution of the ILW disposal cell

### 9.4.1 Narrative

Most interesting chemical evolution in disposal cell is the concrete/steel interaction and the chemical evolution of concrete due to groundwater. Most important chemical reaction is assumed to be the leaching of concrete and the subsequent changes on pH in the environment as well as the direct degradation of concrete. The degradation of the concrete barriers decrease their ability to limit and retard radionuclide transport. Changes of pH of the environment changes the corrosion behavior of the steel. Both the waste itself and reinforcement corrosion is in interest.

The groundwater composition is not very aggressive and thus other degradation processes (sulphate attack, ettringite formation, carbonation, magnesium ingress) impact the concrete at a considerably lower rate. Leaching of concrete occurs in many phases, but can be simplified to only include leaching of portlandite (CH) after which leaching of CSH-gels is initiated. In the process the pH in the concrete gradually decreases.

### 9.4.2 Conceptual model

Modelling chain can be expressed as separate interconnected activities as presented in *Figure 9-2*.

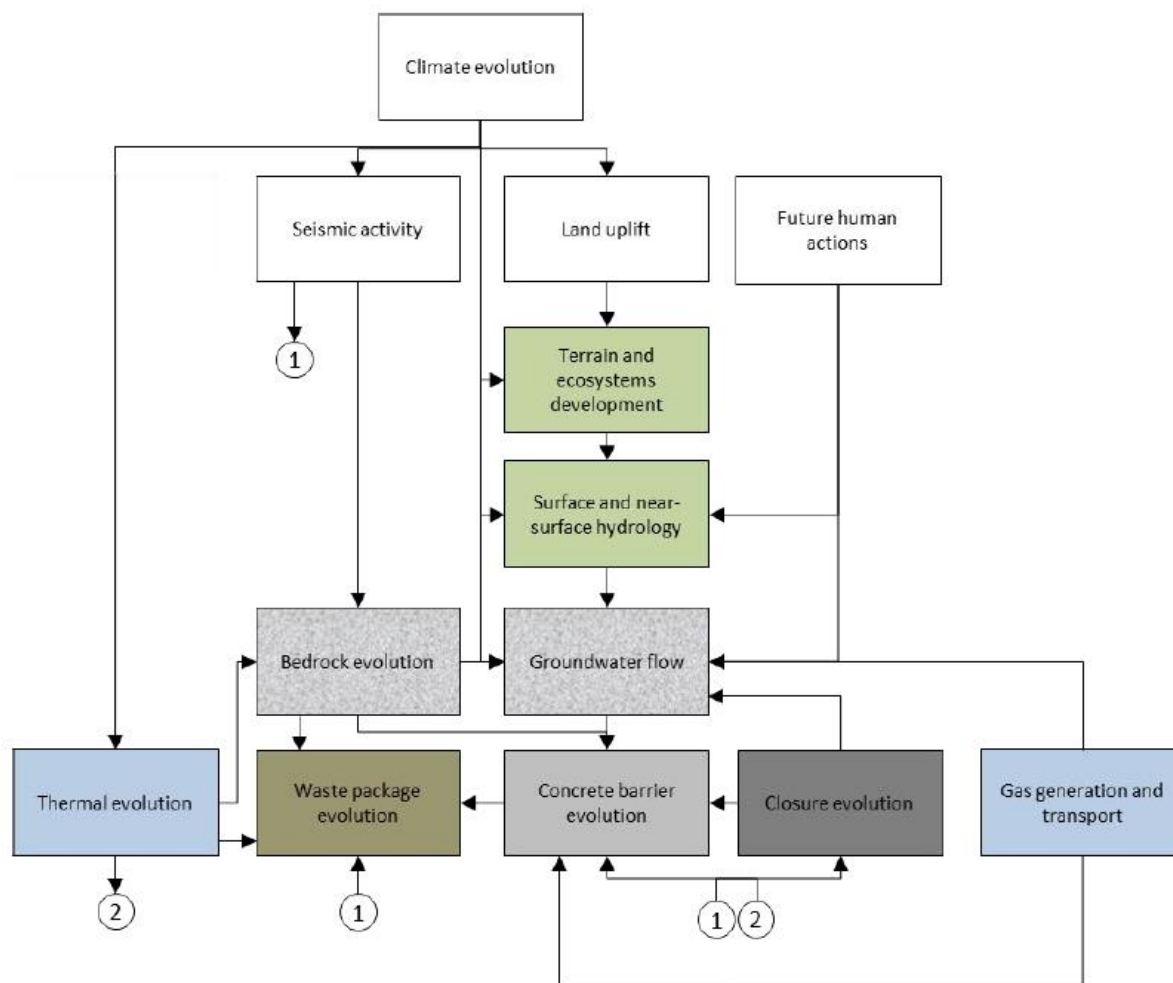


Figure 9-2: The modelling chain in the performance assessment. (Nurmi 2018)

All of these activities must be dealt and the information flow between actions essential. Arrows in the Figure 9-2 present schematic data flow.

### 9.4.3 Mathematical model

Mathematical models are presented in multiple reports, and are mostly available when the exact target of this research is defined.

### 9.4.4 Calculated results

Example of the modelling result is presented Figure 9-3. This presents the degradation of concrete cover due to groundwater leaching in one of the concrete barrier. It can be seen that the total degradation is expected to be slow process in this case.

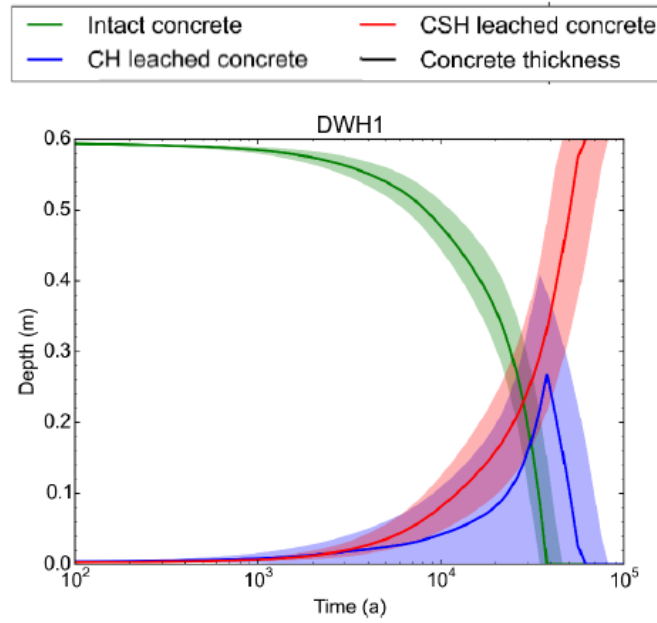


Figure 9-3: Leaching depth of concrete barrier due to groundwater.

## 10. France

ANDRA - Benoît Cochepin, Christelle Martin and Isabelle Munier

### 10.1 Characterization of the HLW disposal cell in clay

#### 10.1.1 Description of materials in disposal cell

##### 10.1.1.1 Description of waste

The HL waste is mostly vitrified waste resulting from spent fuel reprocessing that allows to separate fission products and minor actinides, formed by nuclear reaction within nuclear reactors, from uranium and plutonium, i.e. radioactive materials which can be recovered. Fission products and minor actinides are then calcined and incorporated into a glass matrix. The glass produced is hot cast into a stainless steel container.

Other waste packages, in very limited quantities, are considered as HLW packages. This primarily includes packages of 'technological waste' produced during operations at the La Hague vitrification facility and certain used sealed sources from the CEA (Andra, 2016a).

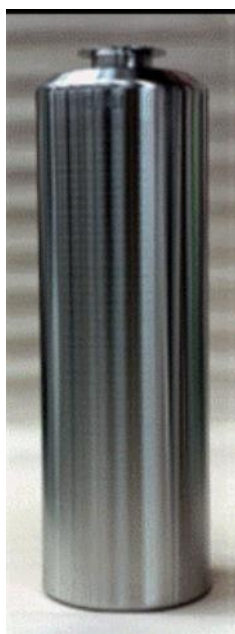


Figure 10-1: Image of a HLW vitrified waste primary package

##### 10.1.1.2 Description of disposal packages

The HLW container body consists of a cylindrical shell made of non-alloy steel with an effective thickness of between 65 and 53 mm, a welded base of a thickness matching the shell thickness, and a cover made of the same grade of steel. All the welded joints are made at full thickness to reduce their singular character in terms of strength and leaktightness. A gripping groove machined into the disposal container lid allows handling, emplacement and possible retrieval of disposal packages during a minimum period of 100 years (Andra, 2016a).

In general, the disposal containers are designed to contain one or two primary packages. For some shorter primary package, the possibility of placing three packages is also studied.

Andra has selected low-carbon unalloyed steel as the material of the container. This choice is based on the predictable corrosion kinetics of the material, in that general corrosion is the predominant

mechanism rather than localised corrosion processes. In particular, the chosen grade of steel and its microstructure limit the risk of stress corrosion (Andra, 2016a).

The functions of the HLW disposal package are mainly related to the operation period of Cigéo (package transfer and handling, standardisation of Cigéo components, etc.). In order to make best use of the containment capacity of nuclear glass, Andra has also chosen to delay the arrival of water on glass, so that the temperature is lower when water finally comes into contact with it: this function concerns the leaktightness of the disposal container. At this stage<sup>10</sup>, Andra intends to ensure that the leaktightness of the HLW disposal container is maintained at least as long as the core temperature of the glass is greater than 50°C for the moderately-exothermic waste (HLW0) delivered before 2075 and above 70°C for the highly-exothermic waste (HLW1/HLW2) delivered after 2075. The higher value used for the HLW1/HLW2 waste is explained by the advances in knowledge about the behaviour of vitrified waste and of radionuclides in solution expected over the coming decades. With the architecture selected for the underground facility, these limits correspond to a period of less than 500 years after the closure of Cigéo (Andra, 2016a).

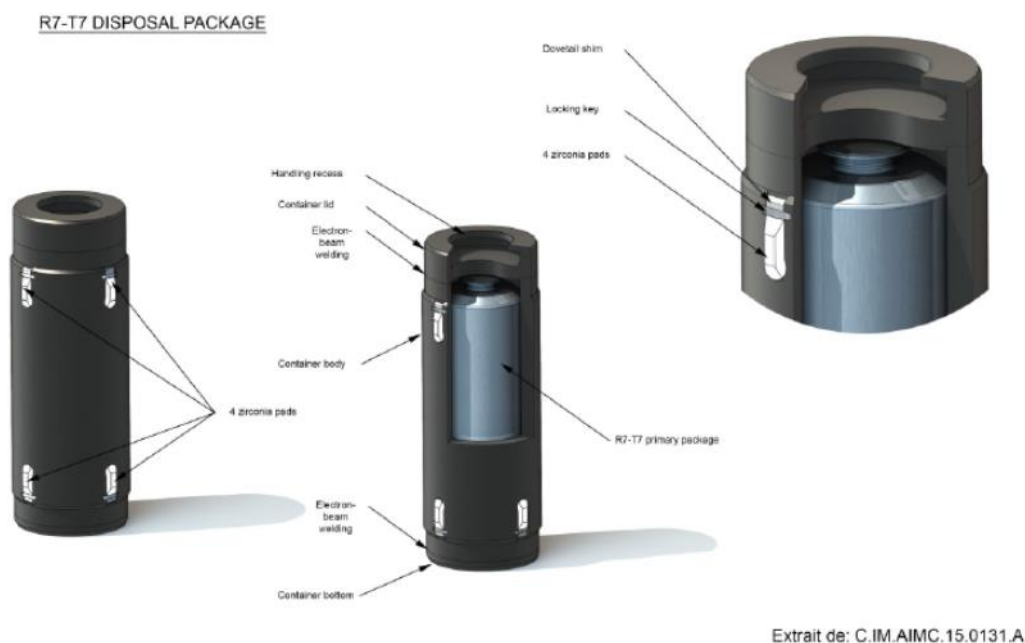


Figure 10-2: R7-T7 disposal package with at top right, a detailed view of its gripping groove.

#### 10.1.1.3 Description of HLW disposal cells

The HLW disposal cells comply with the design principles which serve to justify the performance of the structures in operation and after closure. They are designed as sub-horizontal bores with a slope of 1% to 2 % with the lower end oriented towards the access drift. At this stage of the project, the length of these dead-end cells are of the order of 100 m (Andra, 2016a).

<sup>10</sup> These temperature constraints may be reviewed between now and the construction licence application on the basis of advances in knowledge, in particular on the behaviour of the radionuclides at higher temperature.

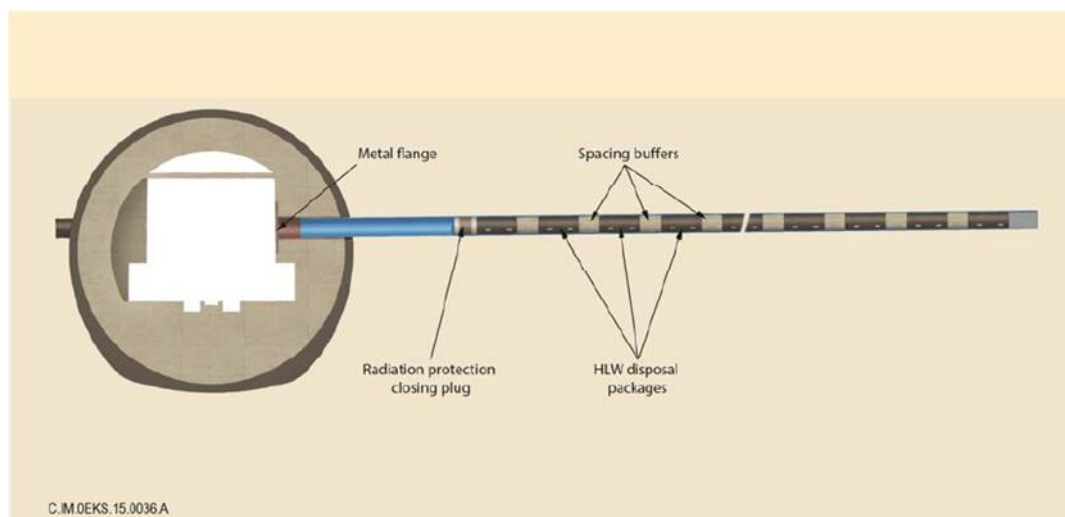


Figure 10-3: Cross section through a HLW1/HLW2 disposal cell: shown here at the end of loading (illustration from end of basic engineering design stage).

According to the current reference design of the disposal cell (Andra, 2016a):

- The disposal cells contain disposal packages and spacers if applicable;
- The sleeving of the HLW disposal cells are made of low-carbon steel. The minimum thickness of 25 mm of the sleeve is designed to ensure its mechanical stability over the period of reversibility (around 100 y). The diameter of the tube is of the order of 700 mm;
- The annular gap between the sleeve and the clay rock is filled with a material that imposes corrosion-limiting environmental condition (cement-based grout).

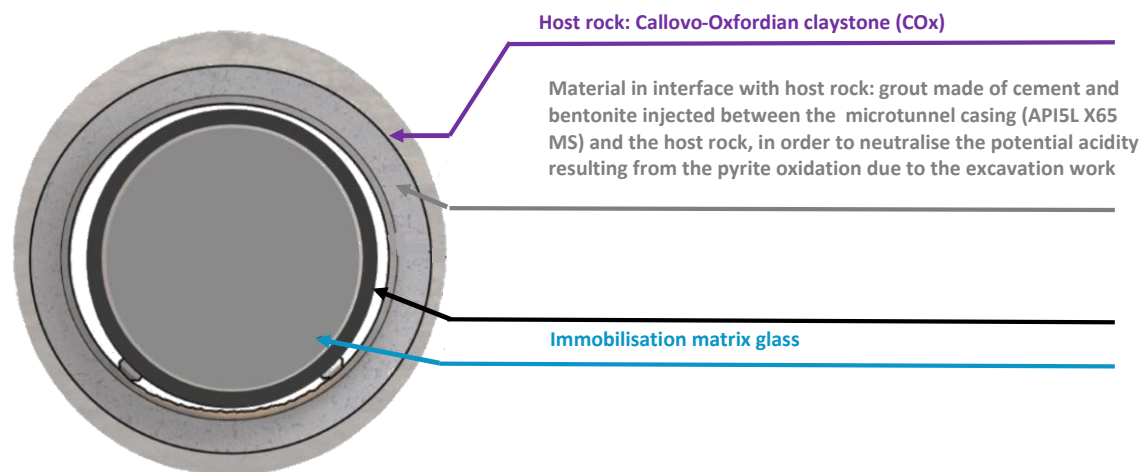
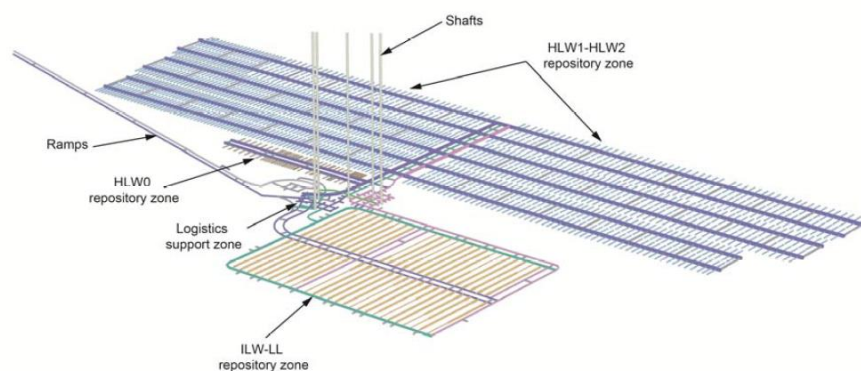


Figure 10-4: Section of a HLW disposal cell with identification of the different materials.

The most exothermic HL waste are grouped together within a same zone (HLW1-HLW2 zone), that is separate from the zone (HLW0 zone) dedicated to the moderately-exothermic HL waste (see the figure of illustrative scheme of Cigéo). The requirements and data taken into account for the design of the repository zones are directly associated with the post-closure safety objectives (Andra, 2016a).



CJM.AMSL16.0057.A



Figure 10-5: Cigéo underground facility.

#### 10.1.1.4 Description of the host rock

Andra is mainly interested in study of Callovo-Oxfordian claystone behaviour (Andra, 2016a). The Callovo-Oxfordian clay formation, dating from the Jurassic, was deposited about 160 million years ago over a period of about 5 million years, in an open and calm marine environment, below a water depth of about a hundred metres. It forms a predominantly clay layer between the limestone formations of the Dogger and the Oxfordian. Its thickness varies from 130 m to 160 m, located at a depth of 500 m to 630 m.

The formation is formed of three main mineralogical phases: a predominantly clayey phase (40% to 45% on average, up to 60% in the middle of the layer), a calcareous phase (mostly calcite, with a few percent of dolomite) and a quartz phase (of fine particle size: silts).

#### 10.1.2 Thermal gradients

The primary packages of HL waste are characterised by heat release, which is taken into account in the dimensioning: Andra has chosen to limit the temperature and the thermo-hydro-mechanical effects on the Callovo-Oxfordian in a range (i) avoiding irreversible degradation of the disposal system characteristics contributing to the safety functions, particularly the Callovo-Oxfordian, and (ii) within which the processes governing changes in the disposal system can be represented and modelled reliably. In particular, it implies a cell temperature always below 100°C (in practice, the criterion applied in the clay rock is 90°C). Compliance with this range is based on the relationship between the heat output of the packages, which is related to their radiological content and the duration of their prior interim storage, and the dimensioning of the underground facility.

To justify the post-closure safety of the repository at the disposal section level, a thermo-hydro-mechanical design of the HLW disposal sections is performed, taking account of (Andra, 2016a):

- the heat induced by the different types of HLW and the diffusion of the heat in the clay rock and the thermal decay associated with the radioactive decay which is a function of the inventory and the preliminary storage time;
- the major horizontal stress perpendicular to the centreline of the access drifts;
- the hydro-mechanical response of the clay rock to temperature increase (changes in interstitial pressure and effective stress with respect to mechanical strength) and the mechanical response of the clay rock to the access drift boring operations (strain, fractures, behaviour of the damaged zone);

- ventilation of the drifts during the operating period and any changes in air flowrate over the successive construction and operating phases and while awaiting closure,
- For the continuation of the detailed engineering design of the HLW1/HLW2 zone, the following design data are used, based on models with conservative thresholds for the failure criteria.

Table 10-1: Number of packages per disposal cell and distance between cells for disposal of highly exothermic HLW approximately 100m long

Waste package family	Age of packages and thermal output on disposal in the repository	Number of packages per disposal cell	Distance between cells Px (m)
A	85 years (275 W per package)	44	33
B	85 years (345 W per package)	38	36
C	85 years (365 W per package)	34	51
D	70 years (448 W per package)	29	45

The Figure 10-6 below shows the temperature change in the clay rock around the warmest HLW2 waste disposal cell, with the present dimensioning. Note that the dimensioning criterion here is the THM criterion, not the criterion of 90°C maximum temperature in the clay rock.

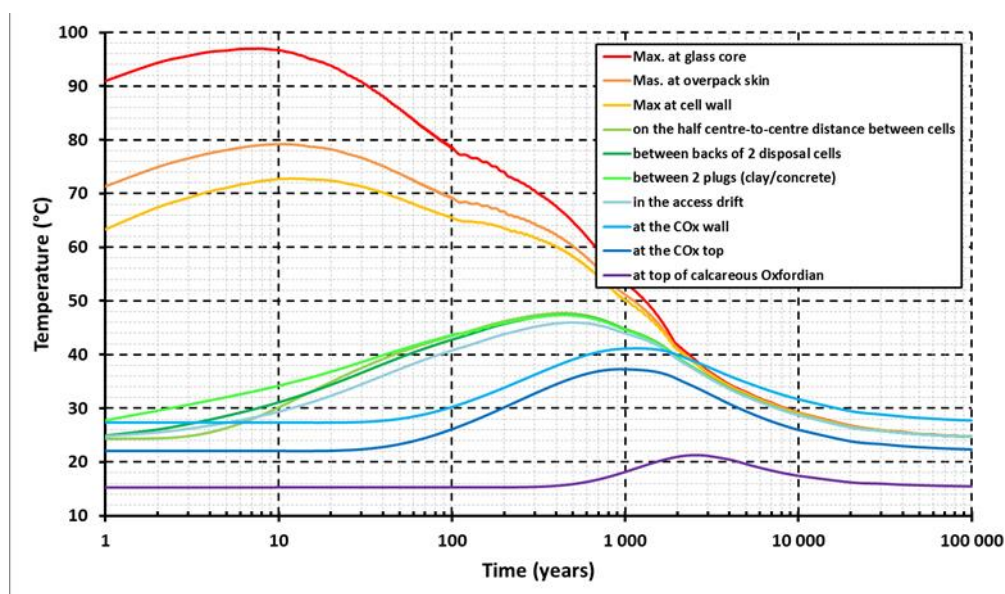


Figure 10-6: Temperature change over time at various points in and around the warmest HLW2 cell (temperature change in the clay rock at the cell wall is given by the yellow curve).

### 10.1.3 Pore water compositions

Callovo-Oxfordian clay layer has been extensively studied, especially from a mineralogical point of view. First, its interstitial water had been described through modelling (Gaucher et al.; 2006 and 2009) before being reinforced by in situ data (Vinsot et al.; 2008).

The modelling of water composition with reactive transport tools takes into account the mineralogy and exchangers composition (see detailed in Table 10-2 and Table 10-3) (Marty et al; 2014a and 2014b, Idiart & Laviña; 2019). The chemical composition of the water is described in Table 10-4.

Table 10-2: Example of mineralogical composition of the Callovo-Oxfordian claystone and molar volumes of the different minerals and secondary minerals (Marty et al. 2014a)

Primary Minerals	M <sub>v</sub> (cm <sup>3</sup> /mol)	mol/kg <sub>water</sub>
Calcite	36.93	27.99
Celestite	46.25	0.69
Dolomite	64.3	2.76
Pyrite	23.94	1.06
Siderite	29.38	1.10
Illite_Imt-2	139.18	10.77
Montmorillonite-BCCa	132.48	2.75
Microcline	108.74	1.37
Quartz	22.69	50.86
Ripidolite_Cca-2	211.92	0.41

Table 10-3: Example of exchangers composition of the Callovo-Oxfordian claystone (Idiart & Laviña; 2019)

Exchanger	Log K	mol/kg water
Cox2Ca	0.7	4.7·10 <sup>-01</sup>
Cox2Mg	0.7	3.3·10 <sup>-01</sup>
CoxNa	0	3.9·10 <sup>-01</sup>
CoxK	1.2	7.8·10 <sup>-02</sup>
Cox2Sr	0.6	1.2·10 <sup>-02</sup>
Cox2Fe	0.8	2.9·10 <sup>-03</sup>
<b>Total (CEC)</b>		2.1

Table 10-4: Example of water composition of the Callovo-Oxfordian claystone (Marty et al. 2014a)

Variable	Value
pH	7.0
pe	-2.8
<b>Totals</b>	<b>Concentration (mol/kg water)</b>
Al	8.4·10 <sup>-8</sup>
C	3.8·10 <sup>-3</sup>
Ca	7.6·10 <sup>-3</sup>
Cl	4.1·10 <sup>-2</sup>
Fe	6.8·10 <sup>-5</sup>
K	5.1·10 <sup>-4</sup>
Mg	5.1·10 <sup>-3</sup>
Na	4.0·10 <sup>-2</sup>
S	1.1·10 <sup>-2</sup>
Si	1.8·10 <sup>-4</sup>
Sr	2.3·10 <sup>-4</sup>

The material injected at the interface with host rock is a grout made of cement and bentonite. Andra is studying a range of material composition more or less alkaline. In a first approximation, this material could be assessed between a “low-pH” and an OPC cement.

## 10.2 Chemical evolution of the HLW disposal cell

### 10.2.1 Narrative

#### 10.2.1.1 Operating period

The main chemical processes affecting the components of Cigéo HLW cells during the exploitation phase are the oxidation processes of the Callovo-Oxfordian claystone in the field close to the structures, the chemical interaction between the host rock and the injected cementitious material and, in a less extent, corrosion processes (Andra, 2016a).

The ventilation of access drift leads concomitantly both a desaturation of the rock (ZFC) and the development of a so-called oxidizing disturbance in the host rock because of its reactivity with oxygen in the air. From a mineralogical point of view, this disturbance corresponds mainly to the oxidation of the Fe-bearing mineral phases (pyrite, siderite, etc.), to the dissolution of the carbonated phases and to the formation of sulphated secondary phases (gypsum, etc.). It leads to a modification of the undisturbed host rock water composition.

During this period, corrosion in a humid atmosphere concerns the inner surface of the liner and the disposal container. This corrosion usually starts when the relative humidity reaches a value of about 70% (formation of a film of water).

To prevent acceleration of sleeve and container from corrosion during this phase, the annular space between the sleeve and the rock is filled with a material intended to neutralise the transient oxidizing/acid disturbance. The formulation of the material is designed to reconcile this objective with the requirement that the pH of water coming into contact with the glass after loss of container leaktightness be as close as possible to neutrality.

#### 10.2.1.2 Post-closure period

The chemical evolution of an HLW disposal cell after closure, that is to say of the Callovo-Oxfordian system (mechanically damaged zone in the near field and mechanically undisturbed Callovo-Oxfordian claystone) and of the engineered components of the cells (cementitious grout, steels of lining and disposal containers, glass matrix) is part of a thermal, mechanical and hydraulic evolution (Andra, 2016b):

- The thermal transient has a duration of a few hundred to thousands of years at most with a maximum within the cell reached in a few tens of years at most. Its intensity and duration are sufficiently limited that it does not involve significant mineralogical transformations in the Callovo-Oxfordian. It intervenes as a parameter of the chemical processes of interactions between the components of the chemical system which represents a HLW cell, and this over a short duration;
- The mechanical evolution intervenes indirectly, mainly by the rupture of the HLW disposal containers, after a few thousand years, which allows the arrival of water (vapor and liquid) on the primary packages (container in stainless steel and supposedly at the same time on the glass), thus allowing its gradual dissolution. The dissolution of the glass depends in intensity of its initial fracturing but also of the fracturing under the mechanical loading by the deferred deformation of Callovo-Oxfordian in the time;
- The hydraulic / gas transient has a duration of several tens to hundreds of thousands of years with first the consumption of residual oxygen, and then the production of hydrogen through anoxic corrosion. The total corrosion of the metallic components leads to the end of the hydrogen source term, and a total resaturation of the disposal cell.

Chemical processes (corrosion, chemical degradation of cementitious materials, etc.) are conditioned by the presence of water (liquid and vapor). The hydraulic-gas transient has therefore an effect on the chemical evolution of an HLW cell. It is then possible to distinguish two main periods:

- The first period includes all the phenomena that occur until the loss of watertightness of the disposal container, i.e. the first few thousand years. This period is marked by the thermal transient of the cell, because of the presence of the waste packages. It is also marked by a "short" period (approximately 100 years) during which the cell is resaturated with water, before it becomes desaturated by the production of hydrogen linked to the corrosion process. This desaturation results in a gaseous mixed hydrogen-water vapor atmosphere within the cell, with a relative humidity greater than 90 %. The chemical system involved during this period consists of metal components, liner and disposal containers, cement filling material and near-field claystone.
- The second period begins when the storage container breaks and spreads over the long term. The temperature in the cell has decreased below 50 °C. It occurs around 4000 years after the installation of the package assuming an average corrosion rate of 10 microns / year<sup>11</sup> and a minimum mechanical thickness at break of a few millimeters. The chemical system involved during this period consists of glass, metal components, liner and disposal containers, cement filling material and near-field claystone. This period can be subdivided into two sub-periods, before and after the water saturation of the cell.
  - For a few tens to hundreds of thousands of years, the cell is not saturated with water. The glass is exposed to an atmosphere consisting of water vapor and hydrogen, except in the lower part where condensation can occur in the corrosion products, which allows the presence of liquid water in contact with the glass. The relative humidity is above 90%.
  - Beyond, and over the long term, the cell is completely saturated with water. The temperature is then imposed by the rock, about 22 ° C.

### Iron/clay interactions

The disposal containers and the sleeve of the HLW cells contain a large quantity of steel, entailing the necessity of verifying the limited character of the impact of iron on the favourable characteristics of the Callovo-Oxfordian.

The iron/clay interactions at the HLW cells are well understood experimentally. They involve the formation of various secondary compounds: iron oxides, iron carbonates, iron silicates and aluminosilicates, sulphides and newly-formed iron-enriched clays. Hydrogen is also formed, some of which is dissolved in the aqueous phase.

Geochemistry-transport simulations show, at the end of the corrosion period, a remineralised zone several centimetres up to some decimetres in extent at the initial iron-clay rock interface and a slightly-disturbed zone a few metres in size in the Callovo-Oxfordian. The clay rock close to the HLW cells is consequently concerned by the disturbance.

In view of its small extent, this disturbance has a negligible impact on radionuclide transfer in the Callovo-Oxfordian host formation.

### Cementitious grout degradation

The current design of HLW cells includes the injection of a cementitious type material between the host rock and the metal liner to prevent any increase of the corrosion rate due to the partial oxidation of the rock during the operating period. The neutralization of the cementitious grout in contact with the oxidized claystone occurs gradually and leads to a silicate-carbonates-clay mixture comparable to claystone, it means with a water composition close to equilibrium with claystone (pH ~7,2).

Assessments carried out by numerical simulation indicate that total dissolution of the smectite phase would take place over a maximum extension of one centimetre from the interface, and a moderate

---

<sup>11</sup> The average corrosion rate will depend among other things on the pH imposed by the cementitious grout.

evolution of the sodium- and calcium-bearing fractions of the ion exchange site after 100,000 years. Similarly, the ionic strength and potassium concentration (K) undergo very little change in the clay rock.

### Waste degradation

Glass alteration by water only starts after the container lose its integrity, due to corrosion processes and to lithostatic pressure. However, the production of hydrogen by anoxic corrosion will probably maintain an unsaturated situation for a few tens of thousands of years in the primary container. Under these conditions, it is very likely that the alteration of the upper part of the glass package starts in contact with water vapor, with relative humidity still close to 100%.

Subsequently, after resaturation of the container, the glass will be altered in contact with the water of site having drilled through the cementitious grout, the corrosion products of the liner and the disposal container. The alteration of the glass is, moreover, directly related to its composition as well as surfaces exposed to water and therefore to its fracturing that essentially results from the initial fracturing (related to cooling).

In unsaturated conditions, the degradation of nuclear glass starts only at a relative humidity of at least 50% and the formation of a monolayer of water on the surface of the glass. The hydration rates depend on the chemistry of the water film on the surface of the hydrated glass: the absence of exchange with the external environment will cause a very strong increase in the concentrations and the pH within this layer of water and the precipitation of crystalline secondary phases (analcime / tobermorite type).

According to literature (Vienna, 2013; Gin et al., 2015), glass alteration in pure water is due to the formation and dissolution of an alteration film, which is likely to incorporate chemical elements from the solution and to act as a diffusion barrier for reactive species. How effective this barrier is primarily depends on the concentration of silicon in solution in the vicinity of the glass.

The phenomenology of alteration of SON68 glass in Callovo-Oxfordian porewater is identical to that observed in pure water (*Figure 10-7*). After the water has penetrated into the glass (hydration) and after a very short initial step marked by a predominant interdiffusion (preferential relaxation of the network modifying elements resulting in the formation of a hydrated layer), the dissolution of the glass becomes congruent for the major elements (Si, B, Al ...) and is dominated by the hydrolysis reaction of the silicate network which corresponds to the alteration regime at initial rate ( $V_0$ ). An alteration film gradually forms on the surface of the glass; it plays a role of diffusion barrier, also called protective role, and induces a fall of the alteration rate. The alteration of the glass then continues at a residual rate ( $V_R$ ).

Beyond the alteration regime through the residual rate which depends on the environmental conditions, an alteration recovery inducing an increase in alteration rates may possibly occur. However, in the case of SON68 glass in repository condition, such a phenomenon is very unlikely. Indeed, it has so far been observed experimentally only under specific conditions ( $\text{pH} > 10.5$  and / or  $T \geq 90^\circ \text{C}$ ) not representative of long-term conditions expected in HLW disposal cells after neutralization of the cementitious grout.

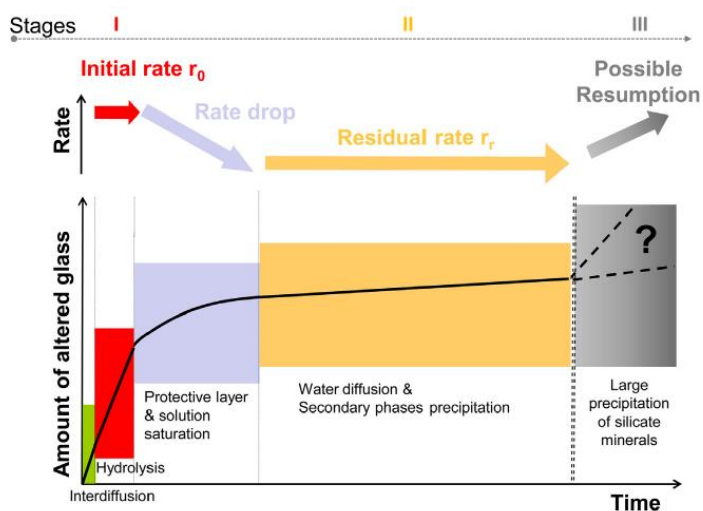


Figure 10-7: Stages of nuclear glass corrosion and related potential rate-limiting mechanisms (Gin et al., 2013).

Corrosion products (CP) resulting from the corrosion of a low-alloy steel in anoxic conditions (conditions expected in the disposal cells after consumption of residual oxygen) are mainly composed of iron oxides such as magnetite, or iron carbonates such as siderite  $\text{FeCO}_3$  or chukanovite  $\text{Fe}_2(\text{OH})_2\text{CO}_3$ . Iron and corrosion products increase glass alteration by maintaining high alteration rates over longer periods than in pure water. The identified associated mechanisms are mainly silicon sorption at surface sites of corrosion products, and iron silicates precipitation.

The silicon released during glass alteration can also interact with other elements transported in the groundwater such as magnesium, whence a distribution/competition between iron silicates and magnesium silicates.

### 10.2.2 Conceptual and mathematical model

The model of nuclear glass alteration in HLW cells takes into account both the glass hydration phase in unsaturated conditions and the alteration in water (Figure 10-8), and assumes a radionuclides release congruent with alteration of the vitreous matrix.

Silicon is a key parameter with respect to the alteration of glass, hence the importance of the interactions of silicon with corrosion products via sorption and coprecipitation processes, as well as with magnesium present in the Callovo-Oxfordian porewater, Callovo-Oxfordian claystone and the cementitious grout.

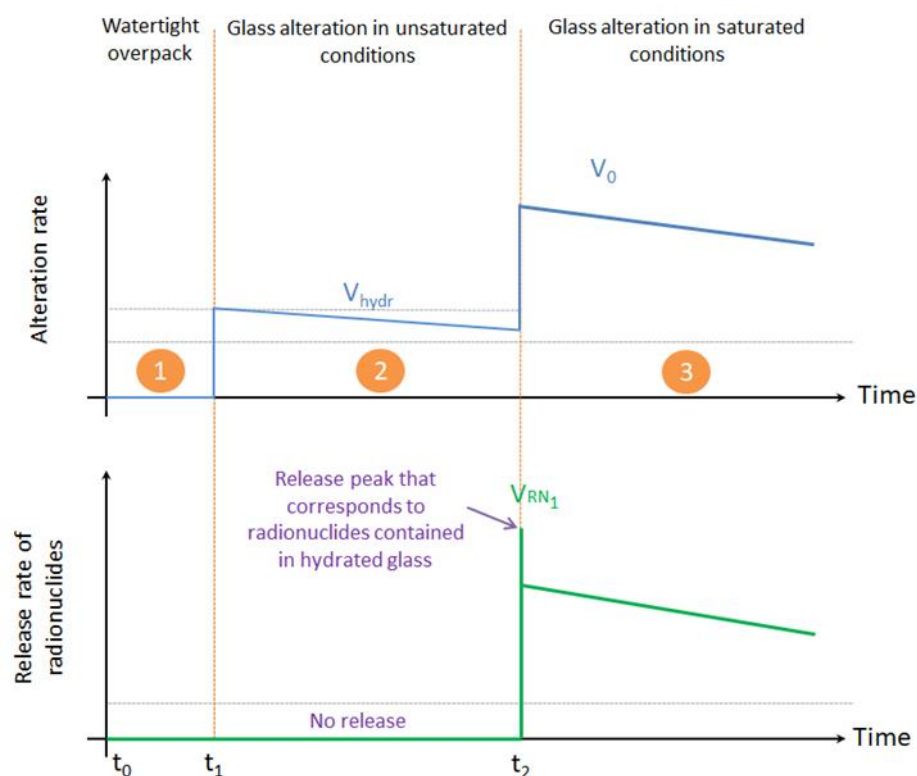


Figure 10-8: Alteration of a glass surface and associated release of radionuclides - (1) sealed container (2) alteration under unsaturated conditions in the vicinity of the glass  $\Rightarrow$  no release (3) as resaturation occurs near the hydrated glass, release of the radionuclides present in the hydrated glass and alteration in  $V_0$  (4) alteration in  $V_R$  - At each moment, until the total resaturation, one part of the glass will alter under unsaturated conditions and another part under saturated conditions thus leading to gradual release of radionuclides.

The parameters of this model, especially the values of  $V_0$  and  $V_R$  are defined on the basis of experiments conducted in Callovo-Oxfordian porewater and in the presence of environmental materials (unalloyed steel, Callovo-Oxfordian claystone<sup>12</sup>).

The duration of the transient between the alteration regime at the initial rate  $V_0$  and that at the residual rate  $V_R$  is a function of the interactions between the silicon and iron. These interactions strongly depend on the iron and silicon fluxes induced by the corrosion processes of the metal components and the glass alteration.

## 10.3 Characterization of an ILW disposal cell in clay

### 10.3.1 Description of materials in disposal cell

#### 10.3.1.1 Elements of geometry

In the French concept, the IL waste is disposed of in "disposal packages", which are placed in "cells" in the underground facility. The cells are spherical or ovoid underground excavations on a horizontal axis or slight slope dug out of the Callovo-Oxfordian formation (Figure 10-9). The tunnels are oriented according to the direction of the principal major stress (Andra; 2016a, 2016b)).

<sup>12</sup> Experiments in cementitious grout porewater and the presence of cementitious grout are still in progress.

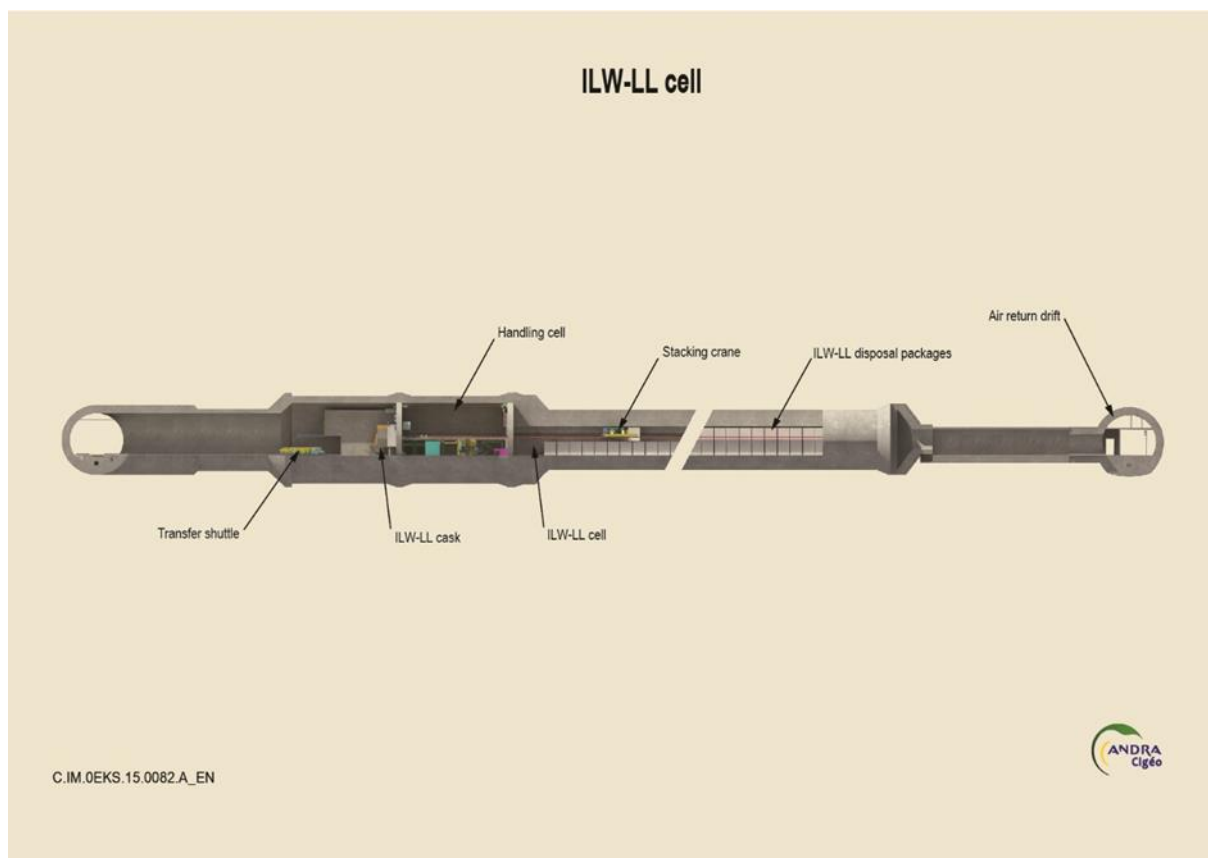


Figure 10-9: Design Principle ILW-LL cell

The standard cross-section of the usable part depends on the type of disposed package. The disposal cells comprise package layouts<sup>13</sup> on one, two or three columns/levels (*Figure 10-10*). The maximum usable part of the disposal cell is approximately 500 m. This length is compatible with the preservation of the undisturbed thickness of clay rock necessary for the justification of post-closure safety. The arrangement considered for one disposal package type is shown in *Figure 10-11*.

The construction of the ILW cell is accompanied by the installation of bolts and a concrete liner to provide the minimum mechanical stability until closure. Filling concrete defines a rectangular disposal cross-section matching the volume occupied by the waste packages.

<sup>13</sup> The various layouts are defined in Volume II, chapter 3 of (Andra, 2016a).

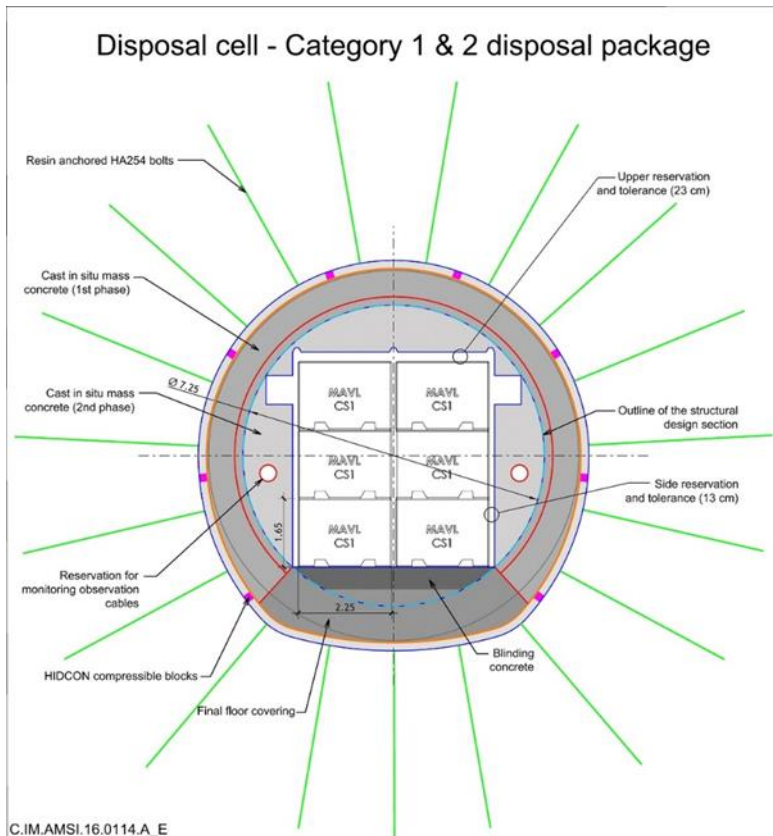


Figure 10-10: Standard section of ILW-LL disposal cell with support and liner. Example of CS1 disposal cells (end of basic engineering design stage).



Figure 10-11: Filling of disposal cells with packages type CS5 (at end of basic engineering design).

It is planned that some or all of the ILW-LL primary packages will be inserted into disposal containers before they are transferred to the underground facility for placement in cells<sup>14</sup>. The functions of these containers concern essentially the operation of Cigéo (package transfer and handling, standardisation of Cigéo components, etc.).

Parallelepipedal concrete containers will be used for most waste packages (CS1 to CS5 disposal containers), while steel containers will be used for a few waste packages (CS6 and CS7 disposal containers).

The technical solution selected by Andra for the concrete containers consists of precast reinforced elements made up of a body and a lid. The lid will be secured by screws on most of the primary packages (Figure 10-12).

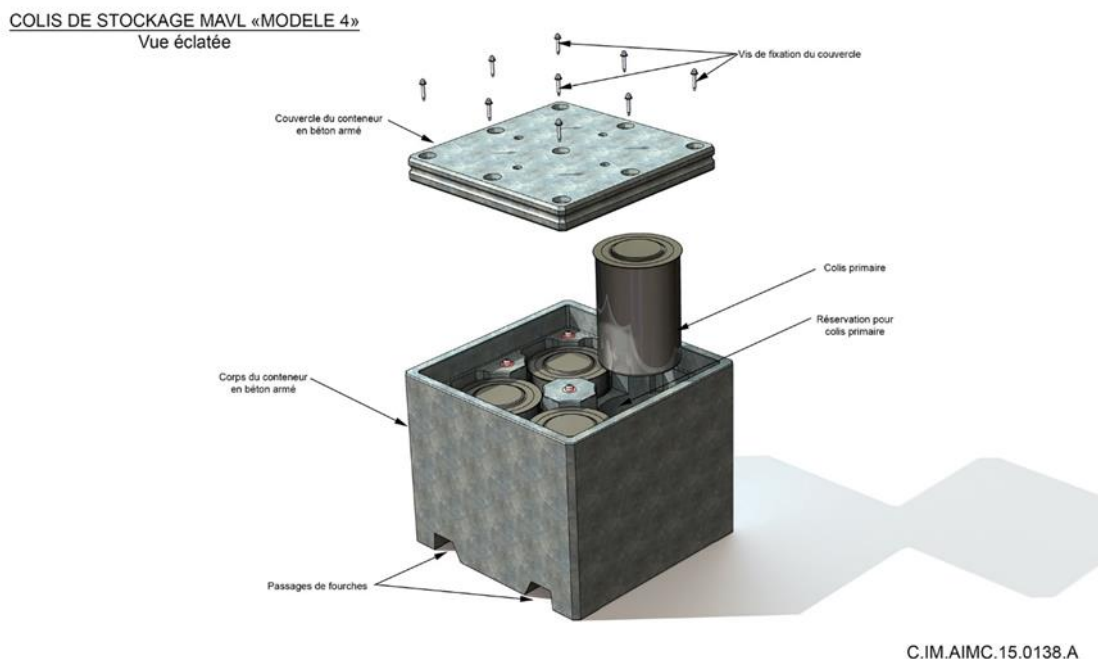


Figure 10-12: CS4 ILW-LL disposal container with lid secured by screws

#### 10.3.1.2 Description of materials

Main materials used in the ILW cells are cementitious materials. They contribute to the post-closure safety function “Limit the release of radionuclides and immobilise them in the repository”. The ILW cell contributes to limiting the release of radionuclides and toxic chemicals and immobilising them in the repository by imposing a cementitious chemical environment<sup>15</sup>.

For the metal waste, a cementitious environment (pH > 11) is required, associated with anoxic redox conditions. These conditions favour slow corrosion kinetics by a passivation effect (for steels), and consequently slow release of the activation products contained in the metal parts.

<sup>14</sup> At this stage, the following solutions are being considered: (i) for the majority of the waste package families, the primary package is placed in a disposal container on arrival at Cigéo; (ii) for some waste package families identified as “eligible for direct disposal”, the primary package delivered to Cigéo is placed directly in the disposal cell, without being placed in a disposal container.

<sup>15</sup> The cementitious materials of the ILW cells ensure high pH conditions over durations longer than 100,000 years. Subsequently, degradation of the concrete leads to a gradual decrease of the pH values until they reach a plateau, remaining above 10.5 over the next million years.

In addition to the effects favouring limitation of the kinetics of radionuclide release, the cementitious environment limits the transfer of radionuclides, in particular actinides, to the Callovo-Oxfordian by favouring their precipitation and retention.

The large body of data acquired over many years on the characterisation of the properties of cementitious materials with respect to speciation highlights, for the physicochemical states of the concretes<sup>16</sup>:

- low solubility of the actinides: the values are based on a large volume of knowledge acquired from equilibrium calculations, apparent measurements made in cementitious solutions, and literature data where considered pertinent with respect to the cementitious water compositions and the measurement protocols;
- significant sorption properties of the cementitious phases: the values are based on direct measurements, models calibrated for a material of interest (on material or according to a top-down approach) and models developed using data obtained from simple systems, such as the calcium silicate hydrates (CSH) (according to a component additivity or bottom-up approach).

#### 10.3.1.3 Description of waste

Several different kinds of nuclear waste will be disposed in Cigéo, such as metallic or organic waste. Organic waste are composed by organic polymers. Among the great variety of organic polymers planned to be stored in Cigéo, Andra is especially interested in the behaviour of PVC and cellulose.

Among other organic molecules, degradation of these both polymers leads to the release of phthalate and iso-saccharinic acid (ISA). The extension of the organic plume in the cell and in the near field is evaluated by the modelling of the evolution of their concentration with time and space.

Metallic waste are mainly composed by technological waste (black steel) and structural waste (stainless steel, Ni-alloys and Zr-alloy, etc.)

#### 10.3.1.4 Description of host rock

The Callovo-Oxfordian claystone is described in the part dedicated to the HLW.

### 10.3.2 Pore water compositions

#### 10.3.2.1 Cementitious components

The cementitious materials considered in the ILW cell are mainly composed by Ordinary Portland Cement (CEM I). The disposal containers are made of CEM V concrete. Modelling of mineralogies and water compositions of these materials are based on different assumptions depending on available data and numeric tool used for modelling (Marty et al.; 2014a, 2014b).

First Andra decided to retain amorphous CSH phases in the initial mineralogical assembly of the model of degradation of the concrete. Indeed, if we consider an amorphous CSH phase 1.6 in the initial assembly, the secondary CSH phases allowed to precipitate will be the CSH 1,2 and 0,8. The simplified composition of BHP CEM I concrete is detailed in *Table 10-5*. The high proportion of calcite is related to the nature of the aggregate incorporated in the concrete. The proportion  $\frac{3}{4}$  of monosulfoaluminate

---

<sup>16</sup> Two states of the cement are considered: undisturbed state, i.e. cementitious material in equilibrium with the portlandite after leaching of the alkalis, and weathered state, i.e. cementitious material in equilibrium with the CSH phases after dissolution of the portlandite.

(MSA) and ¼ ettringite is respected (mass fraction). A porosity of 13% was selected. The aluminum carrier phase is the aluminous pole of the hydrogrenat C3AH6.

Table 10-5: Simplified mineralogical composition of concrete CEM I considering amorphous "CSH 1,6" (the high proportion of calcite is related to the nature of the aggregate incorporated in the concrete).

Mineral	Name in ThermoChimie	Mass fraction	Molar volume (cm <sup>3</sup> mol <sup>-1</sup> )	Molar mass (g mol <sup>-1</sup> )	Volume Fraction*	mol L <sup>-1</sup> solution
Hydrogrenat-Fe	C3FH6	0,02	154,50	436,01	0,02	0,94
Calcite	Calcite	0,75	36,93	100,09	0,72	130,15
CSH amorphe	CSH1,6	0,13	84,68	196,29	0,15	11,54
Ettringite	Ettringite	0,01	710,32	1 255,09	0,01	0,12
Hydrotalcite	Hydrotalcite	< 0,01	227,36	443,32	< 0,01	0,12
Hydrogrenat-Al	C3AH6	< 0,01	149,52	378,29	< 0,01	0,16
MSA	Monosulfoaluminate	0,03	311,26	622,51	0,03	0,72
Portlandite	Portlandite	0,05	33,06	74,09	0,06	11,78
Alcalin	K <sub>2</sub> O	< 0,01	40,38	94,20	< 0,01	0,22
Alcalin	Na <sub>2</sub> O	< 0,01	25,88	61,98	< 0,01	0,09
Chlorure	Cl	< 0,01		35,45		0,04
Porosité	0,13					

\* Excluding porosity

Table 10-6: Simplified mineralogical composition of concrete CEM V considering amorphous "CSH 1,6" (the high proportion of calcite is related to the nature of the aggregate incorporated in the concrete).

Mineral	Name in ThermoChimie	Mass fraction	Molar volume (cm <sup>3</sup> mol <sup>-1</sup> )	Molar mass (g mol <sup>-1</sup> )	Volume Fraction*	mol L <sup>-1</sup> solution
Minéral	Nom dans la base THERMOCHIMIE	Fraction massique	Volume molaire (cm <sup>3</sup> mol <sup>-1</sup> )	Masse molaire (g mol <sup>-1</sup> )	Fraction volumique*	mol L <sup>-1</sup> solution
Hydrogrenat-Fe	C <sub>3</sub> FH <sub>6</sub>	0,01	154,50	436,01	0,01	0,55
Calcite	Calcite	0,76	36,93	100,09	0,73	125,43
CSH amorphe	CSH1,6	0,12	84,68	196,29	0,13	10,01
Hydrotalcite	Hydrotalcite	0,01	227,36	443,32	0,02	0,54
Hydrogrenat-Al	C <sub>3</sub> AH <sub>6</sub>	0,03	149,52	378,29	0,03	1,42
MSA	Monosulfoaluminate	0,04	311,26	622,51	0,05	1,07
Portlandite	Portlandite	0,01	33,06	74,09	0,02	3,04
Pyrite	Pyrite	< 0,01	23,94	119,98	< 0,01	0,07
Alcalin	K <sub>2</sub> O	< 0,01	40,38	94,20	< 0,01	0,36
Alcalin	Na <sub>2</sub> O	< 0,01	25,88	61,98	< 0,01	0,10
Chlorure	Cl	< 0,01		35,45		0,01
Porosité	0,135					

\* Excluding porosity

The interstitial fluid of young age concrete was calculated with ThermoChime database (version 8). The calculated equilibrium is given in Table 10-7. The concentration of chloride reported in Table 10-7 ( $4.0 \times 10^{-2}$  mol L<sup>-1</sup>) is similar to that of the claystone ( $4.1 \times 10^{-2}$  mol L<sup>-1</sup>). Except for the alkaline load (sodium and potassium), the concentration of the other elements is controlled by the mineralogical assembly of the concrete. The simulation is carried out in two stages: (i) the water reacts with the alkalines (present in the concrete before (ii) to be balanced with the minerals constituting the concrete BHP CEM I. The

ionic strength of the solution ( $I = 0.3$ ) lies at the limit of the range of validity of the Debye-Hückel activity model.

Table 10-7: Examples of water composition of CEM I and CEM V cement modelled with ThermoChimie

Elements	CEM I (mol L <sup>-1</sup> )	CEM V (mol L <sup>-1</sup> )
Al	7,7 10 <sup>-4</sup>	1,2 10 <sup>-3</sup>
Fe	6,2 10 <sup>-7</sup>	4,2 10 <sup>-6</sup>
Si	7,7 10 <sup>-5</sup>	1,6 10 <sup>-4</sup>
Sr	--	--
K	2,2 10 <sup>-1</sup>	3,6 10 <sup>-1</sup>
Mg	3,2 10 <sup>-10</sup>	2,1 10 <sup>-10</sup>
Ca	1,5 10 <sup>-3</sup>	8,6 10 <sup>-4</sup>
Na	9,0 10 <sup>-2</sup>	1,0 10 <sup>-1</sup>
Cl	4,0 10 <sup>-2</sup>	1,0 10 <sup>-2</sup>
S(VI)	3,2 10 <sup>-4</sup>	1,0 10 <sup>-3</sup>
S(-II)	--	1,0 10 <sup>-3</sup>
TIC	9,9 10 <sup>-5</sup>	2,7 10 <sup>-4</sup>
pH	13,26	13,46
pe	7,74	-11,02
log P <sub>CO2</sub> (atm)	-13,14	-13,15

#### 10.3.2.2 Callovo-Oxfordian claystone

The porewater composition of the Callovo-Oxfordian claystone is described in the HLW part.

## 10.4 Chemical evolution of the ILW disposal cell

### 10.4.1 Narrative

#### 10.4.1.1 Operating period

The chemical processes that develop during the Cigéo operating period are mainly driven by the hygrometry and saturation conditions of the materials. The ventilation of the ILW cells during this period results in hygrometry conditions between 40 and 70%. This ventilation leads to the gradual desaturation of Callovo-Oxfordian claystone in the near field over the extension of the connected fracturing zone (ZFC) as well as that of the cementitious materials. During this phase, the chemical evolution is little influenced by the thermal conditions which remain moderate ( $T^{\circ} < 50^{\circ}\text{C}$  for the alveoli of exothermic waste).

The main chemical processes affecting the components of Cigéo MA-VL cells during the exploitation phase are the oxidation processes of the Callovo-Oxfordian claystone in the field close to the structures, atmospheric carbonation processes of cementitious materials and, in a less extent, corrosion processes.

#### Claystone oxidation

The ventilation of disposal cells leads concomitantly both a desaturation of the rock (ZFC) and the development of a so-called oxidizing disturbance in the host rock because of its reactivity with oxygen in the air. From a mineralogical point of view, this disturbance corresponds mainly to the oxidation of the Fe<sup>II</sup>-bearing mineral phases (pyrite, siderite, etc.), to the dissolution of the carbonated phases and to the formation of sulphated secondary phases (gypsum, etc.). It leads to a modification of the undisturbed host rock water composition by enhancing content in sulphate and alkalines.

### Concrete carbonation

Concerning the cementitious components, their main chemical evolution is atmospheric carbonation. This process results from the reactivity of carbon dioxide in an alkaline medium, which constitutes an acid source after dissolution in the interstitial water. It neutralizes and causes the dissolution of certain mineral phases (cement hydrates (portlandite), hydrated calcium silicates (C-S-H), etc.) and precipitates mainly in the form of calcium carbonate. The extent of this disturbance is about few centimetres over the operating period and does not affect the material at the reinforcement beds of the various components thus ensuring the maintenance of passivating conditions vis-à-vis their corrosion kinetics, which remain low ( $<1 \text{ micron}\cdot\text{year}^{-1}$ ).

#### 10.4.1.2 Post closure period

### Cementitious components and near field evolutions

In post-closure, the resaturation of the cementitious materials by the water coming from the host rock will cause a progressive degradation of the cementitious materials and an alkaline disturbance within the claystone in interface with the liner.

The development of these different processes is mainly driven by the hydraulic conditions in the cells. Indeed, during this period, the chemical evolution is little influenced by the thermal conditions which remain moderate ( $T \text{ } ^\circ < 50^\circ\text{C}$  for exothermic waste cells). In addition, the mechanical evolution of the structures (liner, containers, etc.) due to, in particular, the corrosion of their metal reinforcement leads to their cracking after a few thousand years. This cracking does not lead to the development of a preferential path in the chemical degradation of the structures because of the predominantly diffusive transfer conditions after the resaturation of the structures.

The resaturation transient of the MA-VL cells is controlled by the production of hydrogen by radiolysis of some waste and by the anoxic corrosion of the metal components of the cells. The development of this transient results in the maintenance of desaturated conditions in the voids for periods of up to several hundred thousand years. The porous materials see their saturation increase after a few hundred years after the closure of the storage until reaching about 80% for cementitious materials and more than 90% for the Callovo-Oxfordian claystone (*Figure 10-13*).

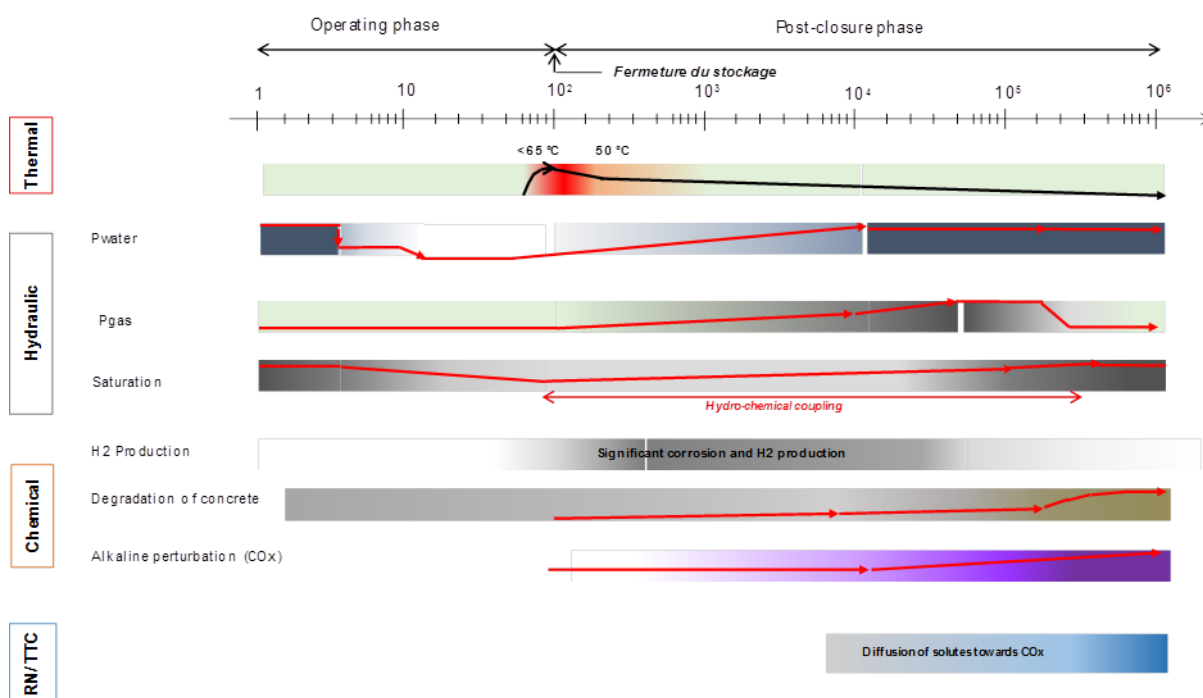


Figure 10-13: Chronogram of main processes occurring in ILW cells during the operating and the post-closure periods.

The main processes responsible for concrete/clay rock interactions are well known. Whatever the nature of the cementitious materials (CEM I, CEM V, etc.), the different studies relating to the alkaline perturbation in the Callovo-Oxfordian claystone make it possible to define a reaction scheme considered as stabilized; mainly resulting in the dissolution of the initial mineral phases (smectites, quartz, etc.) and the formation of secondary mineral phases (saponites, illites, C-S-H, etc.). It also results in reversible ion exchange processes due to the migration of alkaline and alkaline-earth cations from concrete.

The mineralogical modifications of the claystone due to the alkaline disturbance induce changes of the pore structure, of the proportions between the swelling clays and the non-swelling minerals and thus have consequences on the hydraulic properties (porosity, permeability) and mechanical (swelling).

This disturbance is thus mainly expressed by the development of (i) a first so-called "remineralized" zone which corresponds to a significant modification of the mineralogical and geochemical characteristics of the claystone, and thus textural, near the interface with the material (or the cementitious fluid) and (ii) a second zone called "zone affected by an alkaline plume without remineralisation" with little or no remineralisation but with a high pH of the interstitial solution (pH~10) and a modification of the exchangeable cation population position in the clayey mineral layers.

Concrete degradation results mainly in three processes: hydrolysis, carbonation in water and sulphate attack. The most developed is the hydrolysis, which the main consequence is the dissolution of portlandite and calcium sulfoaluminates, as well as the decalcification of C-S-H. These chemical perturbations lead to an evolution of the transfer properties in the degraded zones (in particular an increase of the porosity and its connectivity). This is a slow and continuous process (as long as connected porosity exists) that helps buffer interstitial fluids.

## Waste degradation

The degradation of organic waste by radiolysis and/or hydrolysis under partially saturated cementitious conditions leads to the release of potentially aggressive organic compounds for cementitious components (acid attack) and likely to interact with other solutes (complexation properties) present in the cell and near-field claystone, depending on their nature and inventory. Till now, the release of phthalate is considered as labile. The degradation of cellulose and the release of ISA is kinetics.

These molecules will interact with the different cementitious components in which they will diffuse through (speciation evolution, sorption, etc.). And then, after release, their concentrations will decrease from the waste package according to a centrifuge way toward the near field.

The degradation of metallic waste is represented with corrosion kinetics, which parameters are mainly determined by (i) the size/surface of the piece of waste and (ii) the environmental chemical conditions.

### 10.4.2 Conceptual model

The evaluation of the extension of degradation of the cementitious components and the resulting alkaline disturbance at the level of ILW cells is based on a combination of experiments carried out in the surface laboratory and in underground laboratories, on natural analogues and on numerical simulations.

These different bodies of knowledge provide access to ever larger time and space scales: centimetric and annual thanks to surface laboratory experiments, decimetric and multi-year thanks to underground laboratory experiments. tens or even hundreds of thousands of years for natural analogues and models. To move from the laboratory scale to that of the disposal cell and to evaluate the propagation of the reaction fronts and their long-term consequences with respect to the mineralogical evolution of the materials and their water chemistry, it is necessary to use a geochemical modelling approach coupled with transport phenomena.

After closure of the disposal, chemical interactions develop locally between materials, with kinetics that are, at first, a function of water availability. The increase in the saturation of claystone and cementitious materials in contact initiates the processes of degradation of the latter and in particular hydrolysis. These reactions develop in a coupled manner along a reaction front that advances from the interface with the claystone centripetally to the core of the cementitious component, parallel to the solid/solution interface. They begin while the cell has already mechanically evolved in relation to its initial geometry.

Various numerical evaluations were carried out in order to characterize the spatial and temporal evolution of the ISA and phthalate concentrations in the ILW cells. These quantitative evaluations are based on the implementation of two types of complementary numerical simulations:

- simulations of "reactive-transport" type, making it possible to take into account the complexity of the chemical system at the scale of the package and the cell, on the basis of the knowledge acquired;
- simulations of "performance" type, retaining a simplified representation of the chemical reactivity through a partition coefficient ( $K_d$ ) and a solubility limit. They aim to account for the behaviour of the ILW cells and surrounding Callovo-Oxfordian.

Two indicators were chosen to characterize the extension of the "remineralized" zone due to the alkaline disturbance: (i) the dissolution of 50% of the initial clay phases (= illite + smectite) with regard to a significant decrease in the retention properties of the radionuclides and (ii) the total dissolution of the initial contents of smectite with regard to the degradation of the swelling properties of the claystone. With regard to the first criterion, the alkaline disturbance in the claystone is zero in contact with a liner of a ILW cell after 100,000 years of interaction under saturated conditions. In the case where the criterion retained is the total dissolution of the smectite (initial contents of 8% by mass, the extensions of the disturbances are about few decimetres. Concerning the "zone affected by an alkaline plume without remineralisation", its extension is negligible after 100,000 years.

The criterion used to account for the extension of the hydrolysis of a cementitious material is the dissolution of the initial cementitious phase with the highest Ca/Si ratio: portlandite. In general, considering saturated conditions, the cementitious components undergo hydrolysis over their entire thickness after 100,000 years. The intensity of this hydrolysis shows that over this period, almost all of the cementitious components are in an altered state. This altered state lasts for a million years with a gradual decrease in the Ca/Si ratio of the C-S-H phases.

The extension of organics plume have been evaluated by considering threshold values of concentrations that leading to a reduction in the retention properties of the materials toward radionuclides oxidation degree + IV:  $10^{-4}$  M for the ISA and  $10^{-3}$  M for phthalic acid.

#### 10.4.3 Mathematical model

The mathematical and numerical models used to model degradation ILW cell are described in Marty et al.; 2014a and 2014b. Some elements are also described in Idiart and Laviña; 2019.

## 11. Germany

FZJ - Guido Deissman

UFZ - Vanessa Montoya

In Germany, nuclear wastes originate from electricity generation, industrial, medical and research applications, and military programmes (BMUB, 2014, 2018). After the Fukushima nuclear disaster in March 2011, Germany decided to phase out Nuclear Power and in August 2011 and to shut down eight of its 17 commercial nuclear power plants (NPPs). In June, 2015 and December 2017, two additional reactors were closed. The present action plan in Germany is to shut down the 7 remaining light water reactors (LWRs) by the end of 2022 at the latest. Among these seven reactors still in operation, six are pressurised water reactors (PWRs) and one is a boiling water reactor (BWR). Their fuel assemblies are composed of low-enriched uranium oxide or uranium/plutonium mixed oxide (MOX).

Additionally, there are 7 research reactors still in operation, three of them, namely: the Materials Testing Reactor (MTR) facility BER-II in Berlin, the high-flux reactor FRM II in Garching; and the TRIGA reactor FRMZ in Mainz producing above 50kW of thermal power. The other four (three teaching reactors and one training reactor) only generate a maximum thermal power of 2 W. At present, 39 research reactors are permanently out of operation; 3 of them are permanently shut down, but so far no decommissioning licence has been granted for them. Another seven are under decommissioning and the remaining 29 research reactors had been decommissioned and are released from regulatory control.

The treatment and storage of radioactive waste from military and defence programmes in Germany remains the responsibility of the armed forces. However, the civil sector will take over this responsibility when the waste is disposed of in a final repository. Currently, these wastes are stored in a central facility. If necessary, the waste will be conditioned according to the acceptance criteria of the relevant repository for disposal. All these waste management stages are subject to the same safety provisions as those applicable in the civil sector.

The Federal Government intends to dispose of all types of radioactive waste in deep geological formations. Therefore, it is deemed unnecessary to differentiate between wastes containing short-lived or long-lived radionuclides (BMUB, 2014, 2018). Instead, radioactive wastes in Germany are subdivided into:

- Heat-generating waste.
- Waste with negligible heat generation.

Heat-generating radioactive waste is characterised by high activity concentrations and thus high decay heat and includes, vitrified wastes, hulls and structural components from spent fuel reprocessing, and spent nuclear fuel (SNF) to be disposed of directly. According to BMUB (2015a), the prediction is that about 10,500 Mg heavy metal (HM) in the form of SNF assemblies will be generated in nuclear power plants and will have to be disposed of in the Federal Republic of Germany. This amount will be stored in about 1,100 storage casks. Moreover, an estimated amount of about 8000 waste canisters with waste generated mainly during reprocessing of about 6,700 t SNF in France and the UK have to be disposed of (*Table 11-1*).

Table 11-1: Prediction of the amounts of waste expected from reprocessing that will have to be disposed of in the Federal Republic of Germany (BMUB, 2015a)

Type	Canisters	Containers
Vitrified high-level radioactive waste from France (CSD-V)	3,024	108
Vitrified intermediate-level radioactive waste from France (CSD-B)	140	5
Compacted intermediate-level radioactive waste from France (CSD-C)	4,104	152
Vitrified high-level radioactive waste from the UK (UK-HAW)	571	21
Vitrified high-level radioactive waste from reprocessing at Karlsruhe (HAW-WAK)	140	5
<b>Total</b>	<b>7,979</b>	<b>291</b>

Wastes with negligible heat generation contain distinctively lower activity concentrations encompassing wastes from the operation, decommissioning and dismantling of nuclear facilities (e.g., disused plant components, ion exchange resins, air filters, cleaning agents, contaminated/activated concrete structures) and/or from the application of radioisotopes. According to the national programme of the Federal Ministry for the Environment, Nature Conservation, Building and Nuclear Safety, about 60% of all radioactive waste with negligible heat generation originates from the nuclear industry, 37% comes from research activities, and about 3% from the healthcare sector (BMUB, 2015b).

In general, this classification into heat-generating and negligible heat-generating wastes is consistent with the international classification of nuclear wastes with only slight deviations and is compatible with the classification of the IAEA (IAEA, 2009). Compared to the IAEA waste classification (HLW, ILW, LLW, and VLLW), wastes which are referred to as heat-generating wastes comprise HLW and to some extent ILW, while some wastes referred to as VLLW by the IAEA exceed the current German clearance levels for management as conventional waste and have to be disposed of in a repository.

According to the German Atomic Energy Act (AtG, § 9a para. 3), the provision of disposal facilities for radioactive waste, as well as the establishment of the scientific and technical basis for their realisation, is a federal task. Currently, two deep geological disposal facilities are envisaged for the two types of radioactive wastes: the Konrad disposal facility for radioactive waste with negligible heat generation and a disposal facility for heat-generating radioactive waste at a site yet to be identified (BMUB, 2015b).

The Konrad mine at Salzgitter, a former iron ore mine, is currently being converted into a disposal facility for radioactive waste with negligible heat-generation from the operation and dismantling of the nuclear power plants as well as from industrial, medical and research applications. The emplacement of these wastes is foreseen in a Jurassic iron ore formation beneath a Cretaceous clay formation, at a depth between 800 and 1,300 m below ground level. The Konrad disposal facility is expected to become operational in 2027 and is licenced to accept a waste volume of 303,000 m<sup>3</sup>; the operational phase of this facility is not expected to last more than 40 years.

The radioactive waste that is to be delivered to the Konrad disposal facility in the future has to be appropriately conditioned and subjected to product control by the Federal Company for Radioactive Waste Disposal (BGE) to verify compliance with the waste acceptance criteria of this repository according to the plan approval (BfS, 2017). Until delivery to the Konrad disposal facility, wastes with negligible heat-generation remain in interim storage facilities, at the collecting facilities of the Federal States, or at the collecting facility of the armed forces.

The site of a disposal facility especially for heat-generating radioactive waste (i.e., SNF and reprocessing wastes) will be determined according to a step-wise selection procedure established in the Site Selection Act (Standortauswahlgesetz – StandAG) of 23 July 2013 (amended 20 July 2017). The Site Selection Act stipulates a science-based, transparent and comprehensible selection process with a broad involvement of the general public. Rock salt, clay and crystalline rocks are considered as possible host rocks to be evaluated in a stepwise site selection process, involving application of exclusion criteria, minimal requirements and consideration criteria (comprising aspects from geoscience and regional planning), and performing preliminary safety assessments at the end of each step.

According to the Site selection a repository site should be selected by 2031. The current plan is for the heat-generating waste disposal facility to start operation around 2050; the time frame required for the emplacement of the wastes will depend in particular on the concept and design of the disposal facility.

Until a repository for heat-generating waste is available, spent nuclear fuel and reprocessing wastes are placed in interim dry storage in transport and storage casks. Other than on-site storage facilities at the sites of the NPPs, transport cask storage facilities at Gorleben, Ahaus, and the Rubenow ("Zwischenlager Nord") are available. Licensed storage periods for the transport and storage casks are limited to 40 years at present. Since the availability of a disposal facility within this timeframe cannot be guaranteed at present, technical prerequisites for a prolonged period of interim storage are currently being examined.

## 11.1 Characterization of the HLW disposal cell in crystalline-and clay- rock

### 11.1.1 Description of materials in disposal cell

Regarding deep geological disposal of high-level radioactive waste (i.e. SNF, vitrified wastes and compacted metallic waste from SNF reprocessing), Germany is at the siting stage since 2017, however no host rock type and repository concept have been selected yet. The safety criteria laid down in BMU (2010), which are currently under amendment, contain mainly general protection objectives and safety principles and requirements (e.g., dose criteria, exclusion of criticality, containment of radioactivity in the so called "containment-providing rock zone"), but no specific requirements regarding the repository layout and materials to be used. A notable exception concerns the waste containers, which must fulfil the following safety functions, with due regard for the waste products packaged therein and the backfill surrounding them (BMU, 2010):

- "For probable developments, handleability of the waste containers must be guaranteed for a period of 500 years in case of recovery from the decommissioned and sealed final repository. Care should be taken to avoid the release of radioactive aerosols.
- During the operating phase up until sealing of the shafts or ramps, retrieval of the waste containers must be possible"

Although historically the main focus in Germany has been on HLW disposal in salt domes, throughout the last decade, several conceptual studies have been performed with respect to HLW disposal in argillaceous formations and crystalline rocks, using illustrative and partly generic repository concepts (e.g., Jobmann et al., 2016; Bertrams et al., 2017). None of these concepts has so far been endorsed by the implementer BGE and no assessments of the chemical evolution of the disposal cells have been performed.

Regarding HLW disposal in crystalline (granitic) rock, Jobmann et al. (2016) used the Swedish KBS-3 concept as generic concept in a feasibility study on the development of a safety assessment methodology for HLW disposal in crystalline rocks in Germany. Bertrams et al. (2017) also used the KBS-3 concept as a basis for the development of a technical concept for a generic repository for HLW in crystalline rocks in Germany, addressing also the potential usage of different types of waste containers, including unshielded steel containers (BSK), cast steel containers (POLLUX) and the disposal of transport and storage casks (CASTOR), besides copper canisters as used within the KBS-3 concept.

Concerning HLW disposal in clay rocks, in particular the lower Cretaceous and upper Jurassic clay rock formations in Northern Germany and the Opalinus Clay in Southern Germany have been discussed in the past (e.g., BGR, 2007). Jobmann et al. (2007) discussed concepts for HLW disposal for generic repositories in clay formations in Northern and Southern Germany. In these concepts, SNF disposal either in thick-walled steel containers (POLLUX) placed horizontally in disposal tunnels to be backfilled with bentonite or alternatively in unshielded BSK containers in vertical boreholes (depth up to 50 m),

also to be backfilled by bentonite, were assumed. For vitrified HLW, disposal in BSK steel containers in boreholes was intended using bentonite as backfill. Similar concepts were used in the study of Pöhler et al. (2010) using the Lower Cretaceous clay formations in the Lower Saxony Basin as potential host rock formation for a generic repository. More recently, Jobmann et al. (2017a,b) conducted a R&D project aiming at the development of a first draft of a methodology to demonstrate the safety of a HLW repository in argillaceous formations in Germany. In this study repository concepts adapted specifically to the geological conditions in Northern and Southern Germany were developed (cf. *Figure 11-1*). The emplacement level of the repository was assumed to be between 600 and 800 meters below ground level to avoid any adverse impacts from the surface.

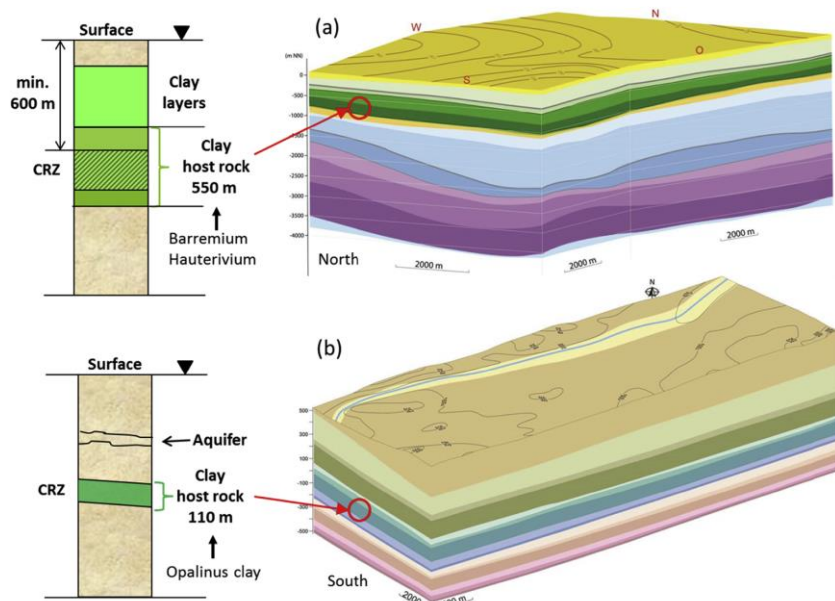


*Figure 11-1: Schematic 3D-geological sections (right) of the repository site models for Northern (a) and Southern (b) Germany and simplified geological profiles (left) illustrating the position of the clay layers (Jobmann et al. 2017b).*

For the thick Lower Cretaceous clay formations in Northern Germany, the option of borehole emplacement of SNF and vitrified HLW in retrievable steel containers (outer diameter  $\approx 0.5$  m; length  $\approx 5$  m) was analysed by Jobmann et al. (2017a), assuming a depths of the vertical boreholes of 27 m (cf. *Figure 11-2*). To ensure the stability of the borehole and to ensure retrievability, the concept assumed that the boreholes will be equipped with an external and an internal liner. Each borehole was assumed to hold three containers; after emplacement the remaining void volume should be filled with sand and the space between the inner and the outer liner filled with a compacted clay buffer. Sealing of each borehole was foreseen using a bentonite plug and a concrete abutment Jobmann et al. (2017a,b). Due to the limited thickness of the Opalinus Clay in Southern Germany (about 100 m), an emplacement concept using horizontal disposal tunnels with a length of 400 m was proposed by Jobmann et al. (2017a) for this scenario. HLW and SNF disposal in thick walled steel containers (POLLUX) was assumed that will be placed on beddings of highly compacted clay (container spacing 23 m) (cf *Figure 11-2*); in this concept the backfilling of the remaining void volume is intended with clay (i.e. reprocessed mined rock, Jobmann et al., 2017b).

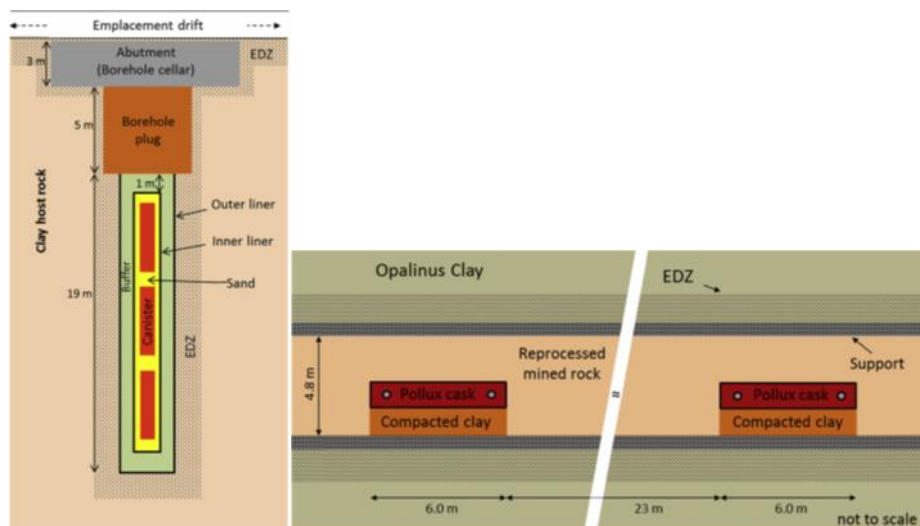


Figure 11-2: Schematic of the concepts for borehole disposal and drift emplacement (Jobmann et al. 2017b).

The temperature of the virgin host rock in a future HLW repository will depend generally on the site and depth of the repository. According to the German Site Selection Act, the minimum cover thickness above the top of the "containment providing rock zone" has to be 300 m; if effects of glaciation or erosion are expected within the assessment time frame (i.e., 1 million years; BMU, 2010), the cover thickness has to be greater than the expected depth of impact of the exogenic processes. Thus a repository depth of > 300 m has generally to be considered in Germany.

### 11.1.2 Thermal and hydraulic gradients

The expected temperatures and thermal gradients in the HLW repository will depend on a large number of factors, such as repository site and depth, repository concept and lay out (incl. the materials used in the engineered barrier system and their properties, e.g. heat capacity/conductivity), the type and properties of the host rock (i.e., salt, clay or crystalline rock), as well as the starting time of the operational phase (and thus the cooling period of the waste) and the loading of waste containers. Due to the state of the siting process, this information is not available to date. However, according to the Site Selection Act, the temperature at the surface of the waste containers should not exceed 100 °C.

Similarly, hydraulic gradients in the disposal cell will depend on the repository concept and site which is not yet selected; however, the hydraulic conductivity of the host rock in the "containment-providing rock zone" should be below  $10^{-10}$  m/s.

### 11.1.3 Pore water compositions

The pore water composition in the disposal cell and its evolution with time is mainly determined by the composition of the natural groundwater at the repository site and the interaction with the materials used for repository construction and within the engineered barrier system and the pore waters contained therein (e.g., pore water in construction concrete or (cementitious) backfill materials or bentonite). To date, due to the status of the German site selection process, no information with respect to the pore water composition and evolution in HLW disposal cells are available. However, the Site Selection Act specifies the following indicators for favourable hydrogeochemical conditions at potential repository sites:

- Chemical equilibrium between the host rock within the "containment-providing rock zone" and the deep groundwater therein,
- Neutral to slightly alkaline (pH 7 – 8) deep groundwaters,
- Anoxic to reducing conditions in the deep groundwater,
- Low concentrations of colloids and complexing species in the deep groundwater, and
- a low carbonate concentration in the deep groundwater.

## 11.2 Chemical evolution of the HLW disposal cell

### 11.2.1 Narrative

n/a

### 11.2.2 Conceptual model

n/a

## 11.3 Characterization of an ILW disposal cell

### 11.3.1 Description of materials in disposal cell

Low and intermediate level radioactive wastes (LILW) with negligible heat generation in Germany are destined to be disposed of in the repository Konrad. The wastes (up to 303,000 m<sup>3</sup>) will be emplaced in a Jurassic iron ore formation at a depth between 800 and 1,300 m below ground level. The permitting process lasted for about 25 years, starting in 1982. Permission for the construction and operation of the repository was finally granted in 2007, after several years of judicial proceedings. Currently, the former iron ore mine is being converted into a repository, the operational phase is intended to start in 2027.

The rock formation hosting the disposal cells is an oolitic Jurassic iron ore ("Korallenoolith", Oxfordian), which is covered by several hundred meters of low permeable clay rocks of Jurassic and Cretaceous age. The emplacement chambers (maximum number 59) are planned to have a width of 7 m and a height of about 6 m, the length can vary between 100 and 1,000 m (NUM, 2002). The roofs and sides of the emplacement chambers will be secured by rockbolts, and, if required by wire netting and shotcreting. After emplacement of the waste containers, the emplacement chambers will be backfilled with a pumpable backfill consisting to 70 wt% of excavated rock material, 10 wt% cement (incl. additives), and 20 wt% water (NUM, 2002). Prior to backfilling, the emplacement chambers will be sealed by shotcrete walls (in 50 m sections). The waste acceptance criteria for the repository Konrad permit the use of various types of waste containers made from either steel, cast iron, or reinforced concrete in different designs and sizes, either cylindrical or box shaped (cf. Table 2; BfS, 2014). The wastes inside the containers have to be fixed using, e.g. cementitious materials or bitumen. If required, the waste containers may include shielding materials on the inside container walls, consisting, e.g. of lead or depleted uranium (BfS, 2014).

Table 11-2: Waste containers permitted for the Konrad repository (BfS, 2014).

Type	Shape	Length/ diameter [mm]	Width [mm]	Height [mm]	Volume (gross) [m <sup>3</sup> ]
Concrete cask Type I	cylindrical	Ø 1060		1370	1.2
Concrete cask Type II	cylindrical	Ø 1060		1510	1.3
Cast iron cask Type I	cylindrical	Ø 900		1150	0.7
Cast iron cask Type II	cylindrical	Ø 1060		1500	1.3
Cast iron cask Type III	cylindrical	Ø 1000		1240	1.0
Container Type I*	box-shape	1600	1700	1450	3.9
Container Type II	box-shape	1600	1700	1700	4.6
Container Type III	box-shape	3000	1700	1700	8.7
Container Type IV	box-shape	3000	1700	1450	7.4
Container Type V	box-shape	3200	2000	1700	10.9
Container Type VI	box-shape	1600	2000	1700	5.4

\*Containers Type I to VI can be made out of steel (3 mm), cast iron, or reinforced concrete

### 11.3.2 Hydraulic gradients

No detailed information about hydraulic gradients in the planned emplacement chambers in the repository Konrad is available. Due to the hydrogeological conditions and the high salinity of the groundwater at repository depth, the migration of radionuclides released from the repository is assumed to be mainly by diffusion (BGR, 2019).

### 11.3.3 Pore water compositions

The pore water composition within the emplacement chambers has not been specified within the documentation used within the permit application process. It will be determined by the composition of the natural groundwater at the repository site and the interaction with the emplaced waste materials and the cementitious backfill. The deep groundwaters at the Konrad site are characterised by a high salinity that increases from about 160 g/L at 600 m depth to about 230 g/L at a depth of 1,300 m below ground level. Exemplarily, the chemical composition of some groundwaters collected in the Konrad mine is given in Table 11-3.

Table 11-3: Mine water composition (Brewitz, 1982 and Tittel et al., 1986)

ID		Schacht Konrad Hils	Schacht Konrad Str. 670	Schacht Konrad Ort 300	Schacht Konrad Pump pit*
pH	-	6.1	6.0	6.0	
E <sub>H</sub>	mV	95	195		
Na	mg/L	54,100	62,000	61,778	77,722
K	mg/L	118	214	286	212
Ca	mg/L	5,050	13,200	11,349	8,939
Mg	mg/L	1,356	2,720	2,280	2,761
Sr	mg/L	568	438	487	376
HCO <sub>3</sub>	mg/L	100	70	60	
SO <sub>4</sub>	mg/L	316	767	600	832
Cl	mg/L	95,970	125,000	117,327	135,556
Br	mg/L	206	840	653	822

\* average 1981

## 11.4 Chemical evolution of the ILW disposal cell

### 11.4.1 Narrative

The chemical evolution of the (L)ILW disposal cells in the Konrad repository has not been addressed in detail within the permit application process. The radionuclide source term has been determined using a stylised scenario, assuming that the emplacement chambers and the remaining voids in the mined repository are spontaneously water saturated in the post closure phase and the emplaced waste containers are instantaneously in contact with water (NUM, 2002).

### 11.4.2 Conceptual model

The conceptual model describing the radionuclide release from the waste packages after instantaneous contact with water post-closure assumes a delay time for the mobilisation of radionuclides depending on their fixation (NUM, 2002). Four different material groups are distinguished, namely bitumen, cementitious materials, metals, and others. The element/radionuclide specific time scales for mobilisation are given in *Table 11-4*; it is assumed that after 600 years the complete radionuclide inventory is released from the waste packages.

*Table 11-4: Element specific time for radionuclide mobilisation form the waste.*

Group	Time for mobilisation	Elements
Bitumen	10 a	Cl, I, Sr, Ra, Ca
	20 a	Cs, C, Se, Sn, Zr, Nb, Tc, Ni, Pd, Mo, Sm, Rb, Co, Eu, Pb
	200 a	Actinides
Cementitious materials	0a	Cs, Rb, Cl
	15 a	Sr, Ra, Ca
	40 a	C, Se, Sn, Zr, Nb, Tc, Ni, Pd, Mo, Sm, Co, Eu, Pb
	600 a	Actinides
Metals	50 a	all
Others	0 a	all

*Table 11-5: Solubility limits used for the near field within the permitting process for Konrad.*

Element	Solubility limit [mol/L]	Element	Solubility limit [mol/L]
C	1E-04	I	1E-02
Cl	1E-02	Cs	1E-02
Ca	1E-02	Sm	1E-04
Co	1E-03	Eu	1E-04
Ni	1E-03	Cm	1E-07
Se	1E-02	Am	1E-07
Rb	1E-02	Pu	1E-07
Sr	1E-02	Np	1E-05
Zr	1E-07	Pa	1E-05
Mo	1E-04	Th	1E-07
Nb	1E-07	U	1E-04
Tc	1E-04	Ra	1E-03
Pd	1E-04	Pb	1E-04
Sn	1E-04	Ac	1E-05

## 12. Hungary

The Hungarian organisation participating in ACED is the Centre for Energy Research MTA EK. Margit Fabian delivered a completed template for the kick-off meeting held in July 2019 that can be found in Appendix A.

Hungary has made a country-wide screening process in which the Boda Clay stone formation in the southwest in Hungary has been concluded to be suitable for the disposal of HLW. Reprocessing of spent fuel is one of the approaches adopted by PURAM, the Hungarian WMO i.e. vitrified HLW is not yet present. Lab studies to assess the post-closure behaviour of vitrified HLW are performed in Hungary.

The website of PURAM shows that Intermediate Level Waste has been disposed in Hungary since 1976. Appendix A shows a photograph of a disposal facility in the operational phase. The facility is hosted in granite and is backfilled with cementitious material. The waste in 200 litre drums has been put in ferro-concrete containers and emplaced by a forklift truck. The safety concept and analysis for the post-closure phase is unfortunately only available in Hungarian.

## 13. Lithuania

LEI - Povilas Poskas, Dalia Grigaliuniene, Asta Narkuniene

There is only one nuclear power plant (NPP) in Lithuania - the Ignalina NPP with two units of RBMK type reactors (RBMK-1500). Ignalina NPP reactors started operation in December 1983 and August 1987, respectively. The reactors were shut down on December 31, 2004 and December 31, 2009. Immediate dismantling strategy for the decommissioning of the Ignalina NPP was selected.

In line with requirements of Council Directive 2011/70/Euratom of 19 July 2011, a new national Program on management of spent nuclear fuel and radioactive waste (with content according to the Directive) was approved in 2015. According to this Program it is foreseen to dispose of the long lived intermediate level radioactive waste in the geological repository. Graphite blocks and sleeves from the reactor core, activated metallic reactor core components, parts of the spent fuel assemblies currently being stored at the Ignalina NPP are among this type of waste.

There is no final decision yet on the repository site, disposal concept, host rock and waste packages, but the research studies related to the repository performance and radionuclide transport are being performed.

### 13.1 Characterization of an ILW disposal cell in granite

#### 13.1.1 Description of materials in disposal cell

Regarding deep geological repository development, Lithuania is at the early conceptualization stage. Considering the outcomes of the desktop studies on the potential host rock for the geological repository in Lithuania [Poskas, 2006], a crystalline rock (granite) has a potential to be selected as the repository host rock. Thus LEI team within ACED WP is focused on the disposal cell in the crystalline rocks.

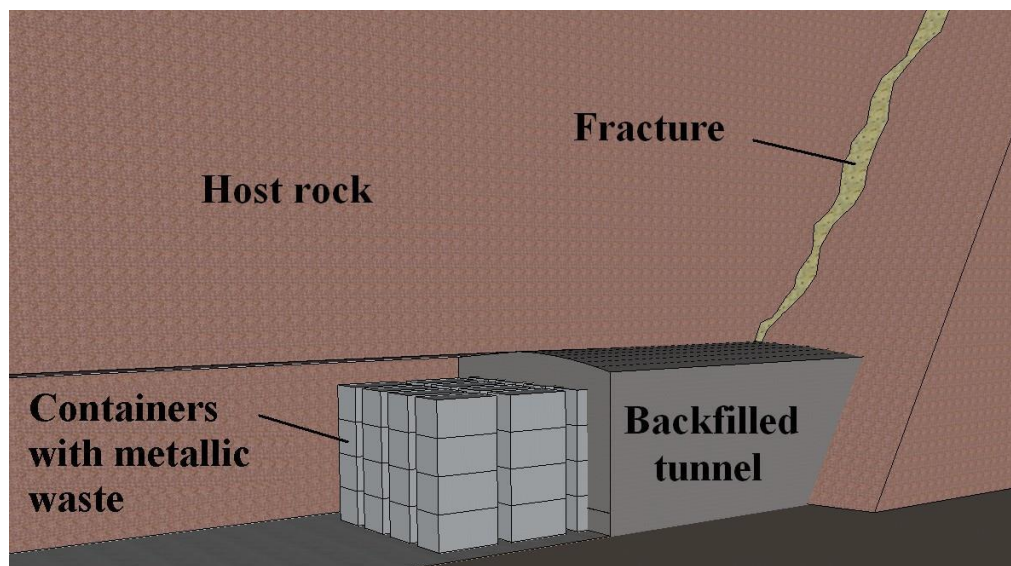


Figure 13-1: Repository concept

For various analysis related to ILW disposal in the crystalline rock, the tunnels of the dimensions of 16 m x 16 m (height x width) are considered [Theramin, 2019]. Steel is assumed as the material of the

container. Dimensions of the steel box (unshielded) would be 1.225 m × 1.72 m × 1.72 m (H × L × W) [Theramin, 2019]. As a material for the immobilisation of the waste, a cement based grout is of interest. Cementitious material (Nirex Reference Vault Backfill (NRVB)) is assumed as a backfill material.

### 13.1.2 Hydraulic gradients

As the site for the geological repository has not been selected, detailed modelling of the groundwater flow in the near field of the ILW disposal cell has not been performed yet. However, in the studies related to investigations of the contaminant transport from the geological repository, hydraulic gradient was assumed to be 0.01. In case of modeling pore water composition after the interaction of the groundwater with the bentonite, water flow was assumed to be negligible considering very low hydraulic conductivity of the bentonite.

### 13.1.3 Pore water compositions

The chemical gradients in pore water compositions are usually the driving forces for the chemical evolution. For the chemical characterization at start of the post-closure phase, the pore water compositions of the materials should be included in order to get a grasp of the potential chemical gradients in the disposal cells considered in your country. Include the methodology how the pore water compositions have been derived.

Porewater composition in the repository near field will depend on the chemical composition of the groundwater flowing in the vicinity of the repository and its interaction with the materials of engineered barriers. As there is no site selected for the geological repository, the site specific and high quality measured data on the crystalline rock groundwater composition are not available yet.

The composition of the porewater reaching the waste could be derived from the modelling of the chemical interaction of the groundwater from the host rock with engineered barriers' materials (steel, concrete grout, etc.). Modelling of the chemical composition changes in the groundwater flowing and interacting with steel and cementitious grout has not been performed. However, there is some experience in the modelling of porewater composition after its interaction with bentonite material.

## 13.2 Chemical evolution of the ILW disposal cell

### 13.2.1 Narrative

The groundwater interacts with the engineered barriers before it reaches the waste, thus it must be well characterized in order to build confidence in the assessment of repository evolution and radionuclide mobility. For the modelling of bentonite porewater, sparse data on the groundwater composition were used. The data corresponds to the groundwater in the crystalline rock in the region of the Ignalina NPP. The crystalline rock contains minerals such as granite, gneiss, etc., thus it is reasonable to expect some concentrations of Fe, Si elements in the water. As these data has not been reported yet, the assumptions on Fe, Si concentration has been made based on the information reported for Swedish crystalline rock (*Table 13-1*).

Table 13-1: Groundwater composition [Vaitkeviciene, 2017]

Element	Na <sup>+</sup> + K <sup>+</sup>	Ca <sup>2+</sup> + Mg <sup>2+</sup>	CO <sub>3</sub> <sup>2-</sup>	Cl <sup>-</sup>	SO <sub>4</sub> <sup>2-</sup>	H <sub>2</sub> SiO <sub>4</sub> <sup>2-</sup>	Fe <sub>tot</sub>	phases
Concentration, mol/l	9.1×10 <sup>-2</sup>	1.9×10 <sup>-2</sup>	2×10 <sup>-3</sup>	2×10 <sup>-4</sup>	2×10 <sup>-2</sup>	7×10 <sup>-5</sup>	3×10 <sup>-5</sup>	magnetite, hematite, goethite, dolomite, calcite, aragonite

Redox, pH are the key data for the modelling of the chemical interactions. As these measured data were not available, the values reported for other crystalline rocks were assigned for the pH, pe, pCO<sub>2</sub>, temperature: pH=7.5, pe=-2.42, pCO<sub>2</sub>=-2.54, t=25 °C.

### 13.2.2 Conceptual model

The bentonite material contains a major part of montmorillonite mineral and some auxiliary mineral phases such as calcite, gypsum, siderite, and dolomite. The later ones can dissolve/precipitate once in contact with the groundwater. Clay particles (montmorillonite mainly) contain at least two types of surface functional groups: permanently charged surface functional groups created by ionic substitution within the crystal structure and variably charged surface functional groups caused by ionisation of surface OH- groups on the edges of clay particles. Considering this, modelling of bentonite porewater composition takes into consideration ion-exchange reactions between ions in the interlayers of montmorillonite and groundwater (Na<sup>+</sup>, K<sup>+</sup>, Ca<sup>2+</sup>, Mg<sup>2+</sup>), protonation and deprotonation reactions at the edge sites and dissolution/precipitation reactions of other minerals in the bentonite (such as calcite, gypsum, siderite, dolomite).

Taking into consideration very low hydraulic conductivity of bentonite water, it is expected that water flow rate within this material will be very low and thus the porewater will be in equilibrium with bentonite. Analysis of the evolution of the chemical conditions over time has not been performed till now. Dissolution of montmorillonite was not considered in the study as it is expected to be insignificant.

The computer code PHREEQC was used for the modelling of bentonite porewater. PHREEQC is a computer program for simulation of chemical reactions and transport processes in natural or contaminated water, in laboratory experiments or in industrial processes. The program is based on equilibrium chemistry of aqueous solutions interacting with minerals, gases, solid solutions, exchangers and surfaces [Parkhurst, 1999].

### 13.2.3 Mathematical model

The equilibrium models require the information on initial water composition (*Table 13-1*), thermodynamic data (log K, its dependence on temperature) for speciation, ion-exchange and surface complexation reactions, information on the amount of mineral phases in contact with water, number of surface sites. It is also important to justify the condition related to CO<sub>2</sub> (close or open system with regard to CO<sub>2</sub>) as this has an impact on pH. Two cases were analysed in the study [Vaitkeviciene, 2017]: when the system is closed (CO<sub>2</sub> partial pressure depends on the overall chemical conditions in the system) and open (fixed CO<sub>2</sub> partial pressure). Data for MX-80 bentonite are presented in *Table 13-2*.

Table 13-2: MX-80 data [Ochs, 2004]

MX-80:	
smectite	88,6 %
quartz	10 %
calcite	0.7 %
soluble impurities:	
halite NaCl	0.007 %
gypsum CaSO <sub>4</sub>	0.34 %
Cation Exchange capacity, CEC	85 meq/100 g bentonite
Exchangeable Na <sup>+</sup>	81.7 %
Exchangeable K <sup>+</sup>	0.3 %
Exchangeable Mg <sup>2+</sup>	3.9 %
Exchangeable Ca <sup>2+</sup>	14.1 %
Number of surface sites:	
SOH site density	2.52×10 <sup>-5</sup> mol/g

The data for ion-exchange reactions and protonation and deprotonation reactions are summarized in Table 13-3.

Table 13-3: Data for chemical reactions

Reaction	log K	Reference
ion-exchange		
$Na^+ + X^- = NaX$	20	[Ochs, 2004]
$NaX + H^+ = HX + Na^+$	23	
$NaX + K^+ = KX + Na^+$	20.26	
$2NaX + Ca^{+2} = CaX_2 + 2Na^+$	40.53	
$2NaX + Mg^{+2} = MgX_2 + 2Na^+$	40.46	
protonation and deprotonation		
$SOH = SO^- + H^+$	-6.7	[Ochs, 2004]
$SOH + H^+ = SOH_2^+$	5.4	
mineral dissolution/precipitation		
Calcite: $CaCO_3 = Ca^{2+} + CO_3^{2-}$	-1.85	[Hummel, 2002]
Gypsum: $CaSO_4 \cdot 2H_2O = Ca^{2+} + SO_4^{2-} + 2H_2O$	-4.58	
Siderite: $FeCO_3 = Fe^{2+} + CO_3^{2-}$	-0.56	
Dolomite: $CaMg(CO_3)_2 = Ca^{2+} + Mg^{2+} + 2CO_3^{2-}$	4.12	

As described in [Parkhurst, 1999], all chemical equations in PHREEQC are written in terms of master species. There is one master aqueous species associated with each element or element valence state plus the activity of the hydrogen ion, the activity of the aqueous electron, and the activity of water.

The dissolved chemical species are assumed to be in thermodynamic equilibrium with one exception; in initial solution calculations, disequilibrium among valence states of redox elements is allowed. The unknowns for each aqueous species *i* are the activity *a<sub>i</sub>*, activity coefficient *y<sub>i</sub>*, molality *m<sub>i</sub>*, and moles in solution *n<sub>i</sub>*.

The numerical method implemented in PHREEQC reduces the number of unknowns (variables to be solved for) to be a minimum number of master unknowns, and iteratively refines the values of these master unknowns until a solution to the set of algebraic equations is found. A modified Newton-Raphson method is used to solve the simultaneous nonlinear equations in PHREEQC.

The master unknowns for aqueous solutions are the natural log of the activities of master species, the natural logarithm of the activity of water *a<sub>H2O</sub>*, the ionic strength *μ* and the mass of solvent water in an aqueous solution *W<sub>a</sub>* [Parkhurst, 1999].

Ion-exchange equilibria are modelled with PHREEQC through heterogeneous mass-action equations and mole-balance equations for exchange sites. The mass-action law equations are based on half-reactions between aqueous species and a fictive unoccupied exchange site.

Surface-complexation processes are modelled with PHREEQC through heterogeneous mass-action equations, mole-balance equations for surface sites, and charge-potential relations for each surface. PHREEQC allows multiple surfaces and surface-site types, termed a "surface assemblage", to exist in equilibrium with the aqueous phase. Two formulations of the mass-action equations for surface species are available in PHREEQC: one that includes electrostatic potential terms and another that excludes all electrostatic potential terms. Electrostatic potential terms were disregarded for modelling of bentonite porewater in the study [Vaitkeviciene, 2017].

Details of mathematical expressions of mass-action equations, activity coefficients, etc. are provided in the PHREEQC manual [Parkhurst, 1999].

## 14. Netherlands

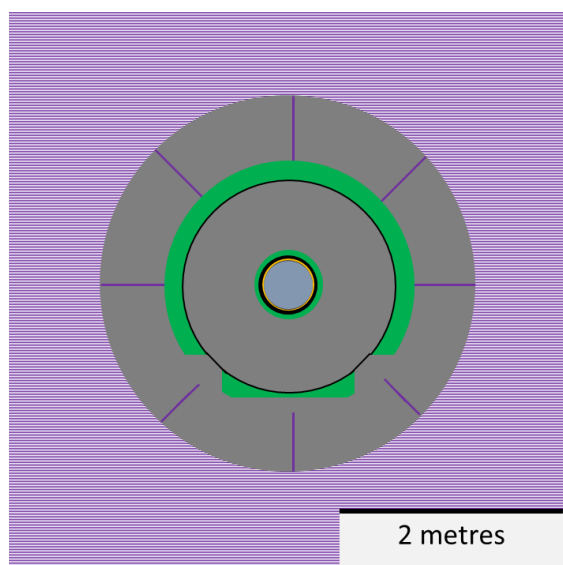
COVRA - Erika Neeft

The Dutch programme into geological disposal of radioactive waste is in the conceptualization stage. The geological formations that are investigated to host a geological disposal facility are poorly indurated clay as well as rock salt. Radioactive waste is intended for disposal after an interim storage period of at least 100 years in the current Dutch policy. Safe interim storage facilities have been built at COVRA's premises because the reference date for implementation lies relatively far into the future.

### 14.1 Characterization of the HLW disposal cell in clay

#### 14.1.1 Description of materials in disposal cell

The Dutch safety concept is adopted from the Belgian programme: there can only be contact between pore water and the waste form when a temperature of the host rock poorly indurated clay is achieved at which nominal migration properties of radionuclides can be relied upon. The thermal phase is defined as the period in time it takes to achieve this temperature at the interface between the engineered barrier system (EBS) and the host rock. Temperature induced hydro- mechanical perturbed radionuclide migration in the clay host rock can then be excluded in a normal evolution scenario. Shielded containers are emplaced in the disposal drifts in order to have contact-handled waste in the operational phase. The left empty volume is backfilled in order to have sufficient heat dissipation from the waste towards the host rock. The following figure shows an image of the disposal cell with the intended materials. The following table shows the dimensions.



**Host rock: clay**

**Material against host rock: concrete segments**

**Material used for backfill: foamed concrete**

**Immobilisation matrix glass,  $\varnothing$  0.420 m**

**Material for overpack: carbon steel overpack**

**Material surrounding the overpack: filler  
+ concrete buffer + stainless steel envelope**

Figure 14-1: Materials used in the disposal cell [Verhoef, 2017]

Table 14-1: Dimensions for the supercontainer for CSD-v

Feature	Dimensions in metres	
Concrete liner support for disposal gallery	Outer diameter	3.348
	Thickness	0.5
Stainless steel envelope	Thickness	0.004
Concrete buffer in disposal package	Outer diameter	1.9
	Thickness	0.642
	Length	2.5
Carbon steel overpack	Outer diameter	0.5160
	Thickness	0.03
Stainless steel canister	Outer diameter	0.43
	Thickness	0.005

There are several criteria and design requirements for the components in the disposal cell in order to satisfy their safety functions:

- **Clay host rock:** the pore water in undisturbed clay host rock can assume to be stagnant i.e. the potential migration of radionuclides is diffusion-controlled. Poorly indurated clays have high smectite contents and there is lack in knowledge how to model the stage at which the gas solubility in these clays is exceeded. The EBS for HLW is therefore designed to prevent exceeding the gas solubility in the host rock in the chemical evolution of the disposal cell. These solubility's are defined as a function of depth, salinity, temperature and porosity. The temperature of the host rock at depth of 500 metre has been estimated to be between 22 and 26 degrees Celsius [Verweij, 2016]. Disposal depths between 200 and 1000 metres are investigated in the Dutch programme.
- **Concrete segments:** hardened segments are to be emplaced by a tunnelling boring machine to prevent convergence of poorly indurated clay. The constructed liner has an additional beneficial function for the post-closure phase: no dehydration of the clay host rock takes place during the operational phase. The compressive strength and thickness of concrete are design requirements for the construction of the disposal facility [Arnold, 2015a&b]. Complementary criteria to satisfy the construction safety function are:
  - the clay host rock is expected to be at least as saline as seawater and therefore the concrete segments are fabricated with a high sulphate resistant cement to prevent delayed ettringite formation;
  - the water-cement ratio is small in order to limit the ingress of dissolved species from the clay pore water and egress of dissolved species from the concrete pore water; the segments are impermeable according to NEN-EN 12390-8 i.e. in engineering terms.
- **Grout backfill:** grout is poured in order limit void volumes in the disposal cell. The hardened foamed concrete should ensure sufficient heat dissipation from the waste to the host rock. A thermal conductivity as small as  $0.09 \text{ W m}^{-1}\text{K}^{-1}$  i.e. the minimum in tailor-made foamed concrete, has been calculated to be sufficient for heat dissipation of the Dutch stored heat-generating waste in the post-closure phase. Complimentary criteria to be able to use this backfill material are:
  - A density limit to prevent floating of the emplaced waste packages when pouring the cementitious fluid. A maximum value of  $2300 \text{ kg m}^{-3}$  is currently used;
  - The necessary compressive strength to have sufficient mechanical support is assumed to depend on the disposal depth e.g. a compressive strength of 10 MPa is necessary for a GDF at 500 metres depth.
- **Concrete buffer:** provides the beneficial physical and chemical conditions for predictable corrosion of the overpack. The hardened concrete containers are, similarly as the hardened concrete segments, designed to be sulphate resistant and have a physical resistance against water flow. Other criteria to satisfy this safety function are:
  - A temperature below 90 till 100 degrees Celsius to eliminate the formation of a gaseous phase by heat generation of the waste;
  - A sufficient thickness of the concrete buffer to provide the chemical beneficial conditions in the thermal phase i.e.  $\text{pH} > 10$  to limit corrosion and prevent pitting of the overpack;

- A sufficient thickness to provide additional shielding in the operational phase i.e. 0.642 metre for Dutch stored vitrified HLW when a density similar to conventional concrete is used as a concrete buffer.
- Carbon steel overpack: prevents contact between the waste form and pore water during the thermal phase. Criteria for the overpack in order to ensure that this contact is prevented are:
  - A sufficient thickness to withstand the lithostatic pressure e.g. 30 mm at 500 metres depth; the mechanical sufficient thickness is also used to calculate the additional necessary shielding by concrete;
  - A temperature below 200 degrees Celsius to remain its mechanical strength.
- Stainless steel canister: no criteria yet set for disposal except the wall thickness which contributes to shielding.
- Vitrified waste form is a product with a homogenised distribution of radionuclides i.e. no hot spots. Consequently, a predictable radionuclide release rate can be assumed in the post-closure phase and the shielding by the waste form can be well predicted for the operational phase. This engineered barrier does not easily dissolve in clay pore water. The heat emission at start of disposal is a maximum of 200 W after the Dutch long interim storage period i.e. on average 130 years. A maximum temperature of 500 degrees Celsius is used as a criterion to prevent glass transition and resulting mechanical stresses. The following figures show the thermal power as supplied by AREVA and the schematics for this waste from France: Colis Standard de Déchets-vitrifiés (CSD-v).

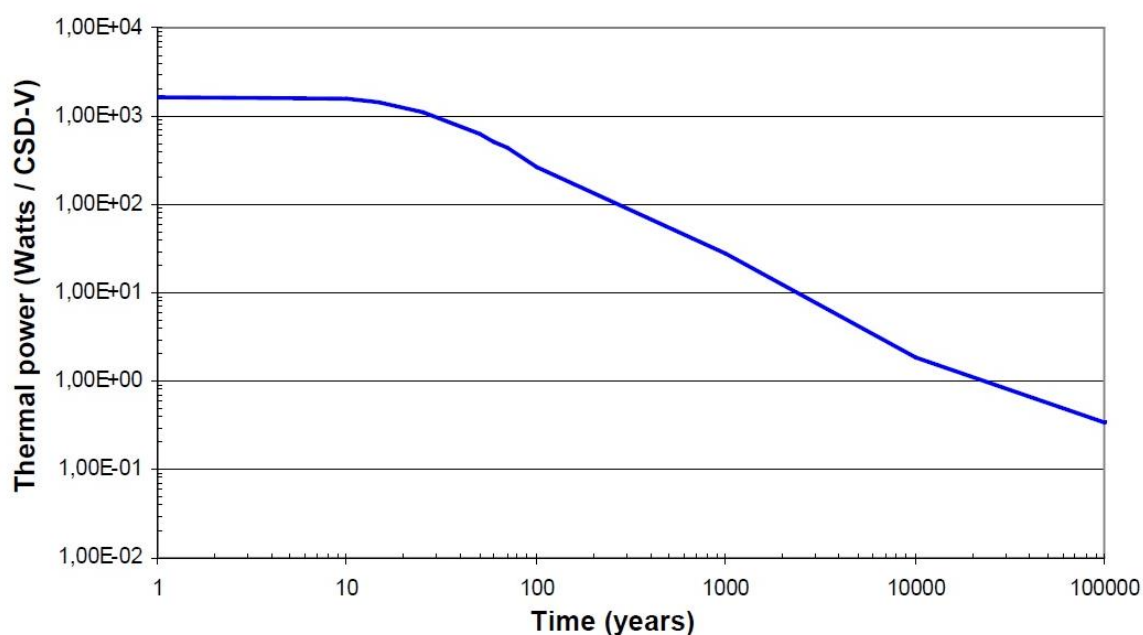


Figure 14-2: Evolution of the thermal power of a typical residue UOX: 44000 MWd/tU initial enrichment 3.8% <sup>235</sup>U and mixed with MOX: 45.000 MWd/tU initial enrichment [AREVA, 2007]. Decay of many short-lived radionuclides takes place in the period smaller than 30 years. Their contribution to the thermal power is assumed not be included.

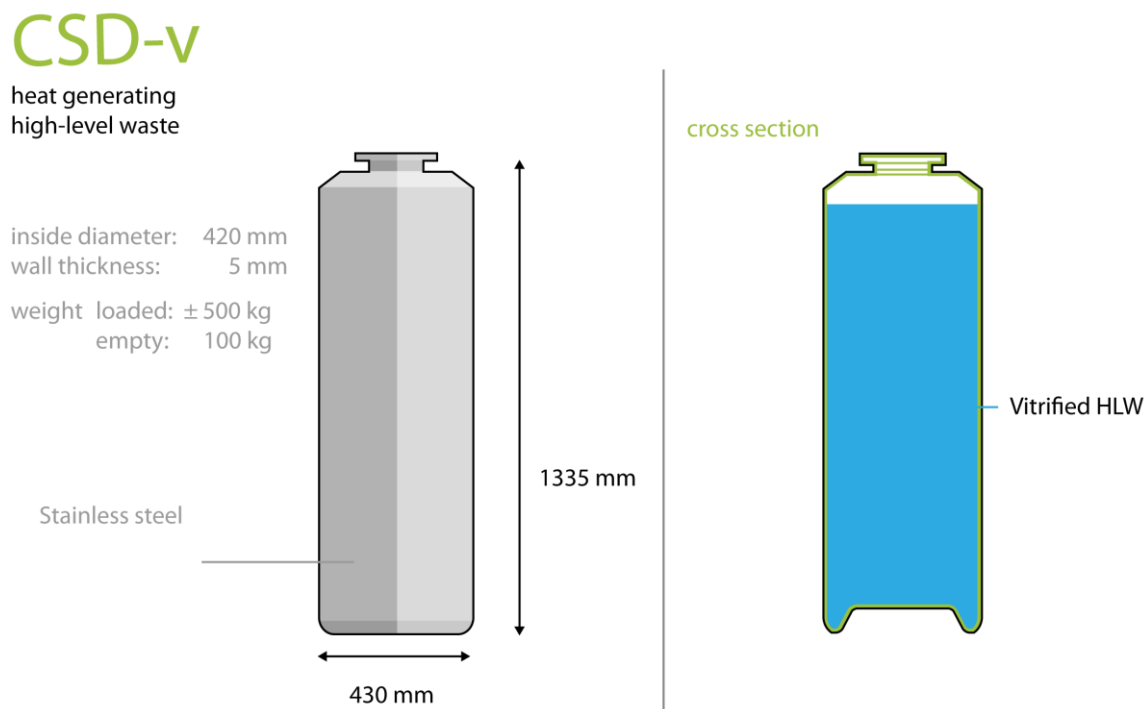


Figure 14-3: Schematics of CSD-v; dimensions in millimetres [AREVA, 2007]

The materials in this disposal cell have been published in the OPERA Safety case [Verhoef, 2017]. A few choices are currently reconsidered:

- The chemical and bacterial evolution at the interface between foamed concrete and the stainless steel envelope surrounding the concrete buffer may result in a too high gas generation rate of the stainless steel. The gas solubility in the clay host rock may be exceeded and this steel envelope is therefore currently suggested to be removed;
- The mechanical design requirement for the backfill i.e. a minimum in compressive strength as a function of disposal depth, may not be necessary;
- The confidence of the use of sulphate resistant Ordinary Portland Cement to manufacture the concrete buffer would rely on certificates. The use of cement blended with Blast Furnace Slag cement eliminates this quality control and is therefore currently considered in the Dutch programme.

## 14.1.2 Thermal gradients

### 14.1.2.1 Conceptual model

The disposal galleries will be backfilled with foamed concrete after emplacement of the concrete containers in the disposal gallery. The emission of heat by the waste form is dissipated into the concrete buffer, backfill, disposal gallery and host rock clay. The emission of heat by the waste reduces as a function of time since the amount of radionuclides, responsible for the heat emission from the waste form, decays as a function of time.

### 14.1.2.2 Mathematical model and parameter values

The dissipation of the heat generated by the waste is through conduction through the materials. The following 2D-axi-symmetric equation is solved:

$$\frac{\partial T}{\partial t} = \sum_{i=1}^n \frac{k_i}{\rho_i C_{p,i}} k_i \nabla^2 T + \frac{Q(t)}{\rho_{waste\ form} C_{p,waste\ form}}$$

where  $k_i$ ,  $\rho_i$  and  $C_{p,i}$  are the thermal conductivity, the density and heat capacity of each material,  $Q(t)$  is the thermal power as a function of time divided by the volume of waste.

The following figure shows the calculated geometry:

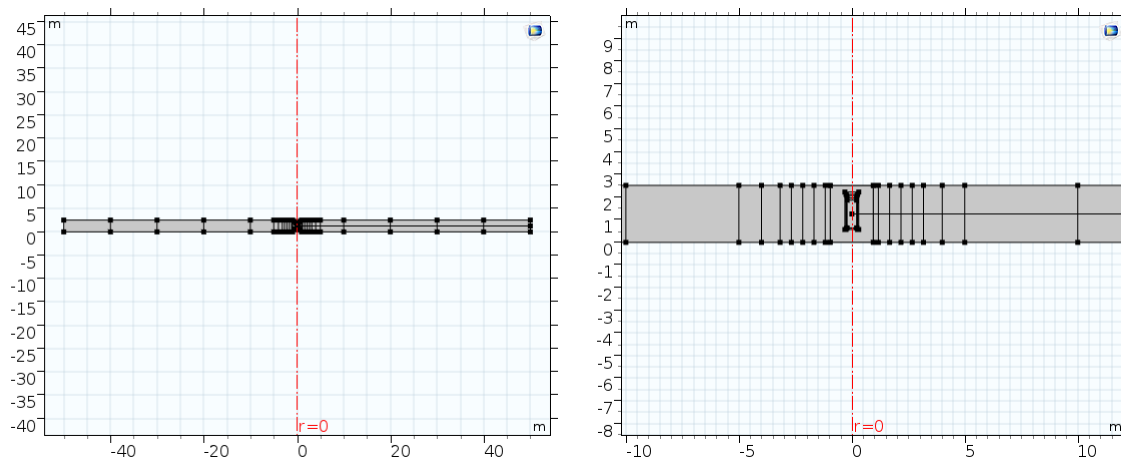


Figure 14-4: Geometry for the calculation of the thermal phase with 100 metre thickness of clay and a magnification with the waste (right). Midpoints are calculated with the line in each positive section in order to obtain maxima in calculated temperatures. The images should be turned 90 degrees in order to visualize these geometries in the disposal concept i.e. horizontal emplacement of disposal packages is envisaged.

The above equation is solved with a variable thermal power  $Q(t)$ , see Figure 14-2, the outer boundary of clay with a temperature  $26^{\circ}\text{C}$ , the initial temperature for all materials with  $26^{\circ}\text{C}$ , and the other outer boundaries as symmetry planes. The following figure shows the calculated temperatures as a function of time after a storage period of a CSD-v of 130 years. It shows these temperatures at midpoints from the materials and at 4 different interfaces. The calculated temperatures at midpoints are expected to be the maxima in temperatures.

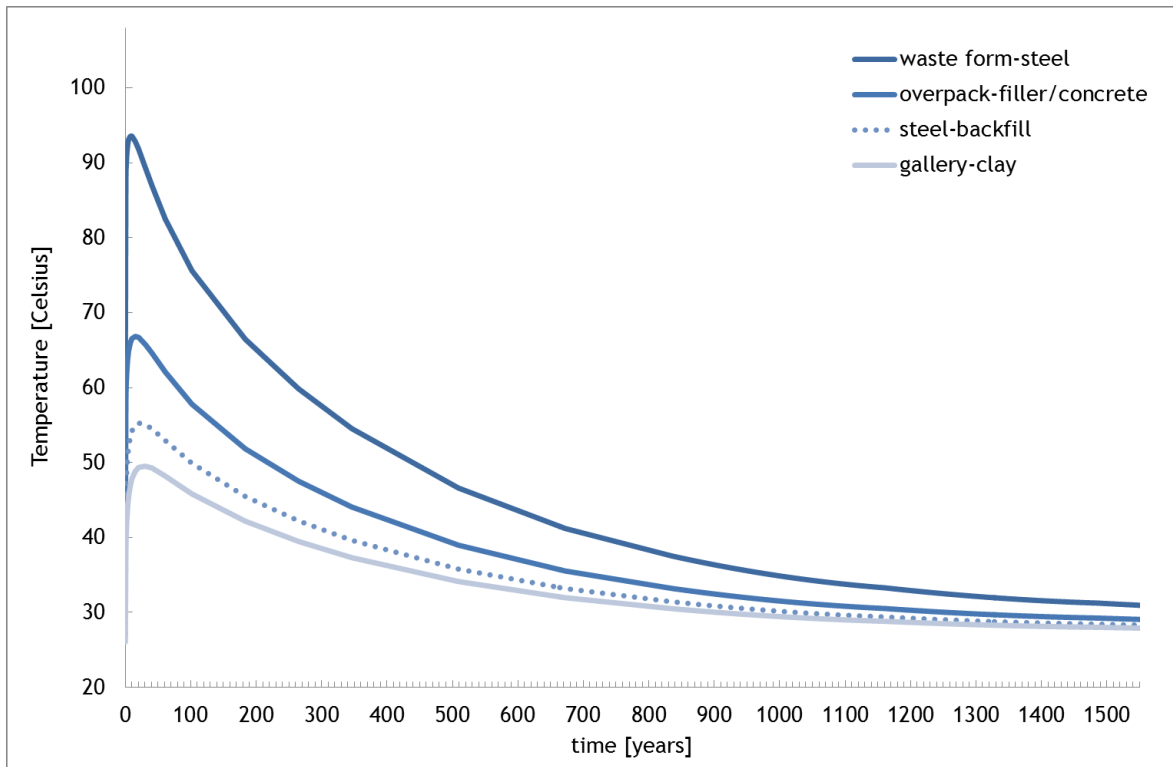


Figure 14-5: Calculated temperatures at different interfaces after a storage period of 130 years for CSD-v; at midpoints; 2D axi-symmetry with thermal power as supplied by AREVA and cooling period of 130 years.

Table 14-2: Description of parameters for thermal gradients

Feature	Parameter	Value and unit	Source	Justification / comments
Heat source in CSD-v	Thermal power as a function of time	Watt / canister	[AREVA, 2007]	A polynomial fit is made of the thermal power of the typical residue supplied by the waste processing facility
Heat volume in CSD-v	Volume of heat source	0.17 m <sup>3</sup>	[AREVA, 2007]	Volume of waste
Waste form glass	Heat conductivity	1.02 W m <sup>-1</sup> K <sup>-1</sup>	[AREVA, 2007]	At 100°C; that is the minimum available thermal conductivity; the thermal conductivity slightly increases with temperature e.g. at 500°C: 1.25 W m <sup>-1</sup> K <sup>-1</sup>
	Specific density	2800 kg m <sup>-3</sup>		
	Specific heat capacity	880 J kg <sup>-1</sup> K <sup>-1</sup>		
Stainless steel canister and envelope	Thermal conductivity	16.2 W m <sup>-1</sup> K <sup>-1</sup>	[AK Steel,1986]	AK Steel 304/304 L, at 100°C, datasheet is public available
	Specific density	8030 kg m <sup>-3</sup>		
	Specific heat capacity	500 J kg <sup>-1</sup> K <sup>-1</sup>		
Air gap	Thermal conductivity		[COMSOL,2018]	COMSOL built-in material
	Specific density			
	Specific heat capacity			
Overpack Carbon steel	thermal conductivity	44.5 W m <sup>-1</sup> K <sup>-1</sup>	[COMSOL,2018]	COMSOL built-in material
	specific density	7850 kg m <sup>-3</sup>		
	specific heat capacity	475 J kg <sup>-1</sup> K <sup>-1</sup>		
Filler + concrete buffer and gallery	thermal conductivity	1.8 Wm <sup>-1</sup> K <sup>-1</sup>	[COMSOL, 2018]	COMSOL built-in material; similar values in the Belgian programme [Weetjens,2009] and [Humbeeck,2007] are comparable to ordinary values of concrete [Soen, 2007]
	specific density	2300 kg m <sup>-3</sup>		
	specific heat capacity	880 J kg <sup>-1</sup> K <sup>-1</sup>		
Foamed concrete	thermal conductivity	0.80 W m <sup>-1</sup> K <sup>-1</sup>	[CUR 181, 1995]	Density 1600 kg m <sup>-3</sup> : wet 0.80 W/mK 95% RH
	specific density	1600 kg m <sup>-3</sup>	[CUR 181, 1995]	Tailor-made product with a compressive strength at least 10 MPa to accommodate lithostatic pressure at 500 metre depth
	specific heat capacity	840 J kg <sup>-1</sup> K <sup>-1</sup>	Joostdevree.nl	Wet larger than dry due to large heat capacity of water
Host rock Boom Clay	thermal conductivity	1.45 W m <sup>-1</sup> K <sup>-1</sup>	[Weetjens, 2009]	Combination of horizontal and vertical conductivity
	specific density	2000 kg m <sup>-3</sup>	[Mazurek, 2003]	Results from large scale in-situ test in a clay pit; water-saturated Boom Clay p.230; also in NIROND,2013 p.89
	specific heat capacity	1420 J kg <sup>-1</sup> K <sup>-1</sup>	[NIROND, 2013]	Deduced from 2.84×10 <sup>6</sup> J m <sup>-3</sup> K <sup>-1</sup> see p.125 in NIROND
	temperature	299.15 K	[Verweij, 2016]	Generic temperature of Boom Clay at 500 metre depth in range 22°C to 26°C; chosen 26°C

### 14.1.3 Pore water compositions and porosity

The pore water compositions in the porous materials used in the Dutch disposal cell, poorly indurated clay and concrete have been deduced from the available literature due to lack in experimental data. The clay pore water is calculated in OPERA(2011-2017) by taking an average of the measured clay mineralogy and calculating the formation waters at three different salinities: a brackish scenario, a seawater scenario and very saline water scenario [Griffioen, 2017]. The brackish-saline interface in the majority of the Netherlands is at a depth smaller than 200 metre [Dufour, 2000] and the available groundwater analysis at suitable disposal depth indicate very saline waters [Griffioen, 2016]. Clay pore water is assumed as saline as seawater as a working hypothesis in the Dutch programme until further information becomes available. The following table shows the calculated pore water compositions for the sea water scenario [Griffioen, 2017] and the calculated porosity [Verweij, 2016].

Table 14-3: Pore water compositions at start of the post-closure phase

Feature	φ	Na	Ca	Mg	Cl	Si	SO <sub>4</sub>	HCO <sub>3</sub>	pe	pH
	%	mmol/kg pore water								
Clay host rock	33	46 1	13.2	56.1	541	0.3	28.4	7.2	-2.8	6.9
Concrete segments	12	-	19.2	-	-	0.007	-	-	-	12.5
Foamed concrete backfill	24	-	15.0	-	-	0.018	-	-	-10.4	12.3
Concrete buffer surrounding overpack	12	-	15.0	-	-	0.018	-	-	-10.4	12.3

The porosity of the cement components is gravimetrically determined [Neeft, 201X]. The measured pH, calcium and silicium concentrations in concrete can be well predicted from the CaO/SiO<sub>2</sub> ratio of the CSH-gel in concrete [Berner, 1992]. The CaO and SiO<sub>2</sub> content in the cements have been taken from the product data sheets for CEM III/B and CEM-II/B-V from the Dutch cement industry: Hollandse Cement Maatschappij. For CEM III/B: 48%(m/m) CaO and 29%(m/m) SiO<sub>2</sub> and for CEM-II/B-V 53%(m/m) CaO and 27%(m/m) SiO<sub>2</sub>. The CaO/SiO<sub>2</sub> ratios are shown in the following figure and the pH and calcium and silicium concentrations have been taken from the data by Greenberg and Change as published in Berner’s paper. Similar results have been obtained in the European Horizon 2020 project Cebama [Vehmas, 2019a]. The redox potential for CEM III/B i.e. foamed concrete and concrete buffer has been taken from a Swiss study that investigated a CEM III/B backfill [Cloet, 2019].

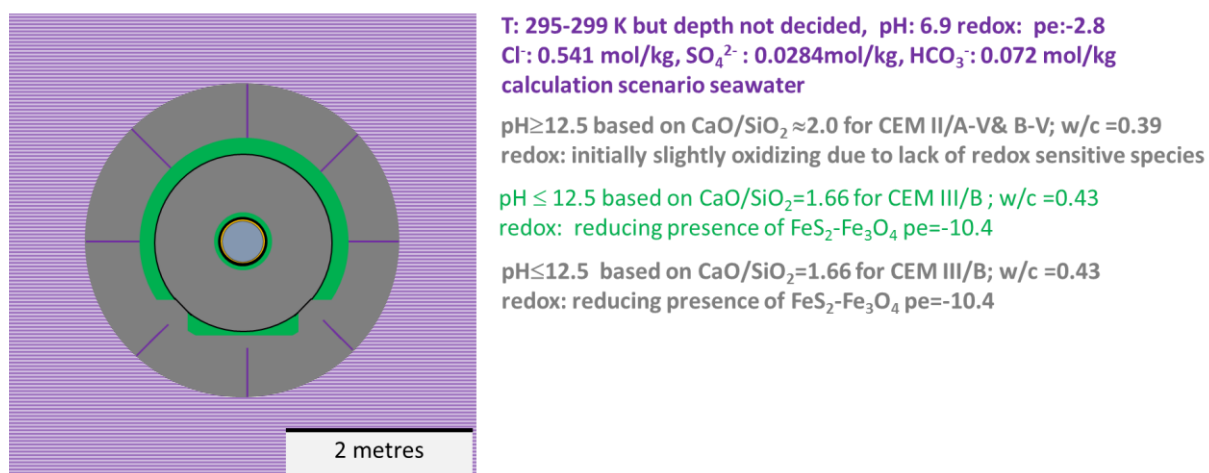


Figure 14-6: Pore water compositions and CaO/SiO<sub>2</sub> ratios for concrete used in the disposal cell.

## 14.2 Chemical evolution of the HLW disposal cell

### 14.2.1 Narrative

In the operational phase, ventilation is expected to be sufficient to keep the Underground Facility with concrete supported liner dry. Salts have been deposited at the intrados of the concrete liner especially at joints between concrete segments. The following figure shows an example from the HADES Underground Research Laboratory in Mol (Belgium) indicating a water flow into the URL.

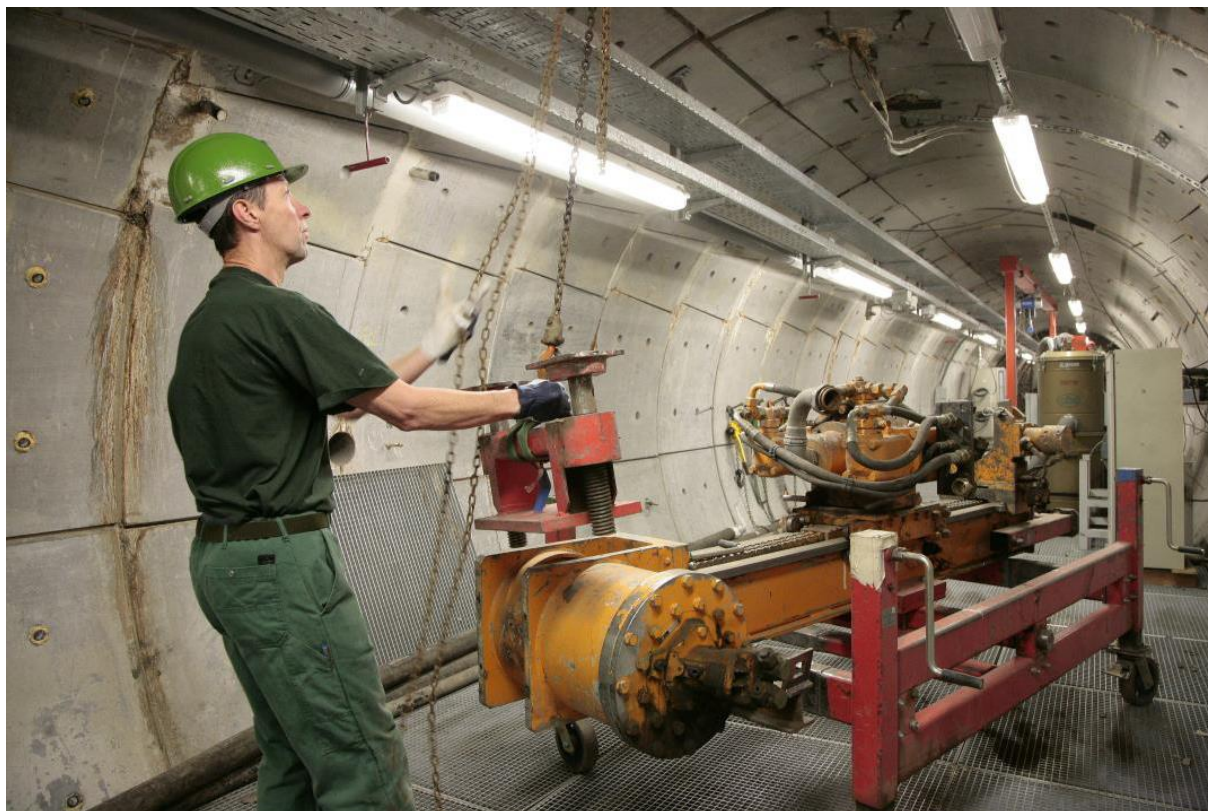


Figure 14-7: Salt deposits at joints between concrete segments in HADES URL. Image from EURIDICE website: presentation 01 EURIDICE general.

The initial preferential pathway for clay pore water transport into the disposal cell is therefore assumed to be along the joints between concrete segments into the cementitious backfill. There is also a slow diffusional inflow of clay pore water species into the concrete segments and cement components diffusing into the surrounding clay. There is some decalcification expected for the concrete segments because the calcium concentration in the concrete pore water is larger than this calcium concentration of the clay host rock. A slow reduction of the pH at the outer surfaces of the concrete segments is caused by the accompanied diffusional flow of hydroxyl ions during decalcification as well as ingress of bicarbonate from the clay pore water. The backfill is more porous than the concrete buffer of the supercontainer i.e. shielded container. Spreading of the dissolved clay pore water species that have interfaced the concrete segments within the backfill is therefore assumed. The carbonate that becomes present in the cementitious materials competes with the calcium in the CSH-gel to precipitate as calcite but the CSH-gel can also sorp carbonate [Pointeau, 2008].

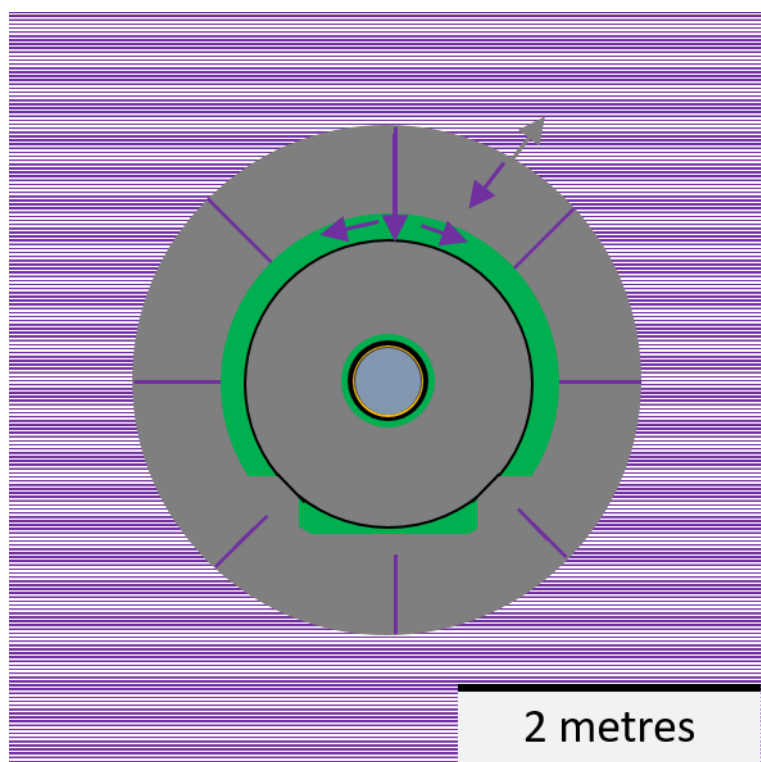


Figure 14-8: Diffusional ingress and egress of dissolved species at start of the post-closure phase

The ingress of dissolved magnesium from the clay pore water is usually assumed to form brucite since  $Mg(OH)_2$  is less soluble than portlandite  $Ca(OH)_2$  [Atkinson, 1985]. The cementitious materials currently considered are made with blended cements which may not have portlandite. Brucite has also been calculated to be formed for the concrete segments made with CEM/IIB-V [Seeratham, 2015]. The ingress of chloride ions from the clay pore water are expected to be sorbed on the positively charged cementitious minerals as long as the pH is above 11.8 since the zeta-potential has then be calculated to become 0 [Poiteau, 2008].

The intrados of the concrete liner – that was dried due to ventilation in a relative humidity below 100% - becomes saturated. The fabricated saturation of a well-engineered concrete buffer is about 90% and the drying in the operational phase is expected to be negligible. The current choice to use cement with Blast Furnace Slag content of at least 66% and blended with Ordinary Portland Cement, has an impact on the start of the gas generation rate. The experimental studies performed at ambient temperature conditions 20-30°C in the nineties for the European study to characterize radioactive waste forms have shown, by measuring the rest potential of steel as a function of time and Raman spectra, that carbon steel-BFS cement interfaces form magnetite immediately [Naish, 1991]. Thermodynamic calculations also show that magnetite is present at alkaline, anaerobic conditions. Anaerobic conditions at the interface between the concrete buffer and carbon steel overpack are therefore assumed; gas generation starts already in the operational phase.

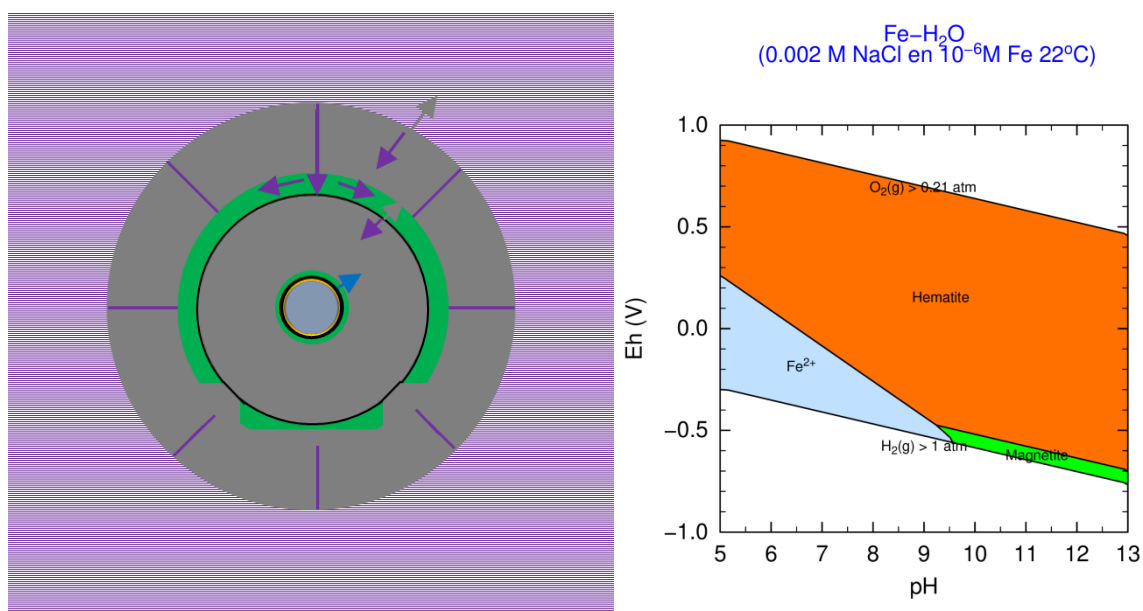


Figure 14-9: Diffusion of dissolved species and gas generation (left) and thermodynamic calculation made with Phreeplot and thermochimie database(right).

The waste form, overpack, concrete buffer, backfill and clay host rock will be heated and slowly cooled down in the post-closure phase. The temperature at the interface between the overpack steel and concrete buffer has been calculated to remain below 80 degrees Celsius, see *Figure 14-5*. The result of shielding calculations show that radiation rate at this interface is 5.2 Gy per hour after a storage period of 130 years [Neeft, 201X]. Anaerobic corrosion experiments at 25 and 80 degrees Celsius with a radiation rate of 0.25 Gy per hour and 25 Gy per hour have been performed in cement and cement solutions in the framework of the Belgian programme [Smart, 2017]. A difference in corrosion rate as a function of temperature, radiation and chlorine concentration has not been measured. A constant small gas generation rate is therefore assumed in the thermal phase and beyond this phase. The gas generated by corrosion has calculated to be sufficiently be dissipated by diffusion i.e. a gas pressure built-up does not occur.

After some time, the clay preferential flow paths along the joints of concrete segments have disappeared due to chemical reactions with clay pore water. The clay host rock and EBS containing waste have cooled down till virgin host rock temperatures. Decalcification and other leaching processes may have increased the diffusion values in the EBS for ingress and egress of dissolved species. The pH of the clay host rock in the local vicinity of the EBS is increased due to egress of hydroxyl ions. The impact can be neglected since the EBS is quite a small volume compared to the clay host rock i.e. the dilution of hydroxyl ions in clay is extensive. The concentration profile of hydroxyl ions of concrete aged in clay for 43 years has been measured to be very steep; the pH of concrete at the interface between concrete and clay has been measured to approach the virgin pH of clay [Atkinson, 1985].

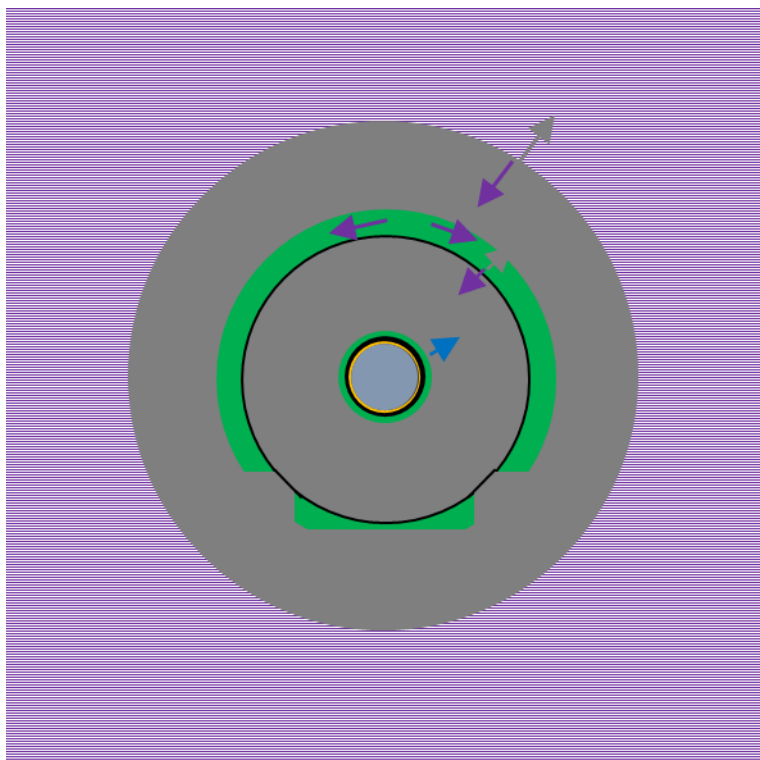


Figure 14-10: Diffusion of dissolved species and gas generation at an evolved stage.

Eventually, there will be contact between pore water and the waste form. The concrete buffer may also still have sufficient mechanical strength against the lithostatic pressure if the interface between the concrete buffer and overpack is as alkaline as emplaced. The contact between the pore water and waste form results from the complete corroding of the overpack as well as stainless steel canister. The complete chemical corrosion of the 30 mm overpack requires at least 3 million years. The corrosion product of the stainless steel canister is different from magnetite i.e. chromite but similar corrosion rates can be assumed i.e. a wall thickness of 5 mm would require at least 0.5 million years. These periods may be too long to allow assuming these alkaline conditions at the overpack-concrete interface. It is therefore assumed that the mechanical strength of the concrete buffer has been reduced significantly by reaction with magnesium and bicarbonate from the evolved clay pore water. The pH of the concrete buffer drops eventually till the pH of clay pore water but it may take thousands of years i.e. far beyond the thermal phase. The reduction in thickness by chemical corrosion of the overpack becomes sufficient to form fractures due to the lithostatic pressure load. These fractures are assumed to be preferentially at the top of the stainless canister since there is empty volume left, see *Figure 14-3*. The contact between the carbon steel overpack and stainless steel results in a larger corrosion rate of the carbon steel since the stainless steel is nobler than the carbon steel overpack.

The residue of reprocessed spent nuclear power fuel is contained in glass. Glass is already an oxidised product and therefore water can only act as a potential dissolver but not as an oxidant. Consequently, no additional gas is expected to be generated when pore water comes into contact with the waste form glass. Glass is an insulator and therefore an electrical contact with both steels is expected to be poor. In a normal evolution scenario, the waste form dissolution rate is assumed to depend on the dissolution rate of glass and the exposed geometric surface area.

The geometric surface is determined by the outer surface of the waste form and a so-called cracking factor. The number of cracks that are assumed to be present within glass were made during pouring melted glass and radionuclides in the canister and subsequent cooling. An X-ray image of a canister

with processed waste to deduce the cracks within the waste form has not been found. The experimental studies performed in the nineties for the European study to characterize radioactive waste forms have demonstrated that it is possible to produce homogeneous and nearly crack free glass blocks by applying appropriate cooling procedures even with non-radioactive simulate HLW [Reimers, 1992]. These old experimental studies have not been modelled but rather theoretical perhaps even unrealistic cases in recent modelling studies [e.g. Barth, 2014]. The presence of radionuclides within glass has some beneficial characteristics to prevent or heal cracks. The thermal power source and the radioactivity work as glass network modifier by producing ionization rays. The following chemistry of decay has been neglected in recent modelling studies. The  $\alpha$ -decay of actinides present in waste diminishes slightly the glass density and its mechanical properties appreciably improve, especially its resistance to cracking [Ribet, 2009]. The evolving helium diffuses at such a high speed at room temperature that helium implantation below room temperature is necessary to make helium observations within glass with neutron activation analysis [Chamssedine, 2010]. Defects generated by stopping the highly energetic alpha particles within the waste form are annealed at room temperature by which helium trapping by defects within the waste form glass does not occur at disposal representative conditions. Consequently, cracks cannot be formed by decay of radionuclides. A geometric surface area determined by a crack-free vitrified waste form seems to be a realistic case with the available experimental evidence.

The glass dissolution rate highly depends on pH. The pore water of a BFS-blended based cement does not contain portlandite,  $\text{Ca}(\text{OH})_2$ ; only C-S-H minerals are available. The maximum in pH of BFS-blended concrete pore water is therefore 12.5. Available glass dissolution rates have been evaluated with OPERA(2011-2017) [Deissmann, 2016]. The available information on the impact of the radiolysis of pore water to the dissolution is scarce but seems to be negligible. The dissolution rates obtained at static conditions seem to be the most representative ones for a normal evolution scenario because only diffusion of dissolved species takes place. There are short term and long-term rates. The long-term rate includes the formed amorphous layer at the exposed surface which no longer dissolves if the solution is saturated with Si, Zr, Al, Ca etcetera. This layer also constitutes a barrier against transport of water towards glass and of solvated glass into solution. The cracking factor of inactive glass i.e. glass not containing radionuclides, is significantly reduced by the formation of this layer from 40 to 5 [Ribet, 2009]. Finally, the layer may result into element-specific radionuclide release.

#### 14.2.2 Conceptual model

The potential release of radionuclides is assumed to take place after the thermal phase in the safety assessment. Cooling periods of 1000, 35000, 70000 and 700000 years have been used for OPERA(2011-2017). The cementitious materials have been assumed to be instantaneously dissolved after a chosen cooling period and radionuclides in these materials are assumed to diffuse directly into the host rock. The vitrified waste form dissolves with a constant rate [Rosca-Bocancea & Schröder, 2017a/b]. The best estimate rate is determined by the weight of the waste form, glass dissolution rate at a pH of 13.5 and a geometric surface area [Deissmann, 2016] i.e. the pH of the interface between the overpack and concrete buffer is assumed to be as emplaced after each cooling period. Consequently, a chemical evolution has been excluded in this assessment. But chemical evolutions for parts of the disposal cell has been modelled in OPERA(2011-2017).

The pH as a function of time at the interface between the concrete buffer and carbon steel overpack has been calculated by assuming a constant clay pore water composition at the outer diameter of the concrete buffer [Kursten, 2015]. The model calculates the evolution of the cement chemistry including pH of the concrete pore water by diffusing of dissolved species and assuming a local equilibrium between dissolved species and cement hydrates [Wang, 2009]. The geochemical evolution of the OPC-based concrete buffer as well as concrete segments has also been calculated as a function of the cumulative leached water [Seetharam, 2015].

The pH and pe as a function of time at the interface between concrete and the clay host rock has been calculated by assuming a constant concrete pore water composition and oxidising potential at this interface. The clay matrix buffers the ingress of dissolved species by ion exchange, sorption at clay minerals and organic matter but also dissolution of SiO<sub>2</sub> in clay. Diffusional flow of species as well as two different advective flows in clay has been used. The chlorine content in clay is calculated to be 'flushed away' from the interface between concrete and clay i.e. the chlorine concentration [Griffioen, 2017].

### Uncertainties

The biggest uncertainty in the safety assessment is the representativeness of data and models.

For the geochemical evolution of the cementitious materials, more or less scoping calculations have been performed to see what a minimum in the period in time for the alkaline beneficial conditions could be. Precipitation and dissolution of mineral phases have been calculated but changes in porosity as a result of these processes have been excluded i.e. constant values for diffusion of dissolved species has been assumed. Sorption of species has been excluded.

The geochemical interaction of the clay host rock with corrosion and degradation products from the EBS were to be assessed in OPERA(2011-2017). Whether concrete interfacing clay is represented by assuming a constant pore water composition is a large normal scenario evolution uncertainty. A large modelling uncertainty is the calculated impact of advective flow i.e. the chlorine concentration is negligible from the clay-concrete till ten metre into the clay. The impact of corrosion gases such as hydrogen has been excluded.

#### 14.2.3 Mathematical model

The chemical evolution of the cementitious materials is calculated by a leaching model in which a local thermodynamic equilibrium is assumed between the dissolved species and cement hydrates [Kursten & Seeratham, 2015].

The chemical evolution of the clay host rock is calculated with an infinite source of concrete pore water with a constant pH and redox potential [Griffioen, 2017].

## 14.3 Characterization of an ILW disposal cell in clay

### 14.3.1 Description of materials in disposal cell

The Intermediate Level Waste described here arises from reprocessing spent fuel from nuclear plants: Compacted waste Standard Residues (Collis Standard de Déchets Compatés: CSD-c). It comprises metal parts from the spent fuel assemblies that have been cut off to extract the spent fuel, then rinsed and dried. A canister of about 170 litres internal volume is filled with either hulls or end pieces. The hulls are made of zircaloy; other metal parts are usually made of Inconel. End pieces are solid stainless steel sections. Drums with other waste arising from reprocessing fuels, such as pumps, stirrers and filters, are primarily made of stainless steel. All drums are compacted to produce pucks that are loaded into CSD-c canisters with similar outer dimensions to those used for vitrified waste, which are welded closed. The void space is about 20% in the canisters. The following figure the schematics for this waste.

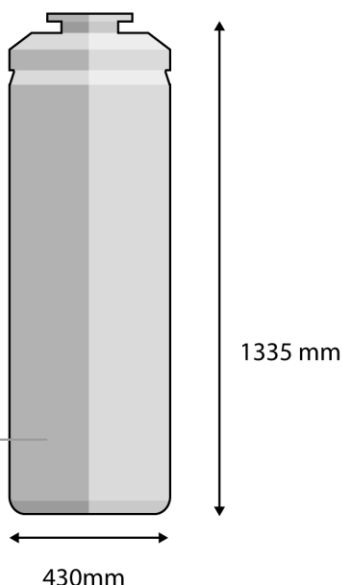
## CSD-c

non-heat generating  
high-level waste

inside diameter 420 mm  
wall thickness 5 mm

weight loaded: >850 kg  
empty: 100 kg

Stainless steel



cross section

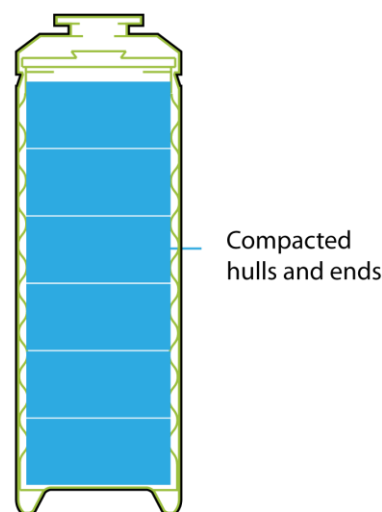


Figure 14-11: Schematics of CSD-c with 6 pucks (compacted drums); dimensions in millimetres [AREVA, 2001]

These stainless steel canisters containing compacted hulls and ends (CSD-c) were envisaged to have the same encapsulation as CSD-v in OPERA(2011-2017) but future work was assigned to investigate another standardised container for non-heat generating waste such as CSD-c [Verhoef, 2017]. The image for the disposal cell is therefore similar to *Figure 14-1* except that the waste inside the stainless canister is metallic waste instead of glass and that the waste form hulls contains radionuclides of two different sources: contamination from the fuel and activation products. Zircaloy has been known to have a higher corrosion resistance than stainless steel in environments such as nuclear plants but also in anaerobic, alkaline environments as shown in the European project Carbon-14 Source Term in which the corrosion rate of Zircaloy is ten times smaller than stainless steel [Neeft, 2018].

### 14.3.2 Pore water compositions

The same approach as described in paragraph 14.1.3 would be used in determination of the pore water compositions. Another standardised container is not yet developed and the pore water compositions in *Table 14-3* are therefore used for the description of the narrative.

## 14.4 Chemical evolution of the ILW disposal cell

### 14.4.1 Narrative

The chemical evolution of the disposal container would be the same as described in paragraph 14.2 until *Figure 14-10*. Eventually, there will be contact between pore water and the waste form. Also for encapsulated CSD-c, it is assumed that the mechanical strength of the concrete buffer has been reduced significantly by reaction with magnesium and bicarbonate from the evolved clay pore water. The pH of the concrete buffer drops eventually till the pH of clay pore water but it may take thousands

of years. The reduction in thickness by chemical corrosion of the overpack becomes sufficient to form fractures due to the lithostatic pressure load. These fractures will be along the length of the canisters since there is empty volume along the length, see *Figure 14-11*. There is electrochemical contact between the carbon steel overpack, stainless steel canister and Zircaloy hulls. The standard electrode potential of Zr is less than Fe, Cr and Ni i.e. Zircaloy hulls would be expected to corrode faster in electrochemical contact with carbon steel overpack and stainless steel canister. But the zirconium-oxide film that is formed during corrosion is less soluble than chromite and magnetite films of stainless steel and the carbon steel overpack. Not only for the neutron transparency (Hafnium-free) Zircaloy hulls are preferred over stainless steel hulls but also for the higher corrosion resistance in the water of a nuclear power plant where the hulls are electrochemically in contact with the stainless steel parts of the fuel assembly. The majority of the hydrogen gas generated during anaerobic corrosion of Zircaloy is not released and determination of the Zircaloy corrosion rate by hydrogen release would underestimate the corrosion rate. The corrosion rates of Zircaloy from measured adsorbed and released hydrogen are as low as corrosion rates determined from released non-radioactive nickel and chromium: below 1 nm per year. The smaller corrosion rates measured with zirconium are attributed to the small solubility product of zirconia [Necib, 2018]. The hydrogen generated during anaerobic corrosion of Zircaloy is picked-up for more than 90% in alkaline and pure water between 30°C and 50°C [Sakuragi, 2017] and this pick-up can be understood from thermodynamic considerations since hydride formation with Zr has been known for decades [Lacher, 1937]. The corrosion rate of Zircaloy has been measured to suddenly increase in CaCl<sub>2</sub> solutions with a higher concentration than 0.05 M caused by the formation of a ternary complex Ca<sub>3</sub>[Zr(OH)<sub>6</sub>]<sup>4+</sup> [Gras, 2014]. The calcium concentration of concrete pore water is smaller than 0.02 M in *Table 14-3* and therefore no sudden increase in corrosion rate is expected. The thickness of PWR claddings is between 0.57 and 0.64 mm. Consequently, it may take at least 285.000 years for a Zircaloy cladding to be corroded. A distinction in the waste inventory for the OPERA Safety case has been made between neutron activated radionuclides and radionuclides as a result of contamination that are present on the surface [Verhoef, 2017/2016]. The release rate of neutron activated radionuclides is expected to be determined by the corrosion rate of Zircaloy and the release rate of radionuclides as a result of contamination are instantaneously released and diffuse into the evolved concrete buffer.

#### 14.4.2 Conceptual model

The potential release of radionuclides is assumed to take place after 1000, 35000 and 70000 years for OPERA(2011-2017). The cementitious materials have been assumed to be instantaneously dissolved after each period and radionuclides in these materials are assumed to diffuse directly into the host rock [Rosca-Bocancea & Schröder, 2017a/b]. Consequently, a chemical evolution has been excluded in this assessment. The parts of the disposal system for which chemical evolutions have been calculated are the same as for HLW i.e. described in paragraph 14.2.2.

The biggest uncertainty in the safety assessment is the representativeness of data and models e.g. instant release of all radionuclides i.e. neglecting the corrosion resistance of Zircaloy.

#### 14.4.3 Mathematical model

The parts of the disposal system for which chemical evolutions have been calculated are the same as for HLW i.e. described in paragraph 14.2.3.

## 15. Romania

Crina Bucur from the Institute for Nuclear Research Pitesti has been asked to complete a template. This completion can be viewed in Appendix B.

Romania investigates disposal of spent fuel since reprocessing of spent fuel is not considered, vitrified HLW is not to be disposed in Romania. Not-site specific safety assessments for the disposal of CANDU spent fuel have been made for a disposal facility hosted in granite as well as clay.

Spent ion exchange resins immobilised in a cementitious matrix is the main type of Intermediate Level Waste to be disposed in a geological formation. There is not yet a handling of the chemical evolution for ILW in the Romanian programme and no safety assessments have been made for disposal of ILW.

## 16. Slovenia

The Slovenian organisation participating in ACED is ZAG. Bojan Zajec prepared together with the Slovenian WMO ARAO the completion of a template for the kick-off meeting held in July 2019 that can be found in Appendix C.

The nuclear power of the plant in Slovenia in Krško is shared with Croatia. The spent fuel is currently stored in a spent fuel pond and there are no plans for reprocessing this waste i.e. vitrified HLW is not expected to be disposed in Slovenia. The KBS-3 concept from Sweden and Finland and other disposal concepts are considered for disposal of spent fuel.

Since 2009, a site for disposal of LILW has been chosen [Viršek, 2011] and the disposal facility, a silo, is being constructed. The silo will be constructed below the groundwater level in low permeable strata at a depth of approximately 15 metre below the surface. Nearly the entire field is covered with gravels. At the location the thickness of this gravel deposit is around 10 m. Groundwater is at a depth of around 5 metre below the surface.

For the primary lining with a thickness of 1.2 metres, reinforced concrete with limestone aggregates and passive soil bolts will be used. For the secondary lining, reinforced concrete with a thickness of 1 m will be used. There will be polyethylene high-density (PEHD) foil between the linings. The waste packages are reinforced concrete containers with an envisaged lifetime of 300 years. The metallic waste within these concrete containers is a mortar with limestone aggregates. When silo will be full, it will be backfilled with a cementitious material covered with a concrete slab and on top of it the clay layer in thickness of approximately 5 m will be built in. All these layers will reduce the water inflow in the silo and will prevent the contamination spreading in the surrounding. The preferential flow of water will be above the silo due to gravel layer.

## 17. Spain

ENRESA - Enrique García

UDC - Javier Samper, Luis Montenegro and Alba Mon

The geological formations considered in the Spanish programme for geological disposal of radioactive waste include granite and clay. Radioactive waste is intended for disposal after an interim storage period. An interim surface storage facility was proposed in Villar de Cañas, but the Project is now stopped.

### 17.1 Characterization of the HLW disposal cell in granite

#### 17.1.1 Description of materials in disposal cell

The materials used in the disposal cell of the Spanish reference concept in granite, named ENRESA 2000 (ENRESA, 2001), are the spent fuel, the carbon steel and the bentonite. The reference system is based in the disposal of spent fuel in carbon steel canisters in long horizontal disposal drifts. Canisters are surrounded by high-density bentonite. Access is accomplished by means of "main drifts" which run perpendicular to the disposal drifts. The main drifts meet at a central area, which includes the required underground infrastructure. Communications between the surface and the central underground area are accomplished by way of 3 access shafts and a ramp. *Figure 17-1* shows an scheme of the underground infrastructure in the Spanish repository concept in granite.

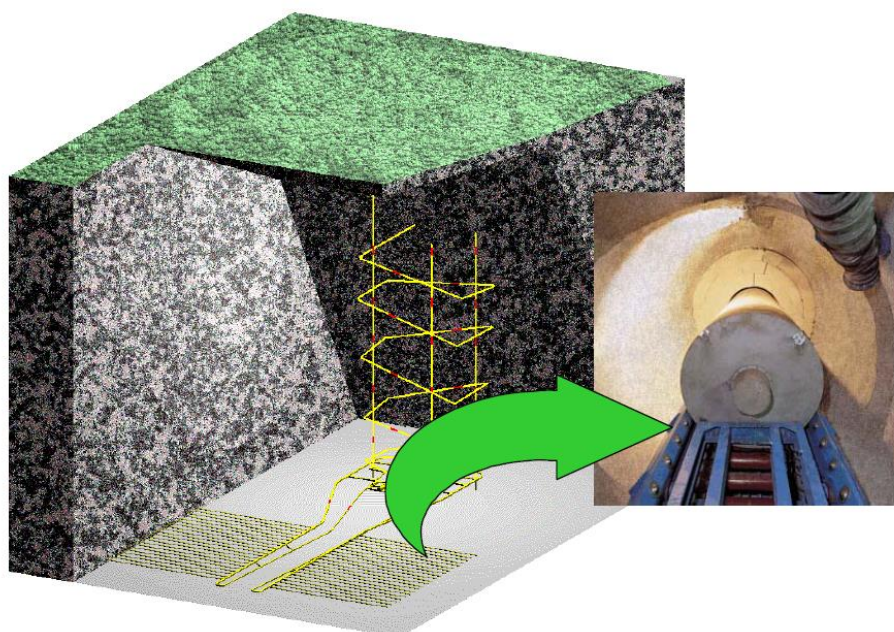


*Figure 17-1: Underground installations in the Spanish repository concept in granite (ENRESA, 2001).*

The canister measures 4.54 m in length and 0.90 m in diameter, and contains 4 PWR or 12 BWR fuel elements in a subcritical configuration. The thickness of the wall of the canister is 0.10 m at the cylindrical shield and 0.12 m at the ends, and is capable of withstanding the pressures to which it is subjected under disposal conditions and of providing a minimum period of containment of one thousand years. After being unloaded from the reactor, the fuel elements are temporarily stored for their thermal power

to decay to a level at which they may be disposed of with a total thermal power of 1,220 W per canister. A total 3,600 canisters will be required for the final waste inventory of spent fuel estimated for the Spanish nuclear power programme.

Canisters are disposed in cylindrical disposal cells, constructed with blocks of precompacted bentonite of 1,700 kg/m<sup>3</sup> dry density (in order to achieve a final dry density of 1,600 kg/m<sup>3</sup>). The blocks are initially non-saturated (degree of saturation of 66% and water content of 14%). The disposal drifts of 500 m in length and 2.4 m in diameter (Figure 17-2) are located at a depth of 500 m in the granitic host formation. Separations of 2.0 m between canisters and 35 m between disposal drifts have been established, in order not to exceed a temperature of 100 °C in the bentonite. The detailed dimensions of an individual “cell” are shown in Figure 17-3.

**DISPOSAL CONCEPT**

- Deep disposal
- Crystalline rock
- Spent fuel
- Carbon steel canister
- Horizontal emplacement
- Bentonite buffer

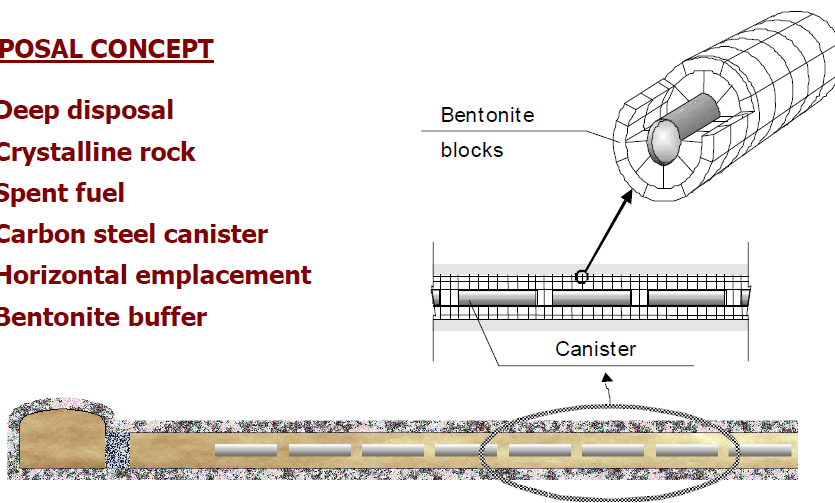


Figure 17-2: Longitudinal section of a disposal drift in the Spanish repository concept in granite (ENRESA, 2001).

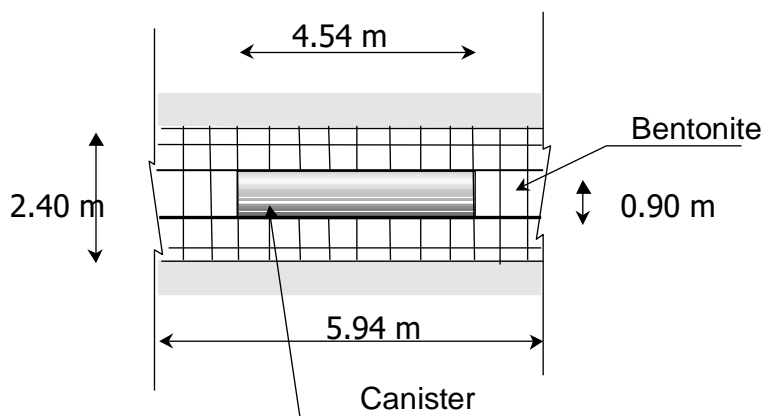


Figure 17-3: Dimensions of an individual disposal cell in the Spanish repository concept in granite (ENRESA, 2001).

Once a disposal drift is completed, it is sealed with a 6 m long seal made of bentonite blocks and closed with a concrete plug at its entry. After completion of all the disposal drifts, main drifts, ramp, shafts and

other remaining rock cavities will be backfilled with a mixture of bentonite and natural sand or an appropriate crushed material. The backfilling material will consist of 10 % bentonite (increasing up to 20 % at the top of the drifts) and suitably graded sand.

ENRESA's disposal facility is supposed to be located at a site, defined on the basis of the known characteristics of Spanish granites, which is called "generic site". The outcropping granitic formations studied in Spain present suitable dimensions to accommodate a geological repository, characterised by low permeability, low fracture density, tectonic stability and low seismicity (ENRESA, (2001)).

The materials used in the disposal cell of the Spanish reference concept in granite, have to satisfy different safety functions and safety requirements. In this section the main requirements of the waste package, which refers to the canister and its content (the waste form and the canister cavity materials), and the bentonite buffer are discussed.

The spent fuel is assumed to retain the radionuclides, which are only released at the pace the different parts that make up the fuel assemblies degrade. The only safety requirement relative to the different spent fuel parts is their own rate of degradation, which is assessed separately for the metallic parts and for the uranium oxide matrix. Degradation only starts once the absolute containment provided by the container is lost.

Canister cavity, which encompasses the materials interposed between the wastes and the canister wall, is not properly a barrier, as its constituents are not intended to perform barrier functions by themselves. The only requirement applicable is that the materials present in that space do not affect adversely to the contiguous barriers.

The main safety function of the canister is to provide absolute containment of the waste during the operational phase and until the thermal transient fades away (about 1000 years after emplacement) so that the temperature in the near field is low (about 80°C and below), which reduces the uncertainties affecting radionuclide transport (especially solubility limits and sorption coefficients). The selection of carbon steel is justified by the predictability of the behaviour of this material in the repository environment (low susceptibility to localised corrosion) and by the reliability of the product (large experience in fabrication and testing methods). The canister is designed to support the acting mechanical loads in both the operational phase and the post closure phase. Lifetime assessments quantify the corrosion rates of the canister materials due to the different plausible degradation mechanisms. Design margins and conservatism result in an expected lifetime between several ten thousand years and a few hundred thousand years.

The bentonite buffer is required to perform a large diversity of safety functions, which can only be fulfilled once the bentonite saturates and swells, closing tightly the construction gaps between the construction blocks and the drift wall or the canister wall on the one hand and between the blocks themselves on the other. The gaps will close quickly upon contact with groundwater; in the case of the outer gaps, this will happen shortly (weeks or months) after buffer emplacement, creating a continuous barrier well before the whole mass of the buffer is fully saturated. The long-term safety functions of the bentonite buffer are the following:

1. It isolates the waste package from the geosphere. Groundwater, and the solutes it contains, have to diffuse through the bentonite pores in order to gain access to the canister and, after the failure of the latter, to the canister cavity, delaying and slowing down harmful chemical reactions (including the inhibition of microbial activity) with waste packages materials. All the same, the products of these reactions are not actively removed, reducing the rates at which they proceed. On the other hand, reactions at the buffer material have not to provide itself a supply of reactants that could cause unacceptable degradation to the waste package. This isolation function is important in relation to the lifetime of the canister, the degradation of the waste form, and the precipitation of many radionuclides within the EBS.
2. The buffer is a containment barrier by itself, as it retains radionuclides on the base of its properties: (1) low hydraulic conductivity, which makes radionuclide advection negligible, (2) sorption of many radioelements, especially with actinides; and (3) filtration of colloids

- and large complex molecules, and inhibition of microbial life, because of the small size of the pores (and for the latter also the low water activity).
3. The bentonite isolates mechanically the canister from limited shear displacements in the disposal drift walls.
  4. The bentonite buffer has to avoid the build up of excessive gas pressure in the near field, without undue impairment of the safety functions.
  5. The bentonite has to be able to transfer radiogenic heat from the waste package to the host rock, avoiding excessive temperatures.

The most important safety function of the near field host rock is the isolation of the EBS. An important safety requirement is that the degradation of the rock properties in the EDZ (fracturation, hydraulic conductivity) is not so large as to impair the performance and properties of the buffer. One relevant parameter in the EDZ is groundwater flow. The reference concept contributes to limit the importance of the EDZ by: selecting a favourable excavation method and choosing a favourable rock cavity shape and size. A criterion considered in the design of the Spanish repository is that the minimum distance from a canister to any major fracture zone or section of rock with high hydraulic conductivity (respect distance) is 100 m.

The isolation function of the near field host rock is part of the larger isolation function that the geosphere as a whole plays within the multibarrier disposal system, which has been referred to above. In this context, retention of radionuclides in the EDZ is not important for repository safety as this compartment represents a small fraction of the geosphere. Nevertheless, it may be useful in showing the robustness of the system, by reducing the releases from the near field further to the engineered barriers.

Geothermal gradient imposes the base temperature of the rock at the repository level. The Spanish generic site considers a geothermal gradient of 35 °C per kilometre and a mean surface temperature of 13 °C, leading to a background temperature at the repository level of 30.5 °C.

## 17.1.2 Thermal and hydraulic gradients

### 17.1.2.1 Conceptual model

The main THM processes which affect the bentonite buffer in a HLW repository are:

1. Bentonite saturation and swelling. The sounding groundwater will slowly saturate the bentonite buffer, bentonite will swell and fill the gaps among the bentonite blocks, bentonite/rock interface and bentonite/canister interface.
2. Early cementation. Vapor generation and bentonite drying can be produced in the bentonite near the heat source, as a consequence mineral phases can precipitate. The cementation can cause bentonite swelling and fragility in a few centimeters near the heat source.
3. Mechanical interactions.
  - a. Bentonite buffer thickness can be reduced due to the consolidation of the canister.
  - b. Swelling of the corrosion products generated by the canister corrosion can be absorb by the bentonite.
  - c. Increasing of the bentonite pressure due to the thermal expansion can be countered by the water flow from the granite.
  - d. Gas generated by the canister corrosion can affect the stability of the bentonite barrier
1. The THM analysis performed in ENRESA (2001) has taken into account the following processes:
  1. Thermal transport by conduction, convection and phase change.
  2. Liquid water flow and water vapor diffusion.
  3. Thermal expansion, bentonite behaviour in function of the stresses, suction and temperarute and linear elastic granite behaviour.

### 17.1.2.2 Mathematical model

The THM early evolution of the bentonite buffer and the surrounding near field granitic rock was analyzed with CODE\_BRIGHT (Olivella et al., 1996). The numerical model was performed by the “Departamento de Ingeniería del Terreno de la Escuela Técnica Superior de Ingenieros de Caminos Canales y Puertos de la Universidad Politécnica de Cataluña (UPC)” and implemented with the code CODE\_BRIGHT (Olivella et al., 1996). The mathematical equations include the equilibrium equation, the mass balance and the energy balance.

The mechanical equilibrium equations are given by:

$$\nabla \cdot \sigma + b = 0$$

where  $\sigma$  are the tensions and  $b$  are the mass forces.

The water mass balance is the following:

$$\frac{\partial}{\partial t} (\theta_l^w S_l \phi + \theta_g^w S_g \phi) + \nabla \cdot (j_l^w + j_g^w) = f^w$$

where  $\theta_l^w$ ,  $\theta_g^w$ ,  $S_l$ ,  $S_g$ ,  $\phi$ ,  $j_l^w$ ,  $j_g^w$  and  $f^w$  are the water content of the liquid phase, the water content of the gaseous phase, liquid saturation degree, gas saturation degree, porosity, water flux in the liquid phase, water flux in gaseous phase and external water flow, respectively.

The thermal balance can be expressed as the following:

$$\frac{\partial}{\partial t} (E_s \rho_s (1 - \phi) + E_l \rho_l S_l \phi + E_g \rho_g S_g \phi) + \nabla \cdot (i_c + j_{Es} j_{El} j_{Eg}) = f^Q$$

where  $E_s$ ,  $E_l$ ,  $E_g$ ,  $\rho_s$ ,  $\rho_l$ ,  $\rho_g$ ,  $i_c$ ,  $j_{Es}$ ,  $j_{El}$ ,  $j_{Eg}$  and  $f^Q$  are the specific energy of the soil phase, the specific energy of the liquid phase, specific energy of the gaseous phase, solid density, liquid density, gas density, conduction thermal flux, solid energy flux, liquid energy flux, gas energy flux and external thermal flux, respectively.

The solid mass balance is the following equation:

$$\frac{\partial}{\partial t} (\theta_s (1 - \phi)) + \nabla j_s = 0$$

where  $\theta_s$  and  $j_s$  are the solid mass content and the solid flux, respectively.

### 17.1.2.3 Dimensions, initial and boundary conditions of the THM numerical model

The steel canister has a inner diameter equal to 0.9 m and 4.54 m long. The thickness of the canister wall, cap and base are equal to 0.10 m, 0.12 m and 0.12 m, respectively. The finite element mesh domain extend 17.5 m width and 1000 m length representing a section along the depth of the middle of the canister (ENRESA, 2000). The finite element mesh has 1308 nodes and 1140 elements. *Figure 17-4* shows the element mesh used for the THM numerical model. The simulation was extend to 40,000 years to obtain the thermal evolution.

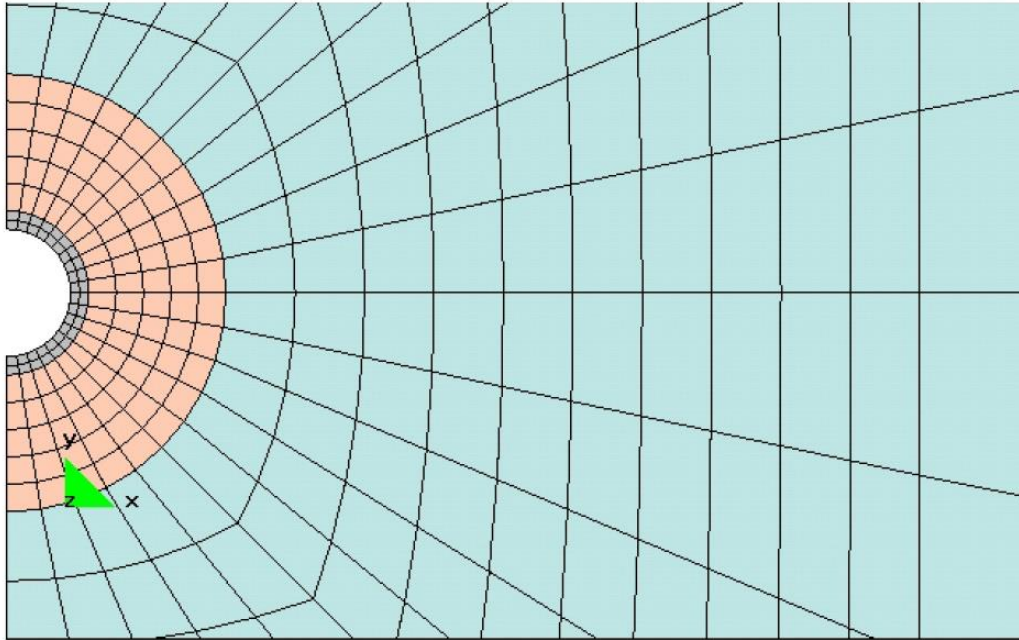


Figure 17-4: Finite element mesh used in the THM numerical model (ENRESA, 2001).

The model assumes that the fuel cooling before the emplacement is equal to 50 years. The thermal power of the fuel when it is placed at the repository is equal to 305.4W.

The initial conditions of the bentonite and granite are the following:

1. Saturation degree of the bentonite is equal to 66 %.
2. Suction pressure of the bentonite is equal to 44.41 MPa.
3. Porosity of the bentonite is equal to 0.407 and equal to 0.01 for the granite.
4. Temperature is equal to 30.5 °C at the depth of the repository and equal to 13 °C at the surface.
5. Hydrostatic tension of the bentonite is equal to 0.24 Mpa.
6. Granitic homogenous medium.

17.1.2.4 TH model parameters

The specific bentonite properties for the THM analysis are listed in Table 1.

Table 17-1: Bentonite parameters used in the THM numerical model (ENRESA, 2001)

Properties	Parameter	Unit	Value
Thermal conductivity $\lambda = \lambda_s S_i \lambda_d^{(1-S_i)}$	$\lambda_s$	W/mK	1.28
	$\lambda_d$	W/mK	0.5
Solid density	$\rho$	kg/m <sup>3</sup>	2630
Specific heat	$c_p$	J/kg°C	1000
Intrinsic permeability $k = k_0 \frac{\phi^3}{(1-\phi)^2} \frac{(1-\phi_0)^2}{\phi_0^3}$	$k_0$	m <sup>2</sup>	6·10 <sup>-21</sup>
	$\phi_0$	-	0.407
Relative permeability $k_{rl} = A S_e^\lambda$	A	-	1
	$\lambda$	-	3
Retention curve $S_i = \left[ 1 + \left( \frac{S}{P} \right)^{\frac{1}{1-\lambda}} \right]^{-\lambda} \quad P = P_0 \frac{\sigma}{\sigma_0}$	$P_0$	MPa	30
	$\sigma_0$	N/m	0.072
	$\lambda$	-	0.39
Diffusive flux $D_m^w = \tau D \left[ \frac{(273,15 + T)^n}{P_g} \right]$	D	m <sup>2</sup> /s/k <sup>n</sup> P	5.9·10 <sup>-6</sup>
	n	-	2.6
	$\tau$	-	1
Plastic behaviour $f = f(\sigma, \epsilon_p, \Delta T)$ $F = \frac{3J^2}{g_s} - \epsilon_p (\rho + P_0) (P_0 - \rho) = 0$ $P_0 = P_0^c \left( \frac{P}{P^c} \right)^{\frac{\lambda(0) - \epsilon_p}{\lambda(0) - \epsilon_0}}$ $P_0^c = P_0^c + 2(\alpha_1 \Delta T + \alpha_2 \Delta T(T))$ $L_p = M/g_s (\theta = -\pi/6)$ $\lambda(s) = \lambda(0)[(1-r)\exp(-\beta s) + r]$ $P_s = k \exp(-\rho \Delta T) s; P_0^c = \frac{1 + e}{\lambda(0) - k_{so}} P_0^c \dot{\epsilon}_p^c$ $G = \frac{3J^2}{g_s} - \alpha \epsilon_p (\rho + P_0) (P_0 - \rho)$ $L_p = M/g_s (\theta = -\pi/6)$	$\lambda(0)$	-	1.5
	r	-	0.75
	$\beta$	MPa <sup>-1</sup>	0.05
	$\rho$	°C <sup>-1</sup>	0.2
	K	-	0.1
	$P^c$	MPa	0.1
	M	-	1.5
	$\alpha$	-	0.395
	$P_0^*$	MPa	8
	Elastic behaviour $\dot{\epsilon}_v^e = \frac{k_j}{1+e} \frac{\dot{P}}{P} + \frac{k_s}{1+e} \frac{\dot{s}}{s+0,1} + (\alpha_0 + 2\alpha_2 \Delta T) \dot{T}$ $k_j = k_{j0} (1 + \alpha_j s)$ $k_s = k_{s0} \left( 1 + \alpha_{sp} \ln \frac{P}{P_r} \right) \exp(\alpha_{ss} s)$ $\dot{\epsilon} = \dot{J}/G; G = E/2(1+\nu)$	$k_{jo}$	-
$k_{so}$		-	0.25
$\nu$		-	0.4
$\alpha_{ss}$		MPa <sup>-1</sup>	0
$\alpha_i$		MPa <sup>-1</sup>	-0.003
$\alpha_{sp}$		-	-0.1609
$P_r$		-	0.01
$\alpha_0$		°C <sup>-1</sup>	1.5·10 <sup>-4</sup>
$\alpha_2$		°C <sup>-1</sup>	0

17.1.2.5 Calculated liquid saturation, porosity, stress and gas saturation time evolution

The time required for the full saturation is 16.4 years (*Figure 17-5*). Near the canister, the bentonite undergoes a drying process due to the sudden increase in temperature. This part of the bentonite reduces the degree of saturation to 0.503 in the first year and thereafter begins to resaturate, reaching full saturation at 16.4 years. By contrast, in the part of the bentonite in contact with the granite the saturation process is progressive, quickly saturating at 2.7 years by the constant supply of water from the granite. A midpoint of bentonite needed 4.6 years to complete saturation.

The results of porosity show that the outer part of the bentonite in contact with the granite swells due to water supply and that the inside near the heat source contracts because of heating. In the stresses that are obtained from the calculations is generally observed a monotonous behavior, except in the instant it reaches saturation in the inner face of the bentonite closest to the heat source. This discontinuity could be due to the coupling between the two behaviors before and after saturation of the bentonite material, and that its effects are reflected throughout the system. The effective stresses after the process of saturation in the bentonite are the order of 5 MPa which corresponds to the value of the swelling pressure of bentonite.

Anaerobic corrosion of various metals in the near field, primarily carbon steel of the canister, results in the formation of hydrogen gas. Other processes such as bacterial activity, radiolysis of water or gas generation by decay of radionuclides within the fuel lead to the formation of hydrogen and other gases, but in amounts that are an order of magnitude lower than the first mentioned process. The presence of hydrogen in the bentonite in significant quantities begins at the moment there is contact of the bentonite pore water with the canister. This actually occurs before the complete saturation of the bentonite. Once corrosion starts hydrogen migrates through the pores of bentonite or through any path accessible through the following mechanisms:

1. Transport by diffusion of gas dissolved in the water in the pores or fractures in the clay barrier.
2. Transport by advection of gas dissolved in the water in the pores or fractures of the bentonite.
3. Transport of gas by forming a free gas phase in biphasic or multiphase flow.

The hypothesis are: first, the air initially contained in the bentonite at the time of emplacement has been associated with hydrogen (to avoid introducing an additional component in the equations) and on the other hand, a constant hydrogen generation rate of 5 mol/year/canister from time zero is assumed. The degree of gas saturation in the bentonite (*Figure 5*), diminishes in most of the bentonite from 40% initially to values that can be considered zero in the early years due to the advance of the water saturation front that expells and compresses the air in the barrier. In the area next to the canister, however, the degree of gas saturation in the first phase increases due to two processes: one is the area of the system in contact with the surface where the gas is being generated and the region away from the water front. On the other hand, heat produces a drying of bentonite increasing the proportion of air over the water. Later, as the water front penetrates in the bentonite, the air is compressed but only to levels of saturation of 2 ‰, the instant when the gas pressure is the same order as the water pressure and the two phases coexist (about 6 MPa). After reaching water saturation and as the corrosion of the canister progresses, hydrogen flows through the connected porosity of the bentonite, expelling a small portion of water (4 ‰ on average). This process of partial hydraulic desaturation takes place from the 30 years after emplacement in the middle of the bentonite. The gas saturation level is higher near the canister (7 ‰) and lowest in the proximity of the granite (0.7 ‰).

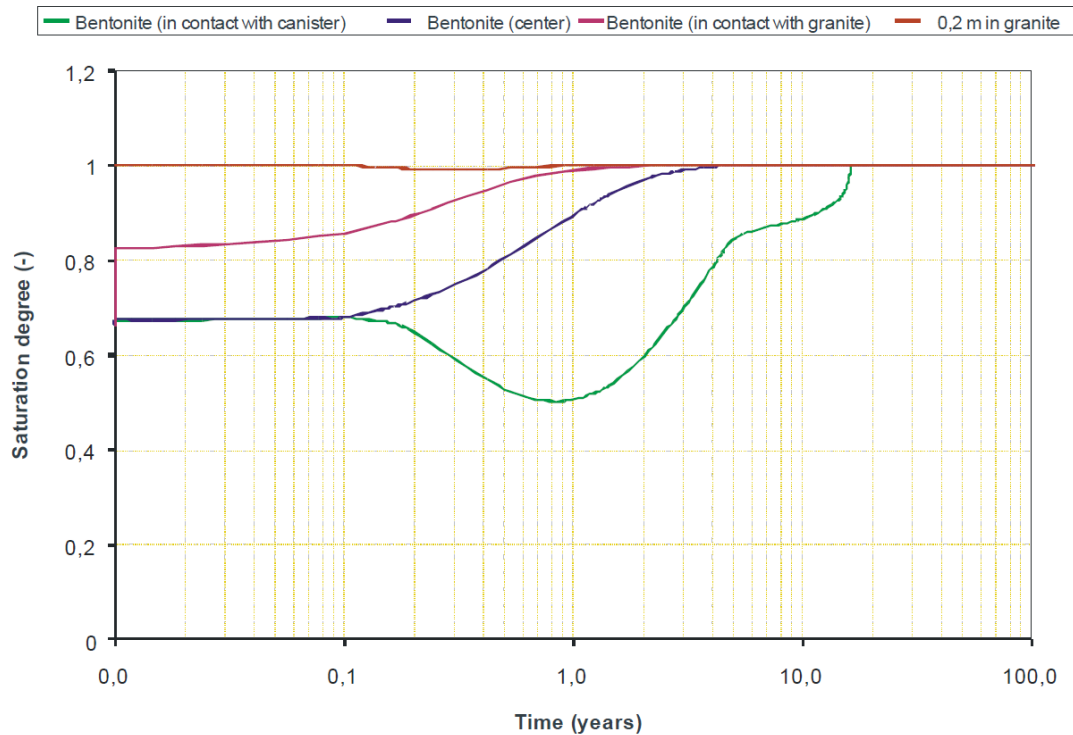


Figure 17-5: Calculated saturation degree time evolution in the Spanish repository concept in granite (ENRESA, 2001).

#### 17.1.2.6 Calculated temperature time evolution

For the configuration of disposal galleries and canisters taken at the reference repository, the maximum temperature does not exceed 100 °C at any time. The maximum temperature (about 97 °C) is reached at the contact with the canister after about 24 years of disposal. Figure 17-6 shows the calculated temperature time evolution at the canister-bentonite interface, in the center of the bentonite, at the bentonite-granite interface and in the granite. These computed results are used in the geochemical evolution model of the Spanish reference concept in granite.

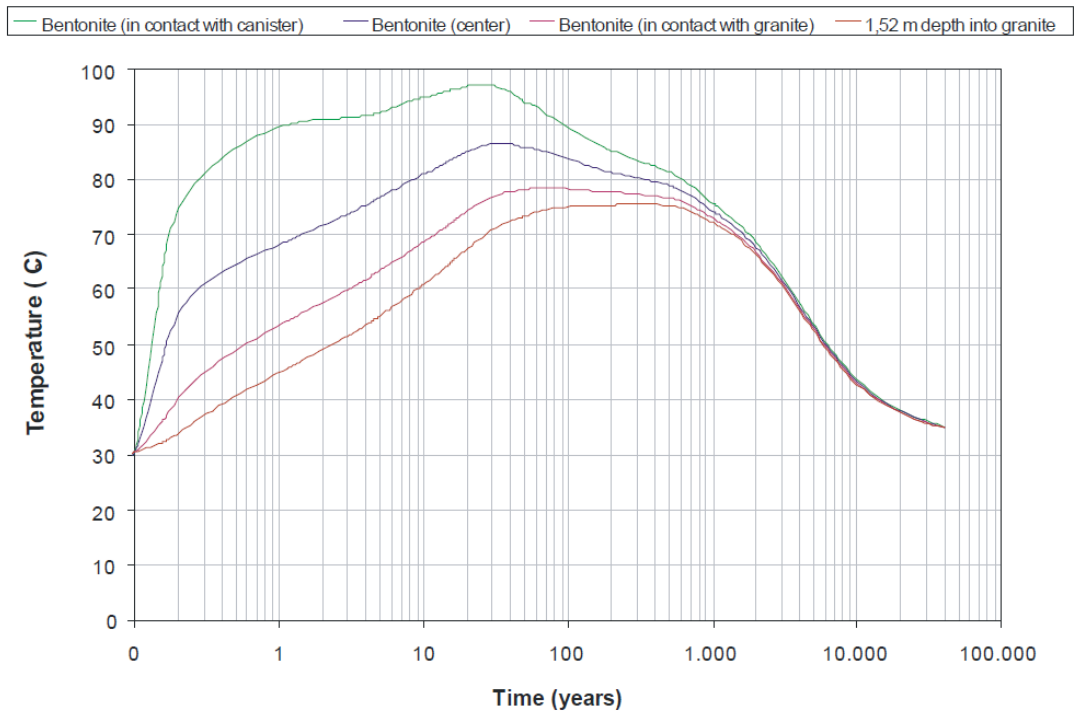


Figure 17-6: Calculated temperature time evolution in the Spanish repository concept in granite (ENRESA, 2001).

Table 17-2: Description of parameters for thermal gradients

Feature	Examples of parameter	Value and unit	Source	Justification / comments
Heat source	Thermal power as a function of time	305.4 W	ENRESA 2001	
Carbon steel canister	thermal conductivity	60 W/m°C	ENRESA 2001	
	specific density	7.850 kg/m <sup>3</sup>	ENRESA 2001	
	specific heat capacity	403.1 J/kg °C	ENRESA 2001	
Bentonite backfill	thermal conductivity	1.28 W/m°C	ENRESA 2001	Dry thermal conductivity equal to 0.5 W/m°C
	specific density	2630 kg/m <sup>3</sup>	ENRESA 2001	
	specific heat capacity	1000 J/kg °C	ENRESA 2001	
Host rock: granite	thermal conductivity	3.65 W/m°C	ENRESA 2001	
	specific density	2630 kg/m <sup>3</sup>	ENRESA 2001	
	specific heat capacity	757.4 J/kg°C	ENRESA 2001	
	temperature	30°C	ENRESA 2001	30°C at the depth of the repository and 13°C at the surface

### 17.1.3 Pore water compositions

The chemical composition of the bentonite porewater in the EBS at the time of the emplacement of the barrier and the granite hydration water are shown in *Table 17-3*. The initial accessory mineral volume fraction considered in the bentonite is presented in *Table 17-4*. The initial value of the cation exchange capacity (CEC) in the bentonite is 101.5 meq/100g.

*Table 17-3: Initial chemical composition of the bentonite porewater and the granite hydration water (ENRESA, 2001).*

Components	Bentonite	Granite
pH	7.75	7.9
pE	12.85	-2.907
HCO <sub>3</sub> <sup>-</sup>	4,361·10 <sup>-4</sup> M	5,048·10 <sup>-3</sup> M
Cl <sup>-</sup>	1,599·10 <sup>-1</sup> M	3,949·10 <sup>-4</sup> M
SO <sub>4</sub> <sup>2-</sup>	3,659·10 <sup>-2</sup> M	1,561·10 <sup>-5</sup> M
Ca <sup>2+</sup>	2,078·10 <sup>-2</sup> M	1,522·10 <sup>-4</sup> M
Mg <sup>2+</sup>	2,230·10 <sup>-2</sup> M	1,604·10 <sup>-4</sup> M
Na <sup>+</sup>	1,455·10 <sup>-1</sup> M	4,350·10 <sup>-3</sup> M
K <sup>+</sup>	1,253·10 <sup>-3</sup> M	5,371·10 <sup>-5</sup> M
Fe <sup>2+</sup>	1,612·10 <sup>-6</sup> M	8,953·10 <sup>-4</sup> M
SiO <sub>2</sub> (aq)	2,646·10 <sup>-4</sup> M	3,761·10 <sup>-4</sup> M

*Table 17-4: Initial mineral volume fraction in the bentonite (ENRESA, 2001)*

Minerals	Content
Quartz	2%
Calcite/Dolomite	0,6%
Gypsum	0,14%
Pyrite	0,02%

## 17.2 Chemical evolution of the HLW disposal cell

### 17.2.1 Narrative

The chemical evolution of the Spanish reference concept in granite was performed with the reactive transport code CORE-LE (Samper et al., 1998). Calculations were focused on the time evolution and the spatial distribution of pH, Eh and the main cations and anions presented in the bentonite porewater and granite water. The conceptual geochemical model includes the following reactions: 1) Aqueous complexation; 2) Acid/base; 3) Redox; 4) Mineral dissolution/precipitation; and 5) Cation exchange of Ca<sup>2+</sup>, Mg<sup>2+</sup>, Na<sup>+</sup> and K<sup>+</sup>. All the reactions were assumed at chemical equilibrium.

The geochemical model was run for two stages, from initial time to the time that the bentonite is saturated and then to 1 Ma. For the first stage (saturation of bentonite), the model only accounts for two material

zones: the bentonite buffer and the granite. The pore fluid from the host rock (granite formation) is taken as boundary water and infiltrates into the bentonite. Then the results of the first stage are taken as initial conditions for the model of the second stage. In the second stage (geochemical evolution after saturation of bentonite), the EDZ and the canister are included in the model domain. This is reasonable because the time to saturate the bentonite (about 20 years) is very short compared to the total simulation time of 1 Ma. It is noted that after bentonite is saturated, solute transport is mainly controlled by diffusion and geochemical reactions. The geochemical evolution after saturation of bentonite can be considered in two periods: 1) The thermal period (100 to 10,000 years), in which canisters are expected to be unbreached; and 2) The “steady-state” period (after 10,000 years), after which the temperature is almost uniform in the repository and is approaching the ambient rock temperature.

### 17.2.2 Conceptual model

The conceptual model of the saturation of bentonite considers only two materials, the bentonite and the granite. The model domain was discretized using a 1-D axisymmetric mesh which has 302 triangular elements (only 2 in the granite) and 304 nodes. Figure 7 shows the geometry and the mesh used in the first stage of the chemical evolution of the Spanish reference concept in granite. The numerical model simulates only the first 100 years.

The thermo-hydro-chemical initial conditions at this first stage are: 1) The initial temperature is the background temperature at the repository level of 30.5 °C; 2) The initial flow condition is calculated with the bentonite initial saturation degree and its suction pressure ( $\Psi=18,5$  MPa); 3) The initial chemical composition in all bentonite nodes is fixed with the bentonite porewater at a water content of 14% (Table 17-3); 4) The initial chemical composition in all granite nodes is fixed with the hydration water in the granite (Table 17-3); and 5) The initial volume fraction of the accessory minerals (Table 3) and initial exchangeable cations composition are fixed only in the bentonite nodes.

The THC boundary conditions at the first stage are: 1) The liquid pressure at the outer boundary ( $r = 1.95$  m) was equal to 5 MPa; 2) A Neuman transport boundary condition was used for solute transport according to which solute flux is equal to the product of water flux times solute concentration of inflow granitic water; and 3) The temperature boundary condition is the calculated temperature in the THM model (Figure 17-6). Figure 8 shows the time evolution of these calculated temperatures at different distances from the central axis of the canister in the THM model (continuous lines) and the used time function in the THC model to reproduce the calculated temperatures (discontinuous lines).

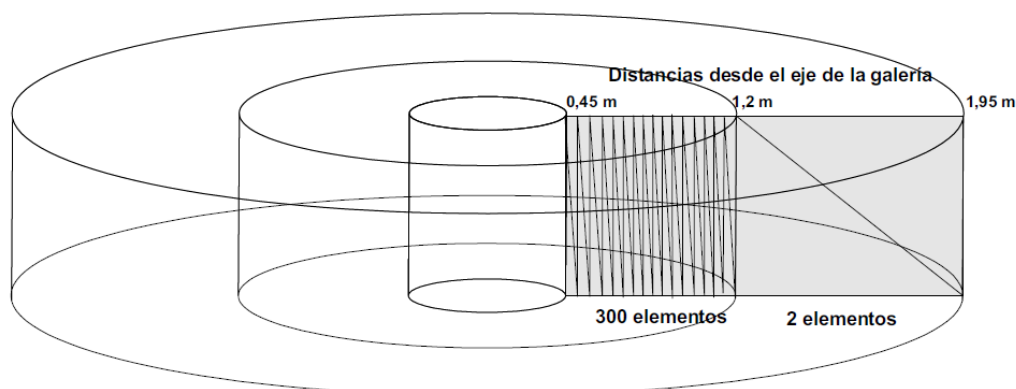


Figure 17-7: Geometry and 1-D axisymmetric mesh used in the first stage of the geochemical model (ENRESA, 2001).

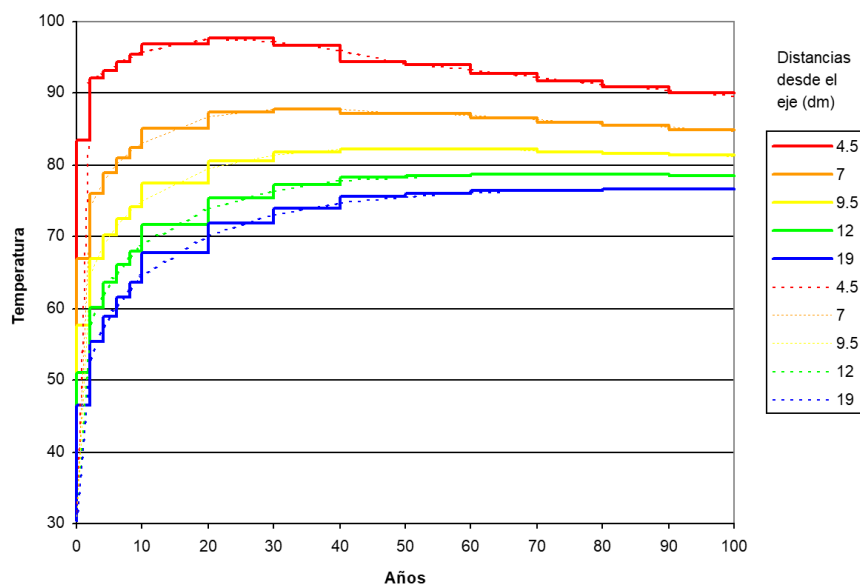


Figure 17-8: Temperature boundary conditions at the first stage of the geochemical model (ENRESA, 2001).

The conceptual model of the geochemical evolution after saturation of bentonite consider four materials: the canister, the bentonite, the EDZ and the granite. The model domain was discretized using a 1-D axisymmetric mesh which has 240 triangular elements (2 in the canister, 136 in the bentonite, 4 in the EDZ and 98 in the granite) and 242 nodes. The mesh discretization is non-uniform,

being more refined near the canister-bentonite interface. Figure 9 shows the geometry and the mesh used in the second stage of the chemical evolution of the Spanish reference concept in granite. Simulations were run for over 1 Ma.

The thermo-hydro-chemical initial conditions at this second stage are: 1) The initial temperature is the calculated temperature at the end of the first stage of the geochemical model; 2) A steady state flow regime was considered (1 L/year per canister); 3) The initial chemical composition in all bentonite nodes is fixed with the calculated chemical composition of the bentonite porewater after saturation (Table 4); 4) The initial chemical composition in all granite nodes is fixed with the hydration water in the granite (Table 2); 5) The initial volume fraction of the accessory minerals (Table 3) and initial exchangeable cations composition are fixed only in the bentonite nodes; and 6) An initial volume fraction of magnetite in the canister nodes as a final product of the canister corrosion.

The mesh was extended to 172 m in order to avoid the influence of the solute boundary conditions in the geochemical processes in the bentonite. The temperature boundary condition is the calculated temperature in the THM model (Figure 17-6). Figure 17-10 shows the time evolution of these calculated temperatures at different distances from the central axis of the canister in the THM model (continuous lines) and the used time function in the THC model to reproduce the calculated temperatures (discontinuous lines).

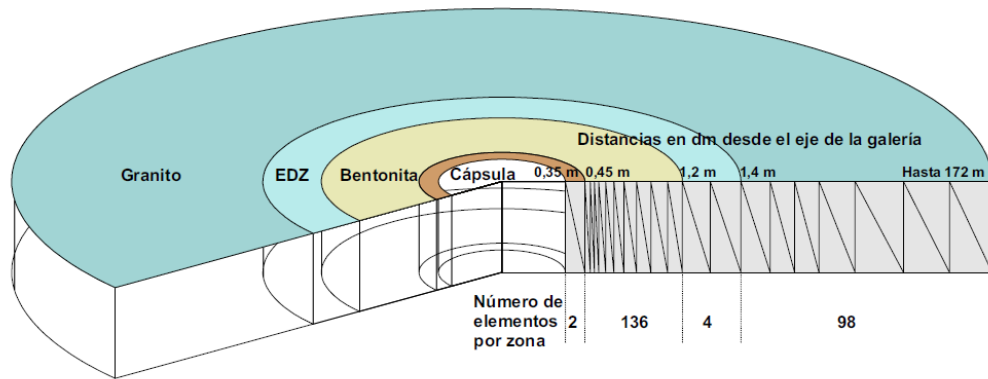


Figure 17-9: Geometry and 1-D axisymmetric mesh used in the second stage of the geochemical model (ENRESA, 2001).

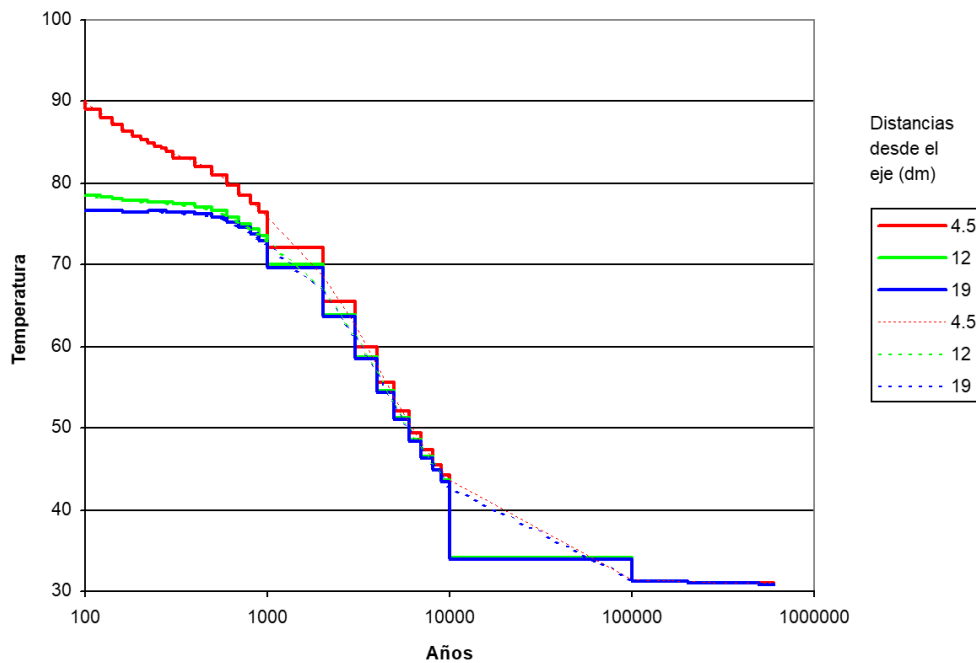


Figure 17-10: Temperature boundary conditions at the second stage of the geochemical model (ENRESA, 2001).

Table 17-5: Calculated chemical composition of the bentonite porewater after saturation (ENRESA, 2001).

Parámetro	Valor
pH	6,6
Eh	-2,79
pe	-0,197
Temperatura	83,07 °C

Especie	Concentración Molar
HCO <sub>3</sub> <sup>-</sup>	1,714E-03
Cl <sup>-</sup>	1,062E-01
SO <sub>4</sub> <sup>-2</sup>	2,094E-02
Ca <sup>+2</sup>	1,119E-02
Mg <sup>+2</sup>	1,607E-02
Na <sup>+</sup>	9,342E-02
K <sup>+</sup>	8,110E-04
Fe <sup>+2</sup>	6,583E-05
SiO <sub>2</sub> (aq)	9,913E-04

### 17.2.3 Mathematical model

The conceptual geochemical model considered in the Spanish reference concept in granite includes the following reactions assumed at chemical equilibrium: 1) Aqueous complexation; 2) Acid/base; 3) Redox; 4) Mineral dissolution/precipitation; and 5) Cation exchange of Ca<sup>2+</sup>, Mg<sup>2+</sup>, Na<sup>+</sup> and K<sup>+</sup>. The mathematical formulation of these chemical reactions is described in Appendix D.

### 17.2.4 Calculated results

During the bentonite buffer resaturation period (first stage of the geochemical model), advection from granite to bentonite is the relevant transport process. Dilution of the chemical concentration of bentonite porewater and mineral dissolution in bentonite are the two main processes produced by resaturation with granitic water. The maximum temperature at the middle point of the bentonite barrier has a value of 83 °C. The value of pH is 6.6 and Eh is -2.8 V. Chloride and sodium presents, respectively, the higher chemical concentration of anions and cations. In general, after a few years of resaturation, chemical changes in the bentonite barrier in terms of porewater, mineralogy and cation exchange complex are not very significant. Changes in porosity of the bentonite and the granite are extremely small.

The thermal period (second stage of the geochemical model from 100 to 10,000 years), in which canisters are expected to be unbreached, starts once bentonite becomes fully saturated. Then solutes diffuse from the bentonite into the granite because concentrations are much larger in bentonite than in granite for all solutes except bicarbonate and silica. As consequence of diffusion, the chemical concentration of sodium and potassium decrease in the bentonite porewater while calcium and magnesium suffer a slight increase in concentration (*Figure 17-11*). The behaviour of bivalent cations could be explained taking into account that calcium diffusion through granite causes calcite and anhydrite dissolution, and, therefore, an increase in the calcium chemical concentration in bentonite porewater. This affects the cation exchange complex because dissolved calcium enters into the

exchange complex and sodium, magnesium and potassium are released to the bentonite porewater. This combination of reactions leads to a slight increase in the concentrations of dissolved calcium and magnesium.

The concentration of chloride in the bentonite porewater decreases by diffusion through granite (Figure 17-12). Bicarbonate increases by diffusion from granite through bentonite and by the effect of calcite dissolution (Figure 17-12). Sulphate increases until 10.000 years by anhydrite dissolution (Figure 17-12). This effect is greater than diffusion through granite during the thermal period. The concentration of dissolved silica decreases in the bentonite porewater due to precipitation of silica solid phases due to the decrease of temperature. The concentration of dissolved iron decreases by diffusion through granite and magnetite precipitation during a period of time from 100 to 1.000 years. After that, from 1.000 to 10.000 years, iron concentration increases by dissolution of the precipitated magnetite and by the presence of canister corrosion products. Finally, pH increases during the thermal period due to the combined effect of decreasing of temperature and calcite dissolution (Figure 17-13). The value of pE presents the opposite behaviour than the pH (Figure 17-13). Its decreasing is caused by temperature and by magnetite dissolution and precipitation.

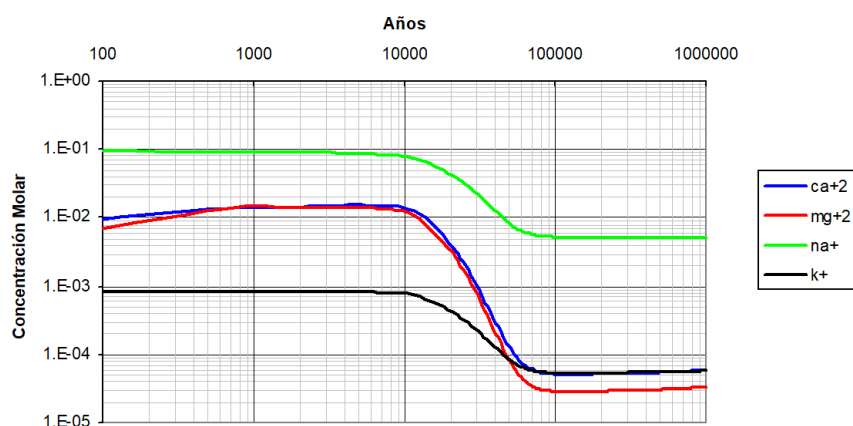


Figure 17-11: Time evolution of the calculated calcium, magnesium, sodium and potassium at the middle point in the bentonite (ENRESA, 2001).

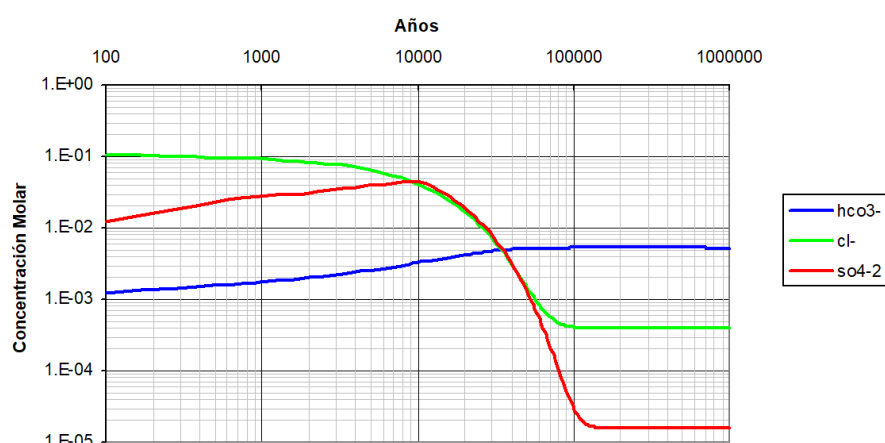


Figure 17-12: Time evolution of the calculated bicarbonate, chloride and sulphate at the middle point in the bentonite (ENRESA, 2001).

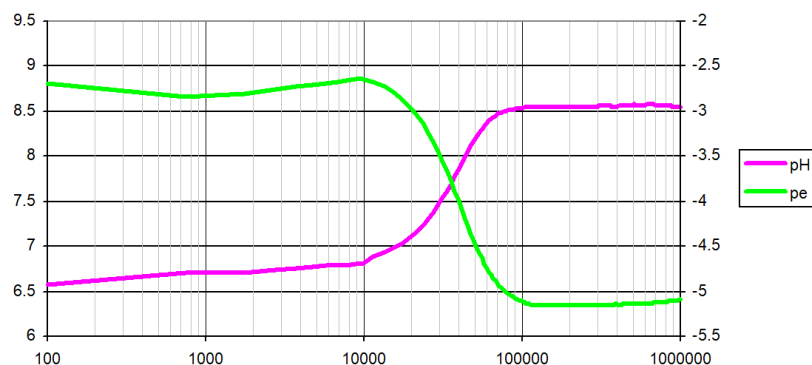


Figure 17-13: Time evolution of the calculated pH and pE at the middle point in the bentonite (ENRESA, 2001).

During the “steady-state” period (second stage of the geochemical model after 10.000 years), after which the temperature is almost uniform in the repository and is approaching the ambient rock temperature, the chemical concentration of sodium, potassium, calcium, magnesium, chloride and sulphate decrease in the bentonite porewater (Figure 17-11 and Figure 17-12). After 100.000 years they reach steady state values. Bicarbonate increases by diffusion from granite to bentonite and by the effect of calcite dissolution (Figure 17-12). Silica chemical concentration continues to decrease in the bentonite porewater by precipitation of its solid phase due to the decreasing of temperature. Iron chemical concentration decreases by diffusion through granite and magnetite precipitation during a period of time from 10.000 to 100.000 years. After 100.000 years, iron concentration increases slightly by decreasing of temperature. The value of pH increases during the “steady-state” period due to the combined effect of decreasing of temperature and calcite dissolution (Figure 17-13). The value of pE presents the opposite behaviour than the pH (Figure 17-13). Its decreasing is caused by temperature and by magnetite dissolution and precipitation. After 100.000 years, pH and pE do not modify almost their values.

#### 17.2.5 Recent updates of the predictions of the chemical evolution of the HLW cell in granite

The predictions of the chemical evolution performed for the ENRESA 2000 Performance Assessment Project have been updated more recently within the context of several EU Research Projects such as NFPRO, FUNMIG, FEBEX, PAMINA, and PEBS. This section presents a summary of the main results of these recent updates.

Samper et al. (2008) presented a 1-D and 2-D axisymmetric water flow and multicomponent reactive solute transport models to simulate canister corrosion, the interactions of corrosion products with bentonite and the long-term hydrochemical evolution of porewater composition in the near field of a repository in fractured granite. Numerical simulations were performed at a constant temperature of 25°C for 0.3 Ma. They used a conceptual and numerical model similar to that of ENRESA (2001). Coupled hydrogeochemical calculations of interactions of corrosion products with bentonite have been performed with CORE<sup>2D</sup>V4 (Samper et al., 2011). They found that: (1) Magnetite is the main corrosion product; (2) Fe diffusion from canister into bentonite leads to magnetite precipitation in the buffer; (3) Siderite precipitation is small due to limited carbonate availability; (4) Corrosion causes an increase of pH in bentonite; (5) Proton surface complexation is the main pH buffering mechanism. Other mechanisms such as Fe<sup>2+</sup> exchange and calcite and iron minerals dissolution/precipitation are much less effective;

and (6) Magnetite precipitation causes a reduction of porosity in bentonite. The largest change occurs at canister–bentonite interface. Corrosion products have a larger volume than carbon-steel, but not large enough to clog bentonite pores.

Lu et al. (2011) presented an updated version of the model of Samper et al. (2008) which considers 3 types of sorption sites in the bentonite, kinetically-controlled canister corrosion and magnetite precipitation, and the competition of  $\text{Ni}^{2+}$  for sorbing sites. Simulations were carried out with CORE<sup>2D</sup>V4 (Samper et al., 2011). Model results show that: (1) Accounting for kinetically-controlled canister corrosion leads to a significant reduction in the corrosion rate; (2) Uncertainties in the surface complexation model play a minor role in the time evolution of the computed pH in the bentonite and the granite. On the other hand, the computed concentrations of dissolved and sorbed Fe are very sensitive to changes in the surface complexation model; (3) The apparent  $K_d$  of Fe is 10 times larger for the triple-site sorption model; (4) The concentration of dissolved Fe computed with kinetic magnetite precipitation is smaller than that obtained at local equilibrium; and (5) The competition of  $\text{Ni}^{2+}$  for sorption sites affects significantly the chemical evolution of the bentonite porewater. The pH in the bentonite porewater decreases compared to the value computed without Ni transport because the sorption of  $\text{Ni}^{2+}$  releases protons. The sorption of  $\text{Ni}^{2+}$  leads to a smaller concentration of sorbed Fe and a larger concentration of dissolved Fe in the bentonite water for  $t < 10^5$  years.

Samper et al. (2016) presented a nonisothermal reactive transport model for the long-term (1 Ma) interactions of the corrosion products and compacted bentonite in a HLW repository in granite. Simulations were carried out with the multicomponent reactive transport code CORE<sup>2D</sup>V4 (Samper et al., 2011). Canister corrosion causes an increase in the pH and the concentration of dissolved  $\text{Fe}^{2+}$  of the bentonite porewater. Iron precipitates as magnetite and siderite and sorbs via cation exchange and surface complexation on weak sites. The largest pH in the bentonite is almost 9.5 at  $2 \times 10^5$  years. Several fronts are observed in the concentration of dissolved  $\text{Fe}^{2+}$ , pH and Eh which are related to sorption and mineral dissolution/precipitation fronts. Magnetite is the main corrosion product and its precipitation reduces significantly the porosity of the bentonite barrier near the canister and could even clog the pores. The thickness of the bentonite zone affected by the decrease of porosity increases with time and is equal to 7 cm at  $t = 1$  Ma. A detailed sensitivity analysis has been performed to changes in model parameters and conceptual model assumptions.

Sensitivity runs were performed to analyse the uncertainties due to the model parameters in: (1) Corrosion rate; (2) Effective diffusion coefficient; (3) Water flow in the granite; (4) Cation exchange selectivities; and (5) Bentonite and granite porewater. The larger the corrosion rate, the larger the magnetite and siderite concentration near the canister-bentonite interface but the smaller their penetration into the bentonite. Therefore, the larger the corrosion rate, the faster the porosity reduction near the canister but the smaller the thickness of affected bentonite. This thickness ranges from  $< 5$  cm for a corrosion rate of  $5 \mu\text{m}/\text{year}$  to nearly 12 cm for  $0.5 \mu\text{m}/\text{year}$ . The larger the effective diffusion,  $D_e$ , the larger the thickness of the bentonite where magnetite, siderite and calcite precipitate and the thicker the bentonite affected by pore clogging. This thickness varies from 4 to 10 cm in the considered range of the  $D_e$ . The bentonite thickness affected by the porosity reduction decreases when the ground water flow through the granite,  $Q$ , increases. Such thickness decreases from 7 cm to 3 cm when  $Q$  increases by a factor of 10. The changes in the bentonite cation exchange selectivities do not affect the computed pH, Eh and the concentrations of other dissolved and precipitated species. The computed magnetite concentration near the canister-bentonite interface is sensitive to changes in the initial chemical composition of the bentonite porewater. By accounting for the dependence of the corrosion rate on the chemical conditions, the thickness of altered bentonite is significantly larger than that of the reference run although the cumulative amount of mineral precipitation near the canister is smaller.

Sensitivity runs were also performed to analyse the uncertainties due to the simplifications of the conceptual model. The sensitivity runs addressed the following features: 1) The thermal field across the bentonite barrier; 2) The dependence of the corrosion rate on temperature; 3) The dependence of the corrosion rate on the chemical conditions; 4) The kinetic magnetite precipitation; 5) The kinetic dissolution of smectite and the neoformation of Fe-clay minerals and zeolites; and 6) The porosity of the canister. The thermal transient and the effect of temperature on the corrosion rate do not have a very significant influence on the geochemical evolution of the bentonite barrier. The thickness of altered bentonite decreases when kinetic magnetite precipitation is considered. Such thickness decreases 3 cm when smectite dissolution and analcime precipitation were taken into account.

## 17.3 Characterization of the HLW disposal cell in clay

### 17.3.1 Description of materials in disposal cell

The Spanish repository concept in plastic clay rock, named ENRESA 2003 (ENRESA, 2004) is based on the disposal of spent fuel in carbon steel canisters in long horizontal disposal galleries. The materials used in the system are the spent fuel, the carbon steel canister, the bentonite, the concrete and the clay.

Canisters are disposed of in cylindrical disposal cells constructed with pre-compacted bentonite blocks of 1.700 kg/ m<sup>3</sup> dry density (in order to achieve a final dry density of 1.600 kg/m<sup>3</sup>). The blocks are initially non-saturated (degree of saturation of 66%). The disposal galleries of 580 m in length and 2.4 m in diameter are located at a depth of 250 m in the host formation. A 0,3 m thick concrete liner is required to deal with the plastic nature of the clay host rock. The separation between canisters is determined mainly by thermal constraints. Separations of 1 m between canisters and 50 m between disposal galleries have been established, in order not to exceed a temperature of 100 °C in the bentonite. Actual separation is a function of the properties of the host rock. Once a disposal gallery is completed, it is sealed with a 6 m long seal made of bentonite blocks and closed with a concrete plug at its entry. After completion of all the disposal galleries, the main drifts, ramp, shafts and other remaining rock cavities will be backfilled with compacted clay from the excavation of the repository, and subsequent projection of clay pellets in the remaining openings. A scheme of the underground facilities in the Spanish repository concept in clay and a schematic diagram of a disposal drift in the Spanish repository concept in clay are shown in *Figure 17-14* and *Figure 17-15*.

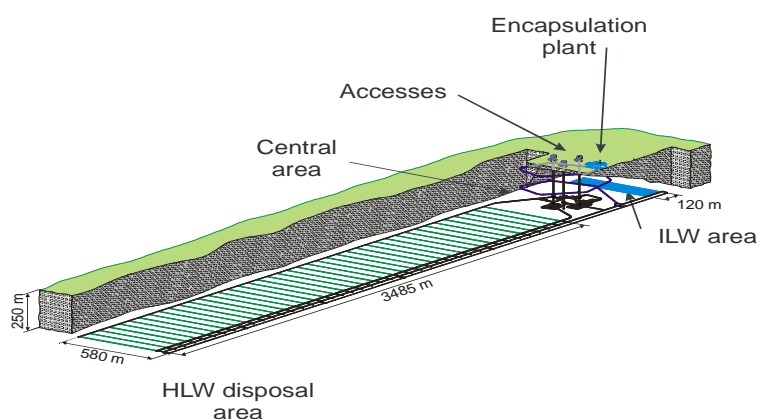


Figure 17-14: Underground installations in the Spanish repository concept in clay (ENRESA, 2004).

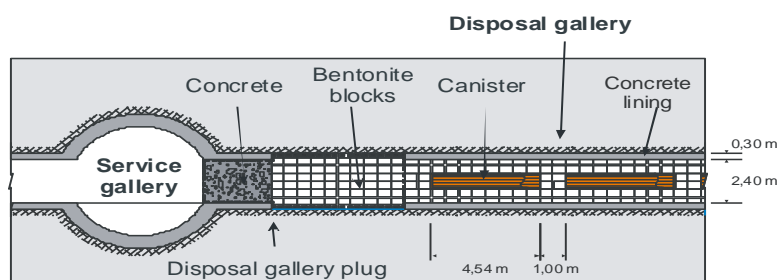


Figure 17-15: Schematic diagram of a disposal drift in the Spanish repository concept in clay (ENRESA, 2004).

The bentonite buffer is required to maintain a large diversity of safety functions, which can only be fulfilled once the bentonite saturates and swells, tightly closing the construction gaps between the bentonite blocks and the liner or the canister wall on the one hand and between the blocks themselves on the other. Nevertheless, there are no safety functional requirements applicable during the time when the canister provides absolute containment. During the resaturation of the buffer, the main concern is the preservation of the favourable properties of the buffer material. As the safety functions assured by the buffer are assumed for the full duration of the quantitative safety assessment (on the scale of a million years), its properties have to be preserved at a sufficient level for commensurate periods of time.

The long-term safety functions of the bentonite buffer are to:

1. Isolate the waste package from the geosphere by limiting advective transport of corroding agents to the canister.
2. Avoid canister sinking in the disposal drift that could result in direct contact of the canister with the rock, hence short-circuiting the buffer.
3. Avoid excessive swelling pressures that could contribute to total pressures that the canister cannot withstand.
4. Avoid excessive temperatures (>100 °C) that could result in chemical alteration of the bentonite and jeopardize its safety functions.
5. The buffer is a containment barrier by itself, as it retains radionuclides based on its properties: (1) Low hydraulic conductivity, which makes radionuclide transport by advection negligible; (2) Sorption of many radioelements, especially actinides; and (3) Filtration of colloids and large complex molecules because of the small size of the pores.
6. Avoid the build-up of excessive gas pressure in the near-field, without undue impairment of the safety functions.
7. Reduce microbial activity to minimize microbial corrosion of the canister.

The geometry of the repository, being understood as such the separations between canisters and between galleries, is determined, mainly, by limitations of thermal order and aspects of security and economy. A thermal analysis was carried out to define the geometry of the disposal area, optimizing its size as small as possible (for safety and economy) without exceeding thermal restrictions, namely the maximum permissible temperature increases in the upper aquifer (5 °C) and on the land surface (0.5 °C), and the maximum permissible temperature in the bentonite buffer (100 °C).

Based on the established repository geological data (including a thermal conductivity value of the clay rock of 1,5 W/m<sup>2</sup>K), on the depth selected for the repository (250 m), and on the initial thermal power of 1.200 W per canister, separations of 1 m between canisters and 50 m between disposal galleries have been established in order to comply with the thermal restrictions imposed.

## 17.3.2 Thermal and hydraulic gradients

### 17.3.2.1 Conceptual model

The main THM processes which affect the bentonite buffer in a HLW repository are:

1. Bentonite saturation and swelling. The surrounding groundwater will slowly saturate the bentonite buffer, bentonite will swell and fill the gaps among the bentonite blocks, bentonite/concrete and bentonite/canister interface.
2. Early cementation. Vapor generation and bentonite drying can be produced in the bentonite near the heat source, as a consequence mineral phases can precipitate. The cementation can cause bentonite swelling and fragility in a few centimeters near the heat source.
3. Mechanical interactions.
  - a. Bentonite buffer thickness can be reduced due to the consolidation of the canister.
  - b. Swelling of the corrosion products generated by the canister corrosion can be absorbed by the bentonite.
  - c. Increasing of the bentonite pressure due to the thermal expansion can be countered by the water flow from the granite.
  - d. Gas generated by the canister corrosion can affect the stability of the bentonite barrier.
4. Increasing of the temperature generated by the spent fuel.

The bentonite buffer in a HLW repository is affected also by the chemical composition of the groundwater and the geochemistry ambient generated by the engineer barrier degradation.

The THM analysis performed in ENRESA (2004), which studied the THM evolution of the near field (the spent fuel, the canister, the bentonite buffer, the concrete and the near host rock) has taken into account the following processes:

1. Thermal transport by conduction, convection and phase change.
2. Liquid water flow and water vapor diffusion.
3. Thermal expansion, bentonite behaviour in function of the stresses, suction and temperature and linear elastic rock behaviour.

### 17.3.2.2 Mathematical model

The THM evolution of the bentonite buffer and the surrounding near field clay rock was analyzed with CODE\_BRIGHT (Olivella et al., 1996, Olivella, 2002). The mathematical formulation have been performed by the Universidad Politécnica de Cataluña (UPC) and implemented with the code CODE\_BRIGHT (Olivella et al., 1996, Olivella, 2002). The code used the finite elements method to solve the coupled THM equations. The mathematical equations include tensional equilibrium, mass balance and energy balance supposing thermal equilibrium.

The mechanical equilibrium is defined as the following equation:

$$\nabla \cdot \sigma + b = 0$$

where  $\sigma$  are the tensions and  $b$  are the mass forces.

The water mass balance is the following:

$$\frac{\partial}{\partial t} (\theta_l^w S_l \phi + \theta_g^w S_g \phi) + \nabla \cdot (j_l^w + j_g^w) = f^w$$

where  $\theta_l^w$ ,  $\theta_g^w$ ,  $S_l$ ,  $S_g$ ,  $\phi$ ,  $j_l^w$ ,  $j_g^w$  and  $f^w$  are the water content of the liquid phase, the water content of the gaseous phase, liquid saturation degree, gas saturation degree, porosity, water flux in the liquid phase, water flux in gaseous phase and external water flow, respectively.

The thermal balance can be expressed as the following:

$$\frac{\partial}{\partial t} (E_s \rho_s (1 - \phi) + E_l \rho_l S_l \phi + E_g \rho_g S_g \phi) + \nabla \cdot (i_c + j_{Es} j_{El} j_{Eg}) = f^Q$$

where  $E_s$ ,  $E_l$ ,  $E_g$ ,  $\rho_s$ ,  $\rho_l$ ,  $\rho_g$ ,  $i_c$ ,  $j_{Es}$ ,  $j_{El}$ ,  $j_{Eg}$  and  $f^Q$  are the specific energy of the soil phase, the specific energy of the liquid phase, specific energy of the gaseous phase, solid density, liquid density, gas density, conduction thermal flux, solid energy flux, liquid energy flux, gas energy flux and external thermal flux, respectively.

The solid mass balance is the following equation:

$$\frac{\partial}{\partial t} (\theta_s (1 - \phi)) + \nabla j_s = 0$$

Where  $\theta_s$  and  $j_s$  are the solid mass content and the solid flux, respectively.

#### 17.3.2.3 Dimensions, initial and boundary conditions of the THM numerical model

The model was performed with a 2-D vertical finite element mesh. The model results are representative of a central section of the canister in the middle of the repository. This is due to the assumption that the galleries length are infinity because their length is much larger than that of the distance between galleries.

The domain extended 25 m width and 540 m length, representing a section along the depth of the middle of the canister. The model included 50 m of aquifer, 110 of marl and 380 m of clay. The finite element mesh was formed by 1170 nodes and 1060 elements. Figure 3 shows a scheme of the model domain and the boundary conditions (the dimensions are not in real scale).

The concrete time life of 1000 years was assumed. The simulation took into account a decreasing of the Young module and the permeability of the concrete after 1000 years of simulation.

The initial conditions of the THM model were the following:

1. Water content of the bentonite is equal to 14 %.
2. Suction pressure of the bentonite is equal to 44.41 MPa.
3. Porosity are equal to 0.407, 0.005, 0.085, 0.328 for the bentonite, canister, concrete and clay, respectively.
4. Temperature is equal to 17.8 °C at the depth of the repository and equal to 10 °C at the surface.
5. Hydrostatic tension of the bentonite is equal to 0.24 MPa.
6. Host rock homogenous medium.

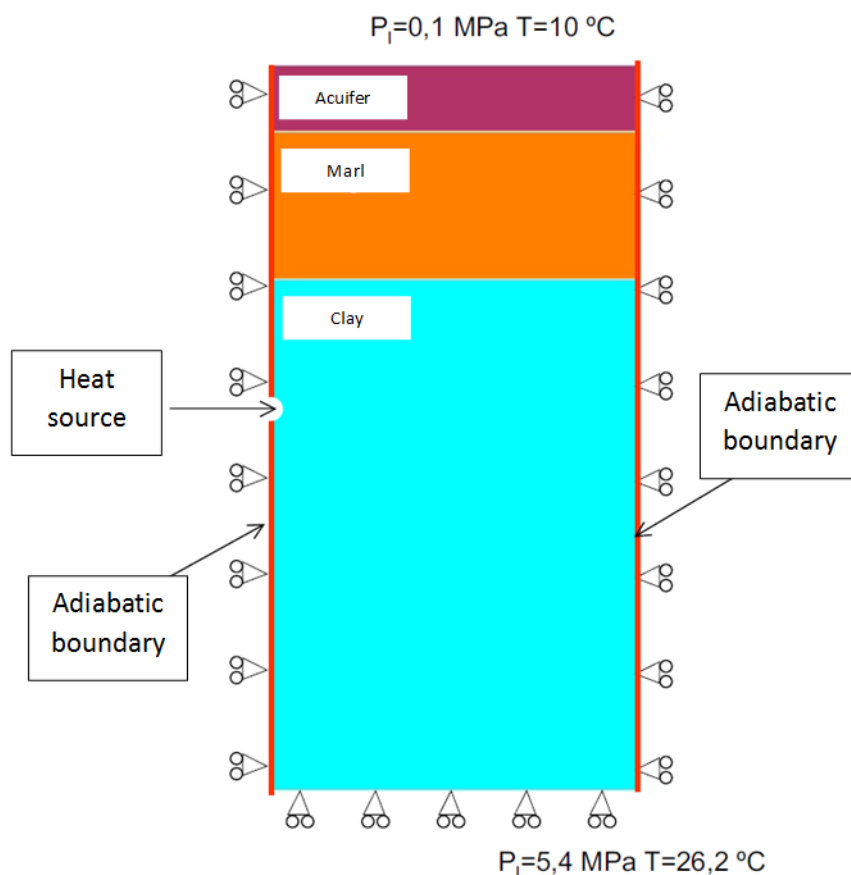


Figure 17-16: Boundary conditions of the numerical model of the near field (ENRESA, 2004).

#### 17.3.2.4 TH model parameters

Table 17-6 shows the THM main parameters of the bentonite, canister, concrete and clay. The intrinsic permeability of the steel, concrete and clay was assumed to be constant and porosity independent. The thermal conductivity of the steel, concrete and clay are assumed to be constant. Table 2 shows the mechanical parameters used for the steel, concrete and clay. An elastic mechanical behaviour was supposed for the steel, concrete and clay.

Table 17-6: Main parameter considered in the THM model of the Spanish reference concept in clay (ENRESA, 2004).

Properties	Parameter	Unit	Bentonite	Steel	Concrete	Clay
Thermal conductivity $\lambda = \lambda_s S_i \lambda_d^{(1-S_i)}$	$\lambda_s$	W/mK	1.15	60	2	1.5
	$\lambda_d$	W/mK	0.47	60	2	1.5
Solid density	$\rho$	kg/m <sup>3</sup>	2630	7800	2300	2740
Specific heat	$c_p$	J/kg°C	735.2+1.38*T	403.1	1374	1117
Intrinsic permeability $k = k_0 \frac{\phi^3 (1-\phi_0)^2}{(1-\phi)^2 \phi_0^3}$	$k_0$	m <sup>2</sup>	2·10 <sup>-21</sup>	10 <sup>-50</sup> (constant)	6·10 <sup>-16</sup> (constant)	4.2·10 <sup>-19</sup> (constant)
	$\phi_0$	-	0.407	0.001	0.085	0.309
Relative permeability $k_{rl} = A S_e^\lambda$	A	-	1	1	1	1
	$\lambda$	-	3	2	2	2
Retention curve $S_i = \left[ 1 + \left( \frac{S}{P} \right)^{\frac{1}{1-\lambda}} \right]^{-\lambda} \quad P = P_0 \frac{\sigma}{\sigma_0}$	$P_0$	MPa	30	100	2.1	20
	$\sigma_0$	N/m	0.072	-	-	-
	$\lambda$	-	0.32	0.33	0.70	0.60
Diffusive flux $D_m^w = \tau D \left[ \frac{(273,15 + T)^n}{P_g} \right]$	D	m <sup>2</sup> /s/k <sup>-n</sup> nP	5.9·10 <sup>-6</sup>	-	-	-
	n	-	2.6	-	-	-
	$\tau$	-	1	-	-	-
Plastic behaviour $f = f(\alpha, \epsilon, \Delta T)$ $F = \frac{3J^2}{G_s} - \epsilon_s (p + P_s)(P_0 - p) = 0$ $P_s = P \left( \frac{P}{P_0} \right)^{\frac{\lambda(0) - \epsilon_s}{\lambda(0) - \epsilon_0}}$ $P_s = P_s^0 + 2(\alpha_s \Delta T + \alpha_s \Delta T / T)$ $L_s = M / G_s \quad (\theta = -\pi / 6)$ $\lambda(s) = \lambda(0)[(1-r)\exp(-\beta s) + r]$ $P_s = k \exp(-\rho \Delta T) s; P_s^0 = \frac{1+\epsilon}{\lambda(0) - k_s} P_s^0 \epsilon_s^0$ $G = \frac{3J^2}{G_s} - \alpha \epsilon_s (p + P_s)(P_0 - p)$ $L_s = M / G_s \quad (\theta = -\pi / 6)$	$\lambda(0)$	-	1.5	-	-	-
	r	-	0.75	-	-	-
	$\beta$	MPa <sup>-1</sup>	0.05	-	-	-
	$\rho$	°C <sup>-1</sup>	0.2	-	-	-
	K	-	0.1	-	-	-
	$P^c$	MPa	0.1	-	-	-
	M	-	1.5	-	-	-
	$\alpha$	-	0.395	-	-	-
	$P_0^*$	MPa	8	-	-	-
	Elastic behaviour $\dot{\epsilon}_v^e = \frac{k_j}{1+\epsilon} \frac{\dot{P}}{P} + \frac{k_s}{1+\epsilon} \frac{\dot{s}}{s+0,1} + (\alpha_0 + 2\alpha_2 \Delta T) \dot{T}$ $k_j = k_{j0} (1 + \alpha_j s)$ $k_s = k_{s0} \left( 1 + \alpha_{sp} \ln \frac{P}{P_r} \right) \exp(\alpha_{ss} s)$ $\dot{\epsilon} = \dot{J} / G; G = E / 2(1+\nu)$	$k_{j0}$	-	0.05	-	-
$k_{s0}$		-	0.25	-	-	-
$\nu$		-	0.4	-	-	-
$\alpha_{ss}$		MPa <sup>-1</sup>	0	-	-	-
$\alpha_i$		MPa <sup>-1</sup>	-0.003	-	-	-
$\alpha_{sp}$		-	-0.1609	-	-	-
$P_r$		-	0.01	-	-	-
$\alpha_0$		°C <sup>-1</sup>	1.5·10 <sup>-4</sup>	-	-	-
$\alpha_2$		°C <sup>-1</sup>	0	-	-	-

Table 17-7: Mechanical parameters of the cantsiter, bentonite and clay of the Spanish reference concept in clay (ENRESA, 2004).

Parameter	Unit	Steel	Concrete	Clay
Thermal expansion coefficient	°C <sup>-1</sup>	1.1·10 <sup>-5</sup>	10 <sup>-5</sup>	10 <sup>-5</sup>
Young module	MPa	1.9·10 <sup>5</sup>	4.7·10 <sup>4</sup>	484.4
Poisson coefficient	-	0.3	0.20	0.3

17.3.2.5 Calculated liquid saturation and mechanical evolution

Figure 4 shows time evolution of the saturation degree at several locations. The inner part of the bentonite buffer dries out due to the large temperature while the external part of the bentonite hydrates in contact with the concrete. The full saturated bentonite buffer is reached after 18.2 years. The concrete layer is fully saturated after a year of simulation. The computed maximum stresses in the bentonite is equal to 7.4 MPa.

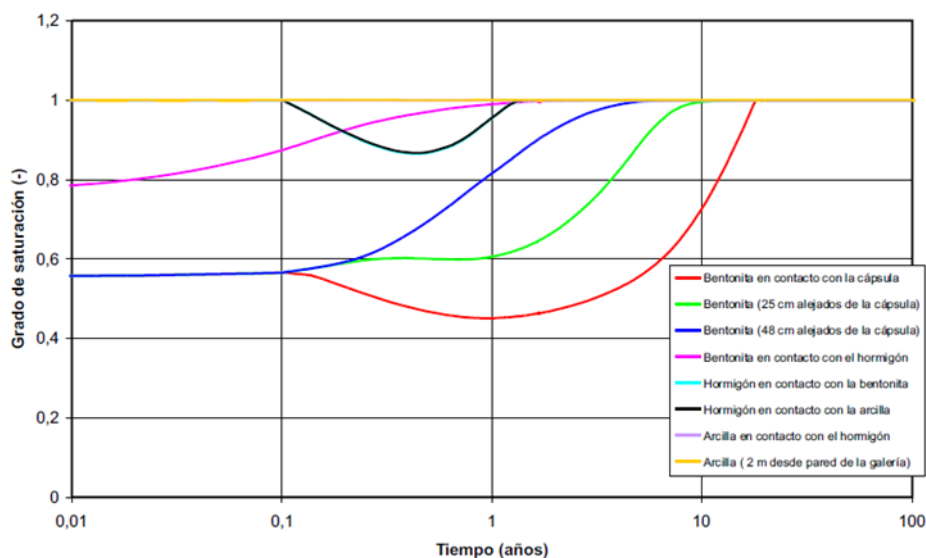


Figure 17-17: . Calculated saturation degree time evolution in the Spanish repository concept in clay (ENRESA, 2004).

17.3.2.6 Calculated temperature time evolution

For the configuration of disposal galleries and canisters taken at the reference repository, the maximum temperature at the bentonite barrier does not exceed 100 °C at any time and the initial temperature at repository depth is 17.8 °C. Figure 17-18 shows the calculated temperature time evolution at different distances at the canister-bentonite interface, the bentonite, the bentonite-concrete interface, the concrete, the concrete-clay interface and the clay. The maximum temperature at the canister-bentonite interface (101.5 °C) is reached at 7 years of disposal. The maximum temperature in the concrete and the clay is 75 °C and 73 °C, respectively, at 21 years. These computed results are used in the geochemical evolution model of the Spanish reference concept in clay.

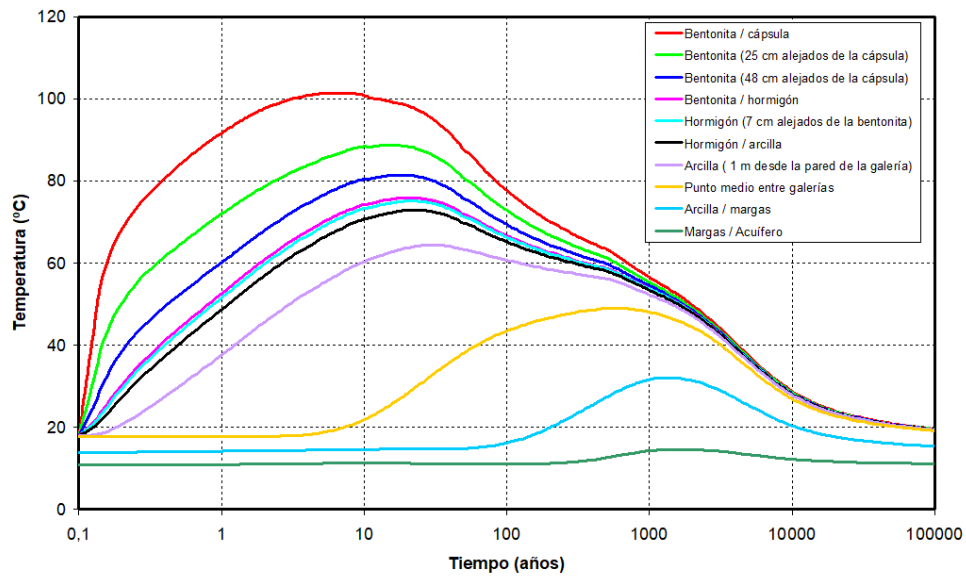


Figure 17-18: Calculated temperature time evolution in the Spanish repository concept in clay (ENRESA, 2004).

Table 17-8: Description of parameters for thermal gradients

Feature	Examples of parameter	Value and unit	Source	Justification / comments
Heat source	Thermal power as a function of time	305.4 W	ENRESA 2001	
Carbon steel canister	thermal conductivity	60 W/m°C	ENRESA 2004	
	specific density	7800 kg/m <sup>3</sup>	ENRESA 2004	
	specific heat capacity	403.1 J/kg°C	ENRESA 2004	
Bentonite backfill	thermal conductivity	1.15 W/m°C	ENRESA 2004	The dry thermal conductivity is equal to 0.45 W/m°C
	specific density	2630 kg/m <sup>3</sup>	ENRESA 2004	
	specific heat capacity	735.2+1.38*T	ENRESA 2004	
Concrete liner	thermal conductivity	2 W/m°C	ENRESA 2004	
	specific density	2300 kg/m <sup>3</sup>	ENRESA 2004	
	specific heat capacity	1374 J/kg°C	ENRESA 2004	
Host rock: clay	thermal conductivity	1.5 W/m°C	ENRESA 2004	
	specific density	2740 kg/m <sup>3</sup>	ENRESA 2004	
	specific heat capacity	1117 J/kg°C	ENRESA 2004	
	temperature	17.8°C	ENRESA 2004	17.8°C at the depth of the repository and 10°C at the surface

### 17.3.3 Pore water compositions

The initial chemical composition of the bentonite porewater, the concrete water and the clay porewater is shown in Table 3. The initial mineral volume fraction considered in the bentonite, the concrete and the clay are presented in Table 4. The initial value of the cation exchange capacity (CEC) in the bentonite is 101.74 meq/100g and 30.17 meq/100g in the clay.

Table 17-9: Initial chemical composition (mol/L) of the bentonite porewater, the concrete water and the clay porewater at 25 °C (ENRESA, 2004).

	Bentonite	Concrete	Clay
<b>pH</b>	7.462	13.25	7.54
<b>Cl<sup>-</sup></b>	1.30E+00	-	2.30E-02
<b>HCO<sub>3</sub><sup>-</sup></b>	2.70E-04	-	1.80E-03
<b>SO<sub>4</sub><sup>2-</sup></b>	1.62E-02	2.00E-03	7.00E-02
<b>Na<sup>+</sup></b>	5.93E-01	1.60E-02	1.30E-01
<b>K<sup>+</sup></b>	4.27E-03	1.00E-01	8.20E-04
<b>Mg<sup>2+</sup></b>	1.60E-01	4.10E-09	8.20E-03
<b>Ca<sup>2+</sup></b>	2.02E-01	1.10E-02	1.10E-02
<b>SiO<sub>2</sub>(aq)</b>	1.93E-04	2.00E-05	2.70E-04

Table 17-10: Initial mineral volumen fraction in the bentonite, the concrete and the clay (ENRESA, 2004)

	Bentonite	Concrete	Clay
<b>Quartz</b>	2%		4%
<b>Calcite</b>	0,6%		16%
<b>Gypsum</b>	0,14%		3%
<b>Dolomite</b>			4%
<b>CSH (tobermorite)</b>		40%	
<b>Portlandite</b>		18%	

## 17.4 Chemical evolution of the HLW disposal cell

### 17.4.1 Narrative

The chemical evolution of the Spanish reference concept in clay was performed with the reactive transport code CORE<sup>2D</sup> (Samper et al., 2011). Calculations were focused on the time evolution and the spatial distribution of pH and the main cations (calcium, magnesium, sodium and potassium) and anions (chloride, bicarbonate and sulphate) presented in the bentonite porewater, the concrete water and the clay porewater. Values of Eh and Fe<sup>2+</sup> were not considered in the THC model. The conceptual geochemical model includes the following reactions: 1) Aqueous complexation; 2) Acid/base; 3) Mineral dissolution/precipitation; 4) Cation exchange of Ca<sup>2+</sup>, Mg<sup>2+</sup>, Na<sup>+</sup>, K<sup>+</sup> and H<sup>+</sup>; and 5) Proton surface complexation. All the reactions were assumed at chemical equilibrium.

The geochemical model was run for two stages, from initial time to the time that the bentonite is saturated and then to 1 Ma. For the first stage (saturation of bentonite), the model accounts for three material zones: the bentonite buffer, the concrete and the clay. Then the results of the first stage are taken as initial conditions for the model of the second stage. In the second stage (geochemical evolution after saturation of bentonite), the same materials are considered in the model domain. It is noted that after bentonite is saturated (19 years), solute transport is mainly controlled by diffusion and geochemical reactions.

### 17.4.2 Conceptual model

The conceptual model of the saturation of bentonite considers three materials: the bentonite, the concrete and the clay. The model domain was discretized using a 1-D axisymmetric mesh which has 422 triangular elements (300 in the bentonite, 120 in the concrete and only 2 in the clay) and 424 nodes. *Figure 17-19* shows the dimensions and the mesh used in the first stage of the chemical evolution of the Spanish reference concept in granite. The numerical model simulates only the first 100 years.

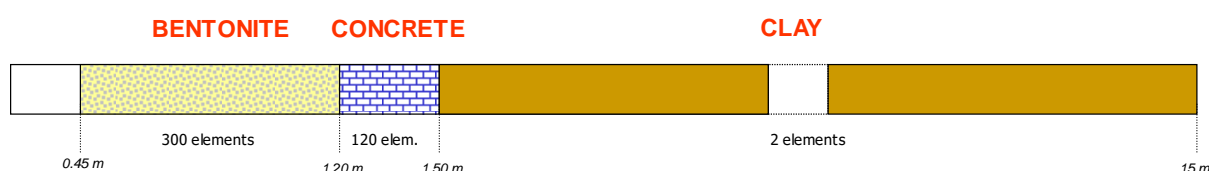


*Figure 17-19: Dimensions and 1-D axisymmetric mesh used in the first stage of the geochemical model (ENRESA, 2004).*

The thermo-hydro-chemical initial conditions at this first stage are: 1) The initial temperature is the background temperature at the repository level of 17.8 °C; 2) The initial flow condition is calculated with the bentonite initial saturation degree and its suction pressure; 3) The initial chemical composition in all bentonite nodes is fixed with the bentonite porewater at a water content of 14% (*Table 17-9*); 4) The initial chemical composition in all concrete nodes is fixed with the concrete water (*Table 17-9*); 5) The initial chemical composition in all clay nodes is fixed with the clay porewater (*Table 17-9*); 6) The initial volume fraction of the minerals is fixed in the bentonite and the concrete nodes (*Table 17-10*); and 7) The initial exchangeable cations composition is fixed in the bentonite nodes.

The THC boundary conditions at the first stage are: 1) The liquid pressure at the outer boundary ( $r = 15$  m) was equal to 2.5 MPa; 2) A Neuman transport boundary condition was used for solute transport

according to which solute flux is equal to the product of water flux times solute concentration of inflow granitic water; and 3) The temperature boundary condition is the calculated temperature in the THM model (Figure 17-18). Figure 17-20 shows the time evolution of these calculated temperatures at different distances from the central axis of the canister in the THM model (continuous lines) and the used time function in the THC model to reproduce the calculated temperatures (discontinuous lines).

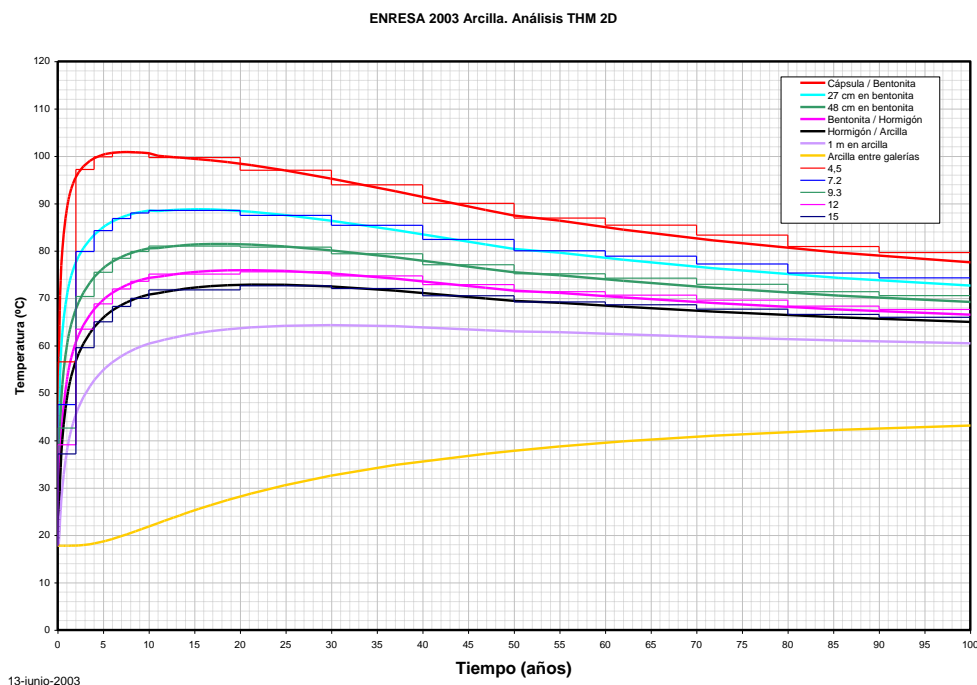


Figure 17-20: Temperature boundary conditions at the first stage of the geochemical model (ENRESA, 2004).

The conceptual model of the geochemical evolution after saturation of bentonite considers four materials: the canister, the bentonite, the concrete and the clay. The model domain was discretized using a 1-D axisymmetric mesh which has 126 triangular elements (20 in the bentonite, 20 in the concrete and 86 in the clay) and 424 nodes. The mesh discretization is non-uniform, being more refined near the interfaces. Figure 17-21 shows the dimensions and the mesh used in the second stage of the chemical evolution of the Spanish reference concept in granite. The mesh was extended to 172 m. Simulations were run for over 1 Ma.

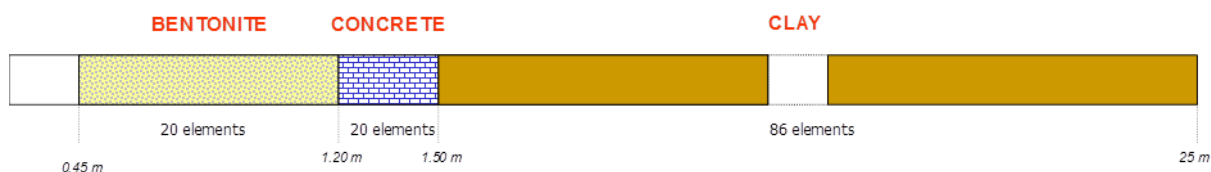


Figure 17-21: Dimensions and 1-D axisymmetric mesh used in the second stage of the geochemical model (ENRESA, 2004).

The thermo-hydro-chemical initial conditions at this second stage are: 1) The initial temperature is the calculated temperature at the end of the first stage of the geochemical model; 2) A steady state flow regime was considered; 3) The initial chemical composition in all bentonite nodes is fixed with the calculated chemical composition of the bentonite porewater after saturation; 4) The initial chemical composition in all concrete nodes is fixed with the calculated chemical composition of the concrete water

after saturation; 5) The initial chemical composition in all clay nodes is fixed with the clay porewater (Table 17-9); 6) The initial volume fraction of the minerals is fixed in the bentonite, the concrete and the clay nodes (Table 17-10); 7) The initial exchangeable cations composition is fixed in the bentonite and the clay nodes; and 8) The initial concentration of sorption sites is fixed only in the bentonite.

The temperature boundary condition is the calculated temperature in the THM model (Figure 17-18: Calculated temperature time evolution in the Spanish repository concept in clay (ENRESA, 2004).). Figure 17-22 shows the time evolution of these calculated temperatures at different distances from the central axis of the canister in the THM model (continuous lines) and the used time function in the THC model to reproduce the calculated temperatures (discontinuous lines).

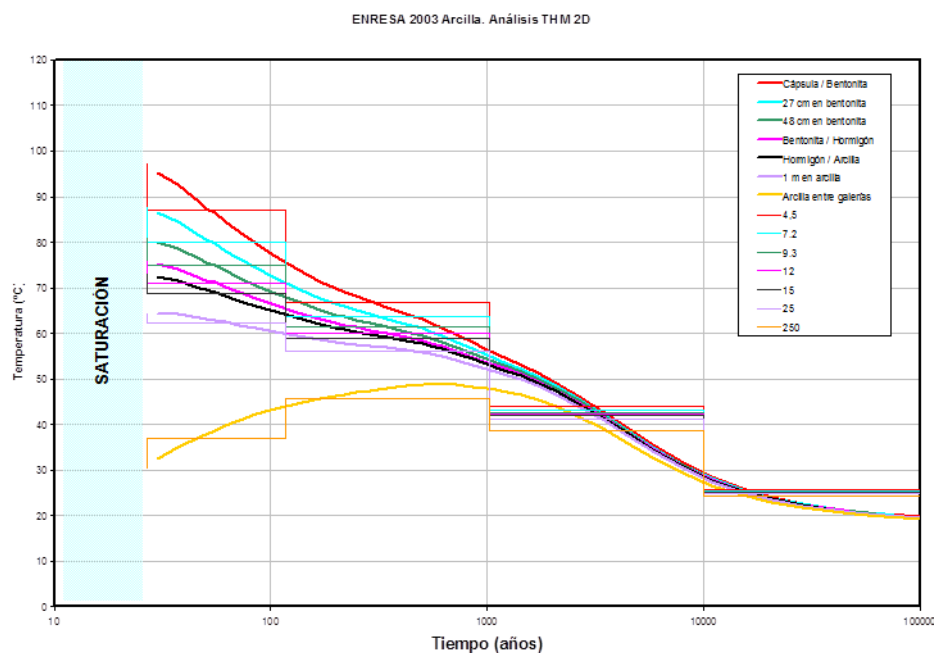


Figure 17-22: Temperature boundary conditions at the second stage of the geochemical model (ENRESA, 2004).

### 17.4.3 Mathematical model

The conceptual geochemical model considered in the Spanish reference concept in clay includes the following reactions assumed at chemical equilibrium: 1) Aqueous complexation; 2) Acid/base; 3) Mineral dissolution/precipitation; 4) Cation exchange of  $\text{Ca}^{2+}$ ,  $\text{Mg}^{2+}$ ,  $\text{Na}^+$ ,  $\text{K}^+$  and  $\text{H}^+$ ; and 5) Proton surface complexation. The mathematical formulation of these chemical reactions is described in Appendix D.

### 17.4.4 Calculated results

During the bentonite buffer resaturation period (first stage of the geochemical model), advection from the clay and the concrete to bentonite is the relevant transport process. Dilution of the chemical concentration of bentonite porewater and mineral dissolution in bentonite are the two main processes produced by resaturation. Bentonite reaches full saturation after 19 years. Figure 17-23 shows the spatial distribution of total concentrations of major cations and anions after bentonite is saturated. Chemical species mainly diffuse from the bentonite into the concrete because concentrations of most ions are smaller in concrete than in bentonite except for  $\text{K}^+$  (Table 17-9). These aqueous concentrations computed results of the first stage of the geochemical model were taken as initial conditions in the second stage. The value of pH in the bentonite increases due to the penetration of the hyperalkaline

plume from concrete while in the concrete decreases by the combination of the thermal effect and the infiltration of clay porewater (Figure 17-24).

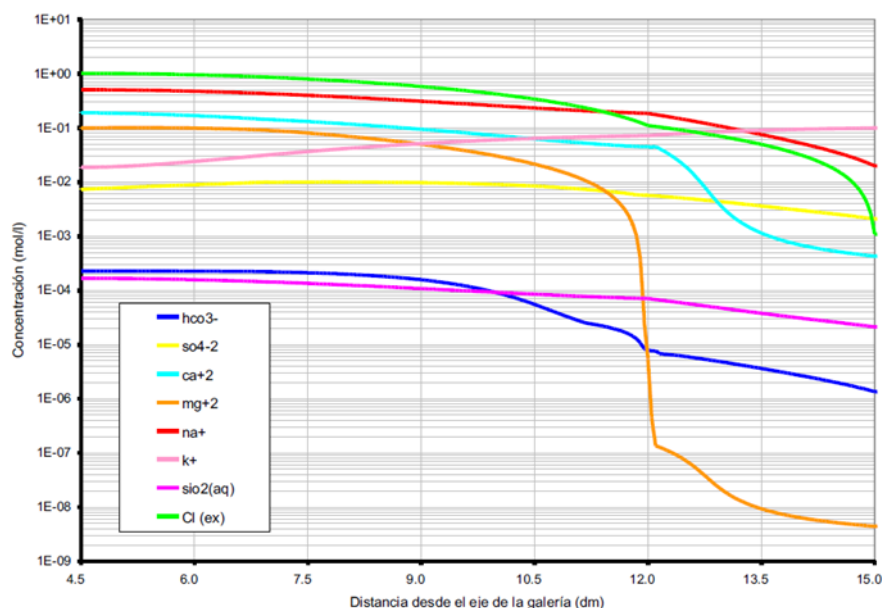


Figure 17-23: Spatial distribution of the calculated calcium, magnesium, sodium, potassium, chloride, bicarbonate, sulphate and silica once bentonite is fully saturated (ENRESA, 2004).

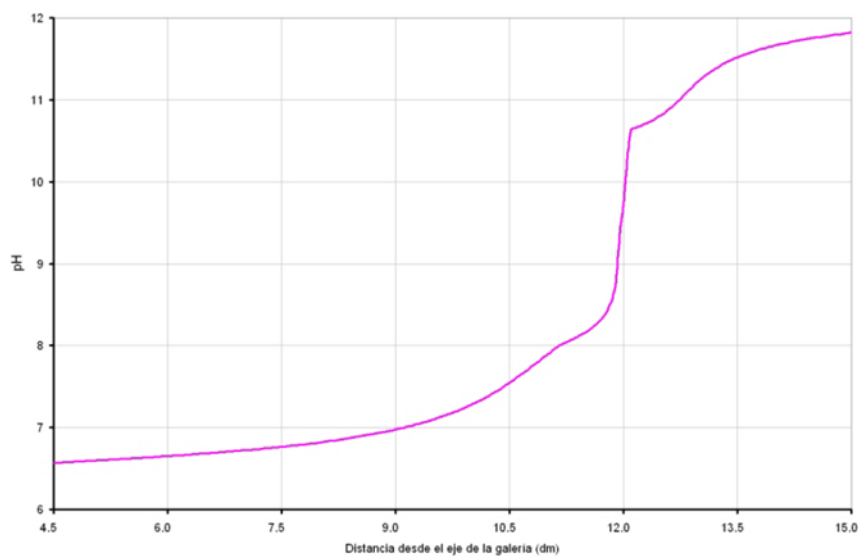


Figure 17-24: Spatial distribution of the calculated pH once bentonite is fully saturated (ENRESA, 2004).

In the second stage (geochemical evolution after saturation of bentonite), which starts once bentonite becomes fully saturated, solute transport is mainly controlled by diffusion and geochemical reactions. Figure 17-25 shows spatial distribution of computed pH at different times. In this figure  $t = 0$  represents the pH distribution in bentonite, concrete and clay after the bentonite is saturated. In the concrete, pH first increases due to the dissolution of portlandite, reaches a maximum value around 10,000 years and then slowly decreases after 40,000 years when portlandite is completely exhausted. In the bentonite pH increases due to the penetration of the hyperalkaline plume from concrete. However, precipitation of calcite, brucite and sepiolite buffers the hyperalkaline plume; pH reaches a maximum value around

10,000 years and then decreases to 9.5 after 1 Ma. The hyperalkaline plume slowly penetrates into the clay formation. The front of the hyperalkaline plume penetrates a radial distance of 0.7 m into the clay formation after 1 Ma.

Figure 17-26 shows the time evolution of total concentrations of major cations and anions at a point located at the middle of bentonite. One can see that ion concentrations decrease after 100 years, reaching minimum values at a time ranging from 2,000 to 10,000 years due to: 1) Diffusion from bentonite into concrete because initial concentrations of major ions in concrete are smaller than those in bentonite; and 2) Mineral precipitation caused by the penetration of the alkaline plume from concrete. The precipitation of calcite leads to a decrease in concentrations of calcium and bicarbonate. The sharp decrease of magnesium, from the initial time to 10,000 years, is mainly caused by precipitation of sepiolite and brucite. Concentrations of  $\text{Ca}^{2+}$ ,  $\text{Na}^+$ ,  $\text{HCO}_3^-$ ,  $\text{SO}_4^{2-}$  and  $\text{Cl}^-$  in bentonite slowly reach steady values after 10,000 years. It is worth noting that after 40,000 years,  $\text{Mg}^{2+}$  concentration increases rapidly due to dissolution of brucite in the bentonite which precipitated previously. Concentration of  $\text{K}^+$  in the bentonite increases slightly before 100 years due to diffusion from the concrete where the porewater has a higher concentration of potassium than in bentonite. After 100 years,  $\text{K}^+$  concentration in bentonite porewater decreases because the porewater in the clay has a very low concentration of potassium.

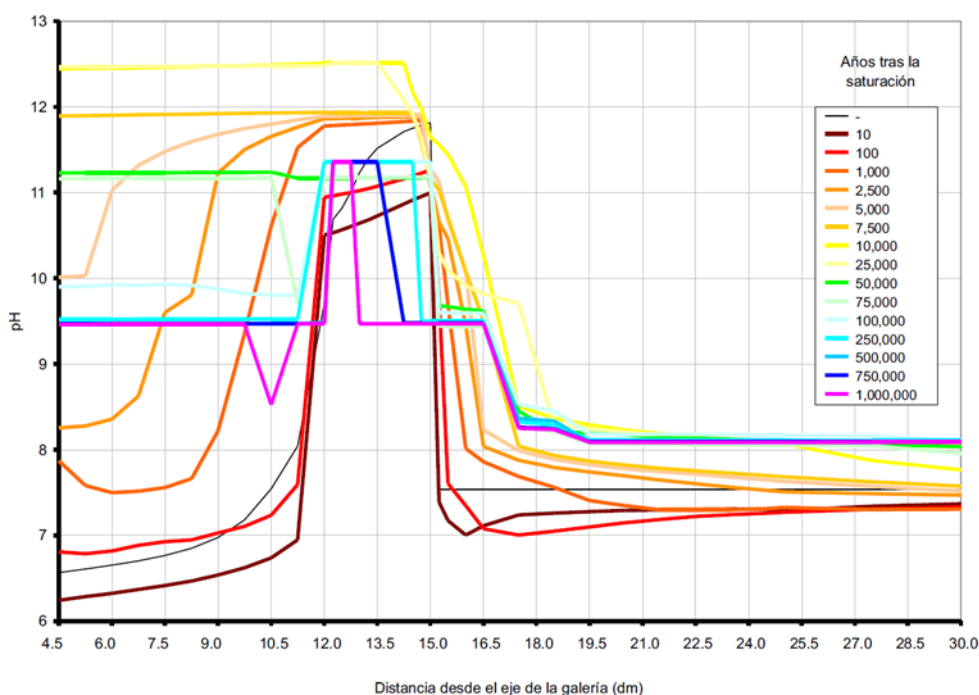


Figure 17-25: Spatial distribution of the calculated pH at different times (ENRESA, 2004).

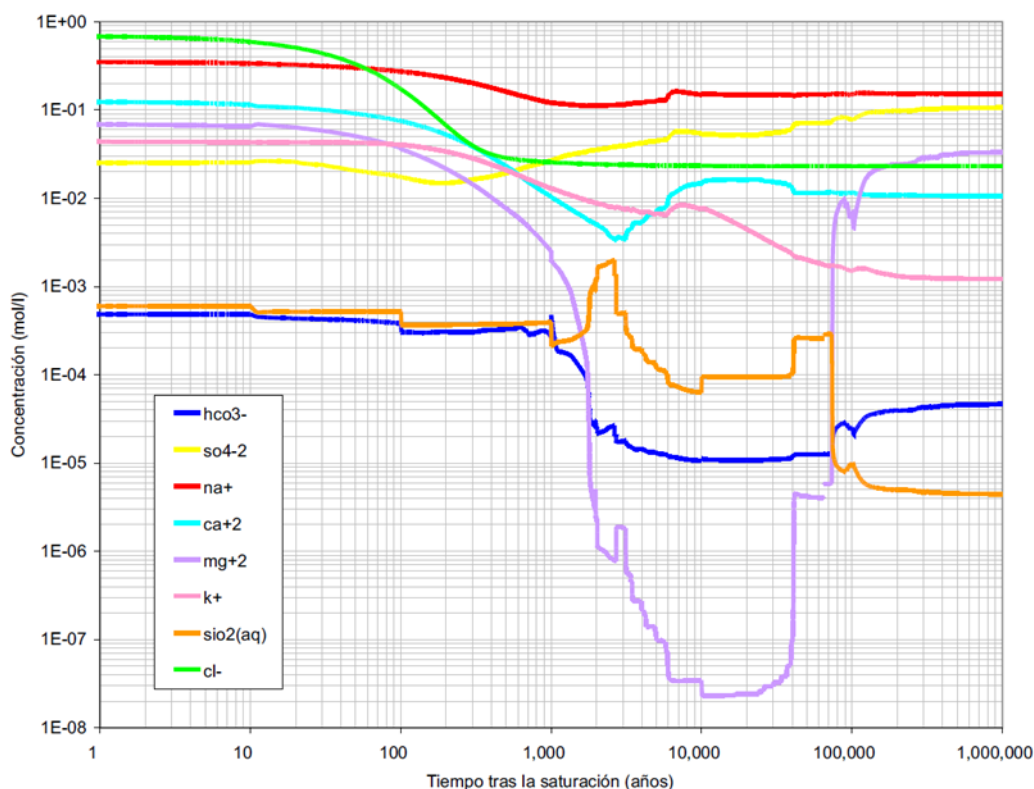


Figure 17-26: Time evolution of the calculated calcium, magnesium, sodium, potassium, chloride, bicarbonate, sulphate and silica at a point located at the middle of bentonite (ENRESA, 2004).

#### 17.4.5 Improvements in the chemical evolution of the HLW cell in clay

The predictions of the chemical evolution performed for the ENRESA 2003 Performance Assessment Project have been updated more recently within the context of several EU Research Projects such as NFPRO, FUNMIG, PAMINA, PEBS and CEBAMA. This section presents a summary of the main results of these recent updates.

Yang et al. (2008) presented a numerical model of coupled saturated/unsaturated water flow, heat transfer and multi-component reactive solute transport to evaluate the long-term (1Ma) geochemical evolution in the bentonite, the concrete and the clay formation for a potential geological radioactive waste repository. They use a conceptual and numerical model similar to that of ENRESA (2004). Changes in formation porosity caused by mineral dissolution/precipitation reactions were taken into account. Simulations were carried out with the multicomponent reactive transport code CORE2D V4 (Samper et al., 2011). Numerical results show that pH in the bentonite porewater can vary from neutral to up to 13 over a time scale of 1 Ma although dissolution of silica minerals and precipitation of secondary calcium silicate hydrate (CSH) minerals in the bentonite buffer the effect of the hyperalkaline plume. Mineral precipitation reduces the volume of pore space in bentonite close to the bentonite-concrete interface due to the precipitation of CSH minerals. Model results indicate that bentonite porosity decreases less than 25%. The hyperalkaline plume from the concrete only extends to a distance of 0.7 m in the clay formation over the time range of 1 Ma.

Mon et al. (2017) presented a non-isothermal multicomponent reactive transport model of the long-term (1Ma) interactions of the compacted bentonite with the corrosion products of a carbon-steel canister and the concrete liner of the engineered barrier of a HLW repository in clay. Simulations were carried

out with CORE2D V4 (Samper et al., 2011). Model results show that: (1) Magnetite is the main corrosion product and its precipitation reduces significantly the porosity of the bentonite near the canister; (2) The degradation of the concrete liner leads to the precipitation of secondary minerals and the reduction of the porosity of the bentonite and the clay formation at their interfaces with the concrete liner. The reduction of the porosity becomes especially relevant at  $t=104$  years; (3) The zones affected by pore clogging at the canister-bentonite and concrete-clay interfaces at 1 Ma are approximately equal to 1 and 3.3 cm thick, respectively; (4) The hyper-alkaline front ( $\text{pH} > 8.5$ ) spreads 2.5 cm into the clay formation after 1 Ma.

Sensitivity runs were performed to analyse the uncertainties in cation exchange selectivities and evaluate the relevance of surface complexation reactions, kinetic smectite dissolution, and Mg-saponite precipitation. Only the concentrations of the exchanged  $\text{Ca}^{2+}$ ,  $\text{Mg}^{2+}$ , and  $\text{Na}^+$  and  $\text{K}^+$  are sensitive to changes in the selectivity coefficients. The computed pH at 1 Ma in the sensitivity run without surface complexation reactions is the same as that of the base run. Accounting for smectite dissolution leads to: 1) Slight changes in the computed pH in the bentonite at 1 Ma; 2) A reduction in the breakthrough of the pH front into the clay formation from 35 to 15 cm; 3) An increase in brucite precipitation in the bentonite near the concrete interface and in the concrete; and 4) A decrease of gypsum precipitation. The run with Mg-saponite precipitation in the bentonite leads to slightly larger pH, slightly smaller magnetite precipitation and smaller smectite dissolution at 1Ma.

## 17.5 Characterization of an ILW disposal cell in clay or granite

No specific studies have been made. Therefore, there is no contribution for this section.

## 18. Sweden

SKB participates in EURAD and has therefore been asked to contribute to this ACED deliverable about the current handling of the chemical evolution in their waste disposal designs and concepts. Klas Källstrom has completed an ACED template that can be found in Appendix E. The following description has been extracted from the refereed SKB reports in his completed template and has been written by Erika Neeft.

Vitrified HLW is not present in Sweden. SKB's work on cemented ILW has therefore been looked at for ACED. Sweden has selected sites for disposal of LILW as well as HLW. The disposal facility for short lived<sup>17</sup> LILW, Slutförvaret för kortlivat radioaktivt avfall (SFR), has been running since 1988 and is located in Forsmark. SFR is going to be extended; the present operating part is called SFR-1 in which mainly operational waste is disposed and the extended one, SFR-3 in which mainly decommissioning waste is disposed<sup>18</sup>. SFR-1 has 4 waste vaults and one silo, a cylindrical vault for ILW and is covered by 60 metres of granitoid rock. SFR-3 is planned to have 6 waste vaults with a rock cover of 120 metres. The safety assessment of the disposal system in SFR includes evolutions of the surface systems, thermal evolutions i.e. the temperature of the disposal facility is determined almost entirely by the exchange of heat between the granitic rock and ground water, mechanical evolutions, site specific hydrogeological evolutions in which it is calculated when the site is submerged or at shore which determine the geochemical evolution of the host rock, near-field hydrological evolution, chemical evolution within the disposal facility and evolution of engineered barriers: bentonite, concrete and macadam i.e. a type of crushed rock [SKB, 2015]. The chemical evolution from the waste form up till the host rock for ILW vaults has been extracted for this ACED description.

### 18.1 Characterization of the LILW disposal cell in granite

The ILW vaults in SFR are called 1BMA in SFR-1 and 2BMA in SFR-3. Waste packages that are emplaced in ILW vaults are 200 litre steel drums, steel moulds, tetramoulds i.e. a mould that can comprise 4 steel moulds and concrete moulds. Organic waste can be spent ion exchange resins, plastics, rubbers and cellulose. Metallic waste can be iron/steel and aluminium/zinc. The safety analysis required the amounts for disposal of cellulose and aluminium/zinc to be limited in 2BMA; degradation of cellulose gives rises to the complexing agent isosaccharinate (ISA) that adversely affects sorption of radionuclides and corrosion of aluminium/zinc may lead to such high gas generation rates that the barriers may become damaged. The largest volume (39%) of envisaged processed waste in 1BMA in SFR-1 is cemented waste containing spent-ion exchange resins, evaporates and sludge in concrete moulds and in 2BMA in SFR-3, this volume (44%) is expected to be tetramoulds containing concrete embedded trash and scrap metal. The walls and roofs of both vaults are lined with shotcrete to stabilise the rock in the operational phase and the caissons, in which the waste packages are emplaced, are casted in the vaults. For the caissons, reinforced concrete is used in 1BMA and unreinforced concrete is envisaged for 2BMA in order to eliminate the potential formation of cracks in concrete by the mechanical stress caused by the increasing thickness of iron corrosion products that have a higher volume than the initial rebars [Höglund, 2014; SKB, 2015]. A lid is put as soon as a compartment is filled and after that a thin concrete layer is casted on top of the lid in order to prevent water intrusion during the operating phase. The caissons are planned to be successively grouted with a similar type of grout that is used for the silo. This grout contributes to the load-bearing capacity of the caissons. The washed crushed rock surrounding the caissons ensures that intruding groundwater preferentially flows away

<sup>17</sup> Short lived waste is defined as radioactive waste that does not contain significant levels of radionuclides with half-lives longer than 31 years; 31 years is used by SKB instead of 30 years as defined in the IAEA Safety glossary, in order to include <sup>137</sup>Cs. A separate facility is envisaged for long-lived radioactive waste that must be isolated from the environment for a longer time than the waste in SFR [SKB, 2015].

<sup>18</sup> The extension is called SFR 3 since the name SFR-2 was used in a previous plan to build vaults adjacent to SFR 1 for disposal for reactor core components and internal parts. The current plan is to dispose of this waste in a separate facility [SKB, 2014a].

from the caissons. The following figure shows the disposal cells for containing the types of waste with the largest volumes.

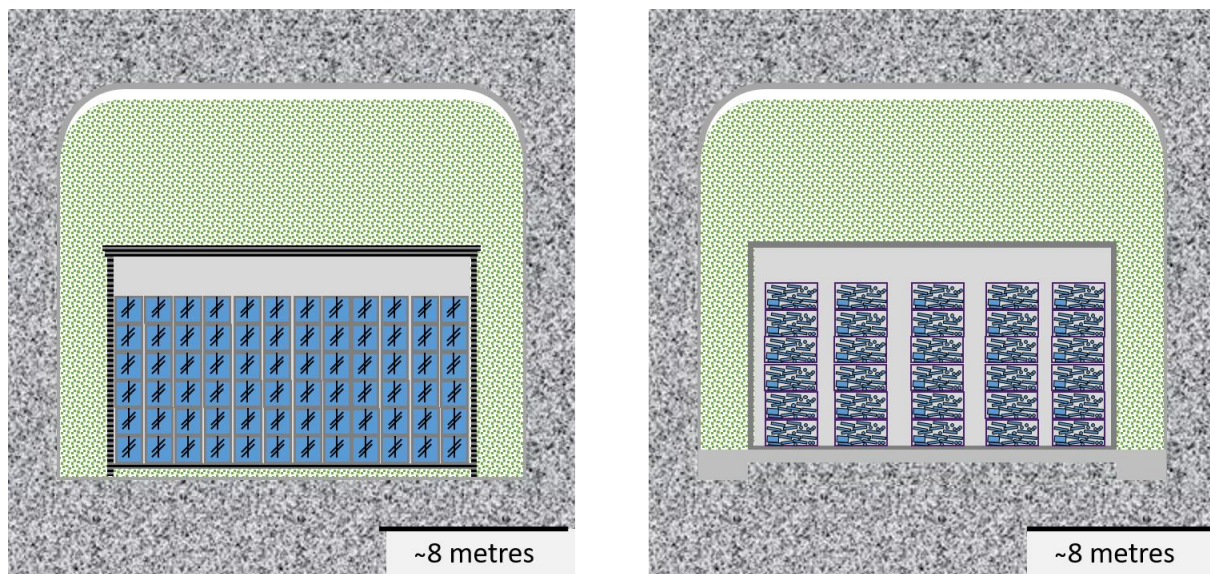


Figure 186-18-1: Disposal cell containing ILW operating (left, 1BMA) and considered in Sweden (right, 2BMA) in the host rock granite, adapted from SKB's report [SKB, 2014a]. Blue = cemented ILW and steel ILW, black = steel sacrificial stirrer, rebar or walls tetramoulds, crushed rock (green), air (white), shotcrete = light grey. A constraining wall of concrete is casted to prevent crushed rock entering the access tunnels. A concrete plug and bentonite seals are fabricated against the constraining wall.

## 18.2 Chemical evolution of the ILW disposal cell

Changes in climate will change the temperature in the disposal facility due to the shallow disposal depth of SFR and after around 52,000 years, a temperature low enough for concrete to freeze ( $-3^{\circ}\text{C}$ ) will occur. The freezing and thawing degrades concrete completely. Also, due to the shallow depth, the current brackish granitic pore water to which the disposal facility is currently exposed will change into fresh granitic pore water after 2,000 years. Reactive transport modelling of multiple chemical components has been performed with the PHAST program [Parkhurst, 2010] in 2 dimensions to evaluate the chemical evolution of the concrete barriers. Two geochemical databases, CEMdata07 and Minteq-2001, have been used to assess the sensitivity of the results to the thermodynamic constants and mineral assemblage assumed in the calculations. The exclusion of Friedel salt in Cemdata07 neglects pore-blocking. The porosity needs to be constant in PHAST but the available models that do include the porosity changes and resulting hydraulic conductivity have not been considered since the gradual deterioration of hydraulic properties is expected to be mainly governed by physical degradation processes that lead to fracture formation. The changes in porosity have been calculated with the evolving mineral assemblage and fracture formation is assumed to be associated when the formation of thaumasite and ettringite results in a smaller porosity than the initial porosity. The formation of these calcium-sulphate minerals makes concrete losing its strength and integrity by peeling off parts of the concrete along moving fronts. This process is taken into account by doubling the effective diffusivity. This formation of these calcium-sulphate minerals would not be identified in parts of concrete that are more located further away from the interface with crushed rock if the hydraulic properties remain unchanged [Höglund, 2014]. The corrosion of grouted metallic waste may cause and rebars in structural concrete may cause fracture of concrete if the strain caused by the formation rate of corrosion products cannot be accommodated by creep of concrete [Höglund, 2014].

## 19. Switzerland

NAGRA participates in EURAD and has been asked to contribute to this ACED deliverable about the current handling of the chemical evolution in their Waste disposal concept. This section is authored by Erika Neeft and has been revised by Lukas Martin from NAGRA.

For the disposal of nuclear waste in Switzerland, Opalinus Clay has been chosen as a reference host rock and NAGRA is currently in the site selection stage. The repository induced effects have been summarised in two NAGRA documents the for disposal of HLW- and L/ILW waste [Leupin, 2016a/b] where the relevance and couplings of temperature, rock-mechanical-, gas-related- and chemical effects have been summarised and assessed. The main waste to be disposed in the Swiss HLW repositories are spent fuel assemblies and vitrified HLW is only a minor waste fraction. Nevertheless, as this ACED work package focuses on vitrified waste, information about the chemical effects for the disposal of vitrified HLW have been extracted and summarised here.

### 19.1 Characterization of the HLW disposal cell in clay

Radionuclides are incorporated into a homogenous borosilicate glass matrix and the glass is poured into thin stainless-steel flasks. Two of these fabricated flask are loaded into a disposal canister. In the Swiss reference design, a carbon steel overpack is foreseen, whereas other materials are being evaluated (e.g. copper coated overpacks) as potential alternatives but not evaluated in the assessment of potential induced effects; a notion is made that if options other than carbon steel were to be implemented, the repository induced impacts related to gas production could be smaller (e.g. in the case of copper). The overpacks are emplaced on a pedestal of compacted bentonite. A cementitious liner is foreseen to support the cavern walls and assure operational safety of the disposal caverns and access tunnels and is designed to withstand the mechanical loads expected to arise during construction and operational phases. The remaining spaces are backfilled with highly compacted bentonite granules. At regular intervals, sealing sections are made in which there is no liner, in order to avoid any hydraulic shortcut along the walls; bentonite forms a watertight contact directly with the Opalinus Clay. The following figure shows an image of the disposal cell from the waste form until the host rock.

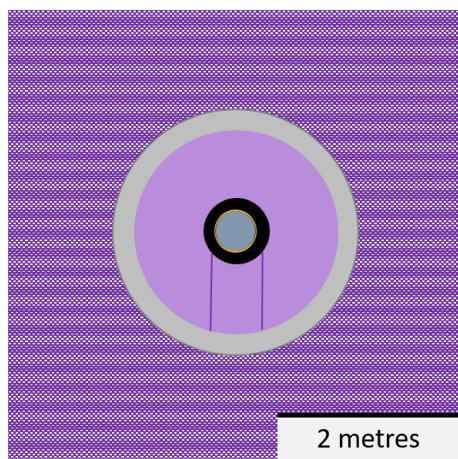


Figure 19-1: Disposal cell containing vitrified HLW considered in Switzerland for the host rock indurated clay. Grey = vitrified HLW, black = steel overpack, bentonite (purple) surrounds the overpack and cementitious liner = light grey.

The average thermal output at the time of closure of an individual waste container is 1350 W whereas the maximum heat output is 1500 W for the HLW containers. Calculated heat generation rates for HLW starting at slightly less than 1500 W show a decrease within the first period of 1000 years to less than 200 W (Fig A-7 in Leupin, 2016a).

## 19.2 Chemical evolution of the HLW disposal cell

The processes taking place during the chemical interactions between the steel overpack and bentonite, bentonite and cementitious liner and cementitious liner and Opalinus host rock have been identified and quantified. The porosities, mineralogical contents and pore water chemistries that have been used to obtain the geochemical modelling results in NAGRA's report [Leupin, 2016a] have been described in Bradbury et al [Bradbury, 2014].

### 19.2.1 Clay-cement interaction

For bentonite, the potential clay dissolution by the leached hydroxyl ions has been assessed by a mass balance calculation in which it takes 4.68 moles of hydroxyl ions to dissolve one mole of montmorillonite. The amount of altered bentonite is then determined by the thickness of the concrete liner. Figure 17 1 shows that the amount of cementitious material is small in the Swiss disposal cell. The extent of altered annulus of bentonite has been calculated to be 0.14 metre if an OPC based cementline with a thickness of 0.20 metre was used . In the Swiss programme, alkaline plumes have been concluded not be safety relevant since the amount of affected clay material, conservatively about 0.2 metre for bentonite and less than 0.1 metre for Opalinus clay, is too small to expect significant effects on dose rates. Pore clogging by precipitation of carbonates and sulphates by chemical interaction between cement and clay has been treated in more detail in order to investigate whether migration of gas could be limited to such an extent that a gas pressure built-up could occur. It has been concluded that it would be unlikely that pore clogging would be continuous along the disposal cells and more likely that the liner itself would be fractured over time allowing gas to migrate directly to the interface with the host rock.

### 19.2.2 Steel-bentonite interaction

The anaerobic corrosion of iron results into the release of dissolved iron species, hydrogen gas and hydroxyl ions. Reactions between montmorillonite, the swelling clay mineral in the bentonite buffer, and these released Fe-species may change the properties of bentonite by which chemical interaction between steel and bentonite is a non-linear process. The Swiss programme refers to Savage's work showing the potential impacts of the iron-bentonite interaction [Savage, 2014]. The released hydroxyl ions could increase the pH and accelerate clay dissolution. The same mass balance as discussed in the previous paragraph is used to determine the clay dissolution but here a clay dissolution rate is used that is determined with the release rate of hydroxyl ions by anaerobic corrosion of iron. Montmorillonite reacts with the dissolved iron species into non-swelling sheet silicates. The impacts of the growth of these silicates are the increase in hydraulic conductivity of the bentonite buffer and decrease in swelling pressure. The dissolved iron species can also be sorbed to montmorillonite and hydrogen gas could reduce sorbed iron. This reduction could increase the surface charge of clay minerals and thereby reducing the swelling pressure and increase the hydraulic conductivity. Reference is made to Didier's work to conclude that this process is not likely to happen [Didier, 2012]. The annular thickness of the altered bentonite as a function of time is determined by the release rate of iron dissolved species by anaerobic corrosion and mineral transformation of montmorillonite into a non-swelling mineral with a mass balance in which it takes 4.18 moles of ferrous ions to dissolve one mole of montmorillonite. Long-term anaerobic corrosion rates are 1 to 2  $\mu\text{m}$  per year [King, 2008] and a mean rate of 1.5  $\mu\text{m}$  per year has been used. The altered annulus of bentonite after 10.000 years becomes 0.08 metre and 0.54 metre after 100.000 years. Reference is made to reaction-transport simulations in which all potential mineralogical alterations are included. These simulation results show that the altered thickness of bentonite after 10.000 years and 100.000 years remains below 0.2 metre, even at 100°C [Marty, 2010].

## 20. United Kingdom

RWM participates in EURAD and has therefore been asked to contribute to this ACED deliverable about the current handling of the chemical evolution in their waste disposal concepts. Mike Poole has completed an ACED template that can be found in Appendix F.

There are no sites for disposal facilities yet in the UK. RWM is developing a generic Disposal System Safety Case (DSSC), which shows how the waste inventory destined for geological disposal could be safely disposed of in a range of geological environments in order to build confidence in the safety of a future geological disposal facility (GDF) for the UK. The latest DSSC has been published in 2016 and the previous one in 2010. The Engineered Barrier System Status Report [RWM, 2016a] and the Generic Post-closure performance modelling [RWM, 2016b] have been looked at for this ACED deliverable. The latest issue additionally includes understanding from research carried out since 2010. The geological formations that are investigated to host a GDF are clay, rock salt and crystalline rock. These clays are called lower strength sedimentary rock in DSSC and the disposal concepts developed by the Swiss WMO NAGRA for HLW and ILW are used as illustrative examples. Crystalline rock is called higher strength rock in DSSC and the illustrative disposal concept example for HLW is KBS-3V which envisages vertical (V) emplacement of copper canisters containing spent fuel, KBS is kärnbränslesäkerhet is the Swedish abbreviation for nuclear fuel safety. Finland is constructing a disposal facility to emplace these copper canisters following KBS-3V. The vitrified HLW is envisaged also to be packaged in copper canisters in the UK if a site with crystalline rock has been found. The material between the canister and granitic host rock is bentonite as in the Swedish and Finnish disposal designs.

RWM has developed its own disposal concept in crystalline rocks for ILW of which the Nirex Reference Vault Backfill (NRVB) is probably best known. NRVB is made with Portland cement, limestone aggregates and water. This backfill provides the alkaline conditions to suppress dissolved concentrations of many important radionuclides and sorption capacity of the ILW disposal concept. It has a high porosity of 50% and consequently a high permeability and a small compressive strength i.e. 6 MPa, 28 days after curing, facilitating retrievability via high-pressure water-jetting (prior to closure). The high permeability and porosity to ensure both homogeneous chemical conditions (so that localised concentrations of materials in wastes will not exhaust the desired chemical conditioning and thereby locally reduce the containment performance) and to permit the escape of gas generated by chemical reactions within the disposal area. The waste packages are steel drums in which ILW has been grouted off.

## 21. References

[AK Steel, 1986] Product data sheet from AK Steel for 316/316L Stainless steel

[Alcolea, 2014] Alcolea A, Kuhlmann U, Lanyon GW, Marschall P, Hydraulic conductance of the ECZ around underground structures of a geological repository for radioactive waste - A sensitivity study for the candidate host rocks in the proposed siting regions Northern Switzerland, NAGRA Arbeitsbericht 13-94 (2014) 1-101.

[Andersson, 1989] Andersson K, Allard B, Bengtsson M, Magnusson B, Chemical composition of cement pore solutions, Cement and Concrete Research nr. 19 (1989) 327-332.

[ANDRA, 2016a] Andra (2016a) Safety Options Report - Operating Part (DoS-Expl).

[ANDRA, 2016b] Andra (2016b) Safety Options Report - Operating Part (DoS-AF).

[Appelo, 1993] Appelo CAJ, Postma D (1993) Geochemistry, Groundwater and pollution. Balkema, Rotterdam.

[AREVA, 2001] AREVA, Specification for compacted waste standard residue (CSD-c) from light water reactor fuel (2001) 1-22 (Confidential document not published openly).

[AREVA, 2007] AREVA, Specification for standard vitrified waste residue (CSD-v) with high actinide content produced at la Hague (2007) 1-23 (Confidential document not published openly).

[Arnold, 2015a] Arnold P, Vardon PJ, Hicks MA, Fokkens J, Fokker PA, A numerical and reliability based investigation into the technical feasibility of a Dutch radioactive waste repository in Boom Clay, OPERA-PU-TUD311 (2015) 1-317

[Arnold, 2015b] Arnold P, Vardon PJ, Hicks MA, Preliminary assessment of tunnel stability for a radioactive waste repository in Boom Clay, Engineering Geology for Society and Territory 6 (2015) 545-549.

[Atabek, 1991] Atabek R, Beziat A, Coulon H Dardaine M, Debrabant P, Eglem A, Farcy C, Fontan N, Gatabin C, Gegout P, Lajudie A, Landoas O, Lechelle J, Plas F, Proust D, Raynal J, Revertegeat E, Near field behaviour of clay barriers and their interaction with concrete, Task 3: Characterization of radioactive waste forms. A series of final reports (1985-1989). No 26 EUR 13877 (1991) 1-63.

[AtG, 1985] AtG, Gesetz über die friedliche Verwendung der Kernenergie und den Schutz gegen ihre Gefahren (Atomgesetz – AtG) vom 15. Juli 1985 (BGBl. I S. 1565), amended 10. Juli 2018 (BGBl. I S. 1122, 1124).

[Atkins, 1991] Atkins M, Beckley N, Carson S Cowie J, Glasser FP, Kindness A, Macphee D, Pointer C, Rahman A, Jappy JG, Evans PA, McHugh G, Natingley NJ, Wilding C, Medium-active waste form characterization: the performance of cementbased systems Task 3 Characterization of radioactive waste forms A series of final reports (1985-1989) No1 EUR 13542 (1991) 1-164.

[Atkinson, 1985] Atkinson A, Goult DJ, Hearne JA, An assessment of the long-term durability of concrete in radioactive waste repositories, Mat Res Soc Symp Proc 50 (1985) 239-246.

[Atomic Act, 2016] Act No. 263/2016 of Coll., OF 14th July 2016, Atomic Act

[Auqué, 2006] Auqué LF, Gimeno MJ, Gómez JB, Puigdomenech I, Smellie J, Tullborg E-L, Groundwater chemistry around a repository for spent nuclear fuel over a glacial cycle – Evaluation of SR-Can, SKB Technical report TR-06-31 (2006) 1-118.

[Barth, 2014] Barth N, George D, Ahzi S, Rémond Y, Joulaee N, Khaleel MA, Bouyer F, Simulation of cooling and solidification of three-dimensional bulk borosilicate glass: effect of structural relaxations, Mech Time-Depend Mater 18 (2014) 81-96.

[Baxter, 2018] Baxter S, Appleyard P, Hartley L, Hoek J, Williams T, Exploring conditioned simulations of discrete fracture networks in support of hydraulic acceptance of deposition holes, Posiva SKB report 07 (2018) 1-109.

[Bernier, 2007] Bernier F, Li XL, Bastiaens W, Ortiz L, Van Geet M, Wouters L, Frieg B, Blümling P, Desrues J, Viaggiani G, Coll C, Chancole S, De Greef V, Hamza R, Malinsky L, Vervoort A, Vanbrabat Y, Debecker B, Verstraelen J, Govaerts A, Wevers M, Labiouse V, Escoffier S, Mathier J-F, Gastalso L, Bühler Ch, Fractures and Self-healing within the Excavation Disturbed Zone in Clays (SELFRAC), EUR 22585 (2007) 1-56.

[Berner, 1992] Berner UR, Evolution of pore water chemistry during degradation of cement in a radioactive waste repository environment, Waste management 12 (1992) 201-219.

[Bertrams, 2017] Bertrams N, Herold P, Herold M, Krone J, Lommerzheim A, Prignitz S, Kuate ES (2017), Entwicklung eines technischen Konzeptes für ein generisches Endlager für wärme-entwickelnde Abfälle und ausgediente Brennelemente im Kristallingestein in Deutschland. DBEtec, Report TEC-20-2017-AB.

[Bethke, 2018] Bethke CM, Yeakel S (2018): The Geochemist's Workbench®, Release 11. GWB Essentials Guide. – Aqueous Solutions, LLC, Champaign, Illinois. 190 str.

[BfS, 2014] BfS (2014), Anforderungen an endzulagernde radioaktive Abfälle (Endlagerungsbedingungen, Stand: Dezember 2014) – Endlager Konrad, Bundesamt für Strahlenschutz, interner Bericht SE-IB-29/08-REV-2, Dezember 2014.

[BfS, 2017] BfS (2017), Federal Office for Radiation Protection: Requirements on radioactive waste for disposal (Waste acceptance requirements as of February 2017) - Konrad Repository; February 2017.

[BGR, 2007] BGR (2007), Bundesanstalt für Geowissenschaften und Rohstoffe: Endlagerung radioaktiver Abfälle in Deutschland – Untersuchung und Bewertung von Regionen mit potenziell geeigneten Wirtsgesteinsformationen, April 2007.

[Blaheta, 2012] Blaheta R, Malik J, Thermal analysis of reference design of DGR for spent fuel assemblies, SURAO report, December 2012 (in Czech)

[BMU, 2010] BMU (2010), Federal Ministry for the Environment, Nature Conservation, and Nuclear Safety: Safety requirements governing the final disposal of heat-generating radioactive waste; September 2010.

[BMUB, 2014] BMUB (2014), Federal Ministry for the Environment, Nature Conservation, Building and Nuclear Safety: Joint Convention on the Safety of Spent Fuel Management and on the Safety of Radioactive Waste Management - Report of the Federal Republic of Germany for the Fifth Review Meeting in May 2015; August 2014.

[BMUB, 2015a] BMUB (2015a), Federal Ministry for the Environment, Nature Conservation, Building and Nuclear Safety: Inventory of radioactive waste - Current inventory as at 31 December 2014 and prediction; August 2015.

[BMUB, 2015b] BMUB (2015b), Federal Ministry for the Environment, Nature Conservation, Building and Nuclear Safety: Program for the responsible and safe management of spent fuel and radioactive waste (National program); August 2015.

[BMUB, 2018] BMUB (2018), Federal Ministry for the Environment, Nature Conservation, Building and Nuclear Safety: Joint Convention on the Safety of Spent Fuel Management and on the Safety of Radioactive Waste Management - Report of the Federal Republic of Germany for the Sixth Review Meeting in May 2018;

[Bock, 2010] Bock H, Dehandschutter B, Derek Martin C, Mazurek M, de Haller A, Skoczylas F, Davy C, Self-sealing of fractures in argillaceous formations in the context of geological disposal of radioactive waste, OECD NEA No. 6184 (2010) 1-310.

[Bradbury, 2014] Bradbury MH, Berner U, Curti E, Hummel W, Kosakowski G, Thoenen T, The Long Term Geochemical Evolution of the Nearfield of the HLW Repository, NAGRA Technical Report 12-01 (2014) 1-134.

[Bruggeman, 2011] Bruggeman C, De Craen M (2012). "Boom Clay natural organic matter. Status Report 2011." SCK•CEN Report ER-189. SCK•CEN Report ER-206.

[Brewitz, 1982] Brewitz, W. (ed.) (1982), Eignungsprüfung der Schachanlage Konrad für die Endlagerung radioaktiver Abfälle. Abschlussbericht GSF-T-136 Vol. 1.

[Carlsson, 2007] Carlsson A, Christiansson, R, Construction experiences from underground works at Forsmark, SKB report R-07-10 (2007) 1-85.

[CCM, 2016] Cibelcor, Belgian company CEM I 52.5 N SR3 LA, September 2016

[Červinka, 2018] Červinka R, Klajmon M, Zeman J, Vencelides T (2018) Geochemical calculations and reactive transport modelling, SURAO technical report 271/2018/ENG

[Chamssedine, 2010] Chamssedine F, Sauvage T, Peugeot S, Fares T, Martin G, Helium diffusion coefficient measurements in R7T7 nuclear glass by  $^3\text{He}(d, \alpha)^1\text{H}$  nuclear reaction analysis, Journal of Nuclear Materials (2017) 175-181.

[Cloet, 2019] Cloet V, Lothenbach B, Lura P, Kosakowski G, Curti E, Wieland W, Lanyon GW, Diomidis N, Leupin O, Cementitious backfill for a high-level waste repository: impact of repository-induced effects, NAB 18-41 (2019) 1-116.

[COMSOL, 2018] Built in Library in COMSOL Multiphysics 5.3a.

[Craeye, 2009] Craeye B, De Schutter G, Van Humbeeck H, Van Cotthem A (2009). Early age behaviour of concrete supercontainers for radioactive waste disposal. Nuclear engineering and design, 239:23-32.

[CUR 181, 1995] Civieltechnisch Centrum Uitvoering Research en Regelgeving (CUR) Werken met schuimbeton, Eigenschappen en toepassingen, Rapport 181 (1995) 1-104, only in Dutch describing foamed concrete

[De Craen, 2004] De Craen M (2004), "Geochemistry of Boom Clay pore water at the Mol site. Status 2004." SCK•CEN report BLG-990.

[De Craen, 2011] De Craen M., Honty M., Van Geet M., Weetjens E., Sillen X., Wang L., Jacques, D., Martens, E. (2011). "Overview of the oxidation around galleries in Boom Clay (Mol, Belgium) - Status 2008." SCK•CEN Report ER-189.

[de Combarieu, 2007] de Combarieu G, Barboux P, Minet Y, Iron corrosion in Callovo-Oxfordian argillite: From experiments to thermodynamic/kinetic modelling, Physics and Chemistry of the Earth, 32 (2007) 346–358.

[Deissman, 2016] Deissman G, Haneke K, Filby A, Wiegers R, Dissolution behaviour of HLW glasses under OPERA repository conditions, OPERA-PU-IBR511A (2016) 1-57, Appendix 1-14.

[Didier, 2012] Didier M, Leone L, Greneche JM, Giffaut E, Charlet L, Adsorption of hydrogen gas and redox processes in clay, Environmental Science & Technology 46[4] (2012) 3574-3579.

[Dizier, 2017] Dizier D, Chen G, Li XL, Rypens J, The PRACLAY heater test after two years of the stationary phase, EURIDICE report EUR\_PH\_17\_043 (2017) 1-65.

[Drake, 2006] Drake H, Sandström B, Tullborg E-V, Mineralogy and geochemistry of rocks and fracture fillings from Forsmark and Oskarshamn: Compilation of data for SR-Can, SKB report R-06-109 (2006\_1-105).

[Dufour, 2000] Dufour FC, Groundwater in the Netherlands,: facts and figures, Netherlands Institute of Applied Geoscience TNO (2000) 1-97.

[Durce, 2018] Durce D, Aertsens M, Jacques D, Maes N, Van Gompel (2018) Transport of dissolved organic matter in Boom Clay: Size effects. *Journal of Contaminant Hydrology*, 208:27-34.

[ENRESA, 2000] ENRESA (2000) Evolución termo-hidro-mecánica del campo cercano. ENRESA-AGP 49-1PP-I-10-01 Rev. A. ENRESA (in Spanish).

[ENRESA, 2001] ENRESA (2001) Evaluación del comportamiento y de la seguridad de un almacén geológico profundo de residuos radiactivos en arcilla. ENRESA (in Spanish).

[ENRESA, 2004] ENRESA (2004) Evaluación del comportamiento y de la seguridad de un almacén geológico profundo de residuos radiactivos en arcilla. Clave: 49–1PP-M-A1–01. ENRESA (in Spanish).

[Fujisawa, 1997] Fujisawa R, Cho T, Sugahara K, Takizawa Y, Horikawa Y, Shiomi T, Hironaga M, The corrosion behaviour of iron and aluminium under waste disposal conditions, *Mat Res Soc Symp Proc* 465 (1997) 675-682.

[Garrels, 1965] Garrels RM, Christ CL, 1965. *Solutions, minerals and equilibria*. Freeman Cooper, San Francisco.

[Gaucher, 2006] Gaucher E. C., Blanc P., Bardot F., Braibant G., Buschaert S., Crouzet C., Gautier A., Girard J. P., Jacquot E., Lassin A., Negrel G., Tournassat C., Vinsot A. & Altmann S. (2006) Modelling the porewater chemistry of the Callovian-Oxfordian formation at a regional scale. *Comptes Rendus Geoscience* 338, 917-930

[Gaucher, 2009] Gaucher E. C., Tournassat C., Pearson F. J., Blanc P., Crouzet C., Lerouge C. & Altmann S. (2009) A robust model for pore-water chemistry of clayrock. *Geochimica et Cosmochimica Acta* 73, 6470–6487.

[Gin, 2015] Gin S., Jollivet P., Fournier M., Berthon C., Wang Z., Mitroshkov A., Zhu Z. & Ryan J. V. (2015) The fate of silicon during glass corrosion under alkaline conditions: a mechanistic and kinetic study with the International Simple Glass, *Geochim. et Cosmochim. Acta*, 151, 68-85.

[Gondolli, 2018] Gondolli J, Dobrev D, Klajmon M, Černoušek T, Kouřil M, Stouilil M, (2018), Corrosion products, SURAO technical report 329/2018/ENG

[Gras, 2014] Gras J-M, State of the art of 14C in Zircaloy and Zr alloys – 14C release form zirconium alloy hulls, (D3.1) CAST report (2014) 1-104.

[Griffioen, 2016] Griffioen J, Verweij H, Stuurman R, The composition of groundwater in Palaeogene and older formations in the Netherlands. A synthesis, *Netherlands Journal of Geoscience* 95[3] (2016) pp. 349-372.

[Griffioen, 2017] Griffioen J, Koenen M, Meeussen H, Cornelissen P, Peters L, Jansen S, Geochemical interactions and groundwater transport in the Rupel Clay. A generic analysis. OPERA-PU-TNO522 (2017) 1-110.

[Gruppelaar, 1998] Gruppelaar H, Kloosterman JL Kloosterman, Konings RJM, *Advanced Technologies for reduction of nuclear waste*, ECN-R—98-008 (1998) 1-103.

[Helgeson, 1974] Helgeson HC, Kirkham DH (1974) Theoretical prediction of the thermodynamic behaviour of aqueous electrolytes at high pressures and temperatures: II. Debye-Hückel parameters for activity coefficients and relative partial molal properties, *Am. J. Sci.* 274, 1199-1261.

[Hermansson, 2004] Hermansson H-P, The Stability of Magnetite and its Significance as a Passivating Film in the Repository Environment, SKI Report 2004:07 (2004) 1-47.

[HCM, 2020] Hollandse Cement Maatschappij Technische Fiche CEM II/B-V 42.5 N, CEM III/A 42.5 N, CEM III/B 42.5 N -LH/SR, February 2020.

[Höglund, 2014] Höglund LA, The impact of concrete degradation on the BMA barrier functions, R-13-40 (2014, updated 2018/03) 1-485.

[Honty, 2012] Honty M, De Craen M Boom Clay mineralogy – qualitative and quantitative aspects – status 2011, SCKCEN-ER-194 (2012) 1-94.

[Hsieh, 2002] Hsieh PA, Winston RB (2002): User's guide to model viewer, a program for three-dimensional visualization of ground-water model results. – U.S. Geological Survey Open-File Report 02-106, 18 p

[Hummel, 2002] Hummel W et al. Nagra/PSI Chemical Thermodynamic Data Base 01/01. Radiochimica Acta 90 (2002) 805–813.

[Hunter, 2007] Hunter F, Bate F, Heath T, Hoch A (2007): Geochemical investigation of iron transport into bentonite as steel corrodes. – SKB Technical Report TR-07-09. Svensk Kärnbränslehantering AB, Stockholm, Sweden.

[IAEA, 2009] IAEA (2009), Classification of radioactive waste, IAEA Safety Standards Series No. GSG1, Vienna; November 2009.

[Idiart, 2019] Idiart A. and Laviña M. (2019) Final results and main outcomes of the Modelling Task. Deliverable n°D3.07. CEBAMA European Project n° 662147

[Ikonen, 2015] Ikonen K, Raiko H, Thermal Analysis of KBS-3H Repository, Working Report 2015-01, Posiva Oy, 2015

[Jackson, 2017] Jackson MD, Mulchay SR, Chen H, Li H, Li Q, Cappelletti P, Wenk H-R, Philipsite and Al-tobermite mineral cements produced through low-temperature water-rock reactions in Roman marine concrete, American Mineralogist Vol. 102 (2017) 1435-1450.

[Jobmann, 2007] Jobmann M, Uhlig L, Amelung P, Billaux D, Polster M, Schmidt H (2007), Untersuchung zur sicherheitstechnischen Auslegung eines generischen Endlagers in Tonstein in Deutschland – GENESIS. DBEtec, Report

[Jobmann, 2016] Jobmann M, Becker DA, Hammer J, Jahn S, Müller-Hoeppe N, Noseck U, Krone J, Weber JR, Weitkamp A, Wolf J. (2016), Projekt CHRISTA – Machbarkeitsuntersuchung zur Entwicklung einer Sicherheits- und Nachweismethodik für ein Endlager für Wärme entwickelnde radioactive Abfälle im Kristallingestein in Deutschland. DBEtec/BGR/GRS, Report TEC-20-2016-AB.

[Jobmann, 2017a] Jobmann M, Bebiolka A, Jahn S, Lommerzheim A, Maßmann J, Meleshyn A, Mrugalla S, Reinhold K, Rübél A, Stark L, Ziefle G (2017a), Projekt ANSICHT – Sicherheits- und Nachweismethodik für ein Endlager im Tongestein in Deutschland. DBEtec/BGR/GRS, Report TEC-19-2016-AB.

[Jobmann, 2017b] Jobmann M, Bebiolka A, Burlaka V, Herold P, Jahn S, Lommerzheim A, Maßmann J, Meleshyn A, Mrugalla S, Reinhold K, Rübél A, Stark L, Ziefle G (2017b), Safety assessment methodology for a German high-level waste repository in clay formations. Journal of Rock Mechanics and Geotechnical Engineering 9, 856-876.

[Johnson, 2000] Johnson J, Anderson F, Parkhurst DL Database thermo.com.V8.R6.230, Rev 1.11. – Lawrence Livermore National Laboratory, Livermore, California.

[Kärki, 2006] Kärki A, Paulamäki S, Petrology of Olkiluoto, Posiva 2006-02 (2006) 1-77.

[Kempl, 2015] Kempl J, Copuroglu O, The interaction of pH, pore solution composition and solid phase composition of carbonated blast furnace slag cement paste activated with aqueous sodium monofluorophosphate, 15<sup>th</sup> Euroseminar on Microscopy Applied to Building Materials, Delft Netherlands (2015) 287-296.

[King, 2008] King F, Corrosion of carbon steel under anaerobic conditions in a repository for SP and HLW in Opalinus Clay, NAGRA Technical Report 08-12 (2008) 1-44.

[Kobylka, 2017] Kobylka D, Thermal dimensioning of DGR for WWER 440 and WWER 1000 spent fuel assemblies, SURAO report 135/2017 (in Czech)

[Kursten, 2015] Kursten B, Druyts F, Assessment of the uniform corrosion behaviour of carbon steel radioactive waste packages with respect to the disposal concept in the geological Dutch Boom Clay formation OPERA-PU-SCK513 (2015) 1-107.

[Lacher, 1937] Lacher JR, A theoretical formula for the solubility of hydrogen in palladium, Proceedings of the Royal Society of London, A 161 (1937) 525-545.

[Lensa, 2008] von Lensa, Werner, Rahim Nabbi, and Matthias Rossbach, (Ed.). (2008), "RED-IMPACT Impact of partitioning, transmutation and waste reduction technologies on the final nuclear waste disposal. Synthesis report." Forschungszentrum Jülich

[Leupin, 2016a] Leupin OX, Smith P, Marschall P, Johnson L, Savage D, Cloet V, Schneider J and Senger R, High-level waste repository-induced effects, NAGRA Technical Report 14-13 (2016) 1-100.

[Leupin, 2016b] Leupin OX, Smith P, Marschall P, Johnson L, Savage D, Cloet V, Schneider J and Senger R, Low- and intermediate-level waste repository-induced effects, NAGRA Technical Report 14-14 (2016) 1-89.

[Lu, 2011] Lu C, Samper J, Fritz B, Clement A, Montenegro L (2011) Interactions of corrosion products and bentonite: an extended multicomponent reactive transport model. Phys. Chem. Earth 36, 1661-1668. <http://dx.doi.org/10.1016/j.pce.2011.07.013>.

[Mäder, 2009] Mäder, U (2009) Reference pore water for the Opalinus Clay and "Brown Dogger" for the provisional safety analysis in the framework of the sectoral plan – interim results (SGT-ZE), NAGRA Arbeitsbericht (2009) 1-45.

[Mallison, 2009] Mallison LG, Davies ILI, A historical examination of concrete EUR 10937 (1987) 1-309.

[Marty, 2010] Marty NCM, Fritz B, Clément A, Michau N, Modelling the long term alteration of the engineered bentonite barrier in an underground radioactive waste repository, Applied Clay Science 47 (2010) 82-90.

[Marty, 2014a] Marty NCM, Bildstein O, Blanc P, Claret F, Cochepin B, Gaucher EC, Jacques D, Lartigue JE, Liu S, Mayer KU, Meeussen JCL, Munier I, Pointeau I, Su D, Steefel CI (2014a) Benchmarks for multicomponent reactive transport across a cement/clay interface. Computational Geosciences. 19, p635-653.

[Marty, 2014b] Marty NCM, Munier I, Gaucher EC, Tournassat C, Gaboreau S, Vong CQ, Giffaut E, Cochepin B, Claret F (2014b) Simulation of cement/clay interactions: Feedback on the increasing complexity of modelling strategies. Transport in Porous Media. 104, 385-405.

[Matsuda, 1992] Matsuda M, Nishi T, Chino K, Kikuchi M, Solidification of spent ion exchange resins using new cementitious material, Journal of Nuclear Science and Technology 29 [11] (1992) 1093-1099.

[Matsuo, 1996] Matsuo T, Matsuda M, Hironaga M, Horikawa Y, Effect of LiNO<sub>3</sub> on corrosion protection of aluminium wastes and their land disposal, Journal of Nuclear Science and technology 33[11] (1996) 85

[Mazurek, 2003] Mazurek M, Joe Person F, Volckaert G, Bock H, Features, Events and Processes Evaluation Catalogue for Argillaceous Media, NEA No 4437 (2003) 1-376.2-862.

[Mazurek, 2011] Mazurek M, Alt-Epping P, Bath A, Gimmi T, Waber HN, Buschaert S, De Cannière P, De Craen M, Gautschi A, Savoye S, Vinsot A, Wemaere I, Wouters L, Natural tracer profiles across argillaceous formations, Applied Geochemistry 26 (2011) 1035-1064.

[Mibus, 2018] Mibus J, Diomidis N, Wieland E, Swanton S, Final synthesis report on results from WP2 (D 2.18) CAST project report (2018) 1-41.

[Milický, 2019] Milický M, Uhlik J, Final 3D groundwater water flow models of potential deep repository sites, SURAO technical report 323/2019/ENG

[Müller-Vonmoos, 1983] Müller-Vonmoos M, Kahr G, Mineralogische untersuchungen von Wyoming Bentonit MX-80 und montigel, NAGRA Technical report 83-12 (1983) 1-15.

[Mon, 2017] Mon A, Samper J, Montenegro L, Naves A, Fernández J (2017) Long-term nonisothermal reactive transport model of compacted bentonite, concrete and corrosion products in a HLW repository in clay. J. Cont. Hydrol. 197, 1-16. <http://dx.doi.org/10.1016/j.jconhyd.2016.12.006>.

[NAGRA, 2008] NAGRA, Effects of post-disposal gas generation in a repository for low-an intermediate level waste sited in the Opalinus Clay of Northern Switzerland, NAGRA Technical report 08-07 (2008) 1-138.

[Naish, 1991] Naish CC, Balkwill PH, O'Brien TM, Taylor KM, Marsh GP, The anaerobic corrosion of carbon steel in concrete, Task 3 Characterization of radioactive waste forms A series of final reports (1985-1989) No 33, EUR 13663 (1991) 1-37.

[Neall, 1994] Neall F, Modelling of the near-field chemistry of the SMA repository at the Wellenberg site: application of the extended cement degradation model. NAGRA Technical report 94-03 (1994) 1-45

[Necib, 2018] Necib S, Ambard A, Bucur C, Caes S, Cochin F, Fulger M, Gras JM, Herm M, Kasprzak L, Legand S, Metz V, Perrin S, Sakuragi T, Suzuki-Muresan T, Final report on 14C behaviour in Zr fuel clad waste under disposal conditions (D3.20) CAST Project Report (2018) 1-35.

[Neeft, 2018] Neeft EAC, 14C exposure from disposal of radioactive waste compared to 14C exposure from cosmogenic origin, Radiocarbon 60[6] (2018) 1911-1923.

[Neeft, 201X] COVRA report: specification for the disposal package for Dutch heat generating waste for a GDF in poorly indurated clay; properties of concrete can be found in ACED D 2.11

[NIROND, 2013] ONDRAF/NIRAS Research, Development and Demonstration (RD&D) Plan for the geological disposal of high-level and/or long-lived radioactive waste including irradiated fuel in considered as waste - State of the art report as of December 2012, NIROND-TR-2013-12 E (2013) 1-411.

[NIROND, 2017] ONDRAF/NIRAS (2017), "Design and construction of the supercontainer for category C waste". NIROND-TR 2017-11E V2

[NIROND, 2017] ONDRAF/NIRAS (2017), "Design and construction of the geological disposal facility for category B and category C wastes". NIROND-TR 2017-12E V2

[NIROND, 2017] ONDRAF/NIRAS (2017), "Design and construction of the monolith B for category B wastes". NIROND-TR 2017-10E V2

[NIROND, 2019] ONDRAF/NIRAS (2019), "Updated GDF layout for the costing 2020", Note 2019-0293.

[Nordquist, 2008] Nordquist R. et al, Groundwater flow and hydraulic gradients in fractures and fracture zones at Forsmark and Oskarsham, SKB report, R-08-103, October 2008

[Nummi, 2018] Nummi O Safety case for Loviisa LILW repository 2018 - Main report. Fortum Report LO1-T3552-00023

[Ochs, 2004] Ochs M Talerico C, SR-Can. Data and uncertainty assessment. Migration parameters for the bentonite buffer in the KBS-3 concept. SKB Technical report TR-04-18, 2004.

[Olivella, 1996] Olivella S, Gens A, Carrera J, Alonso EE (1996) Numerical formulation for a simulator (CODE\_BRIGHT) for the coupled analysis of saline media. Eng. Comput. 13(7), 87-112.

[Olivella, 2002] Olivella S (2002) CODE\_BRIGHT User's Guide. Universidad Politécnic de Cataluña. Departamento de Ingeniería del Terreno. Barcelona. España.

[Padovani, 2017] Padovani C, Kind F, Lilja C, Féron D, Necib S, Crusset D, Deydier V, Diomidis N, Gaggiano R, Ahn T, Keech P, Macdonald DD, Asano H, Smart N, Hall DS, Hänninen H, Engelberg D, Noël JJ, Shoesmith DW, The corrosion behaviour of candidate materials for the disposal of high-level

waste and spent fuel – a summary of the state of the art and opportunities for synergies in future R&D, Corrosion Engineering, Science and Technology 52 S1 (2017) 227-231.

[Parkhurst, 1999] Parkhurst DL, Appelo CAJ (1999) User's guide to PHREEQC (version 2) - A computer program for speciation, batch-reaction, one-dimensional transport, and inverse geochemical calculations - U.S. Geological Survey Water - Resources Investigations Report 99-4259, 312 p

[Parkhurst, 2004] Parkhurst DL, Kipp KL, Engesgaard P, Charlton ASR (2004): PHAST — A program for simulating ground-water flow, solute transport, and multicomponent geochemical reactions. U.S. Geological Survey Techniques and Methods 6–A8. B.m.: U.S. Geological Survey.

[Parkhurst, 2010] Parkhurst DL, Kipp KL, Engesgaard P, Charlton ASR (2010): PHAST Version 2 — A program for simulating ground-water flow, solute transport, and multicomponent geochemical reactions. U.S. Geological Survey Techniques and Methods 6–A35. B.m.: U.S. Geological Survey.

[Parkhurst, 2013] Parkhurst DL, Appelo CAJ (2013) Description of input and examples for PHREEQC version 3—A computer program for speciation, batch-reaction, one-dimensional transport, and inverse geochemical calculations: U.S. Geological Survey Techniques and Methods, book 6, chap. A43, 497 p., available only at z: <http://pubs.usgs.gov/tm/06/a43/>.

[Pitkänen, 1996] Pitkänen P, Snellman M, Vuorinen U, On the origin and chemical evolution of groundwater at the Olkiluoto site, Posiva-96-06 (1996) 1-51.

[Pöhler, 2010] Pöhler, M., Amelung, P., Bollingerfehr, W., Engelhardt, H.J., Filbert, W., Tholen, M. (2010), Referenzkonzept für ein Endlager für radioaktive Abfälle in Tongestein – ERATO. DBEtec, Report TEC-28-2008-AB.

[Pointeau, 2008] Pointeau I, Coreau N, Reiller PE, 2008. Uptake of anionic radionuclides onto degraded cement pastes and competing effect of organic ligands, Radiochimica Acta Vol 96, 367-374.

[Poskas, 2006] Poskas P et al. Generic repository concept for RBMK-1500 spent nuclear fuel disposal in crystalline rocks in Lithuania. In: Proceedings of the International topical meeting TOPSEAL 2006, 2006 Sep 17-20, Olkiluoto information centre, Finland.

[Reimers, 1992] Reimers , Quality assurance of radioactive waste packages by computerized tomography, Task 3 Characterization of radioactive waste forms A series of final reports (1985-1989) No 37, EUR 13879 (1992) 1-74.

[Ribet, 2009] Ribet I, Bétrémieux S, Gin S, Angeli F, Jégu C, Long-term behaviour of vitrified waste packages, Proceedings Global 2009, Paris, France: September 6-11, 2009, paper 9038

[Rosca-Bocancea, 2017] Rosca-Bocancea E, Schröder TJ, Hart J, Safety assessment calculation: central assessment case of the normal evolution scenario OPERA-PU-NRG733 (2017) 1-45.

[RWM, 2016] RWM, Geological disposal - Engineered Barrier System Status report, NDA Report no. DSSC/452/01 (2016) 1-132.

[RWM, 2016b] RWM, Geological disposal - Generic Post-closure performance, NDA Report no. NDA/RWM/138 (2016) 1-143.

[Sakuragi, 2017] Sakuragi T, Final report on Zr alloys corrosion studies at RWMC CAST Project Report 3.17 (2017) 1-35.

[Samper, 1998] Samper J, Juncosa R, Delgado J, Montenegro L (1998) CORE-LE2D: A code for water flow and reactive solute transport. Users Manual. University of A Coruña.

[Samper, 2008] Samper J, Lu C, Montenegro L (2008) Coupled hydrogeochemical calculations of the interactions of corrosion products and bentonite. Phys. Chem. Earth 33, S306-S316. <http://dx.doi.org/10.1016/j.pce.2008.10.009>.

[Samper, 2011] Samper J, Yang C, Zheng L, Montenegro L, Xu T, Dai Z, Zhang G, Lu C, Moreira S, (2011) CORE2D V4: a code for water flow, heat and solute transport, geochemical reactions, and

microbial processes. In: Zhang, F., Yeh, G.-T., Parker, C., Shi, X. (Eds.), Chapter 7 of the Electronic Book Groundwater Reactive Transport Models. Bentham Science Publishers. ISBN: 978-1-60805-029-1, pp. 161-186.

[Samper, 2016] Samper J, Naves A, Montenegro L, Mon A (2016) Reactive transport modelling of the long-term interactions of corrosion products and compacted bentonite in a HLW repository in granite: uncertainties and relevance for performance assessment. Appl. Geochem. 67, 42-51. <http://dx.doi.org/10.1016/j.apgeochem.2016.02.001>.

[Savage, 2010] Savage D, Watson C, Benbow S, Wilson J Modelling iron-bentonite interactions., Applied Clay Science, 47 (2010) 91–98.

[Savage, 2014] Savage D, An Assessment of the Impact of the Long Term Evolution of Engineered Structures on the Safety-Relevant Functions of the Bentonite Buffer in a HLW Repository, NAGRA Technical Report 13-02 (2014) 1-62.

[Schröder, 2017a] Schröder TJ, Hart J, Meeussen JCL, Report on model parameterization - normal evolution scenario OPERA-PU-NRG725 (2017) 1-63.

[Schröder, 2017b] Schröder TJ, Rosca-Bocancea E, Effects of parameter uncertainty on the long-term safety OPERA-PU-732/746 (2017) 1-23.

[Sedighi, 2014] Sedighi M, Bennet D, Masum SA, Thomas HR, Johansson E, Analysis of Temperature Data at the Olkiluoto, Posiva Working report 2013-58 (2014) 1-87.

[Seetharam, 2015] Seetharam S, Jacques D, Potential degradation of the cementitious EBS components, their potential implications on safety functions and conceptual models for quantitative assessments OPERA-PU-SCK514 (2015) 1-91.

[Siitari-Kauppi, 2007] Siitari-Kauppi M, Leskinen A, Kelokaski M, Togneri L, Alonso U, Missana T, García-Gutiérrez M, Patelli A, Physical matrix characterisation: Studies of crystalline rocks and consolidated clays by PMMA method and electron microscopy as a support for diffusion analyses, Informes Técnicos CIEMAT 1127 (2007) 1-44.

[Sillen, 2007] Sillen C and Marivoet J. (2007), “Thermal impact of a HLW repository in clay.” SCK•CEN report ER-38.

[SKB, 2005] SKB, Hydrogeochemical evaluation Preliminary site description Forsmark area – version 2, R-05-17 (2005) 1-403.

[SKB, 2014a] SKB, Initial state report for the safety assessment SR-PSU (2014, updated 2015/10) 1-135.

[SKB, 2014b] SKB, Waste form and packaging process report for the safety assessment SR-PSU, TR-14-03 (2014) 1-237.

[SKB, 2015] SKB, Safety analysis for SFR Long-term safety – Main report for the safety assessment SR PSU, TR-14-01 (2015, updated in 2017/04) 1-500.

[Smart, 2017] Smart NR, Rance AP, Nixon DJ, Fennell PAH, Reddy B, Kursten B, Summary of studies on the anaerobic corrosion of carbon steel in alkaline media in support of the Belgian supercontainer, Corrosion Engineering, Science and Technology 52 [S1] (2017) 217-226

[Snellman, 1998] Snellman M, Pitkänen P, Luukkonen A, Ruotsalainen P, Leino-Forsman H, Vuorinen U Summary of Recent Observations from Hästholmen Groundwater Studies. Posiva Working Report 98-44 (1998) Posiva Oy

[Sneyers, 2008] Sneyers, Understanding and Physical and Numerical Modelling of the Key Processes in the Near Field and their Coupling for Different Host Rocks and Repository Strategies (NF-PRO) EUR 23730 (2008) 1-217.

[Soen, 2007] Soen HMM, Praktische Betonkennis, Cement&Beton centrum (2007) 1-200, in Dutch.

[Spinka, 2017] Spinka O, Grnuwald L, Zahradnik O, Veverka A, Fiedler F, Nohejl J et al., Siting study , Březový potok, SURAO report 139/2017

[StandAG, 2017] StandAG: Gesetz zur Suche und Auswahl eines Standortes für ein Endlager für Wärme entwickelnde radioaktive Abfälle (Standortauswahlgesetz — StandAG) vom 5. Mai 2017 (BGBl. I S. 1074); amended 20. Juli 2017 (BGBl. I S. 2808, 2834).

[Theramin, 2019] Derivation of the preliminary radiological WAC for Lithuania conditions (for untreated and thermally treated waste) /Draft report for Theramin project, 2019.

[Tittel, 1986] Tittel, G., Hollmann, A., Stier-Friedland, G., Warnecke, E. (1986), Ableitung von Sorptionsdaten aus experimentellen Untersuchungen - Schachanlage Konrad. Physikalisch-technische Bundesanstalt, Braunschweig, November 1986.

[Traber, 2013] Traber D, Blaser P, Gesteinsparameter der Wirtgesteine Opalinuston 'Brauner Dogger', Effinger Schisten und Helvetische Mergle als Grundlage für die Sorptionsdatenbank, NAGRA Arbeitsbericht 12-39 (2013) 1-108.

[Vaitkeviciene, 2017] Vaitkeviciene A, Narkuniene A, Application of surface complexation and ion exchange modelling for the estimation of bentonite sorption capacity on selected radionuclides under possible geological disposal conditions in Lithuania. Chemical Technology. 2017. Nr. 1 (68) (In Lithuanian).

[Van Humbeeck, 2007] Van Humbeeck H, De Bock C, Bastiaens W, Demonstrating the Construction and Backfilling feasibility of the supercontainer design for HLW, Proceedings RepoSafe, International Conference on Radioactive Waste Disposal in Geological Formations held in Braunschweig November 6 – 9 2007, 336-345.

[van Eijk, 2000] van Eijk RJ, Brouwers HJH, Prediction of hydroxyl concentrations in cement pore water using a numerical cement hydration model. Cement and concrete research no. 30 (2000) 1801-1806.

[Van Loon, 1995] Van Loon LR, Hummel W, The radiolytic and chemical degradation of organic ion exchange resins under alkaline conditions: effect on radionuclide speciation, NAGRA, Technical report 95-08 (1995) 1-96.

[Vehmas, 2019a] Vehmas T, Itälä A, Compositional parameters for solid solution C-S-H and the applicability for thermodynamic modelling, Proceedings of the 2nd Annual Cebama Workshop Proceedings KIT SR 7752 (2019) 293-300.

[Vehmas, 2019b] Vehmas T, Montoya V, Cruz Alonso M, Vašíček R, Rastrick E, Gaboreau S, Večerník P, Leivo M, Holt E, Ait Mouheb N, Svoboda J, Read D, Červinka R, Vasconcelos R, Corkhill C, Manuscript for peer-reviewed publication on results generated in WP1, Cebama project Deliverable 1.07 (2019) 1-21.

[Verhoef, 2014] Verhoef EV, de Bruin AMG, Wieggers RB, Deissman G, Cementitious materials in OPERA disposal concept in Boom Clay OPERA-PG-COV020 (2014) 1-17.

[Verhoef, 2016] Verhoef EV, Neeft EAC, Deissmann G, Filby A, Wieggers RB, Kers DA, Waste families in OPERA OPERA-PG-COV023 (2016) 1-39.

[Verhoef, 2017] Verhoef EV, Neeft EAC, Chapman NA, McCombie C, OPERA Safety case, COVRA publication (2017) 1-146.

[Verweij, 2016] Verweij JM, Nelskamp S, Definition of the present boundary conditions for the near-field model\_1, OPERA-PU-TNO421\_1 (2016) 1-37.

[Vienna, 2013] Vienna J. D., & Ryan J. V. (2013) Current understanding and remaining challenges in modeling long-term degradation of borosilicate nuclear waste glasses, International J. of Appl. Glass Sci., 4, 283-294.

[Vieno, 2003] Vieno T, Lehtikoinen J, Löfman J, Nordman H, Mészáros F, Assessment of disturbances caused by Construction and Operation of ONKALO, Posiva report 2003-06 (2003) 1-92.

[Vinsot, 2008] Vinsot, A., Mettler, S., and Wechner, S. (2008) - In situ characterization of the Callovo-Oxfordian pore water composition. Physics and Chemistry of the Earth, Parts A/B/C 33, S75-S86.

[Viršek, 2011] Viršek S, Near-surface disposal concept for a low and intermediate level waste repository in Slovenia - Argumentation of safety, Proceedings of the International Conference Nuclear Energy for New Europe, Bovec, Slovenia, Sept. 12-15 2011, 701.1-701.6.

[Vondrovic, 2015] Vondrovic L, [www.posiva.fi/4350/D3](http://www.posiva.fi/4350/D3) 7.1  
[Czech siting programme Vondrovic SURAO 2015.](#)

[Wang, 2009] Wang L (2009). "Near-field chemistry of a HLW/SF repository in Boom Clay – scoping calculations relevant to the Supercontainer design." SCK•CEN Report ER-17.

[Wang, 2010] Wang L, Jacques D, De Cannière P (2010). "Effects of an alkaline plume on the Boom Clay as a potential host formation for geological disposal of radioactive waste." SCK•CEN Report ER-28.

[Wanner, 1994] Wanner H, Albinsson Y, Wieland E, An ion exchange model for the prediction of distribution coefficients of caesium in bentonite, SKB Technical report 94-10 (1994) 1-29.

[Weetjens, 2005] Weetjens E, Sillen X (2005), "Thermal analysis of the Supercontainer concept. 2D axisymmetric heat transport calculations". SCK•CEN report R-4277.

[Weetjens, 2006] Weetjens E, Sillen X, Van Geet M (2006). "Mass and Energy Balance Calculations: contribution from SCK•CEN. Deliverable 5.1.2 of the NF-PRO project." EC, Brussels.

[Weetjens, 2009] Weetjens E, Update of the near field temperature evolution calculations for disposal of UNE-55, MOX-50 and vitrified HLW in a supercontainer based geological repository SCKCEN-ER-86 (2009) 1-14.

[Weetjens, 2012] Weetjens E, Marivoet J, Govaerts J (2012). "Preparatory safety assessment. Conceptual model description of the reference case." SCK•CEN Report ER-215.

[Wenk, 2008] Wenk HR, Voltolini M, Mazurek M, Van Loon L, Vinsot A, Preferred orientation and anisotropy of shales: Callo-Oxfordian shale (France) and Opalinus Clay (Switzerland) Clays and Clay minerals 56 [3] (2008) 285-306.

[Wersin, 2004] Wersin P, Curti E, Appelo CAJ, Modelling bentonite–water interactions at high solid/liquid ratios: swelling and diffuse double layer effects, Appl. Clay Sci. 26 (2004) 249-257.

[Wieland, 2016] Wieland E, Jakob A, Tits J, Lothenbach B, Kunz D, Sorption and diffusion studies with low molecular weight organic compounds in cementitious systems, Applied Geochemistry 67 (2016) 101-117.

[Yang, 2008] Yang C, Samper J, Montenegro L (2008) A coupled non-isothermal reactive transport model for long-term geochemical evolution of a HLW repository in clay. Environ. Geol. 53, 1627-1638. <http://dx.doi.org/10.1007/s00254-007-0770-2>.

[Yu, 2011] Yu, L., Weetjens, E. and Vietor, T (2011). "Integration of TIMODAZ Results within the Safety Case and Recommendations for Repository Design." SCK•CEN report ER-188.

[Yu, 2012] Yu L., Weetjens, E. (2012). "Evaluation of the gas source term for Spent Fuel (SF), Vitrified High-Level Waste (VHLW), compacted waste and MOSAIK." SCK•CEN Report ER-162.

## Appendix A. Presentation kick-off meeting from Hungary

# Kick-off meeting EURAD ACED Country: Hungary Organisation: Centre for Energy Research – MTA EK

Presenter: TBA (Margit Fabian-I can't be present)

Date: 2 July 2019

This presentation can be used in an Appendix for an ACED deliverable that will be published at the EURAD website

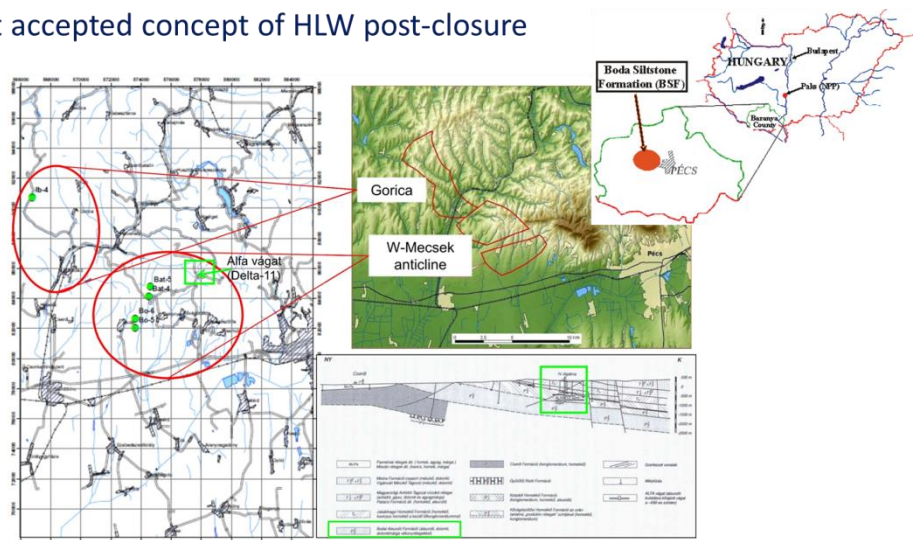
## At start of the post-closure phase: HLW

In Hungary - we have not accepted concept of HLW post-closure

We perform:

- intensive study of the **Boda Claystone Formation** considered as potential host rock for deep geological repository
- vitrification studies in lab-scale (structural studies, leaching tests, irradiation measurements)

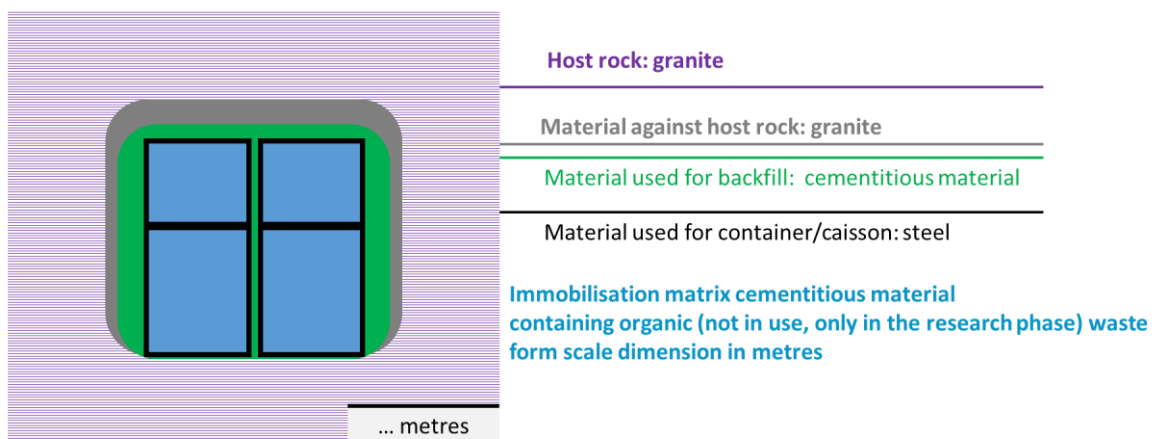
Establishment of deep geological repository:  
2064



## Expected contribution from ACED for HLW disposal cells

- increase understanding the surface reaction (exp. glass/steel, steel/clay)

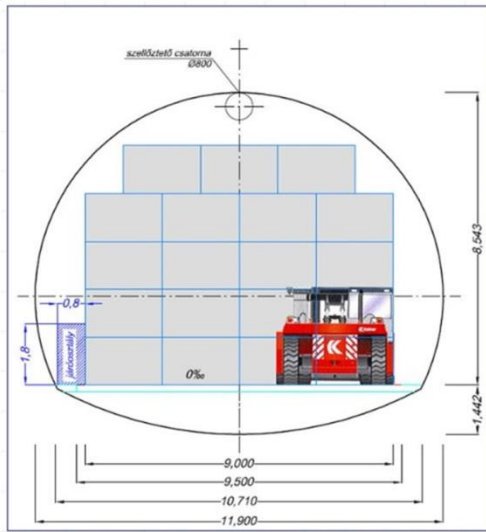
### At start of the post-closure phase: ILW



Reference of materials used in this disposal cell: [http://www.rhk.hu/wp/wp-content/uploads/2018/11/Magyarorsz%C3%A1g-nemzeti-programja\\_v%C3%A9gleges.pdf](http://www.rhk.hu/wp/wp-content/uploads/2018/11/Magyarorsz%C3%A1g-nemzeti-programja_v%C3%A9gleges.pdf) public accessible? Yes (but only in Hungarian)

## At start of the post-closure phase: ILW

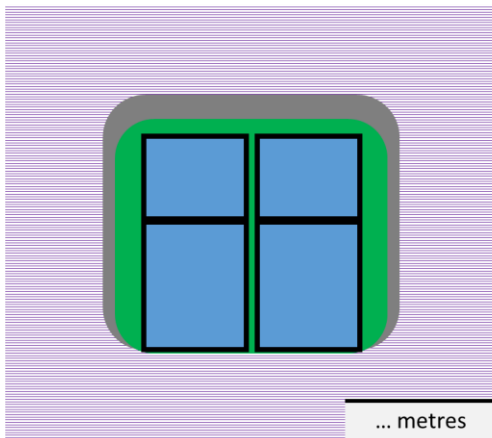
Working disposal system:



- nine container (200 l) in a ferro-concrete container  
- 19 ferro-concrete container in the borehole (in a row)



## Safety concept: ILW



Applying: stochastic, deterministic and fuzzy comparisons

**Criteria for assessing perturbation host rock: applied integrated hydrogeological and geological model**

**Criteria for material against host rock: apply integrated hydrogeological and geological model**

**Criteria for backfill:**

Considering: surface interactions, effect of pore water, failure curve features, gas formation

**Criteria for cementitious immobilisation matrix:**

Considering: diffusion coefficient (ASTM C1308), heat development, consistency, homogeneity, porosity, compressive strength

**+ biosphere model used IFEP list**

**+ natural analogues**

Reference for criteria set in this disposal cell and their rationale:

[http://www.rhk.hu/docs/eloadasok/NRHT\\_konferencia\\_2013/biztonsag/hosszutavu\\_biztonsagi\\_modellezes.pdf](http://www.rhk.hu/docs/eloadasok/NRHT_konferencia_2013/biztonsag/hosszutavu_biztonsagi_modellezes.pdf) public accessible? Yes (but only in Hungarian)

## Expected contribution from ACED for ILW disposal cells

- Preference cementitious matrix containing organic waste
  - Organic material is resin
- What are the reasons for your preference?
  - stabilization of organic waste has not been solved
  - we have a large amount of this type of waste

## Appendix B. Completed template from Romania

Current handling of the chemical evolution  
in Europe for EURAD ACED

Country: Romania

Organisation: Institute for Nuclear Research  
Pitesti

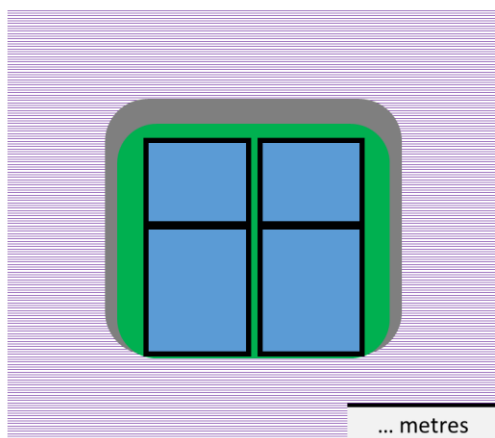
Author: Crina Bucur, Daniela Diaconu

Date: 18.10.2019

These sheets **can** be used in an Appendix for an ACED deliverable that will be published at the EURAD website

### At start of the post-closure phase: ILW

*please remove this sheet and next 3 sheets if intermediated level waste processed with cementitious materials is not considered in your national programme. Please show an image of your disposal cell with a scale dimension and complete the asked details; please remove the respective template sheet for which you cannot complete any requested detail.*



Host rock: no preferred host rock

Material against host rock: not decided yet

Material used for backfill: most probably bentonite

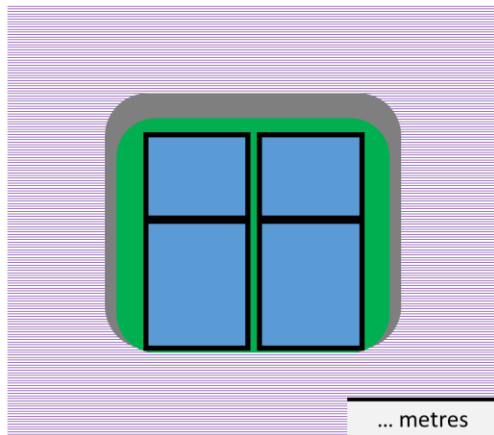
Material used for container/caisson: presumable cement based material

Immobilisation matrix cementitious material  
containing organic waste form  
scale dimension in metres

Reference of materials used in this disposal cell: ...

public accessible? Yes

## At start of the post-closure phase: ILW

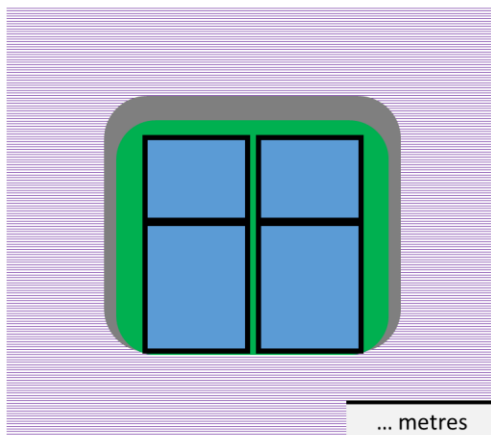


No SA performed up to now in Romania for ILW geological disposal

Reference for pore water compositions in this disposal cell: ...

public accessible? Yes

## Safety concept: ILW



Criteria for assessing perturbation host rock: No such criteria were established yet

Criteria for material against host rock: N/A

Criteria for backfill: N/A

Criteria for cementitious immobilisation matrix: N/A

Reference for criteria set in this disposal cell and their rationale:

public accessible? Yes

## Narrative of the post-closure phase

- *Is there a reference available with a description of processes in a normal evolution scenario?*
- *No*

## Conceptual model for the disposal cell

- *Is there a reference available with a conceptual model for the chemical evolution of this disposal cell in a normal evolution scenario?*
- *No*

## Mathematical model for the disposal cell

- *Is there a reference available with the implementation of the conceptual model for the chemical evolution of this disposal cell in a mathematical model?*
- *No*

## Expected contribution from ACED for ILW disposal cells

- Preference cementitious matrix containing organic waste
  - Organic material is Spent Ion Exchange Resins (SIERs)
- What are the reasons for your preference?
  - SIERs generated at Cernavoda NPP from non-fuel contact systems due to the high  $^{14}\text{C}$  content could not accomplish the WAC for near surface repository and have to be geological disposed of
  - Up to now in the generic SA carried out in RATEN ICN (*M. Pavelescu et al., 2003; D. Buhmann, 2003; Capouet M. et al., 2018*), only the disposal zone for CANDU SF was considered and no SA addressed the ILW disposal. Consequently, the outputs of ACED could be good guidelines on how to treat the evolution of disposal cells for ILW in the Romanian programme.

## References for generic SA performed for CANDU SF disposal:

- M. Pavelescu, A. Ionescu, A. Rizoiu, D. Buhmann, R.Storck - Deep Geological Disposal Research in Romania, 2003
- D. Buhmann, M. Pavelescu, A. Ionescu, A. Rizoiu, R.Storck - Comparison of Long-Term Safety of repositories for Spent CANDU or LWR Fuels in Hard Rock, GRS – 196 SCN-NT 261/2003
- Capouet M. et al., CAST outcomes in the context of the safety case: WP6 Synthesis report (D6.4)

## Appendix C. Presentation kick-off meeting from Slovenia

### Kick-off meeting EURAD ACED Country: Slovenia Organisation: ZAG (& help from ARAO)

Presenter: Bojan Zajec

Date: 2 July 2019

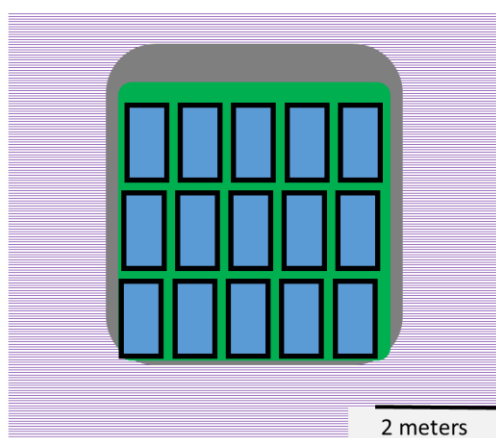
This presentation can be used in an Appendix for an ACED deliverable that will be published at the EURAD website

## HLW

- 1 NPP (Krško) in Slovenia, Westinghouse PWR 1x 730 MW output, ½ to Slovenia, ½ to Croatia. Lifetime extended till 2043. Currently ≈1300 fuel elements stored in the SFP.
- no reprocessed HLW disposal planned in Slovenia
- only direct disposal of spent fuel and HLW (several scenarios under consideration, also KBS3)
- first geological disposal within 90-100 years

## At start of the post-closure phase: ILW

site: Vrbina, near NPP Krško



Host rock: low permeable Miocene silt layer

Material against silt: reinforced concrete (silo) with limestone aggr.

Material used for backfill: concrete

Material used for container: reinforced concrete

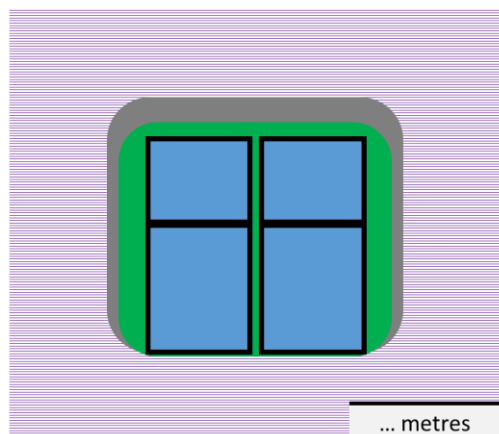
Immobilisation matrix cementitious material  
(concrete mortar with dolomite aggr.)  
containing metallic waste form

scale dimension in metres

\*Please remove 'granite' or 'clay'; \* please remove 'organic' or 'metallic' if your country owns both types of waste than choose the one you are most interested in for an ACED contribution \*Please remove if no additional material is emplaced against the host rock  
Reference of materials used in this disposal cell: ... public accessible? Yes



## At start of the post-closure phase: ILW



pH of silt: between 8.0 and 9.1, increases with depth

pH: ..., redox: ...

pH: ..., redox: ...

pH: ..., redox: ..., CaO/SiO<sub>2</sub>: ..., w/c: ...

Reference for pore water compositions in this disposal cell: ...

public accessible? Yes/No\*

## At start of the post-closure phase: ILW

### Silt chemical properties vs depth:

VOG1							
depth [m]	14	40	64	70	84	102	122
SO <sub>4</sub> <sup>-</sup> [mg/kg]	107	209	130	205	100	840	800
Cl <sup>-</sup> [mg/kg]	7.3	6.5	5	5.8	5	4.9	7
CO <sub>3</sub> ion [%]	12	22	15	21	16	11.8	15.3
VOG2							
depth [m]	18	40			90	101	120
SO <sub>4</sub> <sup>-</sup> [mg/kg]	12	11			130	140	74
Cl <sup>-</sup> [mg/kg]	7	6.7			6.1	8.5	9.6
CO <sub>3</sub> ion [%]	34	17			12	12.2	14.1

Reference for pore water compositions in this disposal cell: ...

### Vrbina groundwater composition:

Spojina	Količina [mg/l]
NH <sub>3</sub> (aq) 25 %	14,3
NH <sub>4</sub> Cl	48,2
NaHCO <sub>3</sub>	1218,8
MgSO <sub>4</sub> ·7H <sub>2</sub> O	436,3
KHSO <sub>4</sub>	192,0
K <sub>2</sub> SO <sub>4</sub>	753

public accessible? Yes/No\*

### Planned activities

- 2017 Environmental impact assessment, cross border impact assessment,
- 2018 Obtaining a construction permit
- 2018-20 Construction

## LILW Repository phases

- |                                  |                  |
|----------------------------------|------------------|
| • Trial operation                | 2020-2021        |
| • Operation I                    | 2022-2024 (2027) |
| • Preparations for idle phase    | 2025 (2027)      |
| • Idle phase                     | 2026-2048        |
| • Preparation for operation      | 2049             |
| • (and second silo construction) | (2049-2050)      |
| • Operation II                   | 2050-2060        |
| • Decommissioning                | 2061             |
| • Closing of the repository      | 2062             |

## Expected contribution from ACED for ILW disposal cells

- Preference cementitious matrix containing metallic and organic waste
  - Metallic material is carbon steel and/or stainless steel
  - Organic (experience with superplasticizers, bio-fibers, plastics in cement matrix)
- What are the reasons for your preference?
  - Experience with steel in concrete.
  - Laboratory for Metals, Corrosion and Anti corrosion protection
  - Laboratory for Stone, Aggregate and Recycled Materials

## Appendix D. Mathematical formulation of chemical reactions

A chemical system is made up of a set of atomic constituents or elements. A chemical species is defined as any chemical entity distinguishable from the rest due to its elemental composition and by the phase at which it is present. Not all species are needed to describe fully the chemical system. The subset of species which is strictly necessary is made up of what are known as components. These components can be chosen arbitrarily among all species. Although the  $N_E$  atomic constituents could serve as a set of components, they are never used as such because the constituents themselves are rarely present in aqueous phases. For this reason, it is more convenient to select as components a subset of  $N_C$  chemical species. These species are also known as the primary species.

CORE-LE allows the user to define a set of aqueous species in the database as a primary species. The code checks that this set of species are initially independent and are able to form together with the sorbed primary species the rest of species (such as secondary species or aqueous complexes, minerals, gases and surface complexes) as a linear combination of primary species.

$$Q_j^S = \sum_{i=1}^{N_C} v_{ji} Q_i^P \quad j = 1 \dots N_S \quad (\text{A1.1})$$

where  $Q_j^S$  and  $Q_i^P$  are the chemical formulae of the  $j$ -th secondary species and the  $i$ -th primary species respectively;  $v_{ij}$  is the stoichiometric coefficient of the  $i$ -th primary species in the dissociation reaction of the  $j$ -th species and  $N_S$  is the total number of secondary species.

CORE-LE assumes local equilibrium among all the chemical species of the system. At a given pressure and temperature, the Gibbs free energy of the system reaches a minimum, and the system cannot spontaneously carry out any chemical work. The derivation from this principle of equilibrium leads to the well-known Mass-Action law expression:

$$K_{j(p,T)} = e^{-\frac{\Delta G^\circ}{RT}} \equiv a_j^{-1} \prod_{i=1}^{N_T} a_i^{v_{ji}} \quad (\text{A1.2})$$

where  $K_j$  is the equilibrium constant which depends on the pressure and temperature of the system,  $a_i$  and  $a_j$  are the thermodynamic activities of the  $i$ -th and  $j$ -th species, respectively,  $N_C$  is the total number of primary species and  $v_{ji}$  is the stoichiometric coefficient of the  $i$ -th primary species in the dissociation reaction of the  $j$ -th species. As a convention the stoichiometric coefficients are positive for species on the right hand side of the reaction, and negative for those on the left hand side. The reactions are always written as the dissociation of one mole of secondary species.

### 1: Aqueous complexation reactions

The continuous motion of dissolved ions together with their large number per unit volume cause numerous collisions making possible the formation of ion pairs and/or dissolved complexes which usually have an ephemeral live (on the order of  $10^{-10}$  s). Since these reactions are almost instantaneous, they can be effectively considered as equilibrium reactions. The equilibrium constant relates the average number of ions pairs or complexes which are being formed. Applying the Mass-Action Law to the dissociation of the  $j$ -th secondary species, one has:

$$K_j = a_j^{-1} \prod_{i=1}^{N_C} a_i^{v_{ji}} \quad (\text{A1.3})$$

where  $a_i$  and  $a_j$  are the thermodynamic activities of the species  $j$  and  $i$ , respectively, and  $\nu_{ji}$  is the stoichiometric coefficient of the  $i$ -th primary species in the  $j$ -th secondary species. This equation allows one expressing the concentration of secondary species or aqueous complexes  $x_j$  in terms of primary species concentrations  $c_i$ :

$$x_j = K_j^{-1} \gamma_j^{-1} \prod_{i=1}^{N_c} c_i^{\nu_{ji}} \gamma_i^{\nu_{ji}} \quad (\text{A1.4})$$

where  $x_j$  and  $c_i$  are molal concentrations and  $\gamma_j$  and  $\gamma_i$  are thermodynamic activity coefficients.

For non-concentrated solutions (less than 1 mol/kg) the value of the activity coefficient of the  $i$ -th aqueous species can be calculated according to the extended Debye-Hückel equation:

$$\log \gamma_i = -\frac{Az_i^2(I)^{\frac{1}{2}}}{1 + Ba_i(I)^{\frac{1}{2}}} + bI \quad (\text{A1.5})$$

where  $I$  is the ionic strength of the solution;  $z_i$  and  $a_i$  are the electric charge and the ionic radius in solution of the  $i$ -th aqueous species, respectively;  $A$  and  $B$  are constants which depend on temperature and dielectric constant of water, and  $b$  is a constant of a given species determined from fitting experimental data. The values of  $A$ ,  $B$  and  $b$  at different temperatures are tabulated in Helgeson and Kirkham (1974). The value of the ionic strength is calculated as:

$$I = \frac{1}{2} \sum_{i=1}^{N_T} c_i z_i^2 \quad (\text{A1.6})$$

The activity of water can be calculated according to Garrels and Christ (1965) as:

$$a_{\text{H}_2\text{O}} = 1 - 0.018 \sum_{i=2}^{N_T} c_i \quad (\text{A1.7})$$

where summation index  $i$  includes all the species in solution except water. The expressions of  $\log \gamma_i$  and  $a_{\text{H}_2\text{O}}$  are only valid for diluted solutions ( $I \leq 0.1$  M).

Accordingly, the total dissolved concentration of a given component  $C_k$  can be written in an explicit form as a function of the concentration of the  $N_c$  primary species:

$$C_k = c_k + \sum_{j=1}^{N_x} \nu_{jk} x_j = c_k + \sum_{j=1}^{N_x} \nu_{jk} K_j^{-1} \gamma_j^{-1} \prod_{i=1}^{N_c} c_i^{\nu_{ji}} \gamma_i^{\nu_{ji}} \quad (\text{A1.8})$$

where  $N_x$  is the number of secondary species. Notice the difference between the concentration of primary species  $c_k$  and the total concentration  $C_k$ . As shown before, the chemical composition of an aqueous system containing  $N_E$  species can be expressed in terms of the concentrations of  $N_c$  components (primary species). This is of great relevance for reactive solute transport modeling because instead of  $N_E$  transport equations only  $N_c$  equations have to be solved. The concentration of the  $N_x$  secondary species can be explicitly computed from the concentrations of primary species. This results in a significant reduction of computing time.

## 2: Acid-base reactions

These reactions include those involving the transfer of protons  $H^+$ . Proton concentration in the solution is obtained by defining a new variable measuring the proton excess or total proton concentration,  $C_H$ , which is defined as:

$$C_H = c_{H^+} + \sum_{j=1}^{N_x} \nu_{jH} X_j \quad (A1.9)$$

where  $C_{H^+}$  is the concentration of free protons and  $\nu_{jH}$  are the stoichiometric coefficients of protons in the acid-base reactions of formation of secondary aqueous species. The total concentration,  $C_H$ , represents the net proton balance or “proton excess” of all acid-base reactions taking place in the solution. Contrary to the total concentrations of all other components,  $C_H$  in some cases may take on negative values.

### 3: Redox reactions

The transfer of electrons between two different atoms changes their chemical valence. This transfer is known as an oxidation-reduction reaction. The redox potential of a chemical system can be described by means of redox pairs such as  $O_2/H_2O$ ,  $SO_4^{2-}/H_2S$ ,  $Fe^{3+}/Fe^{2+}$ , etc. Usually, the redox potential is governed by the most abundant redox pair. Even though this approach seems to be the most adequate, it is rarely used due to the difficulty of obtaining the analytical concentrations of the two species of a redox pair.

Among the different alternative approaches to describe redox reactions the external approach considers hypothetical electron activity as an aqueous component or a master species. Contrary to the protons, which exist in reality as dissolved species, the electron concentration is a hypothetical variable. The definition of this virtual concentration is useful because it allows to complete the redox half-reactions and treat them as the rest of the chemical reactions in the aqueous phase. Each half redox reaction is completed by adding electrons as transferable species. The activity coefficient of this hypothetical species is assumed to be equal to one. It is possible then to define the total electron concentration  $C_e$  as:

$$C_e = c_e + \sum_{j=1}^{N_x} \nu_{je} X_j \quad (A1.10)$$

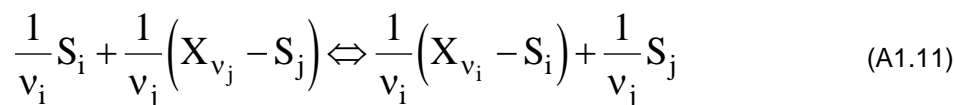
where  $c_e$  is the “free electron concentration” and  $\nu_{je}$  is the stoichiometric coefficient of the electron in  $j$ -th half-redox reaction.

Similar to acid-base reactions, the total concentration  $C_e$  represents the net electron balance or “electron excess” for all redox reactions. Thus,  $C_e$  may take on positive or negative values. In this way, redox reactions can be treated in the same way as the rest of equations. Once the “free electron concentration”,  $c_e$ , is known, the calculation of other redox indicators, such as the counter-part species of a redox pair, the concentration of dissolved oxygen ( $O_2(aq)$ ), or the fugacity of oxygen gas ( $O_2(g)$ ), can be easily calculated by considering them as secondary species (Equation. A1.4)

### 4: Cation exchange.

Cation exchange takes place when free cations in solution exchange with interlayer cations. This process can be described as an equilibrium reaction between an exchangeable cation and an exchange

site. The equilibrium constant is usually known as the exchange coefficient because its value depends on the ionic strength of the solution. A general expression for cation exchange reactions according to the Gaines-Thomas convention is (Appelo and Postma, 1993):



where  $V_i$  and  $V_j$  are the stoichiometric coefficients (equal to their charges) of dissolved and interlayer cations, respectively;  $S_i$  and  $S_j$  denote dissolved cationic species and  $(X_{v_i} - S_i)$  and  $(X_{v_j} - S_j)$  represent exchange sites or exchange interlayer cations. The equilibrium equation for cation exchange is obtained from the Mass Action Law:

$$K_{ij}^* = \frac{\bar{w}_i^{-1/v_i} \cdot a_j^{1/v_j}}{\bar{w}_j^{-1/v_j} \cdot a_i^{1/v_i}} \quad (\text{A1.12})$$

where  $K_{ij}^*$  is the exchange coefficient or selectivity,  $a_j$  is the activity of the  $j$ -th dissolved species and  $\bar{w}_i$  is the activity of the  $i$ -th exchanged species. Activities of dissolved cations are related to concentrations according to the Debye-Hückel theory. Activities of interlayer cations are approximated by their equivalent fractions of the number of exchange sites. Thus, the activity of the interlayer cation  $\bar{w}_i$  is assumed to be equal to its equivalent fraction  $\beta_i$ , and is calculated as:

$$\bar{w}_i \cong \beta_i = \frac{w_i}{\sum_{i=1}^{N_w} w_i} \quad (\text{A1.13})$$

where  $w_i$  is the concentration of the  $i$ -th interlayer cation and  $N_w$  is the total number of such interlayer cations. The sum of concentrations of surface sites or interlayer cations is the so-called cation exchange capacity (CEC). Substituting (A1.13) into (A1.12) yields the general equation for cation exchange:

$$K_{ij}^* = \frac{\beta_i^{1/v_i} \cdot (c_j \gamma_j)^{1/v_j}}{\beta_j^{1/v_j} \cdot (c_i \gamma_i)^{1/v_i}} \quad (\text{A1.14})$$

where the activity of each dissolved species  $a_i$  has been expressed as the product of its concentration  $C_i$  time its activity coefficients  $\gamma_i$ . From this equation, the equivalent fraction of the  $j$ -th interlayer cation can be expressed as

$$\beta_j = (K_{ij}^*)^{-v_j} c_j \gamma_j \left( \frac{\beta_i}{c_i \gamma_i} \right)^{v_j/v_i} \quad j = 1, 2, \dots, N_w \quad (\text{A1.15})$$

From the definition of equivalent fraction, one has:

$$\sum_{j=1}^{N_w} \beta_j = 1 \quad (\text{A1.16})$$

Substituting Equation A1.15 into A1.16 results in:

$$\sum_{j=1}^{N_w} \left( K_{ij}^* \right)^{-v_j} c_j \gamma_j \left( \frac{\beta_i}{c_i \gamma_i} \right)^{v_j/v_i} = 1 \quad (\text{A1.17})$$

which for given dissolved concentrations  $c_i$  can be solved for the single unknown  $\beta_i$ . This equation is quadratic when cation exchange involves only homovalent and divalent cations. However, when cation exchange involves also trivalent cations a cubic equation is obtained. Once the equivalent fraction  $\beta_i$  is known the rest of exchange fractions can be calculated from Equation A1.15. The concentration of the  $i$ -th exchanged cation  $W_j$  (in moles per liter of fluid) can be obtained from the  $i$ -th equivalent fraction according to Equation A1.13 through:

$$w_j = \beta_j \text{CEC} \rho_s z_j \frac{(1 - \phi)}{100\phi} \quad (\text{A1.18})$$

where CEC is the cation exchange capacity (usually measured as the number of milli equivalents of cations per 100 gram of solid),  $\phi$  is the porosity,  $\rho_s$  is the density of the solids (Kg of solids per  $\text{dm}^3$  of solids) and  $z_j$  is the cation charge.

## 5: Mineral dissolution/precipitation reactions

Under equilibrium conditions, mineral dissolution/precipitation reactions can be described by the Mass Action Law which states that:

$$X_m \lambda_m K_m = \prod_{i=1}^{N_c} c_i^{v_{mi}^p} \gamma_i^{v_{mi}^p} \quad (\text{A1.19})$$

where  $X_m$  is the molar fraction of the  $m$ -th solid phase,  $\lambda_m$  is its thermodynamic activity coefficient ( $X_m$  and  $\lambda_m$  are taken equal to 1 for pure phases),  $c_i$  and  $\gamma_i$  are the concentration and activity coefficient of the  $i$ -th dissolved primary species,  $v_{mi}^p$  is the stoichiometric coefficient in the  $m$ -th solid phase, and  $K_m$  is the corresponding equilibrium constant.

The equilibrium condition provides a relationship among the concentrations of the involved aqueous species. The mass transfer needed to achieve this condition is not specified. In fact, the equation does not include the concentration of the  $m$ -th solid phase, and therefore the amount of dissolved/precipitated mineral cannot be computed explicitly. This is an important feature of this type of reactions that is not shared neither by homogeneous reactions nor by the rest of heterogeneous reactions.

## Appendix E. Completed template from Sweden

Current handling of the chemical evolution  
in Europe for EURAD ACED

Country: Sweden

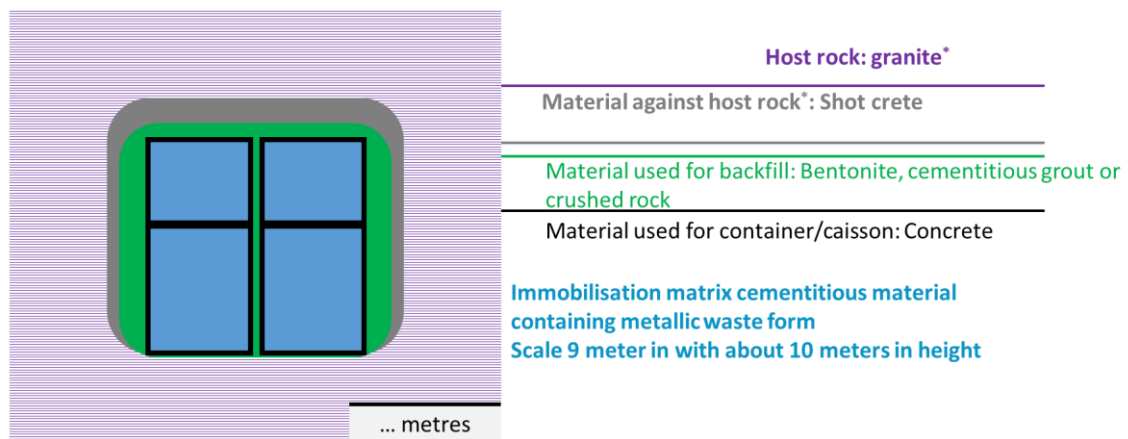
Organisation: Swedish Nuclear Fuel and  
Waste management Company

Author: Klas Källström

Date: 20190815

These sheets can be used in an Appendix for an ACED deliverable that will  
be published at the EURAD website

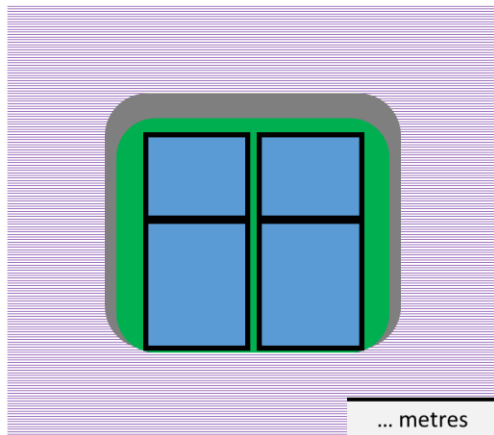
### At start of the post-closure phase: ILW



Reference of materials used in this disposal cell: SKB TR-14-02

public accessible? Yes

## At start of the post-closure phase: ILW



pH: 7,4, redox: -0.210, Cl: 190 mg/l, SO<sub>4</sub><sup>2-</sup>: 50 mg/l, HCO<sub>3</sub><sup>-</sup>: 300mg/l

pH: 13 redox: -0.750

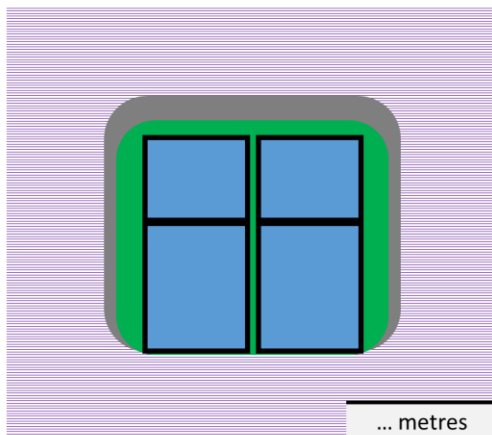
pH: 7,4, redox: -0.210

pH: 13, redox: -0.750 CaO/SiO<sub>2</sub>: 1.8, w/c: 0,47

Reference for pore water compositions in this disposal cell: SKB TR-14-01

public accessible? Yes

## Safety concept: ILW



Criteria for assessing perturbation host rock: NONE

Criteria for material against host rock: NONE

Criteria for backfill: Washed crushed rock

Criteria for cementitious immobilisation matrix: Sulphate resistant  
Minimum of 22 % cement in the concrete. Shall be CEM1 type

Reference for criteria set in this disposal cell and their rationale:

public accessible? Yes/No\*

## Narrative of the post-closure phase

- *Is there a reference available with a description of processes in a normal evolution scenario?*
- **Yes**
- *If yes, can you provide the:*
  - SKB
  - *Waste form and packaging process report (SKB TR-14-03)*
  - 2014
- <http://www.skb.se/upload/publications/pdf/TR-14-03.pdf>
- *If yes, does this narrative also contains a time sequence of features?*
- **Yes**

## Conceptual model for the disposal cell

- *Is there a reference available with a conceptual model for the chemical evolution of this disposal cell in a normal evolution scenario?*
- **Yes**
- *If yes, can you provide the:*
  - *First author* Lars Olof Höglund
  - *Title* Reactive transport modelling of concrete degradation in BMA
  - *Publication date* 2014
- <https://www.skb.se/publikation/2478306/R-13-40.pdf>

\*Please remove 'yes' or 'no'

## Mathematical model for the disposal cell

- *Is there a reference available with the implementation of the conceptual model for the chemical evolution of this disposal cell in a mathematical model?*
- **Yes**
- *If yes, can you provide the:*
  - *First author Lars Olof Höglund*
  - *Title Reactive transport modelling of concrete degradation in BMA*
  - *Publication date 2014*
- <https://www.skb.se/publikation/2478306/R-13-40.pdf>

*\*Please remove 'yes' or 'no'*

## Expected contribution from ACED for ILW disposal cells

- Preference cementitious matrix containing metallic waste
  - Metallic materials is carbon steel/stainless steel
- What are the reasons for your preference?
  - SKB needs to know if corrosion products can cause fractures in the concrete on long time scales. We also need to know how to quantify these eventual cracks and how to change the hydraulic properties of the concrete

## Appendix F. Completed template from United Kingdom

# Current handling of the chemical evolution in Europe for EURAD ACED

Country: Great Britain

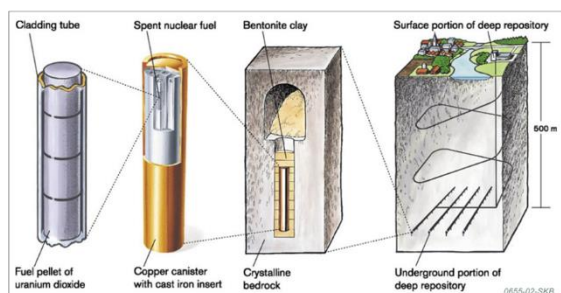
Organisation: Radioactive Waste  
Management Limited (RWM)

Author: Mike Poole

Date: 22/8/19

These sheets can be used in an Appendix for an ACED deliverable that will be published at the EURAD website

## At start of the post-closure phase: HLW



Host rock: higher strength rock

Material against host rock: bentonite

Backfill material in tunnels: bentonite

Immobilisation matrix (for HLW) glass

Material for overpack: copper

Material surrounding the overpack: bentonite

We do not yet have a site in the UK.

The example given is for disposal in higher-strength rock, where we assume the Swedish KBS-3V concept.

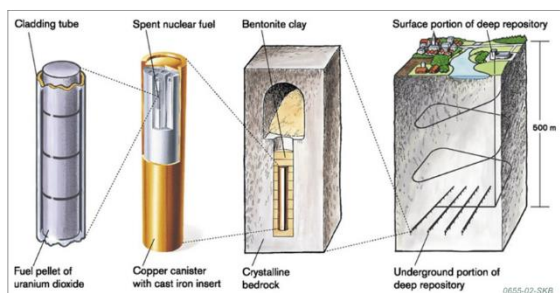
We have alternative example concepts for lower-strength sedimentary rock and evaporite.

The picture shown illustrates for spent fuel, not HLW.

Reference of materials used in this disposal cell: Radioactive Waste Management, *Geological Disposal: Engineered Barrier System Status Report*, DSSC/452/01, December 2016.

Publicly accessible? Here: <https://rwm.nda.gov.uk/publication/geological-disposal-engineered-barrier-system-status-report/>

## At start of the post-closure phase: HLW



It is not possible to give detailed information about pore water compositions in various parts of the engineered barrier system, given that we are at a generic stage and do not have a site in mind, therefore we do not know the likely chemistry of the groundwater and how it will evolve.

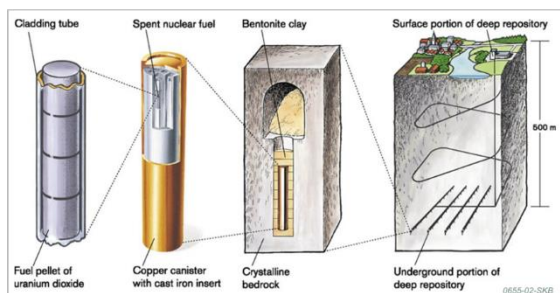
A more general discussion of the engineered barrier system is given in the reference below.

We do not yet have a site in the UK.  
The example given is for disposal in higher-strength rock, where we assume the Swedish KBS-3V concept.  
We have alternative example concepts for lower-strength sedimentary rock and evaporite.  
The picture shown illustrates for spent fuel, not HLW.

Reference of pore water compositions in this disposal cell: Radioactive Waste Management, *Geological Disposal: Engineered Barrier System Status Report*, DSSC/452/01, December 2016.

Publicly accessible? Here: <https://rwm.nda.gov.uk/publication/geological-disposal-engineered-barrier-system-status-report/>

## Safety concept: HLW



It is not possible to give detailed information on criteria for the various engineered backfill components at this generic stage.

However, more general descriptions of the engineered barriers and their evolution is given in the reference below.

We do not yet have a site in the UK.  
The example given is for disposal in higher-strength rock, where we assume the Swedish KBS-3V concept.  
We have alternative example concepts for lower-strength sedimentary rock and evaporite.  
The picture shown illustrates for spent fuel, not HLW.

Reference of criteria set in this disposal cell and their rationale: Radioactive Waste Management, *Geological Disposal: Engineered Barrier System Status Report*, DSSC/452/01, December 2016.

Publicly accessible? Here: <https://rwm.nda.gov.uk/publication/geological-disposal-engineered-barrier-system-status-report/>

## Narrative of the post-closure phase

- *Is there a reference available with a description of processes in a normal evolution scenario?*
- Yes
- *If yes, can you provide the:*
  - *First author: Radioactive Waste Management*
  - *Title: Geological Disposal: Engineered Barrier System Status Report*
  - *Publication date: December 2016*
- *Please provide the hyperlink in this presentation if it is published*
- <https://rwm.nda.gov.uk/publication/geological-disposal-engineered-barrier-system-status-report/>
- *If yes, does this narrative also contains a time sequence of features?*
- Yes

## Conceptual model for the disposal cell

- *Is there a reference available with a conceptual model for the chemical evolution of this disposal cell in a normal evolution scenario?*
- Yes
- *If yes, can you provide the:*
  - *First author: Radioactive Waste Management*
  - *Title: Geological Disposal: Generic Post-closure Performance Modelling*
  - *Publication date: December 2016*
- *Please provide the hyperlink in this presentation if it is published*
- <https://rwm.nda.gov.uk/publication/nda-rwm-138-generic-post-closure-performance-modelling/>

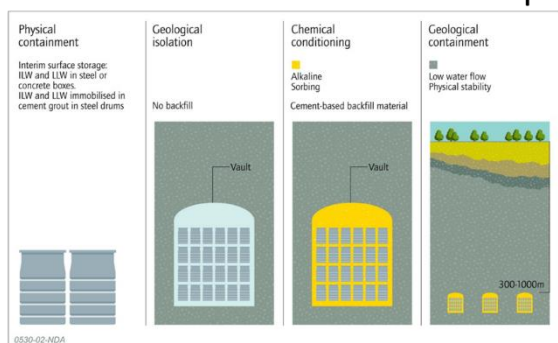
## Mathematical model for the disposal cell

- *Is there a reference available with the implementation of the conceptual model for the chemical evolution of this disposal cell in a mathematical model?*
- Yes
- *If yes, can you provide the:*
  - *First author: Radioactive Waste Management*
  - *Title: Geological Disposal: Generic Post-closure Performance Modelling*
  - *Publication date: December 2016*
- *Please provide the hyperlink in this presentation if it is published*
- <https://rwm.nda.gov.uk/publication/nda-rwm-138-generic-post-closure-performance-modelling/>

## Expected contribution from ACED for HLW disposal cells

- Do you have expected contributions for disposal cells containing vitrified HLW?
- No

### At start of the post-closure phase: ILW



It is not possible to give such detailed information about pore water compositions in various parts of the engineered barrier system, given that we are at a generic stage and do not have a site in mind, therefore we do not know the likely chemistry of the groundwater and how it will evolve.

The cementitious backfill is intended to promote a high pH environment – initially pH 13.5, dropping to about 12.5 for a considerable period of time before dropping further.

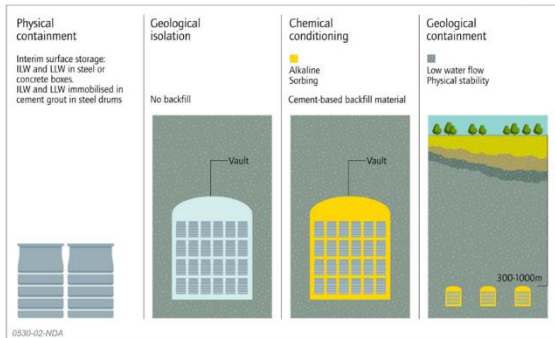
A more general discussion of the engineered barrier system is given in the reference below.

We do not yet have a site in the UK. The example given is for disposal in higher-strength rock, where we assume a cementitious backfill concept. We have alternative example concepts for lower-strength sedimentary rock and evaporite.

Reference of pore water compositions in this disposal cell: Radioactive Waste Management, *Geological Disposal: Engineered Barrier System Status Report*, DSSC/452/01, December 2016.

Publicly accessible? Here: <https://rwm.nda.gov.uk/publication/geological-disposal-engineered-barrier-system-status-report/>

## Safety concept: ILW



It is not possible to give detailed information on criteria for the various engineered backfill components at this generic stage.

However, more general descriptions of the engineered barriers and their evolution is given in the reference below.

We do not yet have a site in the UK. The example given is for disposal in higher-strength rock, where we assume a cementitious backfill concept. We have alternative example concepts for lower-strength sedimentary rock and evaporite.

Reference of criteria set in this disposal cell and their rationale: Radioactive Waste Management, *Geological Disposal: Engineered Barrier System Status Report*, DSSC/452/01, December 2016.

Publicly accessible? Here: <https://rwm.nda.gov.uk/publication/geological-disposal-engineered-barrier-system-status-report/>

## Narrative of the post-closure phase

- *Is there a reference available with a description of processes in a normal evolution scenario?*
- Yes
- *If yes, can you provide the:*
  - *First author: Radioactive Waste Management*
  - *Title: Geological Disposal: Engineered Barrier System Status Report*
  - *Publication date: December 2016*
- *Please provide the hyperlink in this presentation if it is published*
- <https://rwm.nda.gov.uk/publication/geological-disposal-engineered-barrier-system-status-report/>
- *If yes, does this narrative also contains a time sequence of features?*
- Yes

## Conceptual model for the disposal cell

- *Is there a reference available with a conceptual model for the chemical evolution of this disposal cell in a normal evolution scenario?*
- Yes
- *If yes, can you provide the:*
  - *First author: Radioactive Waste Management*
  - *Title: Geological Disposal: Generic Post-closure Performance Modelling*
  - *Publication date: December 2016*
- *Please provide the hyperlink in this presentation if it is published*
- <https://rwm.nda.gov.uk/publication/nda-rwm-138-generic-post-closure-performance-modelling/>

## Mathematical model for the disposal cell

- *Is there a reference available with the implementation of the conceptual model for the chemical evolution of this disposal cell in a mathematical model?*
- Yes
- *If yes, can you provide the:*
  - *First author: Radioactive Waste Management*
  - *Title: Geological Disposal: Generic Post-closure Performance Modelling*
  - *Publication date: December 2016*
- *Please provide the hyperlink in this presentation if it is published*
- <https://rwm.nda.gov.uk/publication/nda-rwm-138-generic-post-closure-performance-modelling/>

## Expected contribution from ACED for ILW disposal cells

- Not applicable

## Appendix G. Complete template from Czech Republic

# Kick-off meeting EURAD ACED Country: Czech Republic Organisation: SURAO

Presenter: Antonín Vokál

Date: 2 July 2019

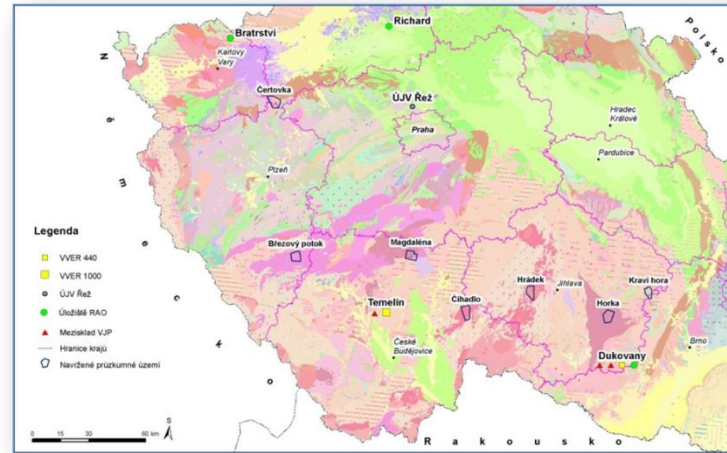
This presentation **can** be used in an Appendix for an ACED deliverable that will be published at the EURAD website

## Czech DGR concept

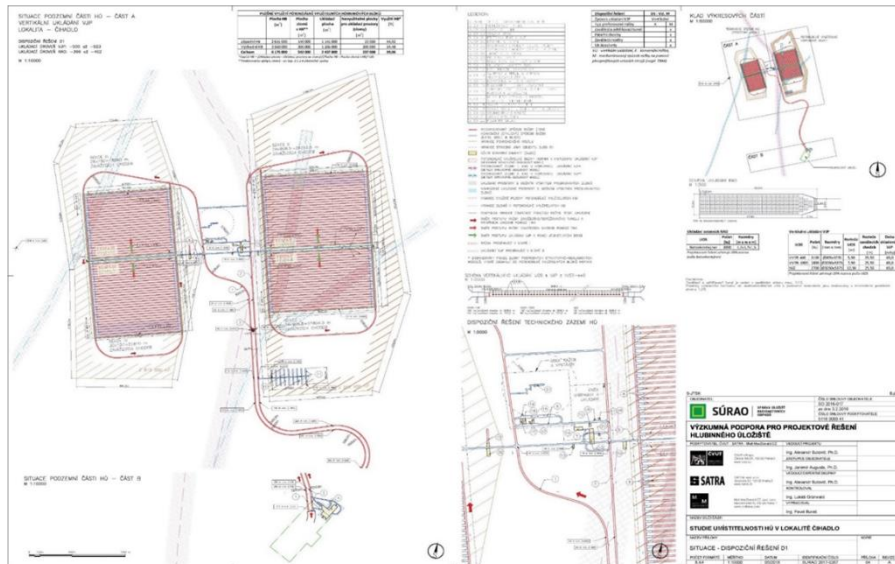
- The Czech DGR disposal concept is based on modified Swedish KBS3 concept for spent fuel
- High and intermediate level waste should be disposed of at the same site at the distance that guarantee that the two repositories will not be mutually affected
- No concrete decisions have been made concerning details of engineered barrier systems

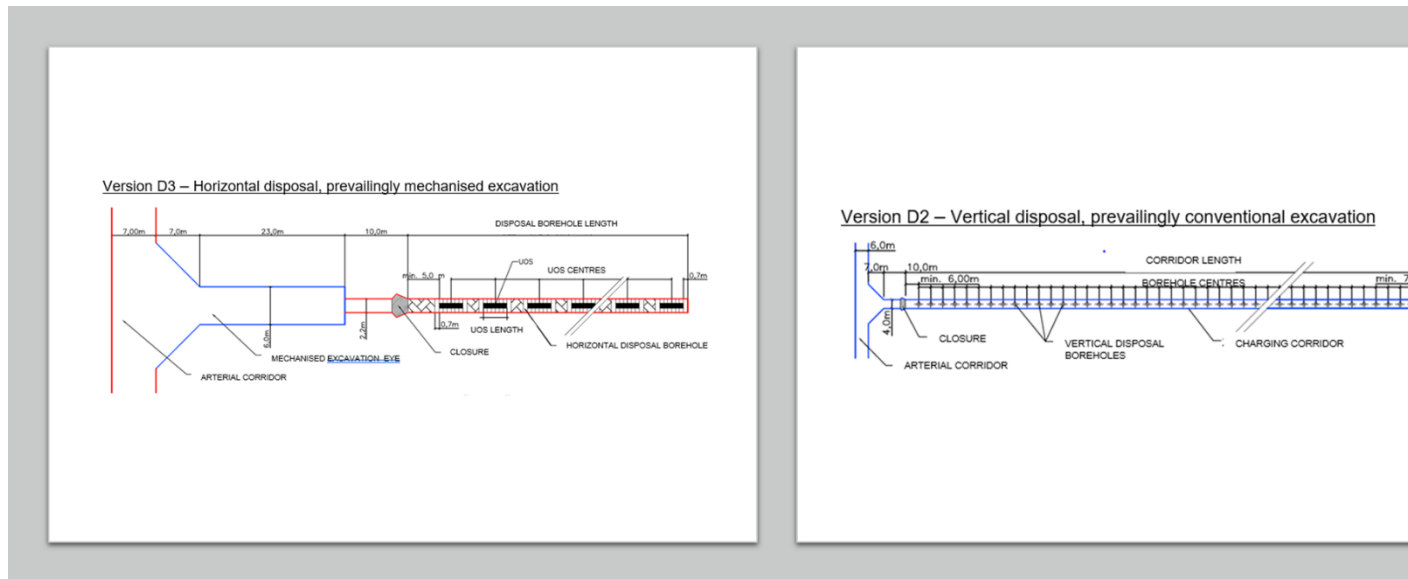
## Candidate sites for DGR

No.	Name	Main type of rock
1.	<b>Březový potok</b>	granodiorite
2.	<b>Čertovka</b>	granite
3.	<b>Čihadlo</b>	granite, gneiss, migmatite
4.	<b>Horka</b>	melagranite, melasyenite (durbachit)
5.	<b>Hrádek</b>	granite
6.	<b>Kraví hora</b>	granulit migmatitized paragneiss
7.	<b>Magdaléna</b>	melagranite, melasyenite (durbachit)
8.	<b>EDU-západ</b>	durbachit, gneiss to migmatite
9.	<b>ETE-jih</b>	migmatitized gneiss



## Preliminary repository layouts of DGR for candidate sites

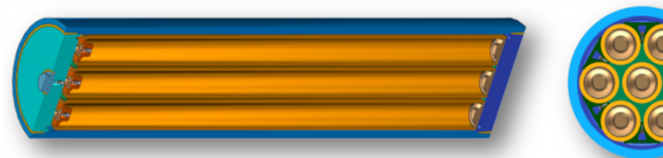




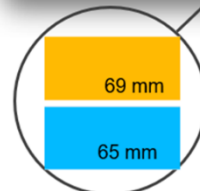
Both horizontal or vertical arrangements are considered

### Waste package characteristics

- **Reference disposal waste packages are based on two layer steel canister concept (carbon steel - outer layer) – stainless steel - inner layer**
- As an alternative copper or titan overpacks are considered

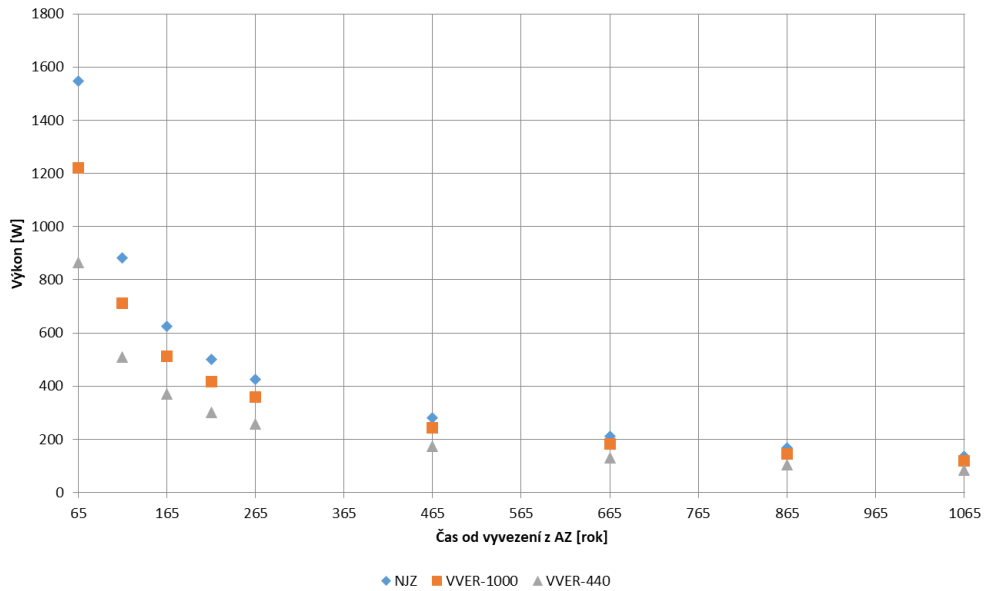


Alternative with independent stainless steel canisters for each SF in carbon steel overpack



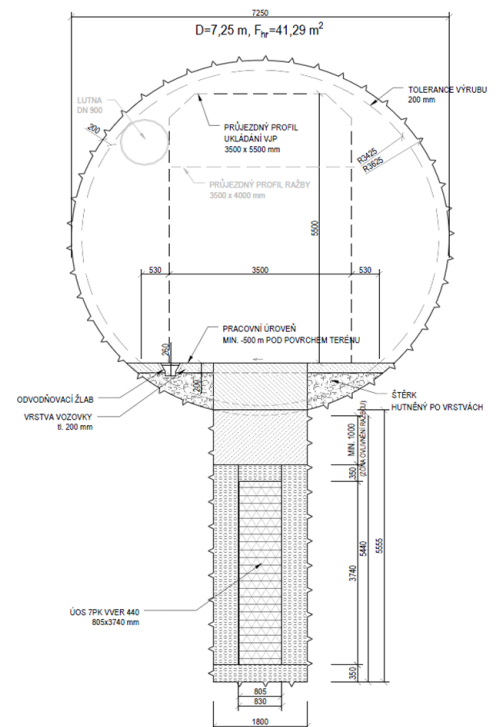
Alternative with one stainless steel canister in carbon steel overpack

# Decay heat of VVER 400/VVER 1000 spent fuel assemblies

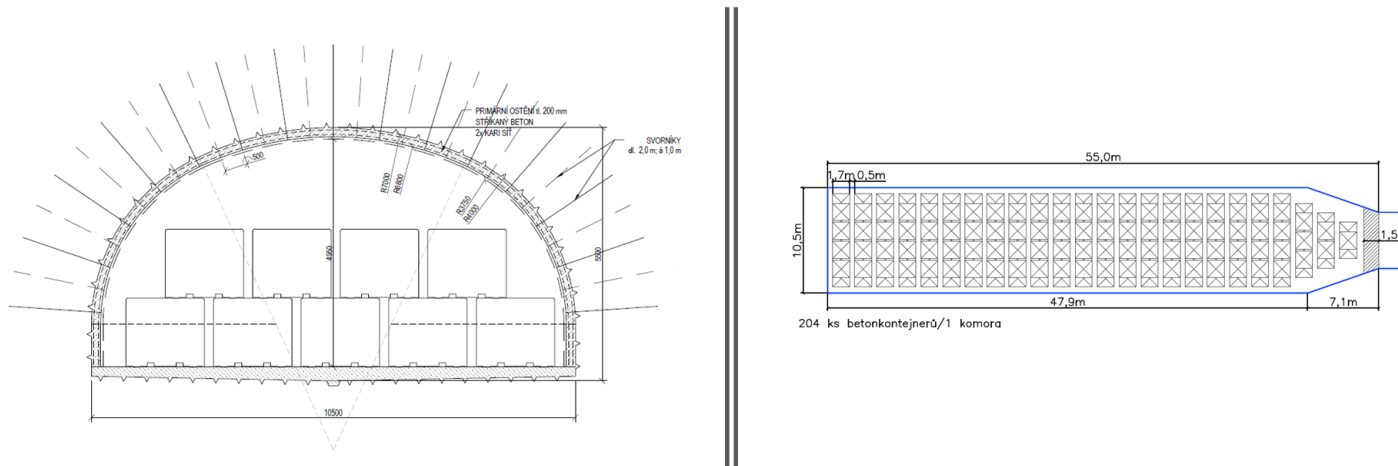


## Other EBS components

- Buffer alternatives
  - **Ca, Mg Bentonite (density 1600 kg/m<sup>3</sup>)**
  - Na Bentonite (Wyoming type)
  - Mixture of bentonite and cement
  - Cement – first layer, bentonite – second layer (similar to Belgian concept)
- Backfill
  - **Mixture of bentonite with ground rock**
  - Mixture of bentonite with sand
- Seals
  - Cement
  - Bentonite
  - Bentonite – cement mixture

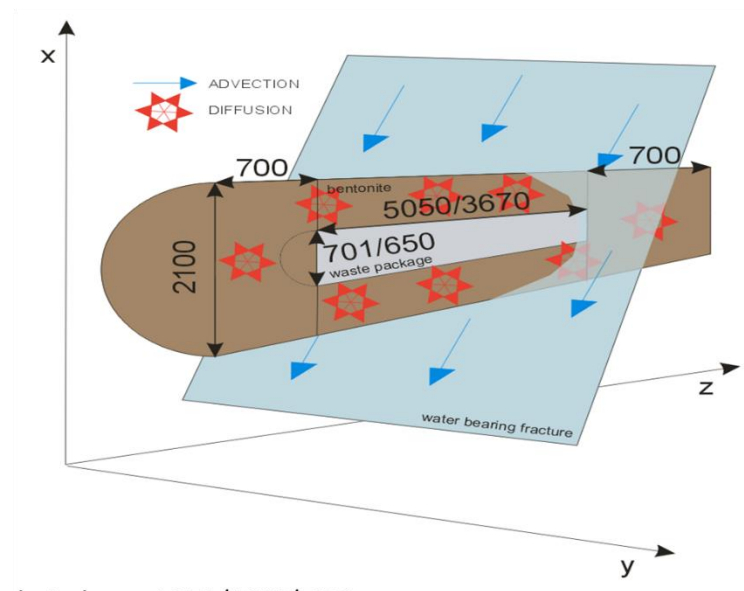


# ILW disposal



No decisions concerning EBS has been made. Preliminary - cement waste form, carbon steel waste packages and cement and bentonite for backfill are envisaged

Preliminary simplified model for reactive transport studies (horizontal layout, carbon steel, bentonite, granite)



Details: SURAO Technical report 271/2018/ENG

## Composition of granitic groundwater

Parameter	Unit	SGW2	B-SGW2-OX	B-SGW2-ANOX	SGW3	B-SGW3-OX	B-SGW3-ANOX
pH		8.2	8.24	7.87	9.4	8.24	8.13
Eh	mV	236.6	731.6	-212.4	236.6	731.7	-257.3
Temperature	°C	25	25	25	25	25	25
Al <sup>3+</sup> *	mol kgw <sup>-1</sup>	3.71E-06	6.34E-08	2.76E-08	3.71E-06	6.32E-08	4.96E-08
Ca <sup>2+</sup>	mol kgw <sup>-1</sup>	8.64E-04	5.12E-05	1.76E-04	3.24E-05	5.11E-05	1.64E-04
Cl <sup>-</sup>	mol kgw <sup>-1</sup>	9.31E-05	2.07E-03	2.06E-03	5.28E-04	2.50E-03	2.49E-03
Fe <sup>2+</sup> *	mol kgw <sup>-1</sup>	1.79E-06	3.60E-12	9.50E-07	1.79E-06	3.60E-12	8.15E-07
HCO <sub>3</sub> <sup>-</sup>	mol kgw <sup>-1</sup>	2.77E-03	9.68E-04	1.32E-03	2.68E-03	9.65E-04	7.55E-04
K <sup>+</sup>	mol kgw <sup>-1</sup>	5.37E-05	8.80E-04	9.04E-04	1.79E-05	8.87E-04	8.80E-04
Mg <sup>2+</sup>	mol kgw <sup>-1</sup>	3.42E-04	1.18E-03	1.03E-03	4.12E-06	1.19E-03	9.78E-04
NO <sub>3</sub> <sup>-</sup>	mol kgw <sup>-1</sup>	0.00E+00	3.18E-03	3.16E-03	0.00E+00	3.18E-03	3.16E-03
Na <sup>+</sup>	mol kgw <sup>-1</sup>	8.65E-04	1.01E-02	1.03E-02	3.81E-03	1.02E-02	1.02E-02
SO <sub>4</sub> <sup>2-</sup>	mol kgw <sup>-1</sup>	2.19E-04	3.59E-03	3.57E-03	1.09E-04	3.48E-03	3.46E-03
SiO <sub>2</sub> (aq)	mol kgw <sup>-1</sup>	5.20E-04	9.67E-05	9.50E-05	4.18E-04	9.67E-05	9.60E-05

Details: SURAO Technical report 271/2018/ENG

## Expected contribution from ACED for HLW disposal cells

- Increase understanding of the evolution of bentonite (blocks and/or pelets) in contact with carbon steel and the interfaces between bentonite and carbon steel and between bentonite blocks and pelets)
- Increase understanding of the cement evolution in contact with carbon steel and the interfaces between cement and carbon steel
- Increase understanding of the interfaces between bentonite and granite